



The University of  
**Nottingham**

UNITED KINGDOM • CHINA • MALAYSIA

School of Molecular Medical Sciences

**IDENTIFICATION, CHARACTERIZATION  
AND FUNCTIONAL ANALYSES OF A NOVEL  
BETA-CATENIN ASSOCIATED PROTEIN, FLYWCH1**

**MEDICAL LIBRARY  
QUEENS MEDICAL CENTRE**

*by*

**Belal Abdul-Rahman Muhammad**  
(BSc, MSc)

Thesis submitted to the University of Nottingham  
for the degree of Doctor of Philosophy

August 2012

# **Declaration**

Except where acknowledged in the text, I declare that this thesis is my own work and is based on research that was undertaken by me in Cancer Genetics & Stem Cell Group, the School of Clinical Sciences, Faculty of Medicine and Health Sciences, University of Nottingham.

Belal A. Muhammad

ID: 4071415

Date: 28/08/2012

## Abstract

The growing knowledge of cell biology and evidence for the role of  $\beta$ -catenin signalling network in homeostasis and carcinogenesis encourages further investigation into the regulatory network of nuclear  $\beta$ -catenin signalling complex. While the role of canonical Wnt signalling in the development of both normal tissue and malignant tumours is well documented, the molecular basis of these functionally distinct nuclear transcriptional programs is poorly understood. Many proteins are associated with cytoplasmic  $\beta$ -catenin for regulation of Wnt/ $\beta$ -catenin pathway activities. However, in the nucleus, the LEF/TCF family of transcription factors, which have DNA binding properties, remains the sole focus as unambiguous partners of  $\beta$ -catenin.

In addition to LEF/TCFs, interaction of  $\beta$ -catenin with several other transcriptional co-activators and/or co-repressors is required for gene regulation. This regulation may also be influenced by alterations of  $\beta$ -catenin protein such phosphorylation of  $\beta$ -catenin which dramatically alters its trafficking and function. Delineation and functional description of nuclear cofactors that interact with unphosphorylated (i.e. nuclear)  $\beta$ -catenin will further unravel the mechanisms of  $\beta$ -catenin-mediated nuclear transcription, and may also identify whether distinct patterns of transcriptional cofactors are engaged in normal development versus tumour progression.

Human FLYWCH1, a conserved member of the mammalian  $C_2H_2$  zinc finger proteins, was identified as one of the phosphorylation-independent Catenin-Interacting-Proteins (CIPs) in a recent screening performed in Dr Nateri's laboratory using a modified yeast-2-hybrid RRS. FLYWCH1 is a previously uncharacterized protein with no known function in mammals. Herein, we have shown that; *i*) in human cells, FLYWCH1 physically interacts with  $\beta$ -catenin and represses its transcriptional activity, *ii*) it regulates the expression of some if not all downstream target genes, *iii*) in the intestine, *Flywch1* marks the crypt-based columnar-cells (CBCs), which function as stem cells, but does not mark any of the differentiated cells in normal villi, *iv*) *FLYWCH1* expression is

strongly down-regulated in CRC cell lines but its expression is up-regulated and restricted to a subpopulation of tumour cells in both human and *Apc*<sup>Min/+</sup> mouse. Our data also showed that  $\nu$ ) FLYWCH1 controls CRC cell morphology and inhibits cell migration through up-regulation of E-cadherin which may not be related to ZEB2-mediated EMT.

Collectively, our data suggest that FLYWCH1 is a novel nuclear  $\beta$ -catenin interacting protein that inhibits cell motility by antagonizing the activity of Wnt/ $\beta$ -catenin signalling pathway. As changes in cell motility is a key step toward invasion and metastasis, FLYWCH1, therefore, may function as a metastasis-suppressing factor which could potentially be of use in the therapeutic field of colon cancer to control cancer spread.

## **Publications:**

- Roya Babaei-Jadidi, Ningning Li, Anas Saadeddin, Bradley Spencer-Dene, Anett Jandke, **Belal Muhammad**, et al. (2011). "FBXW7 influences murine intestinal homeostasis and cancer, targeting Notch, Jun, and DEK for degradation." *The Journal of Experimental Medicine* 208(2): 295-312. <http://jem.rupress.org/content/208/2/295.long>
- Saleh Al-Ghamdi, Abdulkader Albasri, Julien Cachat, Salih Ibrahim, **Belal A. Muhammad**, et al. (2011). Cten Is Targeted by Kras Signalling to Regulate Cell Motility in the Colon and Pancreas. *PLoS ONE* 6(6):e20919. Doi:10.1371/journal.pone.0020919. <http://www.plosone.org/article/info%3Adoi%2F10.1371%2Fjournal.pone.0020919>

## Acknowledgments

I would like to express my sincerest gratitude to my supervisors Dr Nateri for his indispensable guidance, support, and generosity throughout my thesis work and writing up, and Prof. Ilyas for his valuable discussion and support.

My special thanks go to my laboratory advisor, Dr Anas Saadeddin for his invaluable help and advice. My thanks also go to my friends and colleagues in cancer genetics and stem cell laboratory for all their technical and much needed moral support. Further thanks go to my colleagues in pathology group for their valuable help and support.

Many thanks for the Ministry of Higher Education of Iraq and the Iraqi Cultural Attaché in London for sponsoring my PhD project and providing me the financial support during my study at the University of Nottingham. This research project was also supported by the Medical Research Council (MRC) grant to Dr Nateri.

My deepest gratitude goes to my long suffering wife (Srwa), whose support made this whole adventure possible. Finally, I must thank "ALLAH" for giving me the opportunity and ability to finish my PhD and also for granting me two lovely blessing kids (Bahand and Bareen) during the course of my study; by whom I was always inspired.

# List of Figures

Figure 1-1: Schematic representation of Wnt/ $\beta$ -catenin signalling pathway. ....	8
Figure 1-2: Schematic representation of Tcf splice variants and their most conserved domains. ....	12
Figure 1-3: Nuclear interacting proteins of $\beta$ -catenin and TCF4. ....	15
Figure 1-4: The architecture of the small intestinal mucosa. ....	25
Figure 1-5: Multistep genetic model of colorectal carcinogenesis. ....	35
Figure 1-6: The canonical $C_2H_2$ zinc finger structure. ....	38
Figure 1-7 : Model representing Mod(mdg4) proteins as chromatin modules. ...	43
Figure 1-8: Identification of FLYWCH1 as unphosphorylated $\beta$ -catenin interacting protein in yeast. ....	47
Figure 1-9: Outline summary of the experimental research plans applied in this study. ....	49
Figure 2-1: Isolation of plasmid DNA using commercial Miniprep kit. ....	63
Figure 2-2: Isolation of plasmid DNA using manual Miniprep protocol. ....	65
Figure 2-3: Isolation of plasmid DNA using Miniprep kit. ....	66
Figure 2-4: DNA markers used for agarose gel electrophoresis. ....	69
Figure 2-5: DNA extraction from agarose gel. ....	70
Figure 2-6: Overlapping PCR strategy. ....	73
Figure 2-7: Total RNA isolation. ....	76
Figure 2-8: Synthesis of cDNA. ....	77
Figure 2-9: Protein markers used for for SDS-PAGE analysis. ....	88
Figure 3-1: Schematic presentation of FLYWCH motifs within human FLYWCH1 protein. ....	104
Figure 3-2: Multiple sequence alignment of FLYWCH1 in different animals. ...	106
Figure 3-3: FLYWCH1 amino acid sequence alignment in human and mouse. ...	107
Figure 3-4: pBluescriptR (KS+) plasmid (Stratagene). ....	109
Figure 3-5: Single cutter restriction enzyme's map for <i>FLYWCH1</i> ....	110
Figure 3-6: Restriction enzyme digestion analysis of FLYWCH1 IMAGE clone plasmid DNA. ....	112
Figure 3-7: Restriction enzyme digestion analysis of FLYWCH1 IMAGE clone and pI-EGFP2 plasmid vector. ....	114
Figure 3-8: The plasmid map of untagged human FLYWCH1 clone. ....	115

<b>Figure 3-9: Restriction enzyme digestion analysis of untagged FLYWCH1 clone.</b>	116
<b>Figure 3-10: The plasmid map of MYC-tagged FLYWCH1 clone.</b>	117
<b>Figure 3-11: Restriction enzyme digestion analysis of MYC-tagged human FLYWCH1 clone.</b>	118
<b>Figure 3-12: The plasmid map of the eGFP-fused FLYWCH1 clone.</b>	120
<b>Figure 3-13: Restriction enzyme digestion analysis of eGFP-fused human FLYWCH1 clone.</b>	120
<b>Figure 3-14: Western blotting analysis of proteins expressed from different human FLYWCH1 clones in cell culture.</b>	123
<b>Figure 3-15: Nuclear localization of human FLYWCH1.</b>	125
<b>Figure 4-1: Interaction of FLYWCH1 with <math>\beta</math>-catenin in human cell culture.</b>	132
<b>Figure 4-2: Schematic presentation of FLYWCH1 PCR-site directed mutagenesis.</b>	134
<b>Figure 4-3: Restriction enzyme digestion analysis of MYC-FLYWCH1 deletion mutant clones.</b>	136
<b>Figure 4-4: Western blotting analysis of MYC-tagged FLYWCH1 clones.</b>	137
<b>Figure 4-5: Restriction enzyme digestion analysis of eGFP-FLYWCH1 deletion mutant clones.</b>	139
<b>Figure 4-6: Western blotting analysis of eGFP-FLYWCH1 clones.</b>	140
<b>Figure 4-7: Mapping the interaction site of FLYWCH1 with <math>\beta</math>-catenin using Co-IP assay.</b>	142
<b>Figure 4-8: A C-terminal deletion mutant of FLYWCH1 (FLYWCH1-M4) changed the nuclear localisation of this protein.</b>	144
<b>Figure 4-9: Schematic presentation of <math>\beta</math>-catenin site-directed mutagenesis.</b>	146
<b>Figure 4-10: Generation of middle deletion mutant clones of <math>\beta</math>-catenin by overlapping PCR.</b>	149
<b>Figure 4-11: Restriction enzyme digestion analysis of FLAG-<math>\beta</math>-catenin clones.</b>	150
<b>Figure 4-12: Western blotting analysis of FLAG-<math>\beta</math>-catenin mutant clones.</b>	152
<b>Figure 4-13: Mapping the interaction site of <math>\beta</math>-catenin with FLYWCH1 using Co-IP assay.</b>	153
<b>Figure 4-14: Schematic presentation of the interaction sites between FLYWCH1 and <math>\beta</math>-catenin.</b>	160
<b>Figure 5-1: FLYWCH1 represses the transcriptional activity of <math>\beta</math>-catenin/TCF4.</b>	165

<b>Figure 5-2: TCF4 does not rescue the transcriptional repression of FLYWCH1 on <math>\beta</math>-catenin.....</b>	<b>166</b>
<b>Figure 5-3: Suppression of endogenous <math>\beta</math>-catenin/TCF4 by FLYWCH1.....</b>	<b>167</b>
<b>Figure 5-4: FLYWCH1 competes with TCF4 for interaction with <math>\beta</math>-catenin. ....</b>	<b>169</b>
<b>Figure 5-5: A C-terminal deletion of FLYWCH1 (FLYWCH1-M4) lost its suppression activity against <math>\beta</math>-catenin/TCF4.....</b>	<b>171</b>
<b>Figure 5-6: The N-terminal domain of <math>\beta</math>-catenin is required for its functional interaction with FLYWCH1.....</b>	<b>173</b>
<b>Figure 5-7: FLYWCH1 reduces wound-closure capacity of CRC cells.....</b>	<b>175</b>
<b>Figure 5-8: FLYWCH1 has no significant effects on cell proliferation.....</b>	<b>178</b>
<b>Figure 5-9: FLYWCH1 does not affect the total cell growth.....</b>	<b>179</b>
<b>Figure 5-10: FLYWCH1 reduces the migration of CRC cells.....</b>	<b>180</b>
<b>Figure 5-11: FLYWCH1 modulates the expression of Wnt-target genes.....</b>	<b>182</b>
<b>Figure 5-12: FLYWCH1 changes the morphology of CRC cells.....</b>	<b>184</b>
<b>Figure 5-13: FLYWCH1 enhances the expression of E-Cadherin. ....</b>	<b>186</b>
<b>Figure 5-14: Endogenous expression of FLYWCH1 in different human cell lines. ....</b>	<b>188</b>
<b>Figure 5-15: Endogenous expression of FLYWCH1 in normal vs. tumour tissues of intestine. ....</b>	<b>190</b>
<b>Figure 5-16: A simplified diagram shows the mechanism by which FLYWCH1 reduces cell motility.....</b>	<b>200</b>
<b>Figure 6-1: The expression plasmids and the strategy in brief, used to clone eGFP and eGFP-FLYWCH1 into the pLVX-Puro. ....</b>	<b>204</b>
<b>Figure 6-2: Cloning strategy for LVX-eGFP and LVX-eGFP-FLYWCH1-WT clones.....</b>	<b>205</b>
<b>Figure 6-3: Restriction enzyme digestion analysis of Lentiviral constructs containing eGFP and eGFP-FLYWCH1-WT cDNAs.....</b>	<b>206</b>
<b>Figure 6-4: FLYWCH1-WT aberrantly expressed in both HEK293T and HCT116 stable cell lines.....</b>	<b>209</b>
<b>Figure 6-5: Different localization patterns of stably expressed FLYWCH1.....</b>	<b>212</b>
<b>Figure 6-6: PCR amplification of the N-terminal region of the genomic-integrated exogenous <i>FLYWCH1</i>.....</b>	<b>214</b>
<b>Figure 6-7: PCR amplification of the full-length genome-integrated <i>FLYWCH1</i>. ....</b>	<b>215</b>

<b>Figure 6-8: The C-terminus region of the genome-integrated <i>FLYWCH1</i> in HEK293T stable cell line contains an internal in-frame deletion mutation.</b>	217
<b>Figure 6-9: PCR amplification of the genome-integrated <i>FLYWCH1</i> from HCT116 stable cell line.</b>	219
<b>Figure 6-10: The N-terminal region of the genome-integrated exogenous <i>FLYWCH1</i> has not been modified in HCT116 cell line.</b>	220
<b>Figure 6-11: A nonsense point mutation resulted in a stop-codon formation within the N-terminal region of the genome-integrated <i>FLYWCH1</i> in HCT116 stable cell line.</b>	222
<b>Figure 6-12: <i>FLYWCH1</i>/β-catenin transcriptional activity in HCT116 and HEK293T stable cell lines.</b>	224
<b>Figure 6-13: <i>FLYWCH1</i> repression activity on cell migration in HEK293T and HCT116 stable cell lines.</b>	226
<b>Figure 6-14: PCR amplification and restriction enzyme digestion analysis of the automodified exogenous <i>FLYWCH1</i> cDNA.</b>	228
<b>Figure 6-15: Cloning strategy of MYC-<i>FLYWCH1</i>-M5 plasmid.</b>	229
<b>Figure 6-16: The automutated clone of <i>FLYWCH1</i> lost its physical interaction with β-catenin.</b>	231
<b>Figure 6-17: Expression pattern of eGFP-<i>FLYWCH1</i> in both HCT116 and HEK293T stable cell lines.</b>	233
<b>Figure 6-18: Evaluation of eGFP-<i>FLYWCH1</i> protein expression in both HCT116 and HEK293T stable cell lines.</b>	234
<b>Figure 6-19: Stably expressed <i>FLYWCH1</i>-WT but not <i>FLYWCH1</i>-M5 up-regulates E-cadherin in HEK293T cells.</b>	236
<b>Figure 6-20: E-cadherin up-regulation by the wild-type <i>FLYWCH1</i> in HEK293T stable cell lines.</b>	239
<b>Figure 6-21: Effects of the stably expressed <i>FLYWCH1</i> on the morphology of HEK293T cells.</b>	241
<b>Figure 7-1: An overview of Human <i>FLYWCH1</i> cloning.</b>	248
<b>Figure 7-2: Schematic presentation of protein domains involved in the physical and functional interaction of <i>FLYWCH1</i> with β-catenin and vice versa.</b>	251
<b>Figure 7-3: <i>FLYWCH1</i> may modulate intestinal homeostasis and tumourigenesis through controlling cell migration and morphology.</b>	257

## List of Tables

Table 1-1: Proteins that activate the $\beta$ -catenin/TCF signalling.....	17
Table 1-2: A comprehensive list of proteins that repress the activity of $\beta$ -catenin/TCF complex. ....	19
Table 1-3: Examples of Wnt/ $\beta$ -catenin downstream target genes involved in cancer.....	31
Table 1-4: Structural classification of zinc fingers. ....	40
Table 2-1: Common non-commercial solutions and buffers used in this study...	52
Table 2-2: PCR primers used to amplify the full-length (wild-type) and deletion mutants of MYC-tagged FLYWCH1.....	54
Table 2-3: PCR primers used to generate the full-length (wild-type) and deletion mutants of eGFP-FLYWCH1.....	56
Table 2-4: PCR primers used to generate the N-terminus, C-terminus, and the middle deletion mutants of FLAG- $\beta$ -catenin. ....	57
Table 2-5: PCR primers used to amplify mRNA of several $\beta$ -catenin target genes by qRT-PCR. ....	58
Table 2-6 : PCR primers used to amplify the entire sequence and fragments of the exogenous genome-integrated <i>FLYWCH1</i> from the genomic DNA extract of HEK293T and HCT116 stable cell lines.....	59
Table 2-7: List of primary and secondary antibodies used for Western blotting and Immunofluorescent analysis.....	60
Table 2-8: Cycling parameters for the standard polymerase chain reaction.....	71
Table 2-9: Amplification parameters used for the quantitative real time polymerase chain reaction (qRT-PCR). ....	79
Table 2-10: Solution for preparing Resolving Gels for Tris-glycine SDS-PAGE.87	
Table 2-11: Solution for preparing 5% Stacking Gels for Tris-glycine SDS-PAGE.....	87
Table 3-1: Pairwise alignment scores of FLYWCH1 peptide and nucleotide sequences in human versus other animals.....	105
Table 3-2: List of single cutter restriction enzymes used for FLYWCH1 IMAGE clone verification.....	111
Table 4-1: Expected molecular weights of <i>FLYWCH1</i> -recombinant cDNAs and protein molecules.....	135

## Abbreviations

3' UTR	3' Un-Translated Region
5' UTR	5' Un-Translated Region
aa	Amino Acids
AMP	Ampicillin
APC	Adenomatous Polyposis Coli
BMP	Bone Morphogenic Protein
bp	Base Pair
BSA	Bovine Serum Albumin
C <sub>2</sub> H <sub>2</sub>	Cystein2-Histidin2
CBCs	Crypt Base Columnar Cells
CBP	CREB-Binding Protein
CDH1	Cadherin-1 (E-cadherin)
cDNA	Complementary Deoxyribonucleic Acid
ChIP	Chromatin Immunoprecipitation
CKI $\alpha$	Casein Kinase-I Alpha
CMV	Cytomegalovirus
Co-IP	Co-Immunoprecipitation
CRC	Colorectal Cancer
C-terminus	Carboxyl Terminus
CZFPs	Classical Zinc Finger Proteins
DMEM	Dulbecco Modified Eagle Medium
DNA	Deoxyribonucleic Acid
Dvl	Dishevelled
eGFP	Enhanced Green Fluorescent Protein
EMT	Epithelial to Mesenchymal Transition
ESCs	Embryonic Stem Cells
FBS	Fetal Bovine Serum
Fz	Frizzled
GSK-3 $\beta$	Glycogen Synthase Kinase-3 Beta
HA	Hem-Agglutinin
HMG	High Mobility Group
IMAGE	Integrated Molecular Analysis of Genomes and their Expression
ISCs	Intestinal Stem Cells
ISH	In Situ Hybridization
JNK	c-Jun N-terminal Kinase

Kb	Kilo Base pair
kDa	Kilo Dalton
Lgr4	Leucine-rich repeat-containing G-protein coupled Receptor 4
Lgr5	Leucine-rich repeat-containing G-protein coupled Receptor 5
LIF	Leukemia Inhibitory Factor
LRP5/6	Low-density lipoprotein Receptor-related Proteins 5 and/or 6
MCS	Multiple Cloning Site
MEF	Mouse Embryonic Fibroblast
mESCs	Mouse Embryonic Stem Cells
MET	Mesenchymal to Epithelial Transition
NCBI	National Centre for Biotechnology Information
NEB	New England BioLabs
N-terminus	Amino terminus
ORF	Open Reading Frame
PBS	Phosphate Buffered Saline
PCP	Planar Cell Polarity
PCR	Polymerase Chain Reaction
PFA	ParaFormAldehyde
PGE2	Prostaglandin E2
qRT-PCR	Quantitative Real Time Polymerase Chain Reaction
RNA	Ribonucleic Acid
RPMI	Roswell Park Memorial Institute
RRS	Ras-Recruitment System
SCF	SKP-1, Cullin and the F-box protein $\beta$ -TrCP
SDS-PAGE	Sodium Dodecyl Sulfate Polyacrylamide Gel Electrophoresis
TAE	Tris Acetate EDTA
TBS-T	Tris-buffered saline-Tween 20
TCF/LEF	T-Cell transcription Factor (TCF) and Lymphoid Enhancer Factor
TCF4	T-Cell transcription Factor 4
WB	Western Blotting
WIF	Wnt Inhibitory Factor
Wls	Wntless
ZFPs	Zinc Finger Proteins

# Table of contents

<b>Declaration</b> .....	<b>i</b>
<b>Abstract</b> .....	<b>ii</b>
<b>Acknowledgments</b> .....	<b>v</b>
<b>List of Figures</b> .....	<b>vi</b>
<b>List of Tables</b> .....	<b>x</b>
<b>Abbreviations</b> .....	<b>xi</b>
<b>Table of contents</b> .....	<b>xiii</b>
<b>CHAPTER 1 General Introduction</b> .....	<b>1</b>
<b>1.1 BACKGROUND</b> .....	<b>2</b>
1.1.1 <i>Links between transcription and signalling in development and diseases</i> .....	2
1.1.2 <i>The Wnt signalling pathway: outlined definition</i> .....	3
1.1.3 <i>Wnt family of secreted proteins</i> .....	3
<b>1.2 CANONICAL WNT SIGNALLING PATHWAY</b> .....	<b>5</b>
1.2.1 <i>Cytoplasmic events</i> .....	6
1.2.2 <i>Nuclear events</i> .....	10
1.2.3 <i>Regulation of Wnt/<math>\beta</math>-catenin downstream target genes</i> .....	13
1.2.4 <i>Role of nuclear cofactors on canonical Wnt signalling</i> .....	15
1.2.4.1 <i>Activation of <math>\beta</math>-catenin/TCF complex through co-activators</i> .....	16
1.2.4.2 <i>Inhibition of <math>\beta</math>-catenin/TCF complex through co-repressors</i> .....	18
<b>1.3 NON CANONICAL WNT SIGNALLING PATHWAY</b> .....	<b>23</b>
<b>1.4 ROLE OF CANONICAL WNT SIGNALLING IN INTESTINAL BIOLOGY</b> .....	<b>24</b>
1.4.1 <i>The normal architecture of intestine</i> .....	24
1.4.2 <i>Intestinal stem cells and homeostasis</i> .....	26
1.4.3 <i>Cell migration and positioning in intestinal crypts</i> .....	28
1.4.4 <i>Intestinal tumourigenesis</i> .....	30
1.4.5 <i>Multistep carcinogenesis in colorectal cancers</i> .....	33
<b>1.5 THE FAMILY OF ZINC FINGER PROTEINS</b> .....	<b>37</b>
<b>1.6 FLYWCH-TYPE ZINC FINGER PROTEINS</b> .....	<b>41</b>
1.6.1 <i>Origin and description</i> .....	41
1.6.2 <i>Function and importance</i> .....	41

<b>1.7</b>	<b>RATIONAL AND OBJECTIVES OF THIS STUDY .....</b>	<b>45</b>
1.7.1	<i>Rational.....</i>	45
1.7.2	<i>Objectives &amp; Aims.....</i>	48
<b>CHAPTER 2</b>	<b>Materials and Methods.....</b>	<b>50</b>
<b>2.1</b>	<b>MATERIALS .....</b>	<b>51</b>
2.1.1	<i>Cell lines .....</i>	51
2.1.2	<i>Reagents and buffers .....</i>	52
2.1.3	<i>Oligonucleotides.....</i>	54
2.1.4	<i>Antibodies .....</i>	59
<b>2.2</b>	<b>METHODS.....</b>	<b>61</b>
2.2.1	<i>DNA preparation and manipulation.....</i>	61
2.2.1.1	DNA transformation and amplification .....	61
2.2.1.2	Chemical preparation of bacterial competent cells .....	62
2.2.1.3	DNA isolation using Miniprep kit.....	62
2.2.1.4	DNA isolation using manual Miniprep protocol .....	64
2.2.1.5	DNA isolation using Midiprep kit.....	65
2.2.1.6	Genomic DNA isolation .....	67
2.2.1.7	DNA quantification and storage .....	67
2.2.2	<i>Gene cloning techniques .....</i>	68
2.2.2.1	Restriction enzyme digestion .....	68
2.2.2.2	Agarose gel electrophoresis .....	68
2.2.2.3	DNA extraction from agarose gel .....	69
2.2.2.4	DNA extraction from restriction enzyme digestions .....	70
2.2.2.5	Standard polymerase chain reaction (PCR) .....	71
2.2.2.6	Overlapping PCR.....	72
2.2.2.7	Ligation and bacterial transformation.....	74
2.2.2.8	Clone verification .....	75
2.2.3	<i>Ribonucleic acid (RNA) isolation and reverse transcription.....</i>	75
2.2.3.1	RNA isolation.....	75
2.2.3.2	Reverse transcription and complementary Deoxyribonucleic acid (cDNA) synthesis	77
2.2.3.3	Quantitative real time polymerase chain reaction (qRT-PCR).....	78
2.2.3.3.1	Primer design .....	78
2.2.3.3.2	Reaction preparation .....	78
2.2.3.3.3	Data analysis .....	79
2.2.4	<i>General tissue culture techniques .....</i>	79
2.2.4.1	Human cell culture .....	79
2.2.4.2	Transient transfection .....	80
2.2.4.3	Stable transfection .....	82
2.2.4.3.1	Lentivirus production .....	82

2.2.4.3.2	Lentivirus transduction and stable cell line generation .....	84
2.2.5	<i>Protein lysate preparation and analysis</i> .....	85
2.2.5.1	Protein extraction and quantification .....	85
2.2.5.2	Western blotting (WB) analysis.....	86
2.2.5.2.1	Sample preparation and SDS-PAGE electrophoresis .....	86
2.2.5.2.2	Immunoblotting .....	89
2.2.5.3	Co-immunoprecipitation (Co-IP) assay.....	90
2.2.5.3.1	FLAG-conjugated agarose beads.....	90
2.2.5.3.2	Magnetic beads.....	91
2.2.5.3.3	Agarose beads.....	91
2.2.6	<i>Functional analysis</i> .....	92
2.2.6.1	Indirect transcriptional assay .....	92
2.2.6.2	In vitro scratch assay .....	94
2.2.6.3	Trans-well cell migration assay.....	95
2.2.6.4	Cell cycle analysis .....	96
2.2.6.5	Growth curve analysis .....	96
2.2.6.6	Immunofluorescent (IF) analysis .....	97
2.2.6.7	Phalloidin staining .....	98
2.2.6.8	In Situ Hybridization (ISH) assay .....	98
2.2.6.8.1	Probe preparation, specificity and verification .....	98
2.2.6.8.2	In vitro transcription and hybridization protocol .....	99
2.2.7	<i>Statistical analysis</i> .....	100

### **CHAPTER 3 Identification and expression of the human *FLYWCH1***

#### **gene in mammalian cells ..... 101**

3.1	<b>INTRODUCTION .....</b>	<b>102</b>
3.2	<b>RESULTS .....</b>	<b>103</b>
3.2.1	<i>Sequence and domain analysis of FLYWCH1</i> .....	103
3.2.2	<i>Characterization of human FLYWCH1 IMAGE clone</i> .....	108
3.2.3	<i>Cloning of human FLYWCH1 cDNA into mammalian expression vectors</i> .....	113
3.2.3.1	Cloning of untagged human FLYWCH1 cDNA (FLYWCH1-WT).....	113
3.2.3.2	Cloning of MYC-tagged human FLYWCH1 (MYC-FLYWCH1-WT) .....	116
3.2.3.3	Cloning of eGFP-tagged human FLYWCH1 (eGFP-FLYWCH1-WT).....	118
3.2.4	<i>Exogenous expression of human FLYWCH1 cDNA clones in cell culture</i> .....	121
3.2.5	<i>Sub-cellular localization of eGFP-FLYWCH1 protein</i> .....	124
3.3	<b>DISCUSSION.....</b>	<b>126</b>

### **CHAPTER 4 The Interaction of FLYWCH1 with $\beta$ -catenin in Human Cells**

**129**

4.1	<b>INTRODUCTION .....</b>	<b>130</b>
-----	---------------------------	------------

<b>4.2</b>	<b>RESULTS .....</b>	<b>131</b>
4.2.1	<i>FLYWCH1 interacts with <math>\beta</math>-catenin in HEK293T cells.....</i>	131
4.2.2	<i>Site-directed mutagenesis of human FLYWCH1 .....</i>	133
4.2.2.1	MYC-tagged deletion mutants of FLYWCH1.....	135
4.2.2.2	EGFP-tagged deletion mutants of FLYWCH1.....	138
4.2.3	<i>Mapping the interaction site of FLYWCH1 with <math>\beta</math>-catenin .....</i>	141
4.2.4	<i>Site-directed mutagenesis of <math>\beta</math>-catenin cDNA.....</i>	145
4.2.4.1	Cloning of $\beta$ -catenin N-terminal and C-terminal deletions.....	147
4.2.4.2	Cloning of $\beta$ -catenin middle deletion mutants.....	147
4.2.4.3	Validation of FLAG- $\beta$ -catenin (FLAG- $\beta$ -cat) clones .....	150
4.2.5	<i>Mapping the interaction site of <math>\beta</math>-catenin with FLYWCH1 .....</i>	152
<b>4.3</b>	<b>DISCUSSION.....</b>	<b>154</b>
<b>CHAPTER 5 Human FLYWCH1 Inhibits Cell Migration and Alters Cell Morphology of Colorectal Cancer (CRC) Cells through Negative Regulation of Wnt/<math>\beta</math>-catenin Signalling Pathway.....</b>		
		<b>161</b>
<b>5.1</b>	<b>INTRODUCTION .....</b>	<b>162</b>
<b>5.2</b>	<b>RESULTS .....</b>	<b>163</b>
5.2.1	<i>FLYWCH1 represses <math>\beta</math>-catenin/TCF4 transcriptional activity .....</i>	163
5.2.2	<i>FLYWCH1 may compete with TCF4 for binding to <math>\beta</math>-catenin.....</i>	168
5.2.3	<i>The C-terminus domain of FLYWCH1 is essential for its functional interaction with <math>\beta</math>-catenin.....</i>	170
5.2.4	<i>The N-terminal domain of <math>\beta</math>-catenin is required for its functional interaction with FLYWCH1 .....</i>	172
5.2.5	<i>Ectopic expression of FLYWCH1 reduces CRC cell motility .....</i>	174
5.2.5.1	FLYWCH1 suppresses wound closure capacity of CRC cells.....	174
5.2.5.2	FLYWCH1 has no effect on cell cycle progression of CRC cells.....	176
5.2.5.3	FLYWCH1 reduces migration of CRC cells.....	179
5.2.6	<i>FLYWCH1 modulates the gene expression of migration effectors .....</i>	180
5.2.7	<i>Ectopic expression of FLYWCH1 changes the morphology of CRC cells.....</i>	183
5.2.8	<i>Endogenous expression of FLYWCH1 in human cell lines.....</i>	187
5.2.9	<i>Endogenous expression of FLYWCH1 in normal and tumour tissues.....</i>	188
<b>5.3</b>	<b>DISCUSSION.....</b>	<b>191</b>
<b>CHAPTER 6 Generation of Stably-Transfected Cell lines for the Functional Analysis of FLYWCH1 .....</b>		
		<b>201</b>
<b>6.1</b>	<b>INTRODUCTION .....</b>	<b>202</b>
<b>6.2</b>	<b>RESULTS .....</b>	<b>203</b>

6.2.1	<i>Cloning of eGFP and eGFP-FLYWCH1-WT cDNAs into pLVX-Puro</i> .....	203
6.2.2	<i>Transduction and selection of cells with pLVX-eGFP and pLVX-eGFP-FLYWCH1-WT</i>	207
6.2.3	<i>Characterization of cell lines stably expressing eGFP and eGFP-FLYWCH1.....</i>	208
6.2.3.1	Evaluation of FLYWCH1 gene expression by Western blotting analysis .....	208
6.2.3.2	Stably expressed FLYWCH1 shows different expression pattern and sub-cellular localization: fluorescent-microscopic analysis .....	210
6.2.3.3	DNA sequence analysis of genomic PCR products illustrates deletional mutation in FLYWCH1 exogenous gene in HEK293T stable cell line .....	213
6.2.3.4	DNA sequence analysis of genomic PCR products illustrates nonsense point mutation in FLYWCH1 exogenous gene in HCT116 stable cell line.....	218
6.2.4	<i>Functional analyses of stably expressed FLYWCH1</i> .....	223
6.2.4.1	Evaluation of FLYWCH1/ $\beta$ -catenin transcriptional activity in HCT116 and HEK293T stable cell lines .....	223
6.2.4.2	Evaluation of FLYWCH1 repression activity on cell migration in HEK293T and HCT116 stable cell lines.....	224
6.2.5	<i>Cloning the automodified FLYWCH1 recombinant cDNA into mammalian expression vectors</i> .....	227
6.2.6	<i>The automodified clone of FLYWCH1 lost its physical interaction with <math>\beta</math>-catenin</i>	230
6.2.7	<i>New strategy to generate FLYWCH1<sup>+ve</sup> stable cell lines</i> .....	231
6.2.7.1	Evaluation Experiments: Western blotting and fluorescent-microscopic analysis of new stable cell lines.....	232
6.2.7.2	Stably expressed eGFP-FLYWCH1-WT up-regulates E-cadherin in HEK293T stable cell line	235
6.2.7.3	Stably expressed FLYWCH1-WT changed the morphology of HEK293T cells .....	239
6.3	<b>DISCUSSION</b> .....	<b>241</b>
<b>CHAPTER 7 General Discussion</b> .....		<b>244</b>
7.1	<b>INTRODUCTION</b> .....	<b>245</b>
7.2	<b>NOVELTY OF FLYWCH1</b> .....	<b>245</b>
7.3	<b>BIOINFORMATICS ANALYSIS OF FLYWCH1</b> .....	<b>246</b>
7.4	<b>CLONING AND CHARACTERIZATION OF HUMAN FLYWCH1</b> .....	<b>247</b>
7.5	<b>INTERACTION OF FLYWCH1 WITH B-CATENIN</b> .....	<b>249</b>
7.6	<b>BIOLOGICAL SIGNIFICANCE OF FLYWCH1</b> .....	<b>253</b>
7.7	<b>LIMITATIONS OF THIS STUDY</b> .....	<b>259</b>
7.8	<b>CONCLUDING REMARKS &amp; FUTURE DIRECTIONS</b> .....	<b>261</b>
<b>Appendices</b> .....		<b>263</b>

<b>Appendix 1: Multiple sequence alignment of FLYWCH1 aa sequence in different animals .....</b>	<b>264</b>
<b>Appendix 2: Manual plasmid DNA extraction protocol .....</b>	<b>267</b>
<b>Appendix 3: Cell counting using Neubauer haemocytometer .....</b>	<b>269</b>
<b>Appendix 4: pI-EGFP2 vector map .....</b>	<b>272</b>
<b>Appendix 5: pIRES2-EGFP vector map.....</b>	<b>273</b>
<b>Appendix 6: pEGFP-C2 vector map .....</b>	<b>274</b>
<b>Appendix 7: pLVX-Puro vector map.....</b>	<b>275</b>
<b>Appendix 8: pcDNA3 vector map .....</b>	<b>276</b>
<b>Appendix 9: Sequencing data of MYC-tagged FLYWCH1 .....</b>	<b>277</b>
<b>Appendix 10: NCBI primer blast for c-Jun qRT-PCR primers.....</b>	<b>278</b>
<b>Appendix 11: NCBI nucleotide blast of FLYWCH1 probe against human genomic and transcript database. ....</b>	<b>279</b>
<b>Appendix 12: NCBI nucleotide blast of FLYWCH1 probe against mouse genomic and transcript database. ....</b>	<b>280</b>
<b>Appendix 13: Sequencing results for eGFP-FLYWCH1-M2 (<math>\Delta</math>N350)....</b>	<b>281</b>
<b>Appendix 14: Raw data shows the calculation method of luciferase assay as outlined in (section 2.2.6.1). ....</b>	<b>282</b>
<b>Appendix 15: Mapping the interaction site of FLYWCH1 with <math>\beta</math>-catenin using Co-IP assay. This figure represents a long exposure of (Figure 4-7). ....</b>	<b>284</b>
<b>References.....</b>	<b>285</b>

# **CHAPTER 1**

## **General Introduction**

## **1.1 Background**

### **1.1.1 Links between transcription and signalling in development and diseases**

In multicellular organisms, cells have ability to detect the status of the local environment and respond appropriately during embryogenesis and homeostasis. Multiple cytoplasmic signal transduction cascades (pathways) triggered by different ligand/receptor interactions at the cell surface are the mechanisms by which information about the extracellular environment is communicated to the cell. These pathways control almost all cellular biological activities and responses through tight regulation of the transcriptional machinery of the cell (Serup, 2012, Heath, 2010).

Signalling pathways generally recruit specific DNA-binding transcription factors to specified response elements within the promoter of their target genes, thereby, controlling gene transcription. Maintaining a balanced relationship between signalling pathways and the gene expression programme is the only way to guarantee normal development and homeostasis. Accordingly, any disturbance to this system leads to development of various disorders including cancer (Clevers, 2006, Heath, 2010). For example, Wnt signalling through  $\beta$ -catenin maintains the progenitor and stem cell compartment of intestinal-crypts (Miki et al., 2011, Nusse et al., 2008). Deregulation of Wnt signalling may therefore lead to loss of normal intestinal homeostasis. Indeed, around 90% of colorectal cancers (tumours of the large intestine) show deregulated Wnt/ $\beta$ -catenin signalling (Fevr et al., 2007).

Defects in highly conserved Wnt signalling pathway are well known to play key roles in the development of many different types of cancer. This and the above concepts are mechanistically explored in more detail within the following sections throughout this chapter.

### **1.1.2 The Wnt signalling pathway: outlined definition**

The Wnt signalling pathway is an ancient and evolutionarily conserved pathway in metazoan animals (Komiya and Habas, 2008). This pathway involves a large number of signalling molecules including Wnt-ligands, Wnt-receptors, and several cytoplasmic Wnt-signal transducing proteins (see below for detail). Exposure of cells to the extracellular Wnt-ligands stimulates several intra-cellular signal transduction cascades, represented by the canonical ( $\beta$ -catenin dependent) and the non-canonical ( $\beta$ -catenin-independent) pathways.

The Wnt-signal transduction cascades control a huge number of biological phenomena throughout all stages of animal development and adulthood. On the other hand, defective Wnt signalling has catastrophic consequences that underline a wide range of human pathologies including different types of cancer.

### **1.1.3 Wnt family of secreted proteins**

Wnts comprise a highly conserved family of genes throughout the metazoan kingdom. The human genome harbours 19 Wnt genes (*WNTs*) that encode for 19 Wnt proteins (Miller, 2002). Historically, *WNTs* are defined by common conserved amino acid sequences in the original members, i.e. the integrated (*int-1*) in mouse (Nusse and Varmus, 1982, van Ooyen and Nusse, 1984) and the segment polarity gene wingless (*wg*) in *Drosophila* (Rijsewijk et al., 1987). Therefore, the term Wnt, which is a combined name resulted from a fusion of the name of *Drosophila* wingless (*wg*) and mouse *int-1*, was assigned to the members of this family. Proteins encoded by this family of genes are defined as small secreted glycoproteins of about 40 kDa (Cadigan and Nusse, 1997) that share high (27% to 83%) amino acid sequence identity, including a conserved pattern of 23 or 24 cysteine residues (Miller, 2002), a signal sequence for secretion, and many glycosylation sites (Mason et al., 1992).

Wnts function as extracellular ligands for the Wnt signalling pathway, however, their function is highly regulated both intra- and extra-cellularly. The

intracellular modifications include post-translational refinements such as glycosylation (i.e. the enzymatic process that links saccharides to produce glycans, either free or attached to proteins and lipids) and palmitoylation (i.e. the covalent attachment of fatty acids) (Smolich et al., 1993, Willert et al., 2003). These fine adjustments are part of the natural maturation process of Wnt molecules that play crucial roles in secretion, trafficking, spreading and signalling activities of Wnt proteins (Harterink and Korswagen, 2012, Port and Basler, 2010). The mechanisms of secretion of Wnt molecules were further clarified by the discovery of a transmembrane protein called *Wntless* (Wls) (Banziger et al., 2006, Bartscherer et al., 2006, Goodman et al., 2006). This protein is thought to bind to Wnt molecules and facilitates their export from the Golgi to the plasma membrane for release (reviewed by Harterink and Korswagen, 2012, Lorenowicz and Korswagen, 2009, Port and Basler, 2010).

Binding of extracellular signalling molecules to Wnt proteins is among the more common extracellular modifications. In most cases (but not all), these molecules function as antagonists to Wnt activities through interruption of Wnt binding to cell surface receptors. Examples of secreted proteins that antagonize Wnt function are Dickkopf (Dkk) proteins (Glinka et al., 1998), Wnt-inhibitor protein (WIF) (Hsieh et al., 1999), soluble Frizzled-related proteins (SFRP) (Hoang et al., 1998), Cerberus (Bouwmeester et al., 1996), and the context dependent Wnt inhibitor Wise (Itasaki et al., 2003). These molecules prevent Wnt interaction with either Frizzled (Fz) or the LRP5/6 (low-density lipoprotein receptor-related proteins 5 and 6) which eventually leads to inhibition of Wnt signalling pathway (see below).

On the other hand, there are other molecules that function as agonists to promote Wnt signalling pathway such as Norrin (Xu et al., 2004), and R-Spondin2 (Han et al., 2011, Koeneman, 2009, Kazanskaya et al., 2004). Moreover, the adult intestinal stem cell marker Lgr5 (Leucine-rich repeat-containing G-protein coupled receptor 5) and its relative gene Lgr4 were recently identified as mediators of Wnt signalling pathway through R-Spondin receptors (Glinka et al., 2011, de Lau et al., 2011). Considering the importance of Wnt molecules in development and various cellular processes, each of these secreted proteins, therefore, must be tightly regulated during embryogenesis

and cell-fate determination to ensure that a proper level of Wnt-signals is delivered.

After secretion and intervention by intra/extracellular modifications, Wnt molecules eventually function as extracellular ligands to initiate the Wnt signalling pathway through binding to cell surface receptors composed of Fz and LRP-5/6 (Bhanot et al., 1996, Tamai et al., 2000). The intracellular transduction of Wnt-signals activates various signalling pathways that can be categorized into canonical ( $\beta$ -catenin dependent) or non-canonical ( $\beta$ -catenin independent) pathways. Through these signalling pathways, Wnt proteins play fundamental roles in almost every step of embryonic development, starting from mesoderm induction to anterior-posterior body axis formation including embryonic induction (proliferation), generation of cell polarity (migration) and specification of cell fate determination (differentiation) (reviewed by Hendrickx and Leyns, 2008, Logan and Nusse, 2004). Furthermore, this pathway is also implicated in cell biology and homeostasis through maintenance of stem cell properties (Hendrickx and Leyns, 2008, Reya and Clevers, 2005).

## **1.2 Canonical Wnt signalling pathway**

With the discovery of Wnt proteins and their functions as signalling molecules in the early 1980s, the  $\beta$ -catenin-dependent pathway received the most attention and became the best characterized signalling pathway. This pathway is commonly referred to as the canonical Wnt signalling or Wnt/ $\beta$ -catenin signalling pathway which simply means transduction of Wnt-signals through  $\beta$ -catenin, a central signal transducer and a key regulator of this pathway (Figure 1-1). The ultimate function of this pathway is signal transduction from extracellular matrix into the nucleus. This role is accomplished through a series of intracellular events comprising accumulation of stabilized  $\beta$ -catenin in the cytoplasm, followed by its nuclear translocation and subsequent activation of Wnt-target genes. This pathway is represented by two states, the “on” and “off” states, based on the presence or absence of Wnt stimuli (see section 1.2.1 & Figure 1-1). The process of activation and nuclear translocation of  $\beta$ -catenin is

tightly regulated through several cytoplasmic and nuclear regulatory molecules which are explored in more detail in the following sections.

### **1.2.1 Cytoplasmic events**

Regulation of  $\beta$ -catenin in the context of canonical Wnt signalling pathway has been intensively studied both in the presence or absence of Wnt molecules. In the absence of Wnt stimulation, the unbound cytosolic  $\beta$ -catenin is degraded by a destruction complex composed of a scaffolding protein Axin, glycogen synthase kinase-3 beta (GSK-3 $\beta$ ), casein kinase-I alpha (CKI $\alpha$ ), and adenomatous polyposis coli (APC) (Ikeda et al., 1998, Kikuchi, 1999, Kishida et al., 1998, Liu et al., 2002). Within this complex  $\beta$ -catenin is phosphorylated by coordinated action of both CKI $\alpha$  and GSK-3 $\beta$ ; CKI $\alpha$  serves as a priming kinase that phosphorylates Serine 45 (Ser45) of  $\beta$ -catenin and enhances the phosphorylation at Ser33, Ser37, and Threonine 41 (Thr41) by GSK-3 $\beta$  (Amit et al., 2002, Liu et al., 2002). The phosphorylated  $\beta$ -catenin is then ubiquitinated and recognized by the E3-ubiquitin ligase SCF( $\beta$ -TrCP) containing SKP-1, Cullin and the F-box protein  $\beta$ -TrCP (Jiang and Struhl, 1998, Marikawa and Elinson, 1998) and subsequently degraded by the 26S-proteasome machinery (Kitagawa et al., 1999) (Figure 1-1, left panel). This will keep the cytosolic  $\beta$ -catenin at a low level and in such a situation  $\beta$ -catenin does not accumulate in the nucleus (i.e. the pathway is switched off).

Upon extracellular stimulation, Wnt-ligands interact with cell surface receptors consisting of Fz and LRP5/6 to form a ternary complex which leads to inhibition of  $\beta$ -catenin phosphorylation by the Axin destruction complex (consisting of Axin, APC, GSK-3 $\beta$ , and CKI $\alpha$ ), thereby stabilizing  $\beta$ -catenin (Figure 1-1, right panel). Although formation of the trimeric complex between Wnt, Fz and LRP is widely accepted as a prerequisite to trigger Wnt signalling, the precise model of interaction and mechanisms of the subsequent signal transduction is still open to debate. It has long been believed that the interaction between Wnt proteins and its receptors, results in generating a signal which is transduced intracellularly through a cascade of events involving

the Dishevelled (Dvl) protein in a not fully understood manner. These events were thought to inhibit the GSK-3 $\beta$ -dependent phosphorylation of  $\beta$ -catenin and disrupt the Axin/GSK-3 $\beta$ /CKI $\alpha$ / $\beta$ -catenin complex, which in turn increases the cytoplasmic level of  $\beta$ -catenin (Hino et al., 2003, Kishida et al., 1999, Yamamoto et al., 1999).

This model of Wnt-signals transduction in the cytoplasm has recently been revised (Fuerer et al., 2008, Nusse, 2012). According to the current model, Dvl forms a complex with Axin and GSK-3 $\beta$  through its N-terminal domain which is similar to the DIX domain in Axin. Wnt binding to Fz/LRP receptors enhances binding of this complex (Dvl/Axin/GSK-3 $\beta$ ) to Fz. On the other hand, GSK-3 $\beta$  phosphorylates the Axin binding site residues of LRP 6 which then primes the subsequent phosphorylation of another motif of LRP 6 by CK1 $\gamma$ , enabling the scaffolding protein (Axin) to bind to the phosphorylated site of LRP 6. This interaction leads to subsequent inactivation of the destruction complex governed by Axin. Consequently,  $\beta$ -catenin will not be phosphorylated by the GSK-3 $\beta$  (Fuerer et al., 2008, Nusse, 2012) (Figure 1-1, right panel).

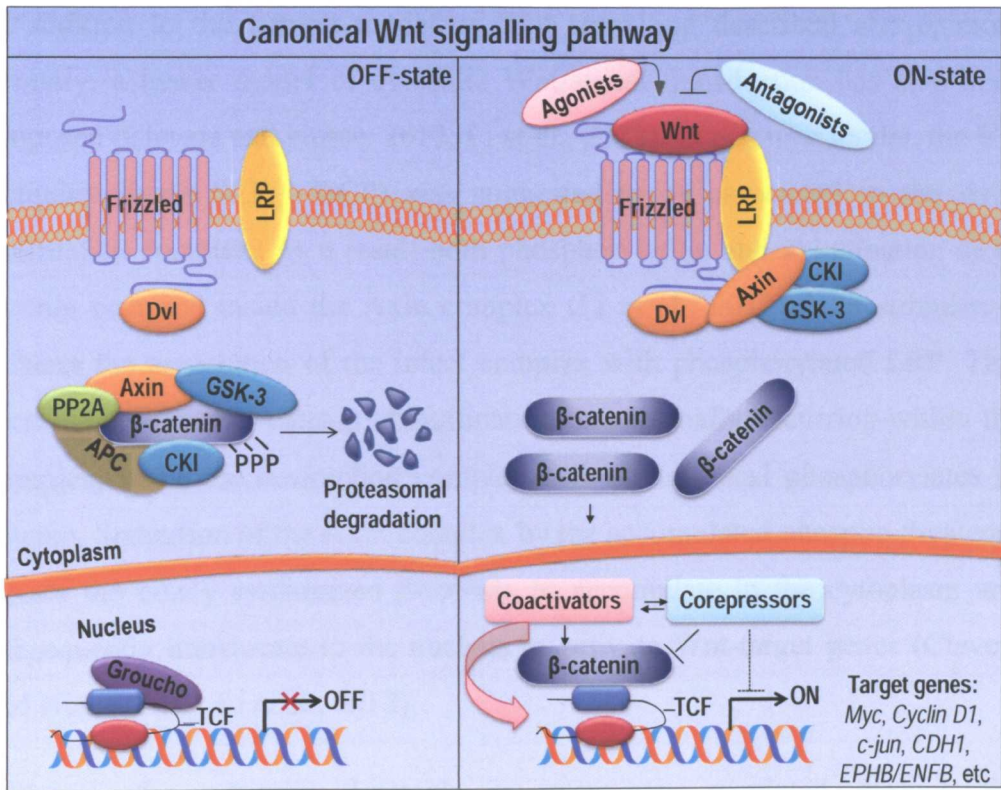


**Figure 1-1: Schematic representation of Wnt/ $\beta$ -catenin signalling pathway.** (Left panel) represents inactive state of Wnt/ $\beta$ -catenin signalling pathway (i.e. OFF-state) in which in the absence of Wnt stimulation,  $\beta$ -catenin levels in the cell are kept low through a dedicated destruction complex that consists of adenomatous polyposis coli (APC), casein kinase I (CKI), glycogen synthase kinase 3 (GSK3), and Axin. This complex targets  $\beta$ -catenin for proteasomal degradation through phosphorylation (P). Conversely,  $\beta$ -catenin stability may also be regulated/enhanced by protein phosphatases (PPs) such as (PP2A) through dephosphorylation of  $\beta$ -catenin (Right panel) represents active state of Wnt/ $\beta$ -catenin signalling pathway (i.e. ON-state) in which Wnt-ligands bind to Frizzled receptors and low-density lipoprotein receptor-related protein (LRP) coreceptors. The cytoplasmic tail of LRP binds to Axin in a Wnt- and phosphorylation-dependent manner. Phosphorylation of the tail of LRP is regulated by GSK-3 $\beta$ , CK1, and Dishevelled (Dvl). As a consequence,  $\beta$ -catenin will not be phosphorylated and/or degraded anymore, which leads to increased cytosolic level of  $\beta$ -catenin, resulting in its translocation into the nucleus. The stabilized nuclear  $\beta$ -catenin then replaces Groucho on TCF/LEF transcription factors (TCF) and recruits other auxiliary cofactors (co-activators and/or co-repressors) to form an active transcriptional complex that regulate the expression of Wnt-target genes. The diagram is adapted from (Nusse, 2012, Saadeddin et al., 2009).

In addition to the current model of Wnt signalling described above, more recently, a newer model of cytosolic Wnt-signal transduction has also been proposed (Clevers and Nusse, 2012, Li et al., 2012). In this new model, the E3-ubiquitin ligase SCF( $\beta$ -TrCP) was suggested to be associated to the Axin destruction complex. As a result both phosphorylation and ubiquitination of  $\beta$ -catenin occurred inside the Axin complex (Li et al., 2012). Wnt stimulation induces the association of the intact complex with phosphorylated LRP. This recruitment blocks  $\beta$ -catenin ubiquitination that normally occurring within the complex, while the destruction complex still captures and phosphorylates  $\beta$ -catenin. Saturation of the Axin complex by the accumulated phospho- $\beta$ -catenin allows the newly synthesized  $\beta$ -catenin to accumulate in the cytoplasm and subsequently translocate to the nucleus to activate Wnt-target genes (Clevers and Nusse, 2012, Li et al., 2012).

Although the cytosolic  $\beta$ -catenin is intensively regulated through the phosphorylation process (see above), in some circumstances,  $\beta$ -catenin can escape from phosphorylation and subsequent degradation even in the absence of Wnt stimulation. For instance, in pathological conditions, when the N-terminal Serine and Threonine residues are mutated (Korinek et al., 1997) or when components of the destruction complex are defective such as APC (Morin et al., 1997) or Axin (Liu et al., 2000). In such conditions, nuclear translocation and accumulation of  $\beta$ -catenin will occur even in the absence of Wnt-signals.

In contrast to the negative role of several kinases such as CKI $\alpha$ , CKI $\gamma$ , and GSK3 $\beta$  in Wnt signalling pathway (see above), protein phosphatases such as PP1, PP2A, and PP2C, have been shown to positively regulate this pathway (Bajpai et al., 2004, Luo et al., 2007, Strovel et al., 2000). Generally, protein phosphatases are signal transducing enzymes that dephosphorylate various intracellular phosphoproteins involved in different pathways including Wnt signalling pathway. (Barford, 1995, Jia, 1997). For example, PP2A was shown to augment Wnt signalling through dephosphorylation of  $\beta$ -catenin (Bajpai et al., 2004, Zhang et al., 2009). Moreover, PP2C and PP1 were also shown to dephosphorylate Axin and, thereby, positively regulate Wnt/ $\beta$ -catenin

signalling pathway (Luo et al., 2007, Strovel et al., 2000). Thus, phosphatases may play crucial role in balancing the cytosolic level of  $\beta$ -catenin through dephosphorylation of  $\beta$ -catenin and/or components of the destruction complex.

The ultimate output of the activated canonical Wnt-pathway is the phosphorylation blockade (stabilization) and cytosolic accumulation of  $\beta$ -catenin. The stabilized  $\beta$ -catenin then enters the nucleus, where it binds to members of T-cell factor (TCF) and lymphoid enhancer factor (LEF) TCF/LEF transcription factors resulting in changes in expression programme of various target genes, including *c-myc*, *c-jun*, *cyclin D1*, *Fra-1*, *CDH1*, and *Axin2* (Bienz and Clevers, 2000, Kikuchi, 2000, Lustig et al., 2002, Seidensticker and Behrens, 2000, Battle et al., 2002). A complete list of Wnt-target genes can be found within the Wnt homepage ([http://www.stanford.edu/group/nusselab/cgi-bin/wnt/target\\_genes](http://www.stanford.edu/group/nusselab/cgi-bin/wnt/target_genes)).

### **1.2.2 Nuclear events**

Whereas the proximal events of Wnt/ $\beta$ -catenin signalling pathway are relatively well documented, the distal events of this pathway are less understood. It seems that going down deeper into the nucleus where the core transcriptional machinery of the cell is located, the pathway becomes more challenging. However, some basic concepts have already been established.

At an early stage after identification of TCF/LEF transcription factors (hereafter TCFs), it has been found that these molecules have a contradictory functions during embryogenesis and development; activating transcriptional processes in one subset of cells, but at the same time repressing the same functions in a different subset. However, identification of  $\beta$ -catenin as a specific binding partner of TCFs not only enabled the scientists to successfully answer the mystery of TCFs function, but it also clarified the mechanism by which TCFs could regulate transcription (reviewed by Hurlstone and Clevers, 2002).

TCFs form a relatively small family of transcription factors comprising four members in vertebrates (TCF1, TCF3, TCF4, and LEF1) and one orthologous form in flies, worms and lower organisms such as Hydra (dTCF/pangolin, POP-1, and hyTCF, respectively) (reviewed by Arce et al., 2006, van Noort and Clevers, 2002). Members of this family are the most studied DNA binding downstream effectors of Wnt/ $\beta$ -catenin signalling pathway. Each contains an N-terminal binding domain for  $\beta$ -catenin and a specific DNA-binding high mobility group (HMG) box (Arce et al., 2006, van Noort and Clevers, 2002). Moreover, through alternative splicing and promoter usage, Tcfs may produce multiple isoforms harbouring diverse functional domains (Figure 1-2) (Hurlstone and Clevers, 2002).

Scientists now appreciate that TCFs function as bipartite regulators of Wnt-target genes. In the absence of stabilized  $\beta$ -catenin, TCFs are bound to members of the Groucho family of co-repressors to keep Wnt-targets silenced. Nuclear accumulation of stabilized  $\beta$ -catenin antagonizes this repression through displacing the co-repressor Groucho (Daniels and Weis, 2005) and recruiting additional co-activators, the process which transcriptionally regulates Wnt-target genes (Kikuchi, 2000, Mosimann et al., 2009). Thus, TCFs can be considered as transcriptional switch, turning on in the presence of stabilized  $\beta$ -catenin, and converting repression to activation (Figure 1-1).

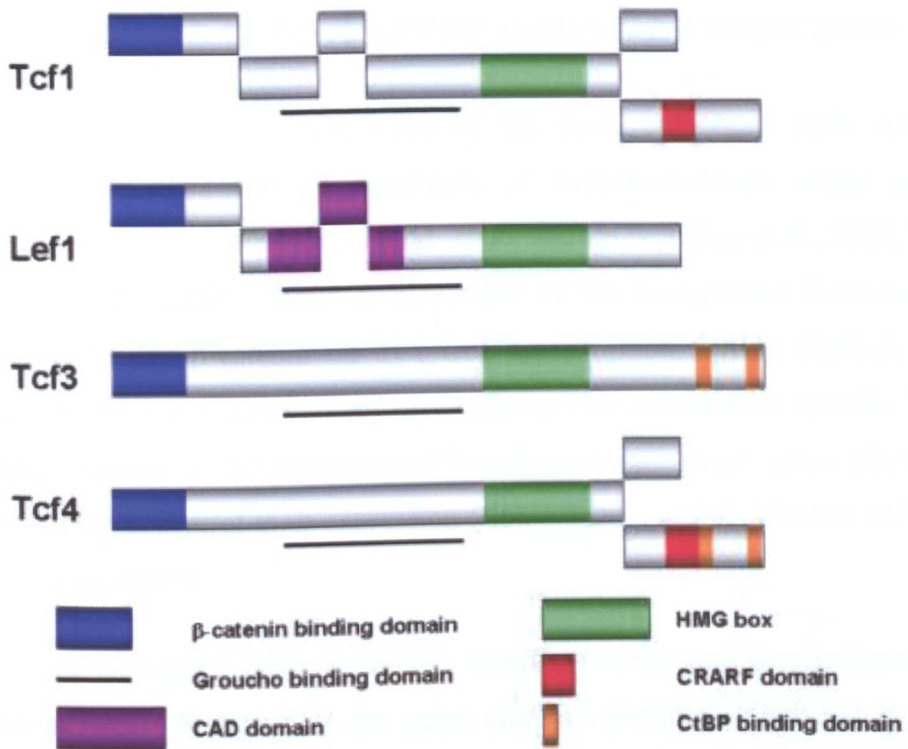


**Figure 1-2: Schematic representation of Tcf splice variants and their most conserved domains.** Short forms of Tcf1 and Lef1 lack the N-terminal domain, which interacts with  $\beta$ -catenin. The CAD domain in Lef1 is required for context-dependent activation of the TCR $\alpha$  enhancer. The HMG box mediates sequence-specific DNA binding. The most divergent region of the Tcf family members is the C-terminus, which in certain longer isoforms contains a conserved motif, CRARF, that serves as an additional DNA-binding domain and a strong transactivator of the WNT pathway (Atcha et al., 2003, Atcha et al., 2007) and two CtBP binding sites. Taken and modified from (Hurlstone and Clevers, 2002).

Historically, identification of  $\beta$ -catenin as a potential co-activator of TCFs further highlighted the importance of  $\beta$ -catenin in the context of the Wnt signalling pathway, especially because it was not clear how  $\beta$ -catenin transduces the signal into the nucleus, as it has no DNA-binding properties. On the other hand, members of TCFs lack transactivation domain but they can bind to DNA through their high mobility group (HMG) box (van Noort and Clevers, 2002). Therefore, interaction of  $\beta$ -catenin with TCFs was a perfect model of coordination between these two proteins.

### 1.2.3 Regulation of Wnt/ $\beta$ -catenin downstream target genes

The activated Wnt signalling pathway has been associated with several biological processes through regulation of Wnt-downstream target genes (Batlle et al., 2002, Clevers and Batlle, 2006, van de Wetering et al., 2002, Van der Flier et al., 2007). Direct displacement of the co-repressor Groucho by stabilized nuclear  $\beta$ -catenin on TCF/LEF transcription factors (Daniels and Weis, 2005) leads to recruitment of  $\beta$ -catenin/TCF complex to specific TCF binding elements in the promoter of Wnt-downstream target genes allowing this complex to control their expression (Behrens et al., 1996, Clevers and van de Wetering, 1997).

Numerous Wnt-target genes have been identified in the past decade; however studies are more focussed on the genes that are positively regulated by this pathway and involved in cancer. One critical example is *c-Myc* which has been identified as a direct target gene of  $\beta$ -catenin/TCF4 complex (He et al., 1998). It has been shown that  $\beta$ -catenin/TCF4 complexes regulate *c-Myc* expression in colon cancer cells through specific Wnt/ $\beta$ -catenin responsive DNA-elements present in the promoter of *c-Myc* (He et al., 1998). Subsequent studies have revealed that the expression of the proto-oncogene *c-MYC* is deregulated (mainly activated) in a variety of human cancers and is often associated with poor prognosis (Pelengaris and Khan, 2003, Pelengaris et al., 2002, Vita and Henriksson, 2006).

In addition to *c-Myc*, many other genes are also targeted and positively regulated by the activated Wnt signalling pathway such as *Cyclin D1* (Shtutman et al., 1999, Tetsu and McCormick, 1999), *c-jun* & *Fra-1* (Mann et al., 1999, Nateri et al., 2005), *EphB2/3* and many other genes (Batlle et al., 2002). A comprehensive list of Wnt target genes can be found on the Wnt homage (<http://www.stanford.edu/group/nusselab/cgi-bin/wnt/>). Moreover, the positive regulation of certain Wnt target genes in response to activated Wnt signalling pathway is very well understood and often used as indicators for the activation status of this pathway. For example, Ito et al. (2008) have used the promoter activity and the protein expression of *cyclin D1* and *c-Myc* to show changes in the transactivational activity of  $\beta$ -catenin/TCF4 in response to

RUNX3 (Ito et al., 2008). Increasing evidence about the link of nuclear localization of  $\beta$ -catenin and downstream target gene activation in various types of cancers led to the general assumption that Wnt/ $\beta$ -catenin signalling is an oncogenic pathway. However, the oncogenicity nature of this pathway has been recently revised (reviewed by Lucero et al., 2010). More details will be found in (section 1.4.4).

Despite the common thought of positive gene regulation by the activated Wnt/ $\beta$ -catenin pathway, negative regulation of this pathway on certain genes has also been reported. For instance, Jamora et al. (2003) found that the Wnt-3a activated Lef1 and stabilized  $\beta$ -catenin together led to direct repression of E-cadherin during epithelial bud formation of hair follicles. This repression was accomplished through direct binding of the  $\beta$ -catenin/Lef1 complex to specific Lef1-binding sites within the E-cadherin promoter (Jamora et al., 2003). E-cadherin was also reported to be indirectly down-regulated in embryoid bodies by high level of Wnt signalling that was induced by Wnt-3a and involved in the process of EMT (ten Berge et al., 2008). In addition to E-cadherin, the gene expression of a tumour suppressor gene, *p16<sup>INK4a</sup>*, was shown to be directly repressed by the activated Wnt pathway through the evolutionary conserved TCF/LEF binding site in the promoter of this gene (Delmas et al., 2007). Furthermore, the transcriptional repression of Wnt signalling pathway on several other genes such as *KAI1* and osteocalcin promoter is also reported (Kahler and Westendorf, 2003, Kim et al., 2005, Spencer et al., 2006). However, it is yet unclear whether the negative effects of Wnt pathway on the later genes are promoter specific and also whether these genes are conventional targets of Wnt signalling pathway.

Often up or down-regulation of Wnt-downstream target genes is cell-type specific and the cellular context, rather than the signal, determines the nature of the response in a not fully understood manner (reviewed by Logan and Nusse, 2004). Therefore, further studies are required to delineate the mechanisms involved in the transcriptional switch of  $\beta$ -catenin/TCF complex to either promote or inhibit gene expression.

### 1.2.4 Role of nuclear cofactors on canonical Wnt signalling

A large body of evidence indicate that the transcriptional activity of  $\beta$ -catenin/TCF complex is tightly regulated in the nucleus through various additional auxiliary proteins (either specific or general transcription co-activators or co-repressors) that are implicated in the transcriptional activity of nuclear  $\beta$ -catenin. These additional cofactors form a complex network of signalling and feedback loops that are required for the tight and precise regulation of  $\beta$ -catenin/TCF complex. It has been established that the nuclear  $\beta$ -catenin acts as a platform to recruit these cofactors (Figure 1-3), in addition to TCFs, to the promoter of Wnt-target genes. In general, these factors can be classified into two groups; **a) co-activators** and **b) co-repressors** as described in the following sections.

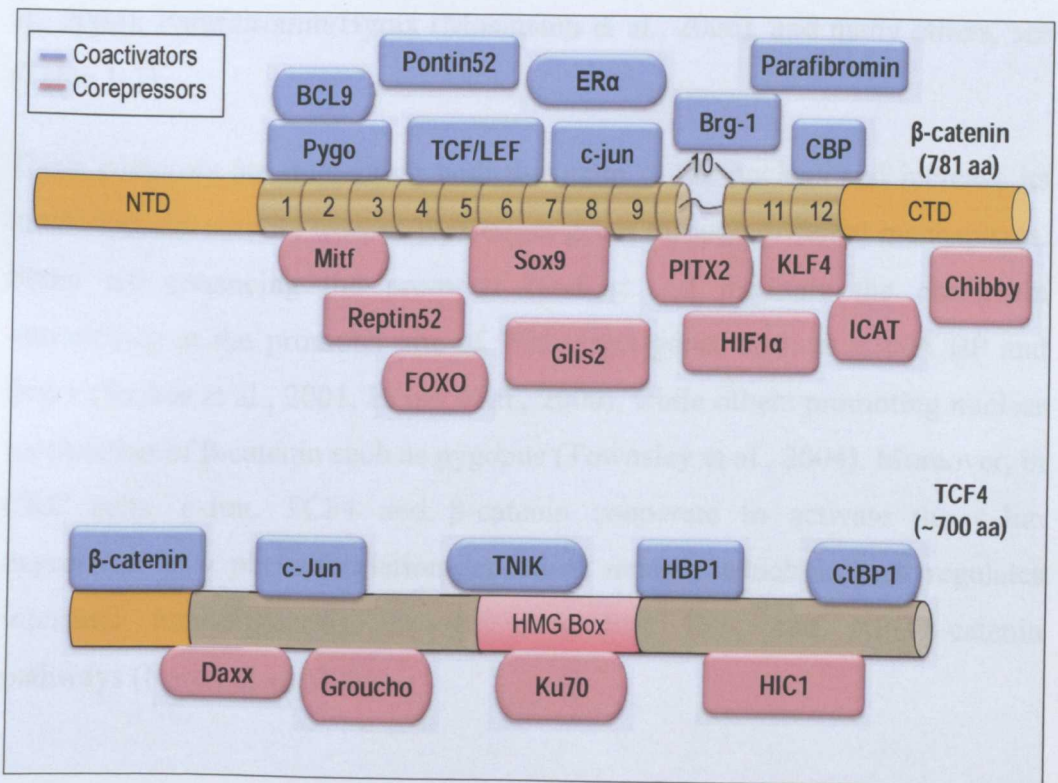


**Figure 1-3: Nuclear interacting proteins of  $\beta$ -catenin and TCF4.** Schematic shows (top panel)  $\beta$ -catenin and (bottom panel) TCF4 molecules with examples of their nuclear cofactors. In both panels, blue boxes represent the positive cofactors (co-activators), whereas red boxes the negative cofactors (co-repressors). The position of

boxes indicates the approximate binding sites of these factors to  $\beta$ -catenin and TCF4. NTD stands for the amino-terminal domain, while CTD for the carboxy-terminal domain of  $\beta$ -catenin. HMG denotes the High-Mobility Group domain of TCF4. Adapted from (Mosimann et al., 2009) and the Wnt home page ([http://www.stanford.edu/group/nusselab/cgi-bin/wnt/protein\\_interactions](http://www.stanford.edu/group/nusselab/cgi-bin/wnt/protein_interactions)).

#### ***1.2.4.1 Activation of $\beta$ -catenin/TCF complex through co-activators***

$\beta$ -catenin itself is acting as a transcriptional co-activator to modulate the transcription of Wnt-target genes after coupling with members of TCFs in the nucleus. Nevertheless, many other proteins (co-activators) have been identified to further augment the activity of the  $\beta$ -catenin/TCF complex. Examples of these proteins are p300/CBP (Hecht et al., 2000, Takemaru and Moon, 2000), Brg-1 (Barker et al., 2001), pygopus (pygo) (Kramps et al., 2002, Townsley et al., 2004), Parafibromin/Hyrax (Mosimann et al., 2006), and many others, see (Table 1-1).

These cofactors are interacting with  $\beta$ -catenin in the nucleus and increase its transcriptional activity toward Wnt-target genes through different mechanisms. Some are enhancing the promoter binding and facilitate the chromatin remodelling at the promoter site of Wnt-target genes such as p300/CBP and Brg-1 (Barker et al., 2001, Hecht et al., 2000), while others promoting nuclear localization of  $\beta$ -catenin such as pygopus (Townsley et al., 2004). Moreover, in CRC cells, c-Jun, TCF4 and  $\beta$ -catenin cooperate to activate the c-Jun expression in a phosphorylation-dependent manner which in turn regulates intestinal tumourigenesis through integrating JNK and APC/ $\beta$ -catenin pathways (Nateri et al., 2005).

**Table 1-1: Proteins that activate the  $\beta$ -catenin/TCF signalling.** Adapted from (MacDonald et al., 2009, Shitashige et al., 2008).

Proteins	Interaction partner(s)	References
AP-1 (both c-Fos & c-Jun)	$\beta$ -catenin	(Toualbi et al., 2007)
Topo II $\alpha$	$\beta$ -catenin	(Huang et al., 2007)
ER $\alpha$	$\beta$ -catenin	(Kouzmenko et al., 2004)
p300/CBP	$\beta$ -catenin	(Hecht et al., 2000, Takemaru and Moon, 2000)
pygopus (pygo)	$\beta$ -catenin	(Kramps et al., 2002, Townsley et al., 2004)
BCL9/legless	$\beta$ -catenin	(de la Roche et al., 2008, Kramps et al., 2002, Townsley et al., 2004)
Parafibromin/ Hyrax	$\beta$ -catenin	(Mosimann et al., 2006)
Brg-1	$\beta$ -catenin	(Barker et al., 2001)
PARP-1	TCF4	(Idogawa et al., 2005)
TNIK	TCF4	(Mahmoudi et al., 2009)
Smad3	LEF1	(Labbe et al., 2000)
c-Jun	$\beta$ -catenin and TCF4	(Gan et al., 2008, Toualbi et al., 2007, Nateri et al., 2005)
PITX2	$\beta$ -catenin and LEF1	(Vadlamudi et al., 2005)
Sox4	$\beta$ -catenin and TCFs	(Sinner et al., 2007)
Mlt10/ Af10-Dot11	$\beta$ -catenin and TCFs	(Mahmoudi et al., 2010)

**AP-1**, Activator Protein 1; **Topo II $\alpha$** , Topoisomerase II alpha; **PARP-1**, Poly(ADP-Ribose) Polymerase-1; **ER $\alpha$** , Estrogen Receptor alpha; **CBP**, CREB-Binding Protein; **PITX2**, Paired-like homeodomain Transcription Factor 2; **TNIK**, Traf2- and NCK-interacting kinase.

#### **1.2.4.2 Inhibition of $\beta$ -catenin/TCF complex through co-repressors**

Although Wnt signalling via the  $\beta$ -catenin/TCF complex is well documented as a prerequisite for activation of Wnt-target genes (Behrens et al., 1996, van de Wetering et al., 1997, Clevers and van de Wetering, 1997, van de Wetering et al., 2002, Van der Flier et al., 2007), this pathway cannot always lead to gene activation. Accumulated evidence over the past decade identified a number of proteins that interact with nuclear  $\beta$ -catenin and antagonize its transcriptional activity leading to transcriptional repression of Wnt-target genes. Accordingly, maintaining the balance between activation and repression of Wnt signalling pathway is an essential task during normal development. In this vein and in certain circumstances, Wnt-signals need to be quenched in order to allow healthy organogenesis during embryonic development. For example, repression of Wnt/ $\beta$ -catenin signalling is found to be required for normal development of the anterior forebrain in zebrafish and mouse embryos. This function can be accomplished by HESX1, a conserved transcription factor and Wnt signalling antagonist, that is required for forebrain development in vertebrates (Andoniadou et al., 2007, Andoniadou et al., 2011).

In addition to normal development, these co-repressors also play pivotal roles in the process of tumorigenesis and cancer development functioning as tumour suppressors through antagonizing the activated Wnt/ $\beta$ -catenin signalling pathway. A comprehensive list of proteins that have been identified as co-repressors for the activated Wnt signalling pathway is presented in (Table 1-2). These proteins are collectively known as Wnt signalling antagonists that negatively regulate the activity of Wnt signalling pathway through different mechanisms; (i) most of these factors interact with  $\beta$ -catenin and/or TCF/LEF and disturb the formation of  $\beta$ -catenin/TCF complex. For example, ICAT (inhibitor of  $\beta$ -catenin and TCF4) and p15RS antagonize Wnt signalling through inhibiting the interaction and formation of  $\beta$ -catenin/TCF4 complex (Tago et al., 2000, Wu et al., 2010), whereas RUNX3, forms a ternary complex with  $\beta$ -catenin/TCF4 by which attenuates Wnt signalling activity (Ito et al., 2008).

**Table 1-2: A comprehensive list of proteins that repress the activity of  $\beta$ -catenin/TCF complex.** Adapted from (Le et al., 2008, MacDonald et al., 2009, Shitashige et al., 2008).

<b>Proteins</b>	<b>Interaction partner(s)</b>	<b>References</b>
ICAT	$\beta$ -catenin	(Tago et al., 2000)
AR	$\beta$ -catenin	(Pawlowski et al., 2002)
E2F1	$\beta$ -catenin	(Morris et al., 2008)
FUS/TLS	$\beta$ -catenin	(Sato et al., 2005)
Foxo3a and Foxo4	$\beta$ -catenin	(Essers et al., 2005, Hoogeboom et al., 2008)
Groucho/TLE	$\beta$ -catenin	(Cavallo et al., 1998, Daniels and Weis, 2005)
Gli3	$\beta$ -catenin	(Ulloa et al., 2007)
GR	$\beta$ -catenin	(Takayama et al., 2006)
HIF1 $\alpha$	$\beta$ -catenin	(Kaidi et al., 2007)
Mitf	$\beta$ -catenin	(Schepsky et al., 2006)
RAR	$\beta$ -catenin	(Easwaran et al., 1999)
Chibby	$\beta$ -catenin	(Takemaru et al., 2003)
Sox6	$\beta$ -catenin	(Iguchi et al., 2007)
Sox9	$\beta$ -catenin	(Akiyama et al., 2004)
Xsox3	$\beta$ -catenin	(Zorn et al., 1999)
Reptin52	$\beta$ -catenin	(Bauer et al., 2000)
Glis2	$\beta$ -catenin	(Kim et al., 2007)
LXRs	$\beta$ -catenin	(Uno et al., 2009)
HBP1	TCF4	(Sampson et al., 2001)
CtBP1	TCF4	(Valenta et al., 2003)

Ku70	TCF4	(Idogawa et al., 2007)
HIC1	TCF4	(Valenta et al., 2006)
Daxx	Tcf4	(Tzeng et al., 2006)
Kaiso	TCFs	(Ilioka et al., 2009, Ruzov et al., 2009, Park et al., 2005)
HESX1	Tcf3	(Andoniadou et al., 2011)
Osx	Tcf1	(Zhang et al., 2008)
p15RS	$\beta$ -catenin and TCF4	(Wu et al., 2010)
Runx3	$\beta$ -catenin and TCF4	(Ito et al., 2008)
Xsox17	$\beta$ -catenin and TCFs	(Chew et al., 2011, Sinner et al., 2007, Sinner et al., 2004, Zorn et al., 1999)
SF1	$\beta$ -catenin and TCF4	(Shitashige et al., 2007a, Shitashige et al., 2007b)
KLF4	$\beta$ -catenin and TCF4	(Evans et al., 2010, Zhang et al., 2006)
SMRT and NCoR	$\beta$ -catenin and TCF4	(Song and Gelmann, 2008)
NLK	$\beta$ -catenin and TCF3/4	(Ishitani et al., 1999)

**SF1**, Splicing Factor-1; **AR**, Androgen Receptor; **FUS/TLS**, Fusion (FUS)/Translocated in Liposarcoma (TLS); **GR**, Glucocorticoid Receptor; **HIF-1 $\alpha$** , Hypoxia Inducible Factor-1alpha; **KLF4**, Kruppel-Like Factor 4; **Mitf**, Microphthalmia-associated Transcription Factor; **CtBP1**, C-terminal Binding Protein 1; **RAR**, Retinoic Acid Receptor; **NLK**, NEMO-like kinase; **HBP1**, HMG-box transcription Factor 1; **HIC1**, Hypermethylated In Cancer 1; **Osx**, Osteoblast-Specific Transcription Factor (Osterix); **SMRT**, Silencing Mediator for Retinoid and Thyroid hormone receptor; **NCoR**, the Nuclear Receptor Co-repressor; **HESX1**, HESX homeobox 1; **LXRs**, Liver X Receptors; **ICAT**, inhibitor of  $\beta$ -catenin and TCF4.

Similar to this mechanism, RAR, Chibby, Sox 9, and HIF-1 $\alpha$  compete with members of Tcf/Lef for binding to  $\beta$ -catenin (Akiyama et al., 2004, Easwaran et al., 1999, Kaidi et al., 2007, Takemaru et al., 2003). *(ii)* Some of the co-repressors regulate Wnt-pathway via more than one mechanism; for example Sox9, in addition to its competition role with members of Tcf/Lef, it can also stimulate phosphorylation and translocation of  $\beta$ -catenin from the nucleus which is subsequently degraded by the ubiquitination/26S proteasome pathway (Akiyama et al., 2004). In addition, the dynamic intracellular localization of  $\beta$ -catenin and the subsequent activation of Wnt/ $\beta$ -catenin pathway were found to be controlled by the nuclear antagonist Chibby through its efficient nuclear/cytoplasmic shuttling (Li et al., 2010b). *(iii)* The third antagonist-mediated inhibitory mechanism of Wnt-pathway involves disruption of TCF binding ability to DNA. For instance, SMRT and NCoR repress  $\beta$ -catenin signaling through indirect binding, via  $\beta$ -catenin and/or TCF4, to the TCF4-binding sites on the promoter of Wnt-target genes including CCND1 (Song and Gelmann, 2008). Moreover, the osteoblast-specific transcription factor Osterix (Osx) was found to interact with Tcf1 through its N-terminal transactivation domain and disrupt Tcf1 binding to DNA (Zhang et al., 2008). *(iv)* Another method of Wnt signal suppression is co-repressor-mediated inhibition of co-activator recruitment by  $\beta$ -catenin. This mechanism is exemplified by KLF4, whose interaction with the C-terminal domain of  $\beta$ -catenin inhibits recruitment of the co-activator, p300/CBP by  $\beta$ -catenin leading to inhibition of p300/CBP-mediated  $\beta$ -catenin acetylation as well as histone acetylation on Wnt-target genes (Evans et al., 2010). The putative  $\beta$ -catenin interaction partners are themselves regulated by several extracellular stimuli. Therefore, it is plausible to expect that their subsequent effects on  $\beta$ -catenin activity are modulated in a context-dependent manner. In this view, different cellular context, may lead to various outcomes of activated Wnt signalling pathway (Lucero et al., 2010).

Alteration of Wnt/ $\beta$ -catenin signalling pathway through  $\beta$ -catenin co-repressors is often involved in crucial biological processes ranging from normal development to cancer. For instance, Sox9 regulates the progression of the chondrocyte differentiation pathway during endochondral bone formation through inhibition of  $\beta$ -catenin (Akiyama et al., 2004), whereas the Wnt

signalling attenuator RUNX3 was proposed to function as a tumour suppressor during intestinal tumourigenesis (Ito et al., 2008). Moreover, expression of Chibby, a nuclear  $\beta$ -catenin associated antagonist of the Wnt/Wingless pathway, was also linked to embryonic development and cancer (Takemaru et al., 2003).

Collectively, these findings indicate that  $\beta$ -catenin co-repressors function as potential gate keepers for the activity of  $\beta$ -catenin/TCF complex, ensuring that the proper threshold of  $\beta$ -catenin is achieved before its interaction with TCFs. This tight regulation of Wnt signalling in the nucleus determines precise downstream effects in both normal and cancer development based on the overall outcome of the interaction between co-activators and co-repressors with the  $\beta$ -catenin/TCF complex. Given the regulatory importance of nuclear cofactors (both co-activators and co-repressors) on Wnt signalling pathway, it is, therefore, predictable that any newly described protein-protein interaction with the nuclear  $\beta$ -catenin could have crucial involvement in normal versus tumour development.

A less understood aspect of Wnt/ $\beta$ -catenin signalling is the discovery and involvement of many DNA-binding transcription factors, other than TCF/LEF, in this pathway. Notably, many of these factors including KLF4, Glis2 and 3, HIC1, and Osx belong to the Cys2-His2 ( $C_2H_2$ ) family of zinc finger proteins characterized by having multiple  $C_2H_2$ -type zinc finger DNA-binding domains (Evans et al., 2010, Kim et al., 2007, Ulloa et al., 2007, Valenta et al., 2006, Zhang et al., 2008, Zhang et al., 2006). These zinc finger-containing  $\beta$ -catenin partners could significantly expand the gene expression programs controlled by Wnt/ $\beta$ -catenin signalling. Due to possessing potential DNA binding properties in addition to their ability to interact with  $\beta$ -catenin and/or TCFs (see above and Table 1-2), zinc finger proteins could disrupt the formation of the  $\beta$ -catenin/TCF complex and recruit nuclear  $\beta$ -catenin to the promoter of specific target genes independently to TCFs. However, this model of nuclear  $\beta$ -catenin recruitment just started to be explored and it needs to be further clarified.

As the current work demonstrates identification and characterization of a novel  $\beta$ -catenin interacting protein called FLYWCH-type zinc finger protein 1

(FLYWCH1), comprehensive information about FLYWCH1 and the family of zinc finger proteins is given in (sections 1.5 & 1.6).

### **1.3 Non canonical Wnt signalling pathway**

In addition to the canonical Wnt-pathway, Wnt-ligands can also trigger non-canonical pathways which are often referred to as  $\beta$ -catenin independent pathways. The non-canonical pathways can be further divided into at least three other distinct branches, the Wnt/ $\text{Ca}^{2+}$ , the Wnt/JNK and the Wnt/planar cell polarity (PCP) pathways. Upstream, the non-canonical pathways also involve Wnt/Fz binding but in an LRP and  $\beta$ -catenin-independent manner. However, the mechanism of downstream signal transduction through these pathways is less understood.

Traditionally, non-canonical pathways were implicated in the regulation of cell movement, polarity, and orientation. However, evidence suggests the involvement of these pathways in various aspects of normal development, diseases and cancer (reviewed by De, 2011, Kikuchi and Yamamoto, 2008, Kohn and Moon, 2005, Sugimura and Li, 2010, Veeman et al., 2003). Moreover, in addition to the Wnt/Fz pathways, other non-frizzled branches of non-canonical Wnt-pathway have also been proposed such as Ryk (Lu et al., 2004), Ror2 (Oishi et al., 2003), and R-Spondin (Kazanskaya et al., 2004) pathways. The non-frizzled Wnt-pathways were also implicated in several important cellular processes such as cell migration and convergent extension (Angers and Moon, 2009, Clark et al., 2012, Semenov et al., 2007).

In general, Wnt signalling pathways (both canonical and non-canonical) are among the most important pathways that have been widely implicated in numerous aspects of development, cell biology and tumourigenesis. However, as outlined above Wnt/ $\beta$ -catenin signalling is of particularly relevance to the normal biology and carcinogenesis of intestine and the following sections explore this in more detail.

## **1.4 Role of canonical Wnt signalling in intestinal biology**

Activated Wnt/ $\beta$ -catenin pathway has important implications in all aspects of intestinal biology ranging from normal development, to cellular homeostasis and carcinogenesis depending on the context of activation and the surrounding microenvironment. The various genetic programs controlled by this pathway through regulation of Wnt-responsive genes are the most important aspect of this pathway.

### **1.4.1 The normal architecture of intestine**

The intestine represents a very attractive experimental model, in terms of both normal intestinal development and cancer formation. Anatomically, it has been divided into the small intestine and the large intestine (comprising the colon and rectum). The small intestine can be further sub-divided into the duodenum, the jejunum, and the ileum. In mammals, the architecture of small intestine is composed of villi and crypts, lined by a single epithelial layer that is renewed continuously every few days (less than one week) (van der Flier and Clevers, 2008). This single layer of epithelium consists of stem cells, transit-amplifying cells and the terminally differentiated subtypes of defensin-secreting Paneth cells, hormone-secreting enteroendocrine cells, mucous-secreting goblet cells, and absorbing enterocytes (Figure 1-4) (Brabletz et al., 2009). Moreover, recently, a new type of secretory cells, known as “tuft” cells, has been added to the list (Gerbe et al., 2011).

The modular organization of the colon epithelium is similar to that of the small intestine, except for the absence of villi and Paneth cells (van der Flier and Clevers, 2008). Many signalling pathways have been reported to play crucial roles during intestinal morphogenesis, among them the Wnt/ $\beta$ -catenin signalling has received the most attention. This pathway often coordinates with other signalling pathways such as Hedgehog, Notch, JNK (c-Jun N-terminal kinases) and BMP (bone morphogenic protein) to create and maintain the

microenvironment required for intestinal development and homeostasis including stem cell regulation, lineage specification and maturation (Miki et al., 2011, Nusse et al., 2008, Saadeddin et al., 2009). Therefore, any disturbance to these pathways may negatively or positively affect the normal structure and organization of the intestine resulting in different type of diseases including cancer (Brabletz et al., 2009, Scoville et al., 2008, Clevers, 2006, Clevers and Nusse, 2012).

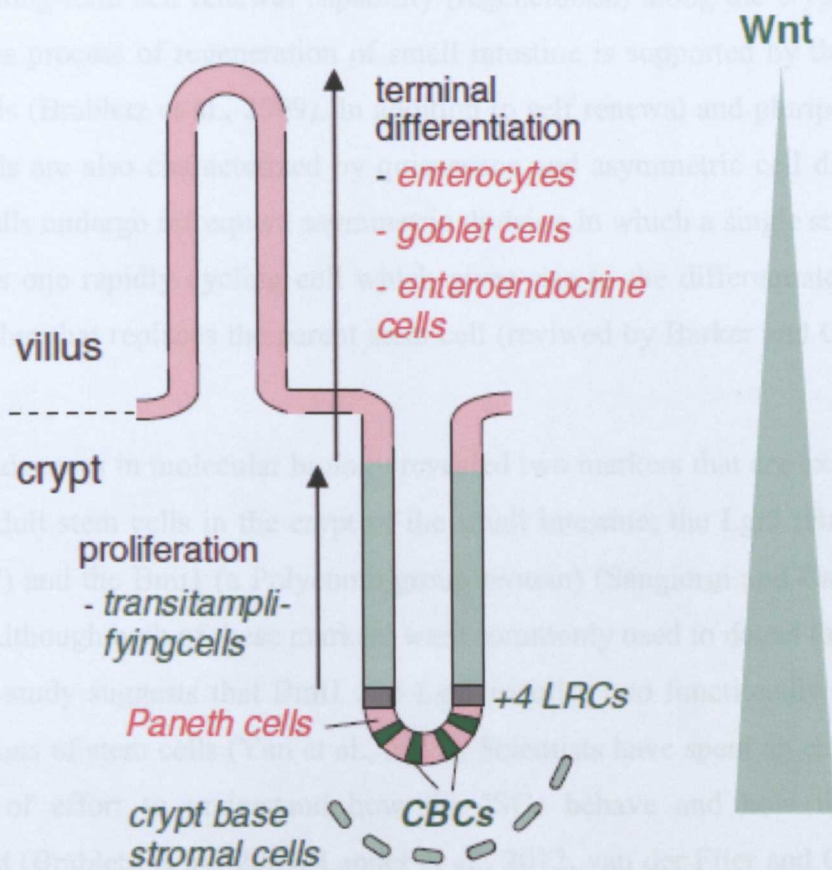


**Figure 1-4: The architecture of the small intestinal mucosa.** Terminally differentiated intestinal epithelial cells (red) are found in the villi; only Paneth cells are located in the crypt base. Green indicates location of putative intestinal stem cells (dark green) and the transit-amplifying cells. Crypt base columnar cells (CBCs) selectively express the Wnt-target gene *Lgr5/GPR49*. Gradients (or components) of Wnt-pathway that induce stemness or proliferation is indicated in green. Taken from (Brabletz et al., 2009).

### **1.4.2 Intestinal stem cells and homeostasis**

Intestinal stem cells (ISCs) are multipotent and self-renewing cells occupying the bottom of the crypt. These cells are cycling slowly, but produce rapidly proliferating progeny cells called transient amplifying cells which gradually differentiate into the five terminally differentiated cell types as described above in (section 1.4.1).

Homeostasis in the context of intestinal epithelium means keeping a balance between cell proliferation and differentiation which is required to maintain the tissue's long-term self renewal capability (regeneration) along the crypt-villus axis. This process of regeneration of small intestine is supported by the adult stem cells (Brabletz et al., 2009). In addition to self renewal and pluripotency, stem cells are also characterized by quiescence and asymmetric cell division. These cells undergo infrequent asymmetric division in which a single stem cell generates one rapidly cycling cell which gives rise to the differentiated cells and another that replaces the parent stem cell (reviewed by Barker and Clevers, 2010).

Recent advances in molecular biology revealed two markers that are expressed by the adult stem cells in the crypt of the small intestine; the *Lgr5* (Barker et al., 2007) and the *Bmi1* (a Polycomb group protein) (Sangiorgi and Capecchi, 2008). Although both of these markers were commonly used to detect the ISCs, a recent study suggests that *Bmi1* and *Lgr5* identify two functionally distinct populations of stem cells (Yan et al., 2012). Scientists have spent an enormous amount of effort to understand how the ISCs behave and how they are regulated (Brabletz et al., 2009, Lander et al., 2012, van der Flier and Clevers, 2008). As a result, the concept of the “stem cell niche”, a supporting microenvironment in which stem cells are found, was proposed (van der Flier and Clevers, 2008). The stem cell niche in the intestine is most likely formed by the subepithelial myofibroblasts (Mills and Gordon, 2001) and is tightly regulated through a long-term crosstalk between epithelial and underlying mesenchymal cells. Although many intrinsic and extrinsic factors are involved, this crosstalk is mainly mediated by conserved signalling pathways, such as Wnt, Hedgehog, Notch, PI3K and BMP (reviewed by Brabletz et al., 2009).

These pathways are ultimately regulating the developmental lineages of stem cells in a predictable and reproducible manner.

Wnt/ $\beta$ -catenin signalling pathway is considered as a dominant force in controlling cell fate and proliferation (homeostasis) of normal intestinal epithelium through stages of development and adulthood (reviewed by Pinto and Clevers, 2005). Several lines of evidence show the accumulation of  $\beta$ -catenin at the bottom of the crypt (Batlle et al., 2002, Lustig et al., 2002) and also show the *in vivo* affects of Wnt signalling on the cell lineage across the crypt-villus axis (Korinek et al., 1998, Pinto et al., 2003). Indeed, active Wnt signalling was shown to be essential for the maintenance of crypt progenitor compartments in the intestine as inhibition of this pathway resulted in significant defects in the regulatory program of the crypt. For instance, in mice lacking the Tcf4 transcription factor, the epithelial stem-cell compartments became deleted (Korinek et al., 1998). Similarly, Fevr et al. (2007) found that upon blocking of Wnt/ $\beta$ -catenin signalling, the transiently amplifying cells were rapidly lost and the intestinal stem cells were also induced to terminally differentiated cells, resulting in a complete block of intestinal homeostasis and fatal loss of intestinal function (Fevr et al., 2007). Moreover, inhibition of Wnt signalling by DKK1 in adult mice reduced cell proliferation and disturbed the normal architectural of small intestine and colon (Pinto et al., 2003, Kuhnert et al., 2004).

Taken together, these observations indicate that Wnt/ $\beta$ -catenin signalling has fundamental roles in regulating homeostasis of the intestinal epithelium through maintaining the crypt stem cell/progenitor compartments. However, the maintenance of the intestinal crypt-villus axis also requires a precise control of the progenitor cell migration during both homeostasis and cancer development. Models that explain the mechanisms of intestinal cell migration and positioning across the crypt-villus axis are outlined below (section 1.4.3).

### **1.4.3 Cell migration and positioning in intestinal crypts**

In normal conditions of small intestine, the transiently amplified progeny of the stem cells undergo bidirectional migration. Paneth cells migrate to the bottom of the crypt, while the other three differentiated cell types (enteroendocrine cells, goblet cells and enterocytes) migrate upward to the apex of the villus (Potten and Loeffler, 1990, Stappenbeck et al., 1998).

Before identification of the role of Wnt signalling pathway in cell movement and positioning across the crypt-villus axis, several alternative mechanisms had been proposed to explain the driving force behind this organised cell movement. For example, Loeffler et al. (1986) proposed a hypothetical mechanism involved a cell-cell interaction leading to a local age-dependent displacement of old cells with newborn cells. In this model, it was assumed that all cells have certain ability to sense the age of their direct neighbours and preferentially divide to displace their oldest neighbours to higher cell positions (Loeffler et al., 1986).

Other researchers suggested a passive mechanism for intestinal cell migration which can be summarized in two steps. First, generation of cells in the crypts transmits a pressure along the crypt-villus axis. Second, gaps left by the expelled mature cells at the top of the villi are immediately reoccupied by new cells. As a result, the attached epithelial cells are forced to migrate upward (reviewed by Heath, 1996). Although the passive model for intestinal cell migration was proposed long time ago, this view is still widely accepted. However, involvement of additional mechanisms such as chemoattraction or repulsion in the regulation of intestinal cell migration cannot be excluded (Solanas and Batlle, 2011).

Essential involvement of the core component of Wnt signalling pathway ( $\beta$ -catenin/TCF complex) in the migration of intestinal epithelium cells was first introduced by Hans Clevers group. Batlle et al. (2002) found that  $\beta$ -catenin/TCF signalling potentially determines cell positioning along the crypt axis in the small intestine. This effect was mainly achieved through controlling the expression of Wnt-targets EphB and ephrinB genes through  $\beta$ -catenin/TCF

signalling (Batlle et al., 2002). Eph receptors comprise the largest known subfamily of receptor tyrosine kinases characterized for binding to membrane-bound ligands known as ephrins. These molecules play key roles in the process of cell migration and adhesion during development (reviewed by Poliakov et al., 2004).

Moreover, the interaction between EphB2/3 and ephrin-B1 was found to compartmentalize the expansion of cancer cells both *in vivo* (in intestinal adenomas) and *in vitro* (in CRC culture) (Cortina et al., 2007). In addition, Ephrin-B2 ligand has been implicated in regulation of endothelial cell morphology and motility independently of Eph-receptor binding (Bochenek et al., 2010), indicating that the receptor/ligand interaction is not always required for the function of these molecules.

The migration of progenitor cells in intestinal epithelium is harmonically orchestrated through differential expression of Eph/ephrin molecules by Wnt signalling pathway. It has been shown that  $\beta$ -catenin/TCF signals promote the expression of EphB2 and EphB3 receptors, whereas they repress the expression of EphB ligands, namely ephrin-B1 and ephrin-B2 (Batlle et al., 2002). The strength of Wnt signal as well as EphB2/3 expression is high in cells resident at the bottom of the crypt, while as cells are migrating upward the Wnt signals/components are reducing gradually permitting gradual increase in expression of ephrin-B1 and ephrin-B2 ligands. The opposite expression of EphB receptors and ephrin-B ligands in different cell compartments along the crypt axis leads to differential adhesion capabilities of the epithelial cells which eventually regulate cell positioning and migration along the crypt-villus axis (Wong et al., 2010a).

Although, the biological effects of Eph/ephrin molecules are relatively well understood, regulatory factors and/or pathways upstream to these molecules are largely unknown. Moreover, the link between gradient concentration of Wnt signalling pathway and the differential expression of Eph-B/ephrin-B proteins along the crypt axis is not fully understood. Furthermore, in addition to Eph/ephrin proteins, many other factors have been involved in regulation of cell adhesion and migration in the intestinal epithelium such as E-cadherin,

p120-catenin, and Small GTPases of the Rho family (reviewed by Solanas and Batlle, 2011). Thus, identification of factors that could provide specificity to the components of Wnt signalling pathway to differentially regulate downstream target genes that involved in cell migration remains of particular interest.

#### **1.4.4 Intestinal tumourigenesis**

Giving the critical roles of Wnt/ $\beta$ -catenin signalling in normal development, stem cells homeostasis, and cell positioning in the intestine (sections 1.4.1 to 1.4.3), it is not surprising that aberrant activation of this pathway is strongly associated to intestinal/colon tumourigenesis. Indeed, it has been found that deregulation of Wnt/ $\beta$ -catenin signalling pathway, the central early event in colorectal carcinogenesis, is implicated in over 90% of human colorectal cancers (Fevr et al., 2007). Most of these cases are linked to mutational inactivation of Wnt/ $\beta$ -catenin pathway components including *APC*, *AXINI* or *CTNNB1* genes. For instance, mutation of *APC*, the most common cause of activated Wnt signalling, occurs in 85% of all sporadic and hereditary colorectal tumours (Kinzler and Vogelstein, 1996). These mutations (both germline and somatic) result in truncated proteins lacking important domains such as AXIN and  $\beta$ -catenin binding sites (reviewed by Segditsas and Tomlinson, 2006). In addition, mutations in *AXINI* and *CTNNB1* genes were also broadly detected in colorectal cancer cell lines (Ilyas et al., 1997, Morin et al., 1997, Shimizu et al., 2002, Webster et al., 2000).

Mutant APC and Axin proteins are unable to form a proper destruction complex with GSK-3 $\beta$  which subsequently impairs the phosphorylation of  $\beta$ -catenin. Similarly, amino acid substitutions in the phosphorylated residues of  $\beta$ -catenin lead to phosphorylation blockade and stabilization of this protein. Either type of disruption leads to accumulation and nuclear translocation of  $\beta$ -catenin which ultimately causes aberrant activation of Wnt signalling pathway. Moreover, alteration of  $\beta$ -catenin expression in colorectal cancer, adenoma, and both dysplastic and nondysplastic aberrant crypt foci (ACF) was also

reported (Mi et al., 2009). Given the importance and influence of Wnt signalling components on the stability of cytosolic  $\beta$ -catenin, appropriate regulation of these components in the context of Wnt-pathway is a crucial step by which the accumulation of nuclear  $\beta$ -catenin can be regulated. In addition,  $\beta$ -catenin is tightly regulated in the nucleus through several regulatory cofactors. The basic concept behind this regulation of  $\beta$ -catenin in both cytoplasmic and nuclear compartments is to transcriptionally modulate Wnt-target genes, including those related to human colon cancer (Table 1-3), in a spatial and temporal manner.

**Table 1-3: Examples of Wnt/ $\beta$ -catenin downstream target genes involved in cancer.** Taken from Wnt homepage hosted by Nusse (<http://www.stanford.edu/~musse/pathways/targets.html>).

Genes	Organism/system in which first identified	References
<i>c-myc</i>	human colon cancer	(He et al., 1998)
<i>Tcf-1</i>	human colon cancer	(Roose et al., 1999)
<i>LEF1</i>	human colon cancer	(Filali et al., 2002, Hovanes et al., 2001)
<i>c-jun</i>	human colon cancer	(Mann et al., 1999)
<i>fra-1</i>	human colon cancer	(Mann et al., 1999)
<i>VEGF</i>	human colon cancer	(Zhang et al., 2001)
<i>EphB/ephrin-B</i>	human colon cancer	(Battle et al., 2002)
<i>Cyclin D1</i>	human colon cancer	(Tetsu and McCormick, 1999)
<i>Cdh1</i> (E-cadherin)	Mouse hair follicle	(Jamora et al., 2003)

It has been established that signalling through  $\beta$ -catenin/TCF complex constitutes the principal driving force behind the biology of the crypt (Korinek et al., 1998). In the same context, Wnt/ $\beta$ -catenin signals resulting from aberrant accumulation of nuclear  $\beta$ -catenin play essential roles in tumourigenesis of the

intestine. This view is strongly supported by the fact that the majority of Wnt-target genes in human colorectal cancer cells are physiologically expressed in intestinal crypts by either Paneth cells or transit-amplifying cells (van de Wetering et al., 2002, Van der Flier et al., 2007). One of the well studied examples of the direct Wnt-target genes expressed in the intestinal crypt are EphB/ephrin-B genes. In addition to their critical implication in cell migration and positioning in the intestinal crypt (section 1.4.3), these molecules were also involved in carcinogenesis of intestine. It has been reported that dissociation of EphB2 kinase-dependent and independent pathways play critical roles in progenitor cell proliferation and tumour suppression (Genander et al., 2009). Moreover, recent data indicate that ephrin-B2 has been strongly involved in tumour angiogenesis and lymphangiogenesis through regulating members of VEGF (vascular endothelial growth factor) family of growth factors (Sawamiphak et al., 2010, Wang et al., 2010). Similarly, deregulation of ephrin-B2 disturbed the normal architecture, function, and vascularisation of the mammary gland and promoted metastasis formation in transgenic mice (Haldimann et al., 2009). Thus, through direct regulation of the Wnt-target genes transcriptional program,  $\beta$ -catenin can potentially control normal development as well as carcinogenesis of the intestine in the context of canonical Wnt signalling pathway.

This classical model of  $\beta$ -catenin involvement in colon cancer became more complicated as many potential  $\beta$ -catenin interacting partners other than TCFs were already discovered and identification of novel partners is still ongoing. On the other hand, the oncogenicity of this pathway has been recently reconsidered in some types of cancer such as melanoma where the stabilized  $\beta$ -catenin was not enough to induce melanoma in mice (Delmas et al., 2007). Furthermore, TCF4, the main downstream effector of Wnt signalling pathway, has been shown to function as a tumour suppressor in a Tcf4 conditional knock out mouse (Angus-Hill et al., 2011). Moreover, activated Wnt/ $\beta$ -catenin signalling in patient tumours, indicated by increased levels of nuclear  $\beta$ -catenin, correlated with an improved rather than poorer prognosis (reviewed by Lucero et al., 2010). This controversial role of  $\beta$ -catenin/TCF4 signalling in

cancer may be further explained by the contribution of other regulatory proteins involved in various roles mediated by  $\beta$ -catenin.

#### **1.4.5 Multistep carcinogenesis in colorectal cancers**

Colorectal cancer (CRC) is the 2<sup>nd</sup> most common cause of cancer-associated death in developed countries (Ricci-Vitiani et al., 2007). It occurs either sporadically as a result environmental and dietary factors, or hereditary in the context of a familial predisposition such as familial adenomatous polyposis (FAP) (Cunningham et al., 2010, Fodde et al., 2001, Pinto and Clevers, 2005). In both cases, CRCs arise from a series of well-defined histo-pathological changes associated with specific genetic alterations in a number of oncogenes and tumour-suppressor genes resulting in malignant tumour development in a stepwise process known as multistep colorectal tumourigenesis (Yamada and Mori, 2007, Fodde et al., 2001, Hughes and Huang, 2011).

The concept of multistep colorectal tumourigenesis was first introduced by Fearon and Vogelstein at early 1990s. In their model they described a process by which normal colonic cells could transform to tumour cells through a number of genetic alterations/mutations in both proto-oncogenes and tumour-suppressor genes (Fearon and Vogelstein, 1990). Since then the accumulated evidence further supported this model and increased our understanding about how solid tumour developed and led to today's knowledge of tumour carcinogenesis.

Although the precise order of alterations necessary for cancer development are not fully understood, it is widely believed that mutation in *APC* (adenomatous polyposis coli), a classic tumour-suppressor gene found on chromosome 5q, is the earliest and essential genetic alteration in the sequential events of colon tumour development (Figure 1-5) (Yamada and Mori, 2007, Huang et al., 1997, Fearon and Vogelstein, 1990, Pinto and Clevers, 2005, Pino and Chung, 2010). Germline mutations in *APC* cause the inherited familial adenomatous polyposis (FAP) syndrome with tumours containing mutated/inactivated wild-type allele of *APC*, most often by deletion (Goss and Groden, 2000, Kinzler and Vogelstein, 1996). People with FAP develop hundreds to thousands of colonic

adenomas at an early age. If not surgically removed, the risk of these polyps developing into cancer rises dramatically with age and during the third to fourth decade of life the lifetime risk of colon cancer approaches 100% (Fodde et al., 2001, Markowitz et al., 2002, Albuquerque et al., 2002). Accordingly, appearance of aberrant crypt foci (ACF) is one of the earliest alterations seen in the epithelium during the adenoma–carcinoma sequence of CRCs development (Bird, 1995, Fodde et al., 2001). ACFs contain dysplastic cells that could progress into benign adenomatous polyps and mutations in *APC* are closely related to the development of dysplasia in these small lesions (Fodde et al., 2001). Subsequent mutations in other genes (see below) along with the alterations in critical signalling pathways such as Wnt/ $\beta$ -catenin pathway lead to gradual progression of the benign adenomatous polyps into carcinoma (Albuquerque et al., 2002, Pinto and Clevers, 2005, Fodde et al., 2001, Hughes and Huang, 2011, Kinzler and Vogelstein, 1996).

One of the well documented roles of *APC* gene is regulation of Wnt/ $\beta$ -catenin signalling pathway. It has been established that APC is an important component of the destruction complex found in the cytoplasm (see section 1.2.1 & Figure 1-1) and responsible for the degradation of the  $\beta$ -catenin protein that involved in the canonical Wnt signalling pathway. Through this degradation, APC protein functions as a suppressor of this pathway, and thereby inhibits the  $\beta$ -catenin mediated transcriptional activity (Aoki and Taketo, 2007, Markowitz et al., 2002). However, mutations in the *APC* gene interfere with this function and lead to an increased cytoplasmic pool of  $\beta$ -catenin which subsequently translocate into the nucleus and activates Wnt-target genes including *c-Myc*, *Cyclin D1*, *c-jun* & *Fra-1*, resulting in increased cell proliferation (He et al., 1998, Shtutman et al., 1999, Tetsu and McCormick, 1999, Mann et al., 1999). Much more detail about the canonical Wnt signalling pathway is mentioned in (section 1.2).

In addition to increased cell proliferation by Wnt signalling pathway, other genetic alterations (see below) activate additional pathways such as transforming growth factor  $\beta$  (TGF- $\beta$ ) pathway that play crucial roles in tumour development (Fodde et al., 2001). These alterations cause gradual

changes in tumour cell physiology which ultimately lead to aberrant biological activities known as hallmarks of cancer such as uncontrolled cell proliferation, resisting cell death, insensitivity to antigrowth signals, angiogenesis...etc (Hanahan and Weinberg, 2000, Hanahan and Weinberg, 2011).

Other genetic alterations including activation of the oncogene *K-RAS* (occurs in 35–50% of CRCs) and inactivation of the tumour suppressor *TP53* (occurs in more than 50% of CRCs), are thought to be later events that occur in the multistep colorectal carcinogenesis (Figure 1-5) (Calistri et al., 2006, Judson et al., 2006, Fodde et al., 2001, Hughes and Huang, 2011, Boland and Goel, 2010, Pino and Chung, 2010).

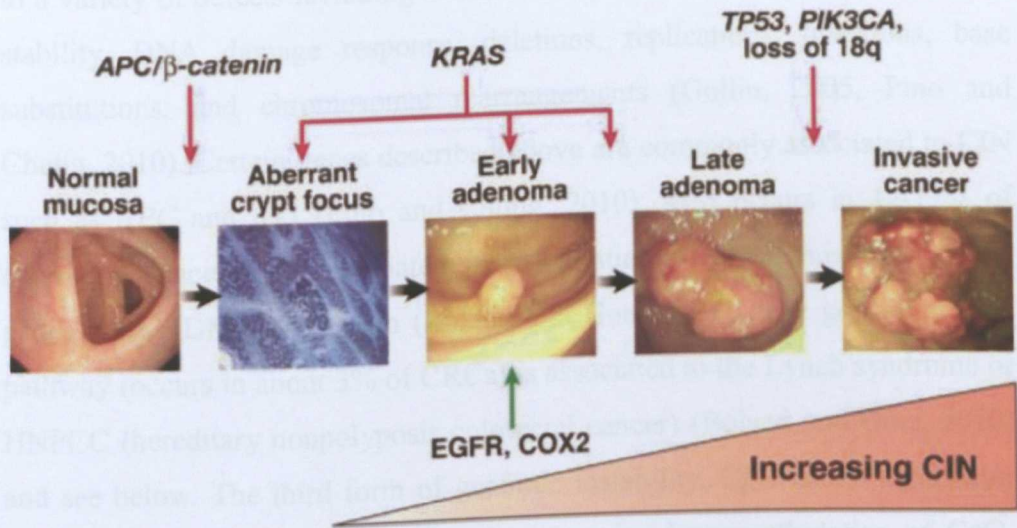


**Figure 1-5: Multistep genetic model of colorectal carcinogenesis.** The initial step in colorectal tumorigenesis is the formation of aberrant crypt foci (ACF). Activation of the Wnt signalling pathway can occur at this stage as a result of mutations in the *APC* gene. Progression to larger adenomas and early carcinomas requires activating mutations of the proto-oncogene *KRAS*, mutations in *TP53*, and loss of heterozygosity at chromosome 18q. Mutational activation of *PIK3CA* occurs late in the adenoma–carcinoma sequence in a small proportion of colorectal cancers. Chromosomal instability is observed in benign adenomas and increases in tandem with tumour progression. Taken from (Pino and Chung, 2010).

In addition to mutations in the above genes, alterations in several other genes have also been identified along the multistage process of colon tumour progression. These include activations of oncogenes such as *B-RAF*, *PIK3CA*, and *CTNNB1* and inactivation of tumour-suppressor genes such as *SMAD2* & *SMAD4*, *DCC*, *Cox-2*, *EGFR*, and *TGFβ* (reviewed by Markowitz et al., 2002, Fodde et al., 2001, Pinto and Clevers, 2005, Boland and Goel, 2010). Moreover, the sequential acquisition of cancer development is promoted by the loss of the genomic stability including chromosomal instability (CIN), microsatellite instability (MSI), and CpG-island methylator phenotype (CIMP) (Dahlin et al., 2010, Boland and Goel, 2010, Pino and Chung, 2010). CIN occurs in 65-70% of sporadic colorectal cancers and characterized by widespread imbalances in chromosome number (aneuploidy) and structure due to a variety of defects including abnormal chromosomal segregation, telomere stability, DNA damage response, deletions, replications, insertions, base substitutions, and chromosomal rearrangements (Gollin, 2005, Pino and Chung, 2010). Certain genes described above are commonly associated to CIN such as *APC* and *p53* (Pino and Chung, 2010). MSI occurs in 12-17% of colorectal cancers and associated to inactivation of DNA mismatch repair genes during DNA replication (Boland and Goel, 2010). The germ-line MSI pathway (occurs in about 3% of CRCs) is associated to the Lynch syndrome or HNPCC (hereditary nonpolyposis colorectal cancer) (Boland and Goel, 2010) and see below. The third form of genomic instability, CpG-island methylator phenotype (CIMP), is characterised by extensive hypermethylation of CpG-rich promoters and associated with microsatellite instability (MSI) and BRAF mutation in colorectal cancer (Issa, 2004, Dahlin et al., 2010, Ogino et al., 2009). CIMP is attributed to 70-80% of sporadic MSI-positive and 15% of total CRCs (Issa, 2004).

Lynch syndrome (HNPCC), is an autosomal dominant disorder and a common cause of hereditary colorectal cancer (Lynch and Lynch, 2000). Patients with this syndrome have an 80% lifetime risk of colon cancer (Markowitz et al., 2002). The genetic basis of HNPCC contributes to microsatellite instability caused by germline mutations in components of the DNA mismatch repair (MMR) genes (Markowitz et al., 2002, Kinzler and Vogelstein, 1996). The

products of these genes recognize and correct base pair mismatches and small nucleotide mutations (insertion/deletion) that occur during DNA replication and, thereby, preserve genomic integrity. Therefore, in cells with MMR defects the mutation rate is much higher (100-1000 folds) than normal cells (Fishel and Wilson, 1997, Narayan and Roy, 2003). In 90% of cases of HNPCC, mutations are found in MSH2 or MLH1, which encode two required components of the mismatch repair complex. In addition to MSH2 or MLH1, mutations in at least two other MMR genes (MSH6, and PMS2) have also linked to HNPCC (reviewed by Jensen et al., 2010, Markowitz et al., 2002).

## **1.5 The family of zinc finger proteins**

The term zinc finger protein (ZFP) is applied to an important family of eukaryotic proteins that have one or multiple zinc finger domains or motifs. A zinc finger motif can be described as a small, functional, independently folded domain that is organized strategically through coordination of one or more zinc ions to stabilize its structure (Iuchi and Kuldell, 2005, Michalek et al., 2011). The main feature of zinc finger motifs is the presence of cysteine and/or histidine residues around a zinc ion forming a tetrahedral geometry (Figure 1-6) (Brayer and Segal, 2008). This domain will be folded to a functional unit only in the presence of zinc; in the absence of zinc the domain will be unfolded and hence unfunctional (reviewed by Michalek et al., 2011).

Historically, zinc finger motifs were first identified by a group of scientists in 1985 in the lab of Aaron Klug at the MRC laboratory of Molecular Biology in Cambridge, where they were working on a *Xenopus* transcription factor, TFIIA (Miller et al., 1985). Thereafter, a large number of proteins (more than 24,000) with similar zinc finger domains have been discovered and annotated as C<sub>2</sub>H<sub>2</sub> (Cys<sub>2</sub>-His<sub>2</sub>) or classical zinc finger proteins (CZFPs) (Iuchi and Kuldell, 2005). Since its discovery, the family of zinc finger proteins has been found to be widespread in nature and has been considered as one of the largest families of regulatory proteins in mammals (Kubo et al., 1998, Iuchi, 2001). Accordingly, recent findings indicate that approximately 3% of the whole

human genome encodes zinc finger proteins (Klug, 2010), suggesting that these motifs could have crucial biological implications.

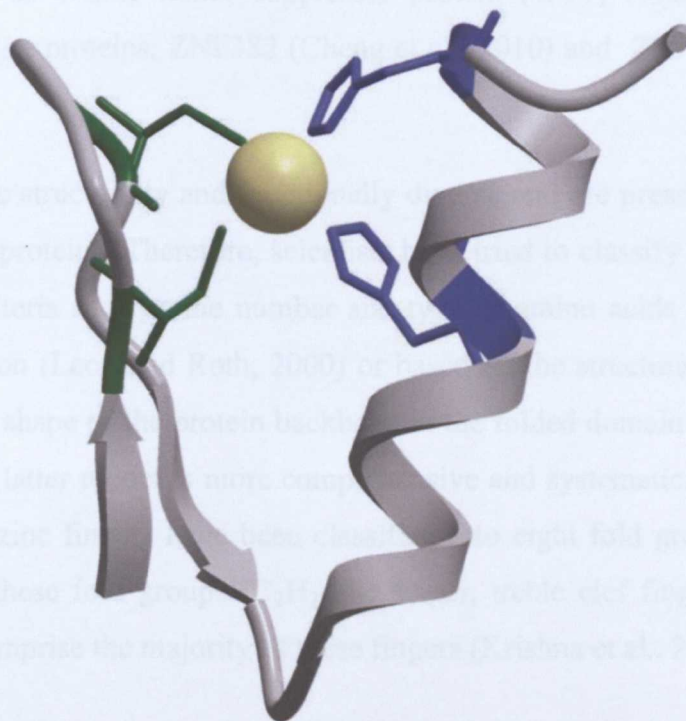


**Figure 1-6: The canonical C<sub>2</sub>H<sub>2</sub> zinc finger structure.** A ribbon diagram of the third C<sub>2</sub>H<sub>2</sub> domain from TFIIIA in *Xenopus laevis* (PDB accession number 1TF3) is showing the canonical stabilization of the ββα fold by the coordination of a zinc ion (yellow) by two cysteine (green) and two histidine (blue) residues. Taken from (Brayer and Segal, 2008).

Although zinc finger motifs were originally identified as DNA-binding domains (Miller et al., 1985), a growing body of evidence has described these motifs as interaction modules that can bind to various compounds such as DNA, RNA, proteins, and small molecules (Brayer and Segal, 2008, Krishna et al., 2003). Some of these fingers support both DNA and protein interactions such as Sp1, and Ying Yang 1 (YY1) (Rotheneder et al., 1999, Seto et al., 1993, Zhou et al., 1995). Thus, it is not surprising that zinc finger-containing proteins have been broadly involved in various biological processes of the cell including gene expression, replication and repair, metabolism, signal transduction, proliferation, differentiation and development (reviewed by Iuchi and Kuldell, 2005, Krishna et al., 2003, Matthews and Sunde, 2002). In

addition, zinc finger-containing proteins, especially those contain the classical C<sub>2</sub>H<sub>2</sub> zinc fingers have been potentially implicated in tumour suppression activities such as Wilms tumor suppressor protein (WT1) (Madden et al., 1993), zinc-finger proteins; ZNF382 (Cheng et al., 2010) and ZNF545 (Wang et al., 2012).

Zinc fingers are structurally and functionally diverse and are present among a vast variety of proteins. Therefore, scientists have tried to classify them based on different criteria such as the number and type of amino acids involved in zinc coordination (Leon and Roth, 2000) or based on the structural properties and the overall shape of the protein backbone in the folded domain (Krishna et al., 2003). The latter model is more comprehensive and systematic. According to this model, zinc fingers have been classified into eight fold groups (Table 1-4), three of these fold groups (C<sub>2</sub>H<sub>2</sub>-like finger, treble clef finger, and the zinc ribbon) comprise the majority of these fingers (Krishna et al., 2003).

As our understanding of zinc fingers has increased, more than 14 different classes and subfamilies of these proteins have been identified such as C2C2, CCHC, CCCH, LIM, RING, TAZ, and FYVE with more focus on the C<sub>2</sub>H<sub>2</sub> classical family of zinc finger proteins (reviewed by Brayer and Segal, 2008, Iuchi and Kuldell, 2005, Michalek et al., 2011). However, up to now the functional involvement of some of these proteins in the biological system of the cell remains unknown.

**Table 1-4: Structural classification of zinc fingers.** Taken from (Krishna et al., 2003), also available at ([http://prodata.swmed.edu/zndb/zndb\\_view.php](http://prodata.swmed.edu/zndb/zndb_view.php)).

Fold groups	Representative structure	Brief description
C <sub>2</sub> H <sub>2</sub> like		Beta-hairpin followed by an alpha-helix. Two zinc ligands are contributed by a zinc knuckle at the end of the beta-hairpin and the other two ligands are from the C-terminal end of the alpha-helix.
Gag knuckle		Two short beta-strands connected by a turn (zinc knuckle) followed by a short helix or a loop. Two N-terminal zinc ligands are donated by the zinc knuckle and two others come from the loop or are placed at both ends of a short helix.
Treble clef		Beta-hairpin at the N-terminus and an alpha-helix at the C-terminus. First two ligands come from the zinc knuckle and the second two ligands are donated by the N-terminal turn of the helix.
Zinc ribbon		Two beta-hairpins forming two structurally similar zinc-binding sub-sites. The ligands are contributed by two zinc-knuckles.
Zn <sub>2</sub> /Cys <sub>6</sub>		Zinc-binding domains in which two ligands are from a helix and two more from a loop.
TAZ2 domain like		Zinc-binding domains where the ligands are located at the termini of alpha-helices.
Zinc binding loops		Zinc binding loops found in larger proteins probably stabilized by zinc and may be viewed as small but separate domains. Common structural feature of these domains is that at least three zinc ligands are very close to each other in sequence and are not incorporated into regular secondary structural elements.
Metallothionein		Cysteine-rich loops, which bind a variety of metals. No clearly defined regular secondary structural elements can be detected and the protein chains are wrapped around a metal cluster with multiple cysteines liganding metals.

## **1.6 FLYWCH-type zinc finger proteins**

### **1.6.1 Origin and description**

The FLYWCH motif is one of the less studied members of the classical C<sub>2</sub>H<sub>2</sub> zinc finger domains. The name “FLYWCH” refers to the amino acid consensus sequence of this motif which is characterized by the presence of four hydrophobic amino acid residues [F (phenylalanine), L (leucine), Y (tyrosine), and W (tryptophan)] in conserved positions in addition to a preserved C<sub>2</sub>H<sub>2</sub> motif. Buchner et al. (2000), first described this domain as an anonymous new member of the classical C<sub>2</sub>H<sub>2</sub> family of zinc finger motifs in the *Drosophila* Modifier of *mdg4* proteins Mod(*mdg4*) (Buchner et al., 2000). Three years later, this domain was annotated as a FLYWCH domain based on the presence of FLYWCH consensus sequence (F/Y-X<sub>n</sub>-L-X<sub>n</sub>-F/Y-X<sub>n</sub>-WXCX<sub>6-12</sub>CX<sub>17-22</sub>HXH; where X indicates any amino acid) (Dorn and Krauss, 2003). Moreover, a later report revealed the presence of this motif in another *Drosophila* protein namely “*Drosophila* GST-containing FLYWCH zinc finger protein” (dGFZF) (Dai et al., 2004).

In addition to *Drosophila*, FLYWCH motifs were also identified in two proteins of *Caenorhabditis elegans* (*C. elegans*); PEB-1 (Beaster-Jones and Okkema, 2004) and FLYWCH transcription factors; FLH-1, FLH-2, and FLH-3 (Ow et al., 2008). Moreover, FLYWCH motifs have also been found in a highly conserved uncharacterized protein in mammals named as FLYWCH1 (Gene ID: 84256). More information about this protein is given below.

### **1.6.2 Function and importance**

The *Drosophila mod(mdg4)* gene, in which the FLYWCH motif was first identified, encodes a family of at least 26 protein isoforms. All these isoforms share a common N-terminal region, but differ in their C-termini which, with a few exceptions, contain a conserved FLYWCH zinc finger motif (Dorn and Krauss, 2003). The *Drosophila* Mod(*mdg4*) proteins were suggested to have a

putative function as chromatin modulators involved in higher order chromatin domains. Moreover, a general model of function of these isoforms in *Drosophila* was also proposed (Figure 1-7) (Dorn and Krauss, 2003). In this model, different Mod(mdg4) protein isoforms were considered as specific chromatin modules that interact with identical partners through their common BTB/POZ (BTB) N-terminal region. Each isoform then selectively interacts and recruits specific proteins to different chromatin sites through their variable C-termini which contain FLYWCH motif.

This proposed function of FLYWCH motif was based on previous evidence that proteins with FLYWCH domain were involved in protein-protein interactions; for example, the *Drosophila* Mod(mdg4)-67.2 isoform interacts with the DNA-binding protein Suppressor of Hairy-wing (Su(Hw)) via its C-terminal region which contains a FLYWCH domain (Gause et al., 2001, Ghosh et al., 2001). Moreover, the specific C-terminal region of another isoform, Mod(mdg4)-56.3/DOOM, containing the conserved FLYWCH motif was shown to be responsible for its interaction with the inhibitor of apoptosis protein of Baculovirus OpIAP (Harvey et al., 1997).

The second *Drosophila* FLYWCH motif-containing protein, dGFZF, possesses a tandem array of four FLYWCH motifs at the N-terminal domain and is expressed through all stages of *Drosophila* embryonic development. Thus, it has been postulated to have an important role in maintaining homeostasis during *Drosophila* development (Dai et al., 2004). dGFZF which is also known as Suppressor of Killer of prune Su(Kpn) (Provost and Shearn, 2006) lacks the nuclear localization signal (NLS) motif and is localized into the cytoplasm in *Drosophila* S2 cells. Therefore, it is not clear whether FLYWCH motifs of this protein could bind DNA. However, its involvement in protein-protein interactions was predicted (Dai et al., 2004, Provost and Shearn, 2006). Thus, FLYWCH motifs within *Drosophila* proteins may play a crucial role in gene regulation and development through interaction with other transcription factors and/or binding to DNA.

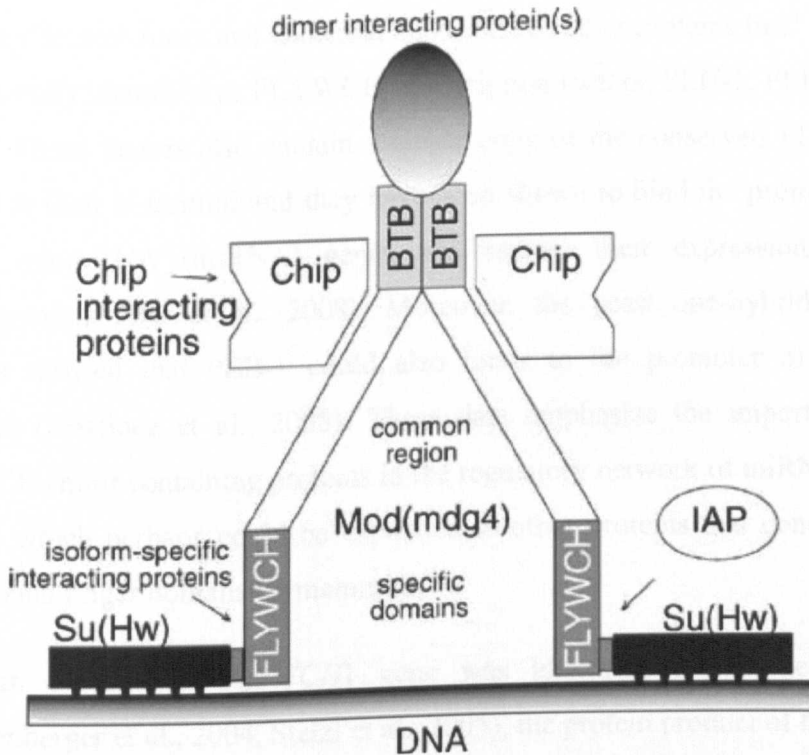


**Figure 1-7 : Model representing Mod(mdg4) proteins as chromatin modules.** A Mod(mdg4) homodimer formed via interactions between N-terminal BTB domains and other proteins is shown. Ahmad, Engel & Prive (1998) postulated such a putative protein binding site formed by the BTB domain dimer (Ahmad et al., 1998). The Chip protein was demonstrated to interact with the common N-terminal region present in all Mod(mdg4) isoforms (Gause et al., 2001). The variable C-terminal regions of different Mod(mdg4) protein isoforms, mostly containing the FLYWCH motif, are postulated to interact with different proteins, and thereby mediating targeting of the proteins to different chromatin sites. The DNA binding protein Su(Hw), which was found to interact with Mod(mdg4)-67.2 (Gerasimova et al., 1995) is shown. The inhibitor of apoptosis protein (IAP) represents another interacting protein, which interacts with the specific domain of Mod(mdg4)-56.3 (Harvey et al., 1997). Taken from (Dorn and Krauss, 2003).

In *C. elegans*, FLYWCH-motif containing proteins have been involved in specific DNA binding (Beaster-Jones and Okkema, 2004, Ow et al., 2008). For instance, PEB-1 is one of four proteins in *C. elegans* which contains a single copy of the conserved FLYWCH motif at the N-terminus domain. This protein was identified as a site-specific DNA-binding protein and the FLYWCH motif was found to be necessary for its DNA binding properties as well as *in vivo*

function (Beaster-Jones and Okkema, 2004). Three other proteins in *C. elegans* were recently identified as FLYWCH transcription factors; FLH-1, FLH-2, and FLH-3. These factors also contain a single copy of the conserved FLYWCH domain at their N-termini and they have been shown to bind the promoters of several microRNA (miRNA) genes and repress their expression during embryogenesis (Ow et al., 2008). Moreover, the yeast one-hybrid (Y1H) analysis showed that PEB-1 could also binds to the promoter of several miRNAs (Martinez et al., 2008). These data emphasize the importance of FLYWCH-motif containing proteins in the regulatory network of miRNA in *C. elegans* which perhaps could be expanded to other proteins that contain this type of zinc finger domains in mammals.

Although the human *FLYWCH1* gene was identified a few years ago (Brandenberger et al., 2004, Stelzl et al., 2005), the protein product of this gene (FLYWCH1) remained uncharacterized. Therefore, information about this protein in human and other mammals is currently very limited. In fact, there is no published report, so far, about FLYWCH1 in mammals. Thus, in the current work, for the first time, human FLYWCH1 was bioinformatically analyzed and experimentally characterized. FLYWCH1 contains a tandem array of five FLYWCH-type DNA-binding zinc finger motifs. However, no evidence for the presence of a transactivation domain within the coding region of this protein is currently available. Importantly, the FLYWCH motifs are highly conserved within all currently identified members of mammalian FLYWCH1 family of proteins including mouse, chimpanzee, dog, cow, and rat (see chapter 3 of the present study).

## **1.7 Rational and objectives of this study**

### **1.7.1 Rational**

While the role of canonical Wnt/ $\beta$ -catenin-signalling in the development of both normal and malignant tissues is well documented, the molecular basis of these functionally distinct nuclear transcriptional programs is poorly understood. It has long been believed that members of TCFs are sole partners of nuclear  $\beta$ -catenin by which the downstream nuclear events of activated Wnt/ $\beta$ -catenin signalling pathway is mediated (Batlle et al., 2002, Graham et al., 2001, Seidensticker and Behrens, 2000). However, the paradox of  $\beta$ -catenin/TCF interaction was challenged by identification of new strategies for  $\beta$ -catenin-dependent but TCF-independent gene regulation. It has been reported that  $\beta$ -catenin interacts with Prop1, a specific homeodomain factor, rather than members of TCFs to regulate the cell lineage determination during pituitary gland development (Olson et al., 2006). In addition,  $\beta$ -catenin was also found to regulate the pluripotency of ESCs through interaction and enhancement of Oct4 activity independently of TCFs factors (Kelly et al., 2011).

Furthermore, the role of TCF4 in tumour development is still a subject of debate. The conventional Tcf4-knockout mouse, dies shortly after birth, shows a loss of proliferating cells in the small intestine, and it is presumed to lack a functional stem cell compartment (Korinek et al., 1998). This finding led to a general assumption that the formation of TCF4/ $\beta$ -catenin complex is cancer-promoting. However, later studies have found that TCF4 is mutated in several cancers such as colorectal and bladder cancer (Lee et al., 2010, Fukushima et al., 2001, Duval et al., 1999). Moreover, recently a gut conditional depletion of mouse Tcf4 increased cell proliferation leading to colon tumourigenesis (Angus-Hill et al., 2011), giving the notion that Tcf4 may function as a tumour suppressor. In addition, the activity of  $\beta$ -catenin/TCF4 complex is tightly regulated in the nucleus through several co-activators and/or co-repressors (see section 1.2.4). Taken together, these findings changed the classical view of the canonical Wnt signalling pathway and encouraged scientists to investigate the

molecular mechanisms involved in regulation of  $\beta$ -catenin signalling in more detail.

In this view, Dr Nateri and his colleagues has previously hypothesised that the diversity of  $\beta$ -catenin interaction with TCF4 and/or other cofactors may be influenced by  $\beta$ -catenin phosphorylation and may also identify whether or not distinct patterns of transcriptional coregulators are engaged in  $\beta$ -catenin signalling during normal vs. tumour development (Dr Nateri, personal communication). To this end, Dr Nateri's laboratory have recently identified several other transcriptional cofactors, in addition to TCFs, that are possibly interacting with  $\beta$ -catenin in a phosphorylation-dependent and independent manner using a modified yeast-2-hybrid based Ras-Recruitment System (RRS) (Figure 1-8, A & B) (Saadeddin A *et al.* unpublished data). These factors may be required for regulation of the downstream Wnt-target genes by  $\beta$ -catenin/TCF4. Among other candidates, CIP1 ( $\beta$ -Catenin Interacting Protein #1) which corresponds to the human *FLYWCH1* gene drew our attention and further characterized in this work.

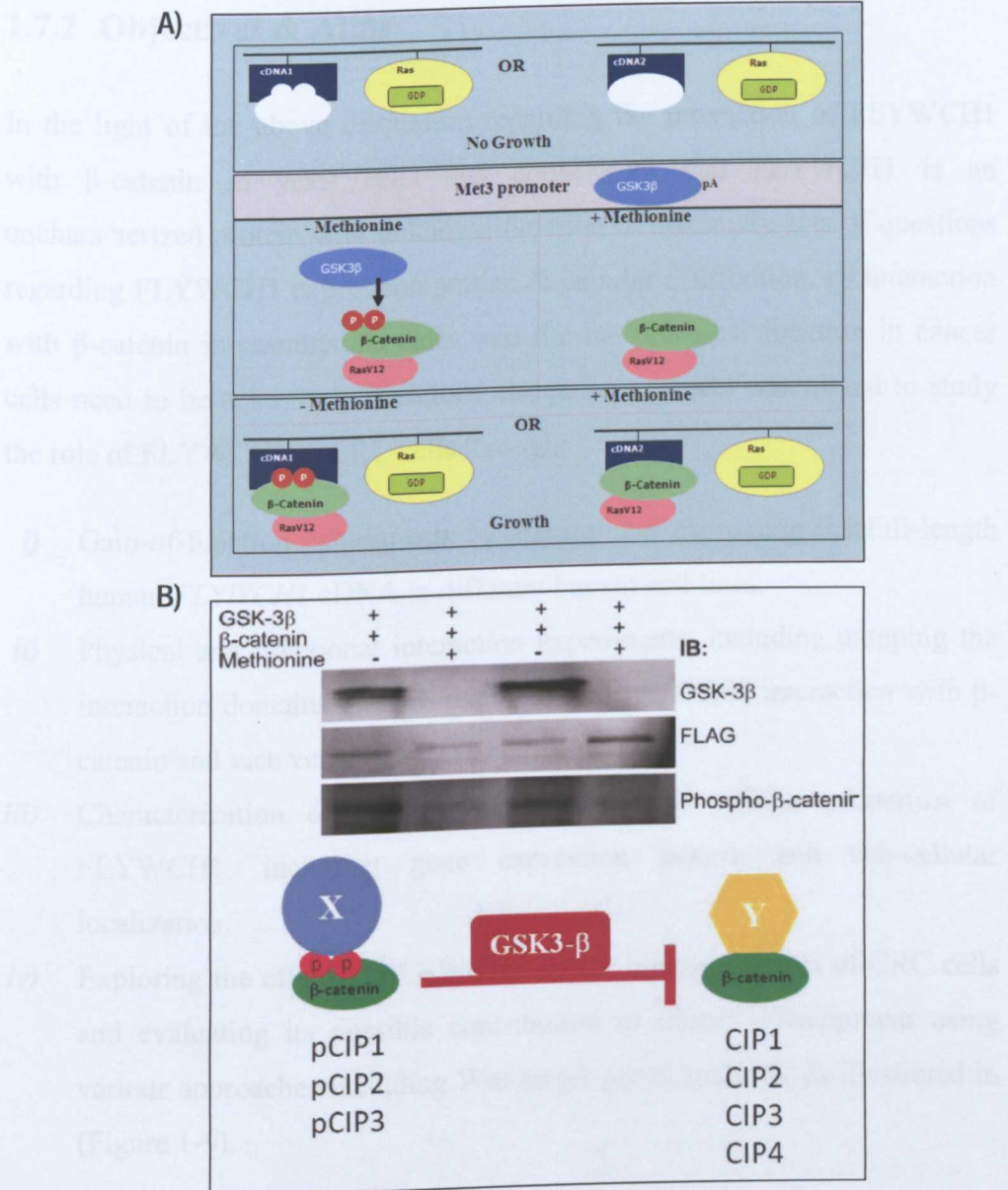


**Figure 1-8: Identification of FLYWCH1 as unphosphorylated  $\beta$ -catenin interacting protein in yeast.** **A)** Schematic representation of the modified yeast two-hybrid Ras Recruitment System (RRS) used to identify new proteins that bind to  $\beta$ -catenin in a phosphorylation-dependent and/or independent manner using mouse embryonic cDNA library (Stratagene). **B)** A Western blot of cell lysates with antibodies to GSK-3 $\beta$ , FLAG and p- $\beta$ -catenin is shown. Phospho- $\beta$ -catenin is induced by withdrawal of methionine. CIP1 ( $\beta$ -catenin Interacting Protein-1), encodes a potential transcription factor with five FLYWCH Zn-finger DNA-binding domains, called "FLYWCH1". It was identified as an interactor that specifically bound to unphosphorylated  $\beta$ -catenin in yeast. Figures are taken from (Saadeddin A *et al.* unpublished data and Dr Nateri, personal communication).

## 1.7.2 Objectives & Aims

In the light of the above discussion regarding the interaction of FLYWCH1 with  $\beta$ -catenin in yeast cells and considering that FLYWCH1 is an uncharacterized protein with unknown function in mammals, lots of questions regarding FLYWCH1 expression pattern & cellular distribution, its interaction with  $\beta$ -catenin in mammalian cells, and the its biological function in cancer cells need to be answered. Therefore, the present project was aimed to study the role of FLYWCH1 in CRC cells through:

- i)* Gain-of-function experiments by cloning and expressing the full-length human *FLYWCH1* cDNA in different human cell lines.
- ii)* Physical and functional interaction experiments, including mapping the interaction domains that are required for FLYWCH1 interaction with  $\beta$ -catenin and vice versa in human cell culture.
- iii)* Characterization of the biochemical and the cellular properties of FLYWCH1, including gene expression pattern and sub-cellular localization.
- iv)* Exploring the effect of FLYWCH1 on the biological traits of CRC cells and evaluating its possible contribution to cancer development using various approaches including Wnt-target genes analyses, as illustrated in (Figure 1-9).

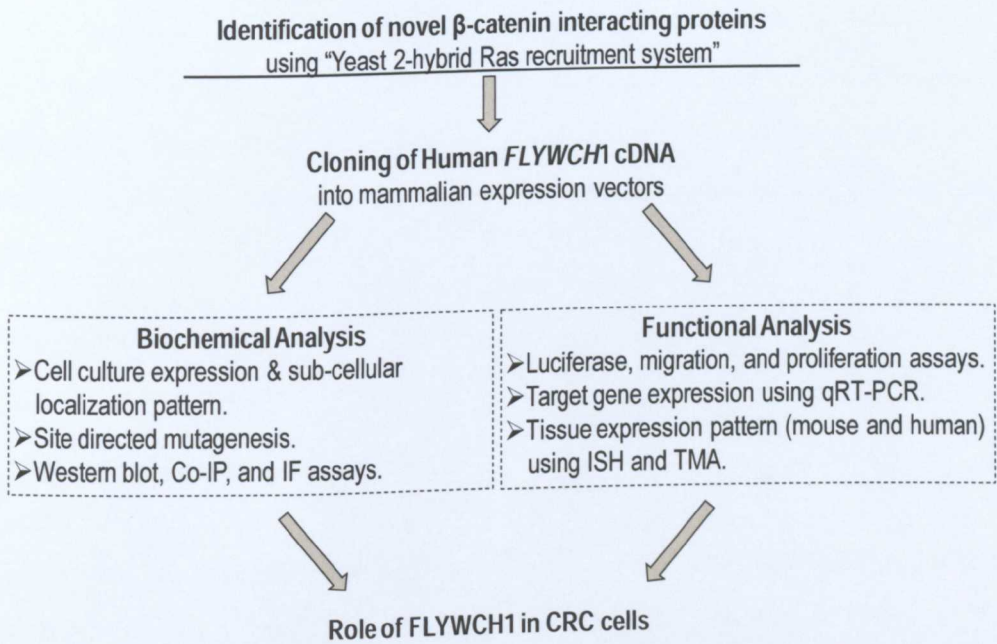


**Figure 1-9: Outline summary of the experimental research plans applied in this study.** The interaction of *FLYWCH1* with  $\beta$ -catenin was originally discovered in Dr Nateri's laboratory in a yeast-2-hybrid assay. In the current work, *FLYWCH1* gene is cloned into different mammalian expression vectors and both biochemically and biologically analysed using various approaches as indicated.

**CHAPTER 2**  
**Materials and Methods**

All procedures were carried out under aseptic condition where appropriate and relevant safety regulations were followed. Standard protocols used throughout the thesis were either developed or followed from previously established templates. Where necessary, modifications were incorporated into the standard protocols for specific use.

## **2.1 Materials**

### **2.1.1 Cell lines**

A transformed human cell line HEK293T (Human Embryonic Kidney), human fibroblast cells (called TIGER cells), and four human CRC cell lines (HCT116, DLD-1, SW620, and SW480) were used throughout this study. HEK293T cell line (Dr Nateri's laboratory) was originally derived from normal human embryonic kidney cells transformed to immortalized cells by sheared DNA from adenovirus type 5 (Graham et al., 1977). These fast-growing cells are relatively easy to transfect with high transfection efficiency and protein yield (Parham et al., 1998, Pham et al., 2006, Soni and Lai, 2011). The human fibroblast cell line (Dr Nateri's laboratory) was a kind gift from professor Gordon Peters (Molecular Oncology Lab, CRUK- London Research Institute). HCT116 adenocarcinoma cell line contains mutation in the  $\beta$ -catenin gene (*CTNNB1*) (Ilyas et al., 1997), while DLD-1, SW480, and SW620 adenocarcinoma cell lines contain different truncated forms of the *APC* gene (Korinek et al., 1997, Morin et al., 1997). SW620 is a metastatic cell line, derived from lymph nodes whereas other cancer cell lines are isolated from primary CRC tumours (Zhuo et al., 2012, Duranton et al., 2003). These cell lines were originally purchased from the American Type Culture Collection (ATCC) (Dr Nateri's laboratory).

The morphology of the cell lines was checked on regular basis for mycoplasma infection and to confirm the correct identity of the cell lines. Whenever required, further investigations for the cell line identities were also performed. All cell lines were maintained as described in (section 2.2.4.1) and used within low passage number (up to 12).

### 2.1.2 Reagents and buffers

All buffers, liquids and solid reagents used for biochemical, molecular and cellular purposes were purchased from Sigma (UK) unless otherwise stated.

Table 2-1: Common non-commercial solutions and buffers used in this study.

Materials	Composition	Stock Conc.	Working Conc.	Storage temp. (°C)
Antibiotics	Kanamycin (50 mg/ml)	1000X	1X	4
	Ampicillin (50 mg/ml)			-20
TSD Buffer 1 (used for chemical competent)	12 g Rubidium-chloride, 9 g Manganese-chloride X2H <sub>2</sub> O, 2.94 g Potassium-acetate, 1.5 g Calcium-chloride X2H <sub>2</sub> O, 150 g Glycerol, dH <sub>2</sub> O to 900 ml, adjust pH to 5.8 then complete to 1	1X	1X	4
TSD Buffer 2 (used for chemical competent)	2.09 g Mops, 1.2 g Rubidium-chloride, 11 g Calcium-chloride X2H <sub>2</sub> O, 150 g Glycerol, dH <sub>2</sub> O to 900 ml, adjust pH to 6.8 then complete to 1 Litre with dH <sub>2</sub> O	1X	1X	4
Agarose gel loading buffer	3 ml glycerol (30%), 25 mg Bromophenol blue (0.25%), dH <sub>2</sub> O to 10 ml	10X	1X	4

SDS-PAGE loading buffer	10% w/v SDS (sodium dodecyl sulfate), 10 mM Beta-mercaptoethanol, 20 % v/v Glycerol, 0.2 M Tris-HCl pH 6.8, 0.05% w/v Bromophenol blue, dH <sub>2</sub> O to the desired volume	5X	1X	-20
SDS-PAGE semi-transfer buffer	30.3 g Trizma-base, 144 g Glycine, dH <sub>2</sub> O to 1Litre	10X	1X	Room temp.
TBS buffer	24.2 g Trizma-base, 80 g Glycine, dH <sub>2</sub> O to 1Litre, pH 7.6	10X	1X	Room temp.
RIPA buffer	150 mM NaCl, 25 mM Tris-HCl pH 7.6, 1% NP-40 , 0.1% SDS, dH <sub>2</sub> O to the desired volume	1X	1X	4
Luria Broth (LB) medium	10 g Tryptone, 5g Yeast extract, 10g NaCl, dH <sub>2</sub> O to 1 Litre, autoclave before use	1X	1X	4
LB Agar medium	Luria Broth with 1% bacteriological agar	1X	1X	4

### 2.1.3 Oligonucleotides

The oligonucleotides used in this study (Table 2-2 to Table 2-6) were designed either manually for standard polymerase chain reaction (PCR) (section 2.2.2.5) or with the help of the primer3 web based primer design tool (Version 0.4.0, available at <http://frodo.wi.mit.edu/primer3/>) for quantitative real time polymerase chain reaction (qRT-PCR) (section 2.2.3.3). The specificity of the primers was checked by blasting the primer sequences against the NCBI human transcript database (<http://www.ncbi.nlm.nih.gov/tools/primer-blast/>) and an example is given in the (Appendix 10). All primers were supplied by Sigma and upon arrival they were spun down and resuspended in an appropriate volume of Sigma distilled water to give a final concentration of 100 micromolars ( $\mu\text{M}$ ) as a stock and stored at  $-20^{\circ}\text{C}$  until use.

**Table 2-2: PCR primers used to amplify the full-length (wild-type) and deletion mutants of MYC-tagged FLYWCH1. Restriction enzyme sites are underlined, MYC-epitopes\* within the forward primers are shown in italic, and the stop codons within the reverse primers are shown in bold. The core primer sequences are highlighted in grey.**

Clones	Primer sequences 5' to 3'	Restriction sites
MYC-FLYWCH1-WT	<b>Forward:</b> GGCTAGCATG <i>GAGCAGAAACTCATCTCTGAAGAAGATCTG</i> <i>GAACAGAAGCTCATCTCTGAGGAAGATCTG</i> ATGCCCCTGCCCGAGCCCA	<i>NheI</i>
	<b>Reverse:</b> TGGATGGCGAGTCCAG <b>TGATAATAG</b> <u>GAATTC</u> GT	<i>EcoRI</i>
MYC-FLYWCH1-M1	<b>Forward:</b> <u>GCTAGC</u> <i>ATGGAGCAGAAACTCATCTCTGAAGAAGATCTG</i> <b>TTCGGGGGCGCCTCCTG</b>	<i>NheI</i>

	<p><b>Reverse:</b>  TGGATGGCGAGTCCCAG<b>TGATAATAG</b><u>GAATTC</u>GT</p>	<i>EcoRI</i>
MYC- FLYWCH1-M2	<p><b>Forward:</b>  GCTAGCATGGAGCAGAAACTCATCTCTGAAGAAGATCTG  CTGCTGCAGGCTGGGCAGGACGG</p>	<i>NheI</i>
	<p><b>Reverse:</b>  TGGATGGCGAGTCCCAG<b>TGATAATAG</b><u>GAATTC</u>GT</p>	<i>EcoRI</i>
MYC- FLYWCH1-M3	<p><b>Forward:</b> GGCTAGCATG  GAGCAGAAACTCATCTCTGAAGAAGATCTG  GAACAGAAGCTCATCTCTGAGGAAGATCTG  ATGCCCTGCCCGAGCCCA</p>	<i>NheI</i>
	<p><b>Reverse:</b>  CTCCGGCCCCTGGAGTTC<b>TGAGAATTC</b></p>	<i>EcoRI</i>
MYC- FLYWCH1-M4	<p><b>Forward:</b> GGCTAGCATG  GAGCAGAAACTCATCTCTGAAGAAGATCTG  GAACAGAAGCTCATCTCTGAGGAAGATCTG  ATGCCCTGCCCGAGCCCA</p>	<i>NheI</i>
	<p><b>Reverse:</b>  CAAGTGGACACGCTGCTC<b>TGAGAATTC</b></p>	<i>EcoRI</i>

\*: The forward primers of M1 and M2 contain one copy of MYC-epitope; however two copies of MYC-epitope were added to the forward primers of the wild-type and deletion mutants M3 and M4.

**Table 2-3: PCR primers used to generate the full-length (wild-type) and deletion mutants of eGFP-FLYWCH1.** Restriction enzyme sites within both forward and reverse primers are underlined, while the stop codons within the reverse primers are shown in bold. The core primer sequences are highlighted in grey. Nucleotides A and C (AC) within the forward primers (shown in bold *Italic*), retains in-frame ORF within the N-terminal eGFP tag.

Clones	Primer sequences 5'to 3'	Restriction sites
eGFP-FLYWCH1-WT	<b>Forward:</b> AGATCT <u>AC</u> ATGCCCCTGCCCGAGCCCA	<i>Bgl</i> II
	<b>Reverse:</b> TGGATGGCGAGTCCCAGTGAT <b>TAATAG</b> <u>GAATTC</u> GT	<i>Eco</i> RI
eGFP-FLYWCH1-M1	<b>Forward:</b> GGC <u>AGATCT</u> <b>AC</b> TTCGGGGGCCGCTCCTG	<i>Bgl</i> II
	<b>Reverse:</b> TGGATGGCGAGTCCCAG <b>TGATAATAG</b> <u>GAATTC</u> GT	<i>Eco</i> RI
eGFP-FLYWCH1-M2	<b>Forward:</b> GGCAGATCT <b>AC</b> CTGCAGGCTGGGCAGGACGG	<i>Bgl</i> II
	<b>Reverse:</b> TGGATGGCGAGTCCCAG <b>TGATAATAG</b> <u>GAATTC</u> GT	<i>Eco</i> RI
eGFP-FLYWCH1-M3	<b>Forward:</b> AGATCT <b>AC</b> ATGCCCCTGCCCGAGCCCA	<i>Bgl</i> II
	<b>Reverse:</b> CTCCGGCCCCTGGAGTTC <b>TGA</b> <u>GAATTC</u>	<i>Eco</i> RI
eGFP-FLYWCH1-M4	<b>Forward:</b> AGATCT <b>AC</b> ATGCCCCTGCCCGAGCCCA	<i>Bgl</i> II
	<b>Reverse:</b> CAAGTGGACACGCTGCTC <b>TGA</b> <u>GAATTC</u>	<i>Eco</i> RI

Table 2-4: PCR primers used to generate the N-terminus, C-terminus, and the middle deletion mutants of FLAG- $\beta$ -catenin. Restriction sites are underlined, FLAG-epitopes within the forward primers and the stop codons within the reverse primers are shown in bold. The overhang complementary sequences of the internal forward primers are shown in italic. The core primer sequences are highlighted in grey.

Clones	Primer sequences 5' to 3'	Restriction sites
FLAG- $\beta$ -catenin- $\Delta$ N	<b>Forward:</b> AAAAGGATCC <u>ATGGATTACAAGGATGACGACGATA</u> <u>AGGAACCATCACAGATGCTGAA</u>	<i>Bam</i> HI
	<b>Reverse:</b> <u>TGGTTTGATACTGACCTGTAA</u> <u>GCGGCCGTTTT</u>	<i>Not</i> I
FLAG- $\beta$ -catenin- $\Delta$ C	<b>Forward:</b> AAAAGGATCC <u>ATGGATTACAAGGATGACGACGATA</u> <u>AGATGGCTACTCAAGCTGATTTG</u>	<i>Bam</i> HI
	<b>Reverse:</b> <u>CCATTCCATTGTTTGTGCAGTAA</u> <u>GCGGCCGCTTTT</u>	<i>Not</i> I
FLAG- $\beta$ -catenin-MD1	<b>Forward (internal):</b> <i>GATGCTGCTCATCCCACT</i> <u>GGTGGGCTGCAGAAAAT</u> <u>GG</u>	....
	<b>Reverse (internal):</b> <u>GATGCTGCTCATCCCACT</u>	....
FLAG- $\beta$ -catenin-MD2	<b>Forward (internal):</b> <i>TTACATCAAGAAGGAGCT</i> <u>GCAGTTCGCCTTCACTA</u> <u>TGGA</u>	....
	<b>Reverse (internal):</b> <u>CCTTTTATTACATCAAGAAGGAGCT</u>	....
FLAG- $\beta$ -catenin-MD3	<b>Forward (internal):</b> <i>GACCAGCCGACACCAAC</i> <u>CCTAGCTATCGTTCTTTTC</u> <u>AC</u>	....
	<b>Reverse (internal):</b> <u>CGTCATCTGACCAGCCGACACCAA</u>	....

All deletions (MD1, MD2, and MD3)	<b>Forward (external) :</b> AAAAGGATCCATGGATTACAAGGATGACGACGATA AGATGGCTACTCAAGCTGATTTG	BamHI
	<b>Reverse (external) :</b> TGGTTTGATACTGACCTGTAA <u>GCGGCCGCTTTT</u>	NotI

Table 2-5: PCR primers used to amplify mRNA of several  $\beta$ -catenin target genes by qRT-PCR.

Target genes	Primer sequences 5'- 3'
<i>c-Jun</i>	<b>Forward:</b> ACCCCAAGATCCTGAAACAG <b>Reverse:</b> ATCAGGCGCTCCAGCTCG
<i>c-Myc</i>	<b>Forward:</b> AAAACCAGCAGCCTCCCGC <b>Reverse:</b> GGCTGCAGCTCGCTCTGC
<i>cyclin D1</i>	<b>Forward:</b> GCTGGAGGTCTGCGAGGA <b>Reverse:</b> CATCTTAGAGGCCACGAACA
<i>CDH1</i> (E-cadherin)	<b>Forward:</b> GTCTGTAGGAAGGCACAGCCTGTCTG <b>Reverse:</b> AGGACCAGGACTTTGACTTGAGC
<i>EPHB2</i> (EphB2)	<b>Forward:</b> AGGATTACCCTGTGGTGGTC <b>Reverse:</b> TACAACGCCACAGCCATAAA
<i>EPHA4</i> (EphA4)	<b>Forward:</b> CGACAAAGAGCGTTTCATCA <b>Reverse:</b> GCTTCACCCAAGTGGACATT
<i>ENFB1</i> (ephrin-B1)	<b>Forward:</b> GGCAAGCATGAGACTGTGAA <b>Reverse:</b> ACTCCAAGGTGGCATTGTTC
<i>ENFB2</i> (ephrin-B2)	<b>Forward:</b> CTGCTGGATCAACCAGGAAT <b>Reverse:</b> TCTAGCACAGACGGCAACAG

Table 2-6 : PCR primers used to amplify the entire sequence and fragments of the exogenous genome-integrated *FLYWCH1* from the genomic DNA extract of HEK293T and HCT116 stable cell lines. Stop codons within the reverse primer that used for cloning (Full-FLYWCH1-Rev-C) are shown in bold, while the restriction enzyme site is underlined. The core primer sequence is highlighted in grey.

Primer use		Primer sequence 5' to 3'	Restriction site
Amplification of the genome-integrated eGFP-FLYWCH1	All PCR amplifications	<b>Forward (GFP-Fwd) :</b> CATGGTCCTGCTGGAGTTCGTG	-----
	N-terminal domain (1.0 Kb)	<b>Reverse (FLYWCH1-Rev990) :</b> CTGTGATGCGTGGGCACTGC	-----
	Full-length (2.2 Kb)	<b>Reverse (Full-FLYWCH1-Rev) :</b> TGGATGGCGAGTCCCAGTGA	-----
	Full-length for cloning (2.2 Kb)	<b>Reverse (Full-FLYWCH1-Rev-C) :</b> <u>TGGATGGCGAGTCCCAGT</u> <b>GATAATAG</b> <u>GAATTCGT</u>	<i>EcoRI</i>
	N-terminal + part of the C-terminal domain (1.4 Kb)	<b>Reverse (FLYWCH1-Rev1446) :</b> CGTGGTCACTGCCACCCGCCCGAC	-----

### 2.1.4 Antibodies

Different types of primary and secondary antibodies were used throughout this study for both Western blotting and immunofluorescent analysis. Details about the source of these antibodies and the dilution factors used are given in (Table 2-7).

Table 2-7: List of primary and secondary antibodies used for Western blotting and Immunofluorescent analysis. "NA" means not applicable.

Primary antibodies	Source & catalogue number	Dilution used	
		WB	IF
FLAG	Monoclonal Mouse ANTI-FLAG® M2 antibody (Sigma, # F1804)	1:1000	NA
MYC (9E10)	Polyclonal Mouse antibody (Sigma)	1:1000	NA
GFP	Polyclonal Mouse antibody (Invitrogen)	1:1000	NA
FLYWCH1*	Mouse polyclonal to FLYWCH1 (Abcam, # ab69284)	1:500	1:50
E-Cadherin	Monoclonal Mouse IgG2a, κ (BD Biosciences, # 610181)	1:5000	1:100
β-Catenin	Monoclonal Mouse IgG1 (BD Biosciences, # 610154)	1:2000	1:100
ZEB2, [SIP1 (H-260)]	Polyclonal Rabbit antibody (Santa Cruz, # SC-48789)	1:1000	1:50
Vimentin (RV202)	Mouse monoclonal antibody (Santa Cruz, # sc-32322)	1:1000	1:100
β-actin	Mouse monoclonal (AC-15) to beta Actin (Abcam, # ab6276)	1:10,000	NA
Secondary antibodies	Source & catalogue number	Dilution used	
		WB	IF
Goat anti-mouse IgG-HRP	(Santa Cruz, # sc-2005)	1:5000	NA
goat anti-rabbit IgG-HRP	(Santa Cruz, # sc-2004)	1:5000	NA
Rabbit anti-Goat IgG-HRP	(DakoCytomatio, # P 0160)	1:2000	NA
Rabbit Anti-Mouse IgG (H+L)	Alexa Fluor® 488 (Invitrogen, # A11059)	NA	1:400
Goat Anti-Mouse IgG (H+L)	Alexa Fluor® 594 (Invitrogen, # A11005)	NA	1:400
Goat Anti-Rabbit IgG (H+L)	Alexa Fluor® 594 (Invitrogen, # A11037)	NA	1:400

\*: FLYWCH1 antibody was purchased from Abcam, however, this antibody was not widely used in this project due to its low detection efficiency and none economical usage (for more detail see the discussion part of chapter 3).

## **2.2 Methods**

### **2.2.1 DNA preparation and manipulation**

#### ***2.2.1.1 DNA transformation and amplification***

Plasmid DNAs were transformed into *Escherichia coli* (*E. coli*); either commercially available XL1-Blue (XL1-B) competent cells (Stratagene, # 200249) or chemically prepared competent cells from DH5 $\alpha$  and XL1-Blue bacterial cells (see section 2.2.1.2). In both cases, 50 to 500 ng DNA was mixed with 50  $\mu$ l competent cells in 1.5 ml sterile eppendorf tubes and incubated on ice for 30 minutes. The mixture was heat shocked at 42°C for 50 seconds then chilled on ice for 2-3 minutes. 500  $\mu$ l of Luria Broth (LB) medium (Table 2-1) was added to the tubes and incubated horizontally at 37°C for 1 hour in a shaking incubator. A small amount (15-20  $\mu$ l) of this culture was spread on plates of LB agar containing 1X concentration of a suitable antibiotic (Table 2-1). Plates were incubated overnight at 37°C in a bacterial growth incubator. A single colony was selected and recultured in LB medium containing 1X concentration of appropriate antibiotic. The broth culture was incubated overnight at 37°C in a shaking incubator then used for DNA isolation. Miniprep Kit (section 2.2.1.3) was used for isolation of small amounts of DNA, whereas, Midiprep Kit was used for isolation of large amounts of DNA (section 2.2.1.5).

### ***2.2.1.2 Chemical preparation of bacterial competent cells***

Chemical competent cells were prepared from strains of *E. coli* either XL1Blue or DH5 $\alpha$  under a sterile condition as follow: A pre-culture of cells was prepared by incubating 10  $\mu$ l XL1Blue or DH5 $\alpha$  in 5 ml LB medium at 37°C in a shaking incubator. After an overnight incubation 2 ml of the pre-culture was added to 500 ml LB medium and incubated at 37°C in a shaking incubator. The cell density was determined by the optical density (OD) readings of the culture using S2100 Diode Array Spectrophotometer (biochrom, UK) at 600 nm. Once the OD reading reached 0.5-0.6, the culture was split into two sterile bottles and incubated on ice for 30 minutes then centrifuged at 2500 rpm for 12 minutes. The pellet of each bottle was resuspended in 20 ml TSD buffer1 (Table 2-1). The whole suspension was then transferred into a 50 ml Falcon tube and incubated on ice for 15 minutes followed by centrifugation at 2500 rpm for 9 minutes. The pellet was resuspended in 7 ml TSD buffer2 (Table 2-1). Immediately after resuspension, the competent cells were aliquoted into eppendorf tubes and stored at -80°C until use.

### ***2.2.1.3 DNA isolation using Miniprep kit***

Small amounts of DNA (up to 20  $\mu$ g of total DNA) were prepared using GenElute Plasmid Miniprep Kit (Sigma, # PLN350). An optimized manufacture's protocol applied in this study is illustrated below (Figure 2-1).

2.2.1.4 DNA isolation using

Manual Miniprep protocol, a

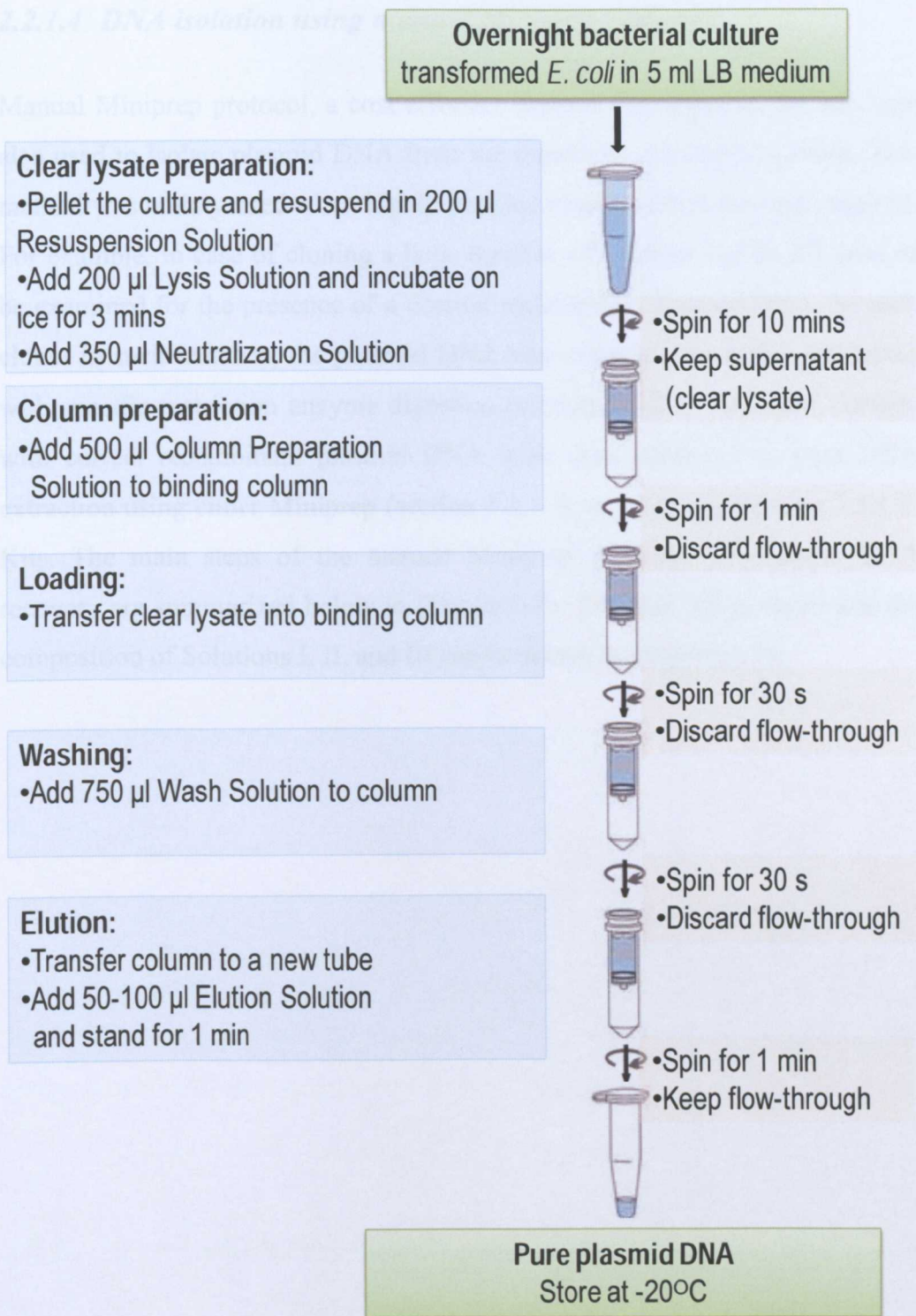


**Figure 2-1: Isolation of plasmid DNA using commercial Miniprep kit.** Steps of pure plasmid DNA isolation using Sigma GenElute Plasmid Miniprep Kit. All centrifugations were performed at 13,000 rpm using a micro-centrifuge at 4°C.

#### ***2.2.1.4 DNA isolation using manual Miniprep protocol***

Manual Miniprep protocol, a cost effective method developed in our lab, was also used to isolate plasmid DNA from the transformed bacterial culture. This method was mainly used when highly purified plasmid DNA was not required. For example, in case of cloning a huge number of colonies (up to 20) need to be examined for the presence of a desired recombinant plasmid DNA for each clone. In such instance, the plasmid DNA was extracted manually and tested with specific restriction enzyme digestion (section 2.2.2.1). Bacterial cultures with correct recombinant plasmid DNA were then subjected to pure DNA extraction using either Miniprep (section 2.2.1.3) or Midiprep (section 2.2.1.5) Kits. The main steps of the manual Miniprep protocol for plasmid DNA recovery are summarized below in (Figure 2-2). The detailed protocol and the composition of Solutions I, II, and III can be found in (*Appendix 2*).

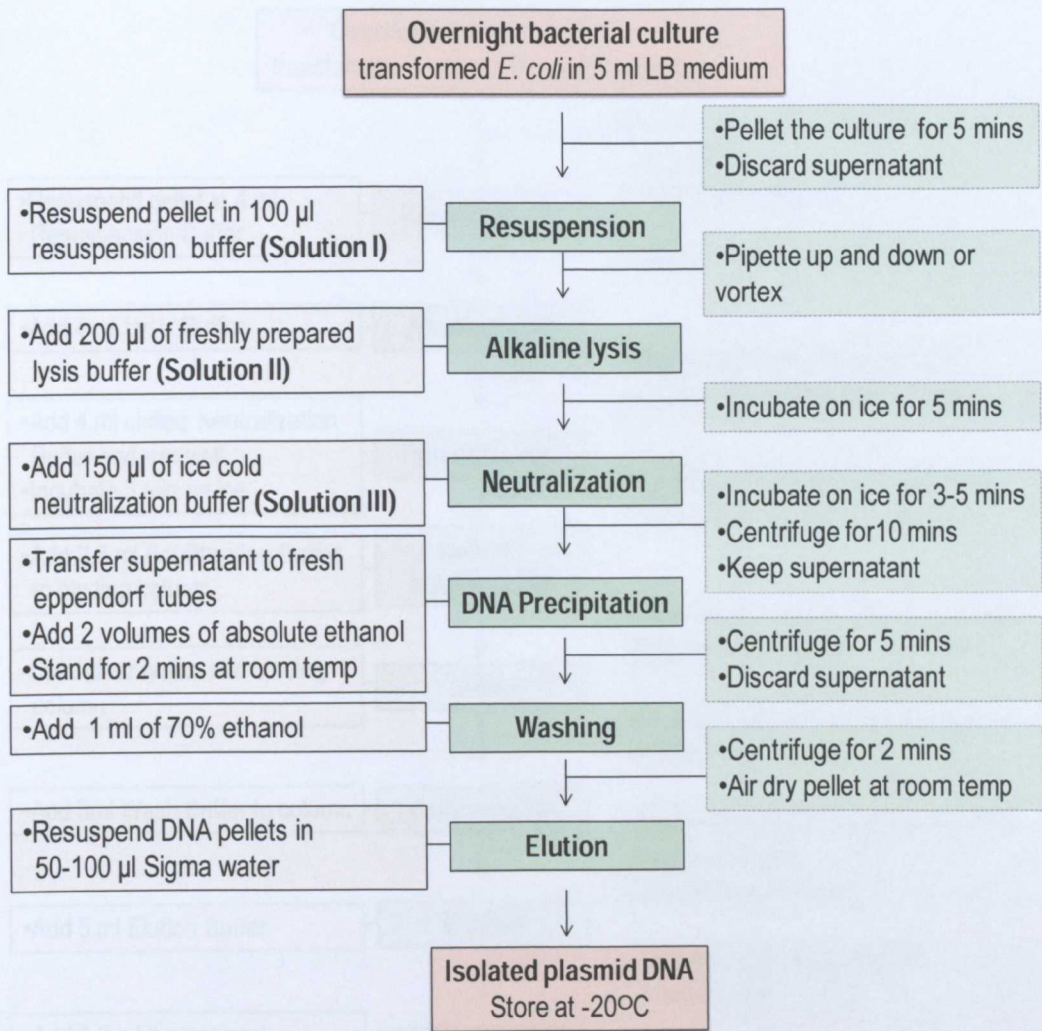
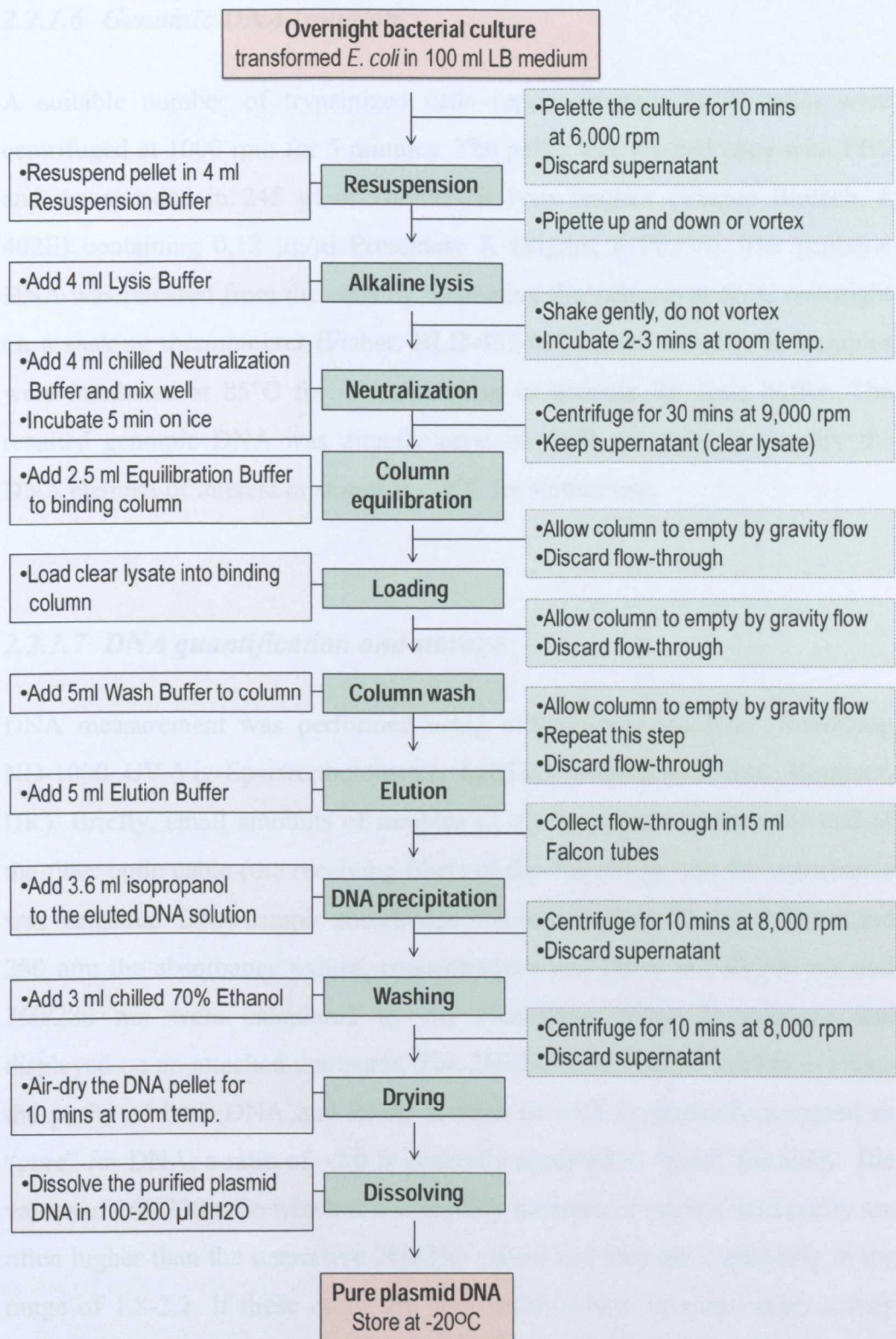


Figure 2-2: Isolation of plasmid DNA using manual Miniprep protocol. Steps of plasmid DNA recovery using a manual Miniprep protocol. All centrifugations were performed at 13,000 rpm using a micro-centrifuge at 4°C.

### 2.2.1.5 DNA isolation using Midiprep kit

Large amounts of DNA (up to 300 µg of total DNA) were isolated using Genopure Plasmid Midi Kit (Roche, # 03143414001) following the manufacture’s instruction as illustrated below (Figure 2-3).



**Figure 2-3: Isolation of plasmid DNA using Miniprep kit.** Steps of pure plasmid DNA purification using Roche Genopure Plasmid Midi Kit. All centrifugations were performed at 2-8°C using an ultra-centrifuge at speeds indicated.

### **2.2.1.6 Genomic DNA isolation**

A suitable number of trypsinized cells (approximately  $2 \times 10^6$  cells) were centrifuged at 1000 rpm for 5 minutes. The pellet was washed once with PBS and resuspended in 245  $\mu$ l of DirectPCR lysis reagent (Viagen Biotech, # 402E) containing 0.12  $\mu$ g/ $\mu$ l Proteinase K (Sigma, # P6556). The genomic DNA was released from the cells by incubating the samples at 56°C overnight on a shaking thermomixer (Fisher, BLD-455-010C). At the end, the samples were incubated at 85°C for 45 minutes to in activate the lysis buffer. The resulted genomic DNA was directly used for PCR reactions to amplify the DNA element of interest or stored at -20°C for further use.

### **2.2.1.7 DNA quantification and storage**

DNA measurement was performed using a NanoDrop machine (NanoDrop ND-1000 UV-Vis Spectrophotometer, LabTech International Ltd, Ringmer, UK). Briefly, small amounts of samples (2  $\mu$ l) were pipetted onto the end of the fiber optic cable (the receiving fiber) of the NanoDrop and the absorbance was measured. DNA sample absorbance was measured at 230 nm, 260 nm and 280 nm; the absorbance values, concentrations and ratios at 230/260 nm and 260/280 nm were calculated by the NanoDrop ND-1000 software and displayed on an attached computer. The 260/280 ratio can be used to evaluate the purity of both DNA and RNA. A ratio of  $\sim 1.8$  is generally accepted as “pure” for DNA; a ratio of  $\sim 2.0$  is generally accepted as “pure” for RNA. The values of 260/230 ratio which is a secondary measure of nucleic acid purity are often higher than the respective 260/280 values and they are commonly in the range of 1.8-2.2. If these ratios are appreciably lower in either case, it may indicate the presence of co-purified contaminants. More detail can be found in the user manual provided by the manufacture. All DNA samples were stored at -20°C until use.

## **2.2.2 Gene cloning techniques**

### ***2.2.2.1 Restriction enzyme digestion***

Plasmid DNAs were digested using specific Restriction Endonucleases purchased from NEW ENGLAND BioLabs (NEB) according to manufacturer's guidelines. Generally, 1  $\mu$ l of a restriction enzyme was used to digest 1  $\mu$ g of a plasmid DNA within 2-3 hours in a 20  $\mu$ l reaction containing 1X NEB buffer. Suitable NEB buffer and incubation temperature were used for each particular restriction enzyme according to the manufacturer's instruction. The efficiency and the specificity of these enzymes were analyzed by running digested DNA samples on 1% agarose gel.

### ***2.2.2.2 Agarose gel electrophoresis***

1% agarose gel, which was commonly used for DNA electrophoresis, was prepared by adding 1 gm of agarose powder (Eurogentec, # EP-0010-05) to 100 ml of 1X Tris Acetate EDTA (TAE) buffer (Sigma, # T9650). The powder was dissolved and homogenized by gentle shake and heat using a microwave for 1-2 minutes. The melted gel was allowed to cool down at room temperature to 45-50°C then a small amount of Ethidium bromide (EtBr) (10-15  $\mu$ l) (Sigma, # E1385) was added and mixed well. The final concentration of the EtBr in the gel should be 0.05  $\mu$ g/ $\mu$ l. Meanwhile, a gel apparatus with an appropriate comb was prepared. The gel was poured into the apparatus and left at room temperature to solidify.

DNA samples were prepared by adding a small amount of 10X loading buffer (the final concentration of the loading buffer should be 1X). Samples were marked carefully and loaded into the gel in a desired order. DNA markers; either "1 Kb DNA ladder" (Invitrogen, #15615-016) or "DNA LADDER, DIRECTLOAD, 1KB" (Sigma, # D 3937) were also loaded with each set of DNA samples to determine the size of DNA molecules (Figure 2-4). Generally, gels were run at 100 volts for 50 minutes using 1X TAE solution as running

buffer. Bands of digested plasmid DNAs or PCR products were visualized and captured using an ultraviolet transilluminator unit (UVidoc).

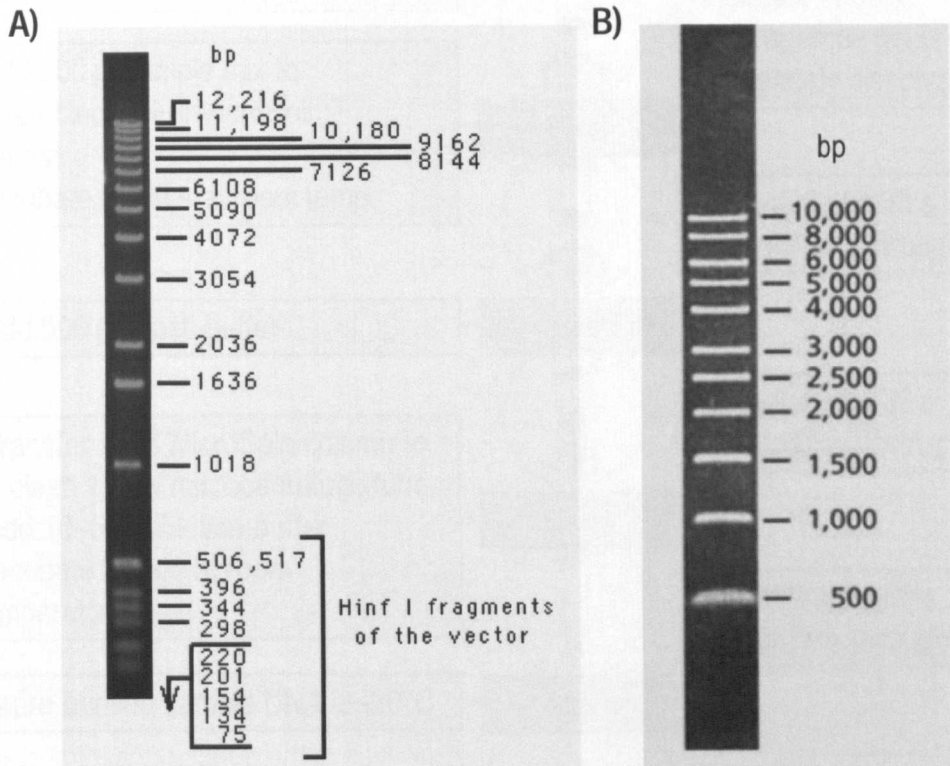


**Figure 2-4: DNA markers used for agarose gel electrophoresis.** A) Represents the 1 Kb DNA ladder from Invitrogen and B) Represents the 1KB DNA LADDER, DIRECTLOAD from Sigma. Both markers were used to determine the size of DNA molecules on agarose gel.

### **2.2.2.3 DNA extraction from agarose gel**

Desired bands of DNA with expected molecular sizes were excised from the gel under Ultra Violet (UV) light. The UV exposure time should be as short as possible to avoid DNA damage. The agarose gel slices were transferred into clean eppendorf tubes and the DNA molecules were purified using GFX<sup>TM</sup> PCR DNA and Gel Band Purification Kit (GE Healthcare, # 28-9034-70) following the manufacturer's protocol which can be summarized as below (Figure 2-5).

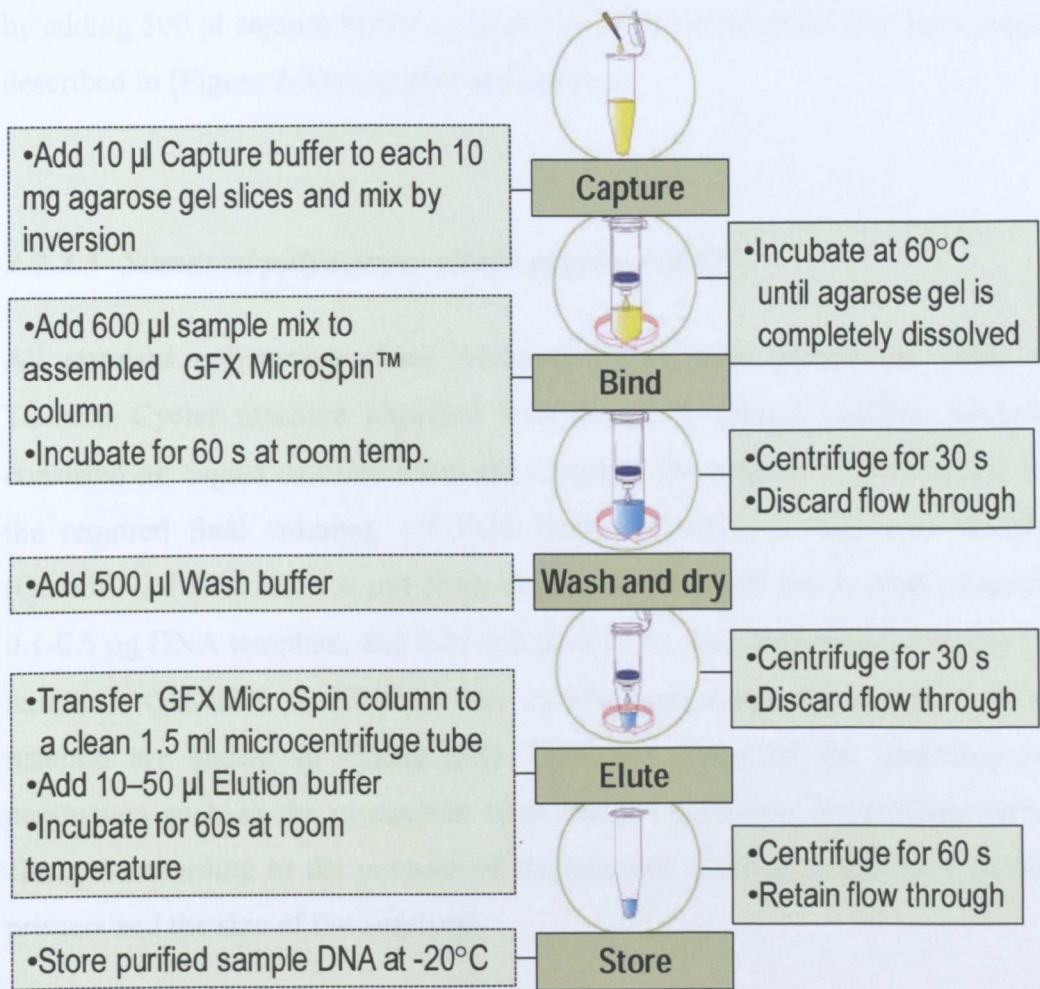


**Figure 2-5: DNA extraction from agarose gel.** Steps of DNA extraction from agarose gel using GE Healthcare GFX™ PCR DNA and Gel Band Purification Kit. All centrifugations were performed at 16,000 rcf using a micro-centrifuge at room temperature.

#### 2.2.2.4 DNA extraction from restriction enzyme digestions

The same protocol described above in (section 2.2.2.3) is used for DNA extraction from restriction enzyme digestions. According to the manufacturer's instruction, the size of the DNA molecules that can be retained by the GFX™ Purification Kit is restricted between 50 bp and 10 kb. Thus, if the unwanted digested DNA fragments were smaller than 50 bp, DNA samples were not run on agarose gel in order to be separated from the undesired DNA fragments. Alternatively, DNA molecules in an enzymatic reaction were directly purified

by adding 500 µl capture buffer to up to 100 µl of the reaction. The same steps described in (Figure 2-5) were also applied here.

**2.2.2.5 Standard polymerase chain reaction (PCR)**

All standard polymerase chain reactions (PCR) were carried out using a Thermal Cycler machine (Applied Biosystem). A typical reaction mixture consisted of: Sigma distilled water (to complete the volume of the reaction to the required final volume), 1X PCR Buffer (QIAGEN), 0.25 mM dNTPs (QIAGEN, # 201913), 1.0 µM from each of the forward and reverse primers, 0.1-0.5 µg DNA template, and 0.25-1.0 µl of DNA Taq-Polymerase enzyme (5 units/µl) (QIAGEN, # 201205). The cycling parameters for a typical PCR reaction are shown in (Table 2-8). However, some of the amplification parameters such as the elongation time and the annealing temperature were changed according to the purpose of the reaction, melting temperature of the primers and the size of the amplicon.

**Table 2-8: Cycling parameters for the standard polymerase chain reaction.**

Cycle Steps	Temperature (°C)	Time	Number of cycles
Initial Denaturation	95	5.0 minutes	1
Denaturation	95	20 seconds	35
Annealing	55	20 seconds	
Extension	72	1.0 minute	
Final Extension	72	7.0 minutes	1
Cooling	4	∞	–

### **2.2.2.6 Overlapping PCR**

The overlapping PCR strategy was used in this study to generate specific middle deletions within the sequence of the gene (cDNA) of interest such as  $\beta$ -catenin and FLYWCH1. The overlapping PCR was performed in two steps; **step one** was aiming to amplify specific nucleotide sequences of the gene of interest in two fragments (A & B), whereas **step two** was aiming to fuse these two fragments in-frame (without making any frame-shift mutations) leaving a distinct sequence of nucleotides (fragment C) to be deleted as summarized in (Figure 2-6).

The primers mentioned here are just examples to outline the overlapping PCR strategy. More details about the gene of interest and the primer sequences used can be found in this Chapter (section 2.1.3) and in Chapter 4 (section 4.2.4.2 & Figure 4-10). In general, for each deletion made, specific external and internal primers have been used. OL1-F (a forward external primer) together with OL4-R (a reverse internal primer) were used to amplify the N-terminal fragment (fragment A). Similarly, OL2-R (a reverse external primer) and OL3-F (a forward internal primer) were used to amplify the C-terminal fragment (fragment B). The internal primers (OL3-F and OL2-R) share complementary sequences which help to modify (mutate/delete) the region of interest and facilitate the recombination of the amplified fragments in one unit as illustrated in (Figure 2-6). Suitable restriction sites were also engineered to the 5' and 3'-ends of the external primers for cloning.

The PCR cycling parameters shown in (Table 2-8) were also applied here to amplify the desired fragments. Minor changes have been made to the elongation time and annealing temperature according to the size of the amplicon and the annealing temperature of the primers.

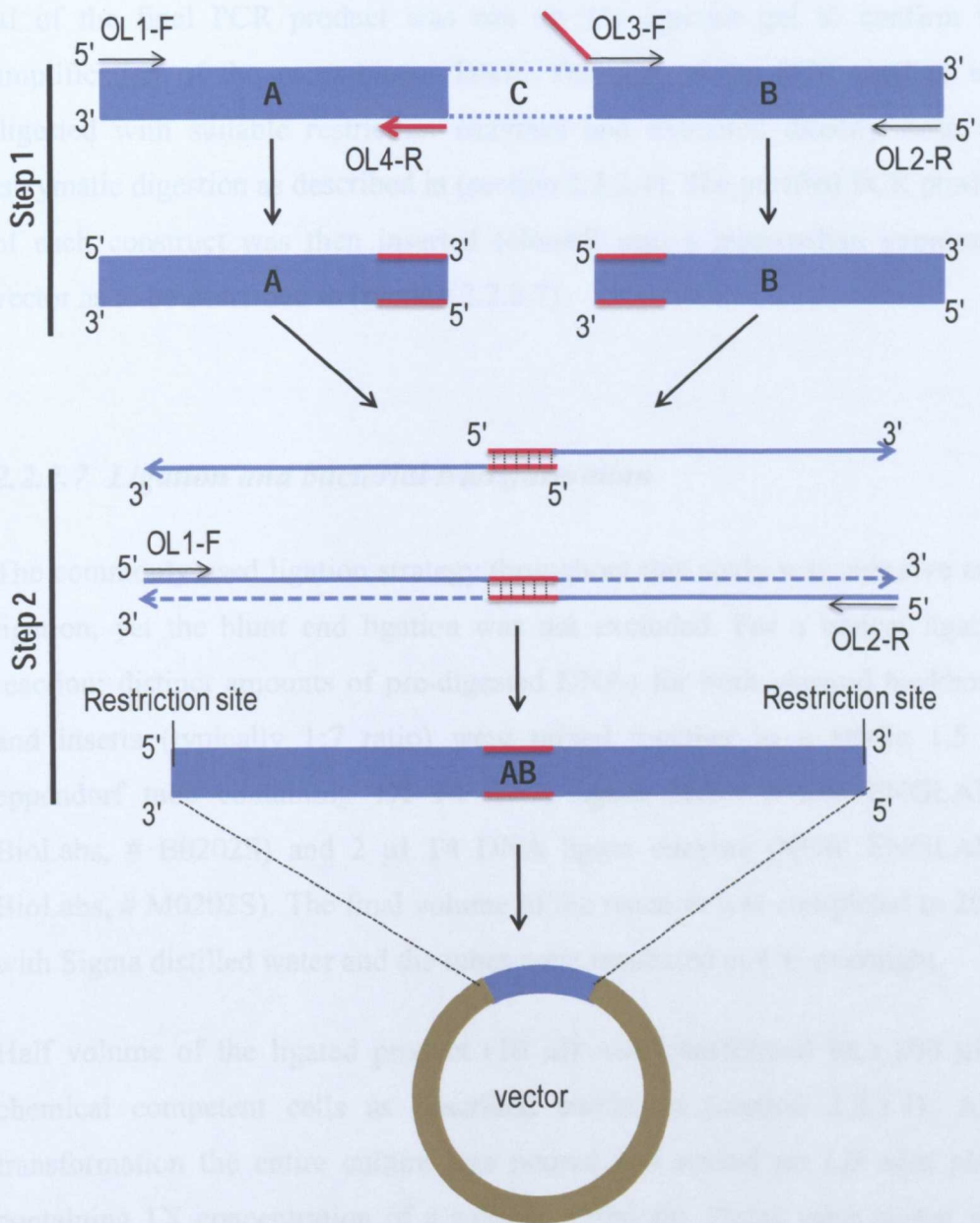


**Figure 2-6: Overlapping PCR strategy.** A schematic presentation of overlapping PCR technique; in step 1, both N-terminal and C-terminal domains (fragments A and B, respectively) were specifically amplified and used as a template for step 2 of the PCR to generate a recombinant gene (cDNA) lacking a distinct nucleotide sequence (fragment C) as indicated.

The PCR product of step one was electrophoresed on 1% agarose gel and the predicted DNA bands were extracted from the agarose gel as outlined in (section 2.2.2.3). Small amounts of the purified PCR products (both fragment A and B) were used as a template for the PCR reaction in step two. Lastly, 2-3

$\mu\text{l}$  of the final PCR product was run on 1% agarose gel to confirm the amplification of the recombinant DNA. The rest of the PCR product was digested with suitable restriction enzymes and extracted directly from the enzymatic digestion as described in (section 2.2.2.4). The purified PCR product of each construct was then inserted (cloned) into a mammalian expression vector as to be described in (section 2.2.2.7).

### ***2.2.2.7 Ligation and bacterial transformation***

The commonly used ligation strategy throughout this study was cohesive ends ligation, yet the blunt end ligation was not excluded. For a typical ligation reaction; distinct amounts of pre-digested DNAs for both plasmid backbones and inserts (typically 1:7 ratio) were mixed together in a sterile 1.5 ml eppendorf tube containing 1X T4 DNA ligase buffer (NEW ENGLAND BioLabs, # B0202S) and 2  $\mu\text{l}$  T4 DNA ligase enzyme (NEW ENGLAND BioLabs, # M0202S). The final volume of the reaction was completed to 20  $\mu\text{l}$  with Sigma distilled water and the tubes were incubated at 4°C overnight.

Half volume of the ligated product (10  $\mu\text{l}$ ) was transformed into 100  $\mu\text{l}$  of chemical competent cells as described earlier in (section 2.2.1.1). After transformation the entire culture was poured and spread on LB agar plates containing 1X concentration of a suitable antibiotic. Plates were closed with their lids and left at room temperature for 5-10 minutes to absorb the liquid culture then incubated at 37°C for 24 hours. Several individual colonies (typically 10-12 colonies) were selected and re-grown in LB media. Finally, the plasmid DNA was manually extracted from the bacterial cultures using a manual plasmid DNA extraction protocol (section 2.2.1.4).

### **2.2.2.8 Clone verification**

The incorporation of a right insert into a backbone vector was initially verified using enzymatic digestions. Some constructs were further verified through automated DNA sequencing (Sequencing Facilities, Queen's Medical Centre, Nottingham University). The protein expression of all plasmid clones were also confirmed by Western blotting analysis. The details of specific enzymes and antibodies used to verify each clone is mentioned in Chapter 4 of this thesis.

## **2.2.3 Ribonucleic acid (RNA) isolation and reverse transcription**

### **2.2.3.1 RNA isolation**

The total RNA was extracted from an appropriate amount of cells using RNeasy Mini Kit (QIAGEN, # 74104). Cells were washed once with PBS and lysed (either directly in the plates or after trypsinization) following the manufacturer's protocol as illustrated below (Figure 2-7).

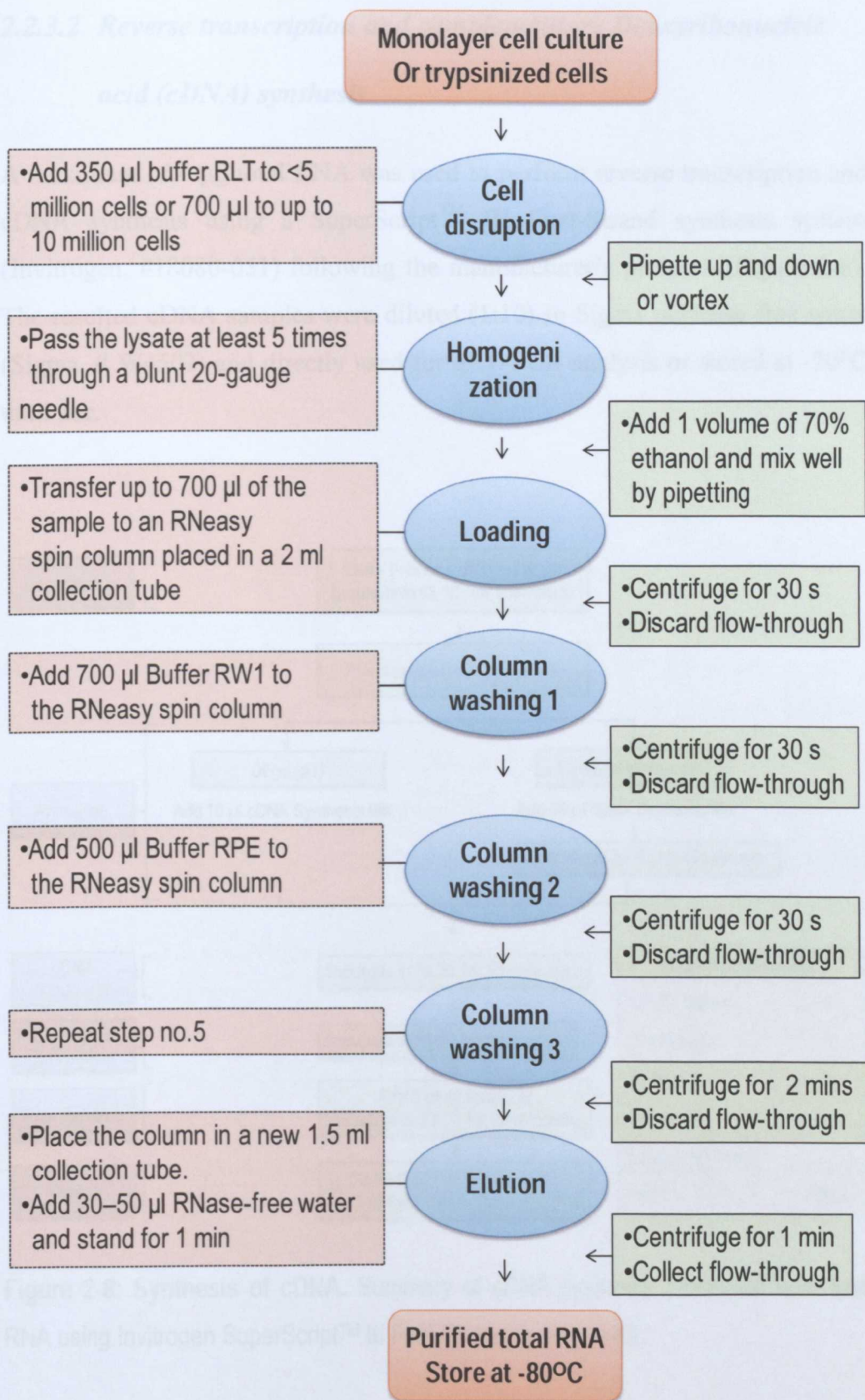


**Figure 2-7: Total RNA isolation.** Summary of total RNA isolation/purification procedure using Qiagen RNeasy Mini Kit. All centrifugations were performed at 8,000 rcf using a micro-centrifuge at room temperature.

2.2.3.2 Reverse transcription and complementary Deoxyribonucleic acid (cDNA) synthesis

A maximum of 4 µg total RNA was used to perform reverse transcription and cDNA synthesis using a SuperScript™ III First-Strand synthesis system (Invitrogen, #18080-051) following the manufacturer’s protocol (Figure 2-8). The resulted cDNA samples were diluted (1:10) in Sigma nuclease free water (Sigma, # W4502) and directly used for qRT-PCR analysis or stored at -20°C until use.

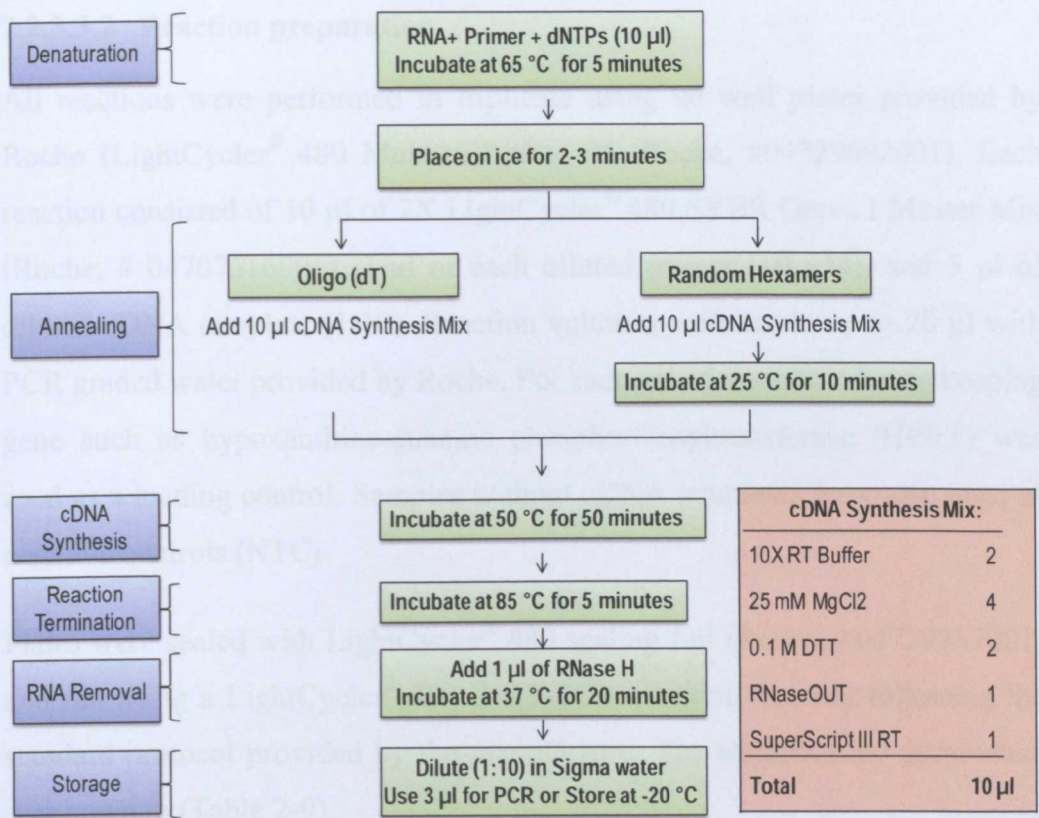


Figure 2-8: Synthesis of cDNA. Summary of cDNA synthesis procedure from total RNA using Invitrogen SuperScript™ III First-Strand synthesis Kit.

### **2.2.3.3 Quantitative real time polymerase chain reaction (qRT-PCR)**

#### **2.2.3.3.1 Primer design**

The primer3 web based primer design tool (Version 0.4.0) available at <http://frodo.wi.mit.edu/primer3/> was used to design primers for qRT-PCR. Generally, primers were designed so that a pair of primers for a specific gene of interest was selected in two different exons and the size of the amplicon was limited to 100-200 base pairs. Moreover, the specificity of the primers was checked by blasting as outlined in (section 2.1.3).

#### **2.2.3.3.2 Reaction preparation**

All reactions were performed in triplicate using 96 well plates provided by Roche (LightCycler® 480 Multiwell plate 96, Roche, #04729692001). Each reaction consisted of 10 µl of 2X LightCycler® 480 SYBR Green I Master Mix (Roche, # 04707516001), 2 µl of each diluted primer (10 µM), and 5 µl of diluted cDNA template (1/10). Reaction volumes were made up to 20 µl with PCR graded water provided by Roche. For each set of reaction a house keeping gene such as hypoxanthine-guanine phosphoribosyltransferase (HPRT) was used as a loading control. Samples without cDNA templates were also used as negative controls (NTC).

Plates were sealed with LightCycler® 480 sealing foil (Roche, #04729757001) and run using a LightCycler® 480 II RT-PCR machine (Roche) following the standard protocol provided by the manufacture. The amplification parameters are shown in (Table 2-9).

Table 2-9: Amplification parameters used for the quantitative real time polymerase chain reaction (qRT-PCR).

Cycle Steps	Temperature (°C)	Time	Number of cycles
Pre-incubation	95	5.0 minutes	1
Amplification	95	10 seconds	40
	55	10 seconds	
	72	10 seconds	
Melting curve	95	5.0 seconds	1
	65	1.0 minutes	
	97	—	
Cooling	40	30 seconds	1

#### 2.2.3.3.3 Data analysis

The qRT-PCR data was analyzed using the comparative CT ( $2^{-\Delta\Delta CT}$ ) method as described previously (Livak and Schmittgen, 2001). CT values for each reaction were first read by the LightCycler<sup>®</sup> 480 software (Roche, release 1.5.0) then exported to a Microsoft Excel file for further calculation and statistical analysis.

## 2.2.4 General tissue culture techniques

All tissue culture works were performed in a class II cabinet hood under aseptic condition. Separate hood and incubator were used for primary cell cultures.

### 2.2.4.1 Human cell culture

The human cell lines described in (section 2.1.1) were maintained in RPMI medium (Roswell Park Memorial Institute medium, RPMI-1640, Sigma, # R0883) supplemented with 10% Fetal Bovine Serum (FBS) (Sigma, # F7524),

1% Penicillin-Streptomycin (Pen Strep) mixture solution (Invitrogen, # 15140-122) and 1% L-Glutamine (Invitrogen, # 25030-081). In some occasions DMEM (Dulbecco Modified Eagle Medium) (Sigma, # D6677) supplemented with the same components mentioned for RPMI was also used.

Cell lines were incubated at 37°C in T-75 flasks (Corning Incorporation, UK) with 5% CO<sub>2</sub> in a tissue culture specific incubator. The growth medium was changed every 2-3 days and cells were passaged before they become confluent. Generally, when the culture reached 90% confluency, cells were rinsed once with sterile phosphate buffered saline (PBS) (Sigma, D8537) then 2 ml of 1X Trypsin/EDTA solution (Sigma, # T3924) was added to the culture. Flasks were incubated at 37°C for 3-5 minutes and gently shook to allow cell disassociation and detachment. The action of Trypsin/EDTA was then stopped by adding 10 ml fresh complete RPMI medium and the cells were further disassociated by gentle pipetting for several times through 10 ml pipettes. Small amount of the cell suspension (typically ratio of 1:4) was expanded and maintained in complete RPMI medium using T-75 flasks. The sub-cultivation ratio can be varied from 1:3 to 1:5 according to the growth rate of the cell line of interest.

#### **2.2.4.2 Transient transfection**

The transient transfection of various plasmid DNAs into different human cell lines was accomplished using either lipofectamine<sup>TM</sup> 2000 (Invitrogen, # 11668-019) or FuGENE® HD (Roche, # 04709713001) transfection reagents following the manufacturer's guidelines. Briefly, one day before transfection, sub-confluent growing cell lines were washed and trypsinized as outlined in (section 2.2.4.1). The trypsinized cells were diluted to a desired concentration (this depends on cell type and confluency of the culture) in complete RPMI medium and subcultured into sterile tissue culture plates. Depending on the purpose of the experiment, various tissue culture treated plates such as 24-well plates, 6-well plates, or cell culture dishes were used. The subcultured cells were allowed to grow overnight or longer to reach 60-70% confluency.

The transfection mixture was prepared as follow: for a typical 6-well plate transfection, 10 µl of a transfection reagent (either lipofectamine<sup>TM</sup> 2000 or FuGENE® HD) was diluted in 250 µl of Opti-MEM® I Reduced Serum Medium (Invitrogen, # 31985-047) in a sterile eppendorf tube and left for 5 minutes at room temperature. In the mean time, 4 µg of a plasmid DNA was diluted in 250 µl of Opti-MEM in another sterile eppendorf tube. The diluted plasmid DNA and transfection reagent were combined together and mixed well by pipetting to produce the transfection mixture. This mixture was incubated for 15 minutes at room temperature. Meanwhile, during the last 5 minutes of the incubation, the cell culture to be transfected was washed once with Opti-MEM or PBS and the whole transfection mixture was added gently to the well by pipetting down slowly along the side of the well. Plates were rocked gently to get equal distribution of the transfection mixture and incubated at 37°C in a tissue culture incubator. Six hours later, the transfection mixture was replaced with fresh RPMI medium and further incubated for 36 hours. Eventually, the transfected cells were used for different experiments and analysis.

The above described protocol for transient transfection was chosen based on manufacturer's recommendations from Invitrogen (<http://products.invitrogen.com/>) and Roche ([http://www.roche-applied-science.com/proddata/gpip/3 5 3 18 1 9.html](http://www.roche-applied-science.com/proddata/gpip/3_5_3_18_1_9.html)) and published data (O'Reilly et al., 2003, Hawcroft et al., 2003, Fischer et al., 2005). Moreover, these protocols were also very well established in Dr Nateri's laboratory and successfully applied to transfect and overexpress many plasmid DNAs (including β-catenin which is frequently used in this study) in different human cell lines including those used in the current work (see section 2.1.1) (Babaei-Jadidi et al., 2011, Nateri et al., 2004, Nateri et al., 2005, Ibrahim et al., 2012). Based on the information provided by these references and my laboratory advisor (Dr Anas Saadeddin), the ratio 2.5:1 of the transfection reagent to DNA and 36-48 hours expression time was used for transient transfection as outlined above. These conditions, however, resulted in a sufficient transfection efficiency and protein expression. The transfection efficiency was validated through a visual assessment of the GFP fluorescence of the EGFP-fusion construct of FLYWCH1 (section 3.2.3.3) using a fluorescent microscope and

the protein expression was validated by Western blotting analysis (sections 3.2.4). Experiments with poor transfection efficiency (less than 50%) were neglected. It should be mentioned that we did not observe noticeable changes in the intensity of the GFP fluorescence during the post-transfection time, especially between 36-48 hours, which is mainly used to harvest the cells. Moreover, all the conditions used to overexpress FLYWCH1,  $\beta$ -catenin, and their deletion mutants in human cell culture including the promoter activity of the backbone vectors, the culture conditions, and the cell lines used, have been previously optimized and established in our lab and by others as detailed above. Therefore, further optimization steps through varying the DNA and/or lipofectamine concentrations or varying the post-transfection times before harvesting the cells were not conducted in this study. However, as information about the half-life of FLYWCH1 protein is currently unavailable, further investigations of FLYWCH1 expression time and stability in different cell lines may yield valuable information.

#### **2.2.4.3 Stable transfection**

In order to obtain stable gene expression, a Lentiviral-Based Gene Delivery system was used to achieve a permanent or a long term integration of the gene of interest into the genome of specific cell lines. This system comprises two main steps; the Lentiviral production and the cell transduction as detailed below.

##### **2.2.4.3.1 Lentivirus production**

The Lentiviral Expression plasmid backbone vector (pLVX-Puro) (*Appendix 7*) and packaging plasmids (see below) were kindly provided by Dr. Dominique Bonnet (Cancer Research UK- London Research Institute). An optimized protocol for viral particles production, and the transduction time for the Lentiviral particles has been produced in our lab by Mr. Mohammed Abuzinadah and other colleagues (Dr. Nateri's lab) (Babaei-Jadidi et al., 2011,

Ibrahim et al., 2012) and a similar strategy is applied in this study as detailed below.

**A) Transfection:** The transfection was started with seeding HEK293T cells in T-75 tissue culture flasks (in triplicate) in complete RPMI medium. Cells were incubated overnight to reach 70-80% confluency. Just before the transfection started, the RPMI medium of each cell culture was replaced with 9 ml Opti-MEM and the flasks were returned back to the incubator. For each transfection, distinct amounts of plasmids (9 µg of the Lentiviral Expression plasmid encoding the gene of interest, 6 and 3 µg of the packaging plasmids; pCMV delta R8.74 and pMDG2 respectively) were diluted in 250 µl Opti-MEM in a sterile 1.5 ml eppendorf tube. In the mean time, 43 µl of FuGENE is diluted in 650 µl of Opti-MEM in a separate sterile tube and incubated at room temperature for 5 minutes. The diluted plasmid DNA and FuGENE were combined together, mixed well, and incubated at room temperature for 15 minutes. After incubation, the transfection mixture was added to the cell culture flasks containing 9 ml Opti-MEM. The flasks were swirled gently to get equal distribution of the transfection mixture and incubated overnight at 37°C. In the following day, the transfection mixture was replaced with 11 ml complete culture medium and returned to the incubator. From now on the culture medium was considered as a viral soup.

**B) Viral soup collection:** The culture medium containing viral particles (i.e. the viral soup) was collected for three respective days. Each time the soup was collected, the transfected cells were re-fed with 11 ml of fresh complete RPMI medium and the cultures were returned to the incubator. The viral soup was kept in the fridge until the last collection was made.

**C) Viral soup concentration:** After the 3<sup>rd</sup> collection of the viral particles, the viral soup was concentrated as follow. The soup was centrifuged at 4000 rpm for 10 minutes to remove large particles/contaminants (e.g. flushed out cells) from the soup. The supernatant was transferred to new falcon tubes and passed through 0.45 µm pore size filters to eliminate any possible non viral particle substances.

Using a pasture pipette, equal amounts of the viral soup (~9 ml) was gently added to specific centrifuge tubes containing 1 ml of 20% filter sterilized Sucrose solution using pasture pipettes. This should make two layers of solutions, the bottom layer of Sucrose solution and the top layer of viral soup. The Lentiviral particles were precipitated at 40,000 rpm for 2 hours using a BECKMAN L8-60M Ultracentrifuge. Finally, the viral pellet in each tube was resuspended in 40 µl PBS and the tubes were incubated at room temperature for 10 minutes, then at 4°C for 1 hour. The concentrated viral particles were aliquoted into eppendorf tubes in small amounts (60 µl per tube). At this stage, the viral particles are ready to infect cells or they can be kept at -80°C for up to 6 months without losing their efficiency.

The calculation procedure of the functional Lentivirus titre or the multiplicity of infection (MOI) that produced by the above described protocol was also optimized by Mr. Mohammed Abuzinadah (Dr. Nateri's lab). The amount of viral particles or MOI required to transduce the cell line of interest were then calculated according to the equation below:

$$X = \frac{\text{MOI required for transduction} * \text{Number of cells to be infected}}{\text{Calculated Lentivirus titer}}$$

Where:

X= stock volume of Lentivirus particles required for transduction.

#### **2.2.4.3.2 Lentivirus transduction and stable cell line generation**

Lentiviral particles encoding the gene of interest were used to transduce various human cell lines as follow: Cells were subcultured and allowed to grow in DMEM medium to reach 60-70% confluency in 6-well plates. The culture medium was replaced with fresh DMEM medium containing 8 µg/ml polybrene (Hexadimethrine bromide) (Sigma, # H9268). Twenty microlitres of the concentrated Lentiviral particles (~6 x 10<sup>9</sup> viral particles) were directly added to the culture medium in each well. Plates were rocked gently to obtain equal distribution of the viral particles in the cell culture and incubated at

37°C. After an overnight incubation, the transduced cells were selected with Puromycin by replacing the growth medium with new DMEM containing 15 µg/ml Puromycin (Sigma, # P8833). The selection was continued for two weeks then the resistant cells were trypsinized, counted and seeded into 96-well plates (one cell per well). Cells were allowed to grow in Puromycin selection for several days. Finally, the resistant cells were further amplified and the stable expression of the gene of interest was validated through Western blotting and/or PCR analysis.

## **2.2.5 Protein lysate preparation and analysis**

### ***2.2.5.1 Protein extraction and quantification***

The total cellular protein was extracted from different cell lines either transfected or untransfected as summarized below. The culture medium was removed and the cells were rinsed once with PBS. Appropriate amounts (typically 250-350 µl per one well of 6-well plate) of freshly prepared RIPA lysis buffer (Table 2-1) containing protease inhibitor (Sigma # P8340) were directly added to the surface of the cell culture and the plates were gently rocked at 4°C for 15 minutes. The highly adhesive cells such as SW480 were mechanically detached from the plate with a scraper. The cell lysate was transferred into 1.5 ml eppendorf tubes and further incubated on ice for 10-15 minutes then centrifuged at 13000 rpm for 10 minutes at 4°C. The supernatant (total cell lysate) was transferred into new eppendorf tubes and labelled properly.

The protein quantification was performed using a BioRad Protein Assay reagent (BIO-RAD, # 500-0006) following the manufacture's guidelines. The BioRad reagent was diluted 1:5 in distilled water (dH<sub>2</sub>O) and series standard dilutions of BSA (Bovine Serum Albumin) (Sigma, # A4503) (0.1, 0.3, 0.5, and 0.7 µg/µl) were also prepared in dH<sub>2</sub>O. The blank was prepared by adding 20 µl of dH<sub>2</sub>O to the first well of a 96-well micro test plate (Scientific laboratory supplies, # MIC9038). This followed by adding 20 µl of each BSA

standard dilutions into separate microplate wells. The protein samples were diluted (1/10) directly in the wells of the microplate by mixing 2  $\mu$ l of the protein lysate with 18  $\mu$ l dH<sub>2</sub>O. Finally, 200  $\mu$ l of the diluted BioRad reagent was added to the wells of the microplate and incubated at room temperature for 5 minutes.

The absorbance of the protein-dye mixture was measured at 595 nm by a Benchmark Plus microplate Spectrophotometer (BIO-RAD) using the Endpoint protocol. The protein concentration was automatically calculated by the machine's software (Microplate Manager, version 5.2.1 Build 106) on attached computer based on the BSA standard curve. The quantified protein samples were directly used for Western blotting analysis or stored at -80°C until use.

### ***2.2.5.2 Western blotting (WB) analysis***

#### **2.2.5.2.1 Sample preparation and SDS-PAGE electrophoresis**

The protein samples were prepared by mixing small portions of the cell lysates (typically 30  $\mu$ g) with appropriate amount of 5X loading buffer (Table 2-1). The final concentration of the loading buffer in the sample should be 1X. Samples were boiled for 4 minutes at 95°C on a thermoblock heater and cooled down on ice for 5 minutes. The SDS-PAGE (sodium dodecyl sulfate polyacrylamide gel electrophoresis) gel is composed of two parts, the stacking and the resolving gels. The stacking gel is less concentrated than the resolving gel and they both contain the following chemicals (dH<sub>2</sub>O, acrylamide mix, Tris, SDS, ammonium persulfate, and TEMED) in distinct compositions as detailed below in (Table 2-10) and (Table 2-11).

Table 2-10: Solution for preparing Resolving Gels for Tris-glycine SDS-PAGE.

Solution components	Component volumes (ml) per gel				
	mold volume of				
	5 ml	10 ml	15 ml	20 ml	25 ml
<b>8%</b>					
H <sub>2</sub> O	2.3	4.6	6.9	9.3	11.5
30% acrylamide mix	1.3	2.7	4	5.3	6.7
Tris (1.5 M, pH 8.8)	1.3	2.5	3.8	5	6.3
SDS (10%)	0.05	0.1	0.15	0.2	0.25
10% ammonium persulfate	0.05	0.1	0.15	0.2	0.25
TEMED	0.003	0.006	0.009	0.012	0.015
<b>10%</b>					
H <sub>2</sub> O	1.9	4	5.9	7.9	9.9
30% acrylamide mix	1.7	3.3	5	6.7	8.3
Tris-Cl (1.5 M, pH 8.8)	1.3	2.5	3.8	5	6.3
SDS (10%)	0.05	0.1	0.15	0.2	0.25
10% ammonium persulfate	0.05	0.1	0.15	0.2	0.25
TEMED	0.002	0.004	0.006	0.008	0.01

Table 2-11: Solution for preparing 5% Stacking Gels for Tris-glycine SDS-PAGE.

Solution components	Component volumes (ml) per gel				
	mold volume of				
	1 ml	2 ml	3 ml	4 ml	5 ml
H <sub>2</sub> O	0.68	1.4	2.1	2.7	3.4
30% acrylamide mix	0.17	0.33	0.5	0.67	0.83
Tris (1.0 M, pH 6.8)	0.13	0.25	0.38	0.5	0.63
10% SDS	0.01	0.02	0.03	0.04	0.05
10% ammonium persulfate	0.01	0.02	0.03	0.04	0.05
TEMED	0.001	0.002	0.003	0.004	0.005

Gels with desired concentrations and combs (e.g. 10% gels with 10-well combs) were casted and the protein samples along with protein markers were loaded into the wells of the gel. Generally, two types of protein markers; either “pre-stained Full range Rain Bow marker” (GE Healthcare, # RPN800E) or “ColorPlus Prestained Protein Ladder, Broad Range” (NEW ENGLAND BioLabs, # P7711S) were used to determine the size of the protein bands (Figure 2-9).

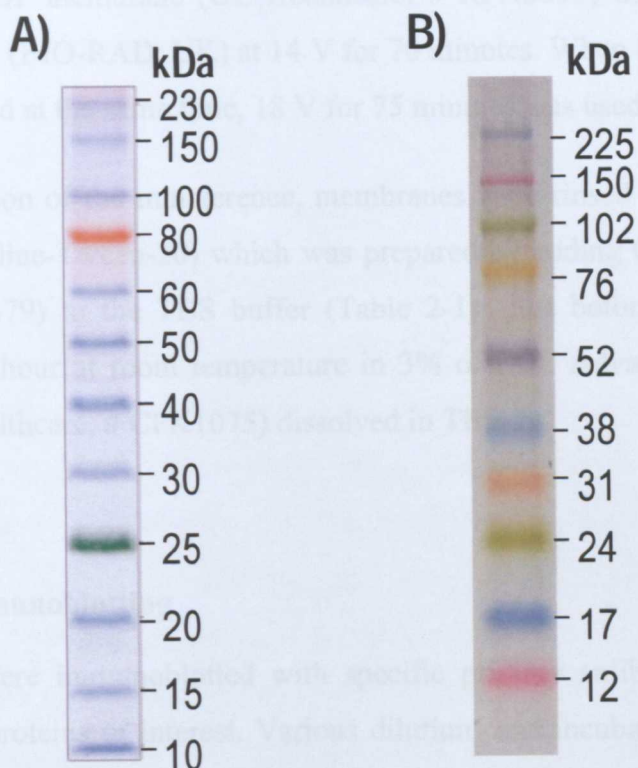


**Figure 2-9: Protein markers used for for SDS-PAGE analysis. A)** Represents the “ColorPlus Prestained Protein Ladder, Broad Range” marker from NEW ENGLAND BioLabs and **B)** Represents the “pre-stained Full range Rain Bow” marker from GE Healthcare. Both markers were used to determine the size of protein molecules during Western blotting analysis.

The upper and the lower compartment of electrophoretic unit (miniVE Vertical Electrophoresis System, Amersham/Biosciences, # 80-6418-77) were filled with 1X TGS running buffer (Tris/Glycine/SDS buffer, BIO-RAD, # 161-0772) and the gel was run at 120 V for 2 hours using a BIO-RAD PowePac supply. Based on the molecular size of the protein of interest, less concentrated SDS-PAGE (e.g. 8%) and longer running time (up to 3 hours) with higher voltage (up to 180) was also used in some occasions. Upon a desired separation of the protein molecules (indicated by the colour and distance between the pre-stained bands of the protein marker), the protein samples were transferred to a Hybond-P PVDF membrane (GE Healthcare, # RPN303F) using a semi-dry transfer system (BIO-RAD, UK) at 14 V for 70 minutes. When two membranes were transferred at the same time, 18 V for 75 minutes was used.

Upon completion of the transference, membranes were rinsed once in TBS-T (Tris buffer saline-Tween-20) which was prepared by adding 0.1% Tween-20 (Sigma, # P1379) to the TBS buffer (Table 2-1) just before use and then blocked for 1 hour at room temperature in 3% of ECL Advance<sup>TM</sup> blocking agent (GE Healthcare, # CPK1075) dissolved in TBS-T.

#### **2.2.5.2.2 Immunoblotting**

Membranes were immunoblotted with specific primary antibodies to detect bands of the proteins of interest. Various dilutions and incubation times were used according to the initial concentration of the primary antibodies and the strength of the protein signal. Details of different types of primary and secondary antibodies and their dilution factors used throughout this study are given in (Table 2-7).

Briefly, membranes were incubated with suitable amounts of specific primary antibodies diluted either in blocking reagent or in TBS-T and rolled for a short time (up to 3 hours) at room temperature or longer time (overnight) at 4°C using a Roller mixer (Stuart SRT6, UK). Membranes were washed three times with washing buffer (TBS-T), 5-10 minutes each. The membranes then incubated with appropriate amounts of secondary antibodies diluted in TBS-T.

After incubation for 1 hour at room temperature the membranes were washed three times with TBS-T, 5-10 minutes each. Finally, the ECL Advance™ Western Blotting detection Kit (GE Healthcare, # RPN2135) was used to visualize the protein bands using a FluorChem®FC2 Imaging System (Alfa Innotech, UK) following the manufacture's guidelines.

### ***2.2.5.3 Co-immunoprecipitation (Co-IP) assay***

In the current work, three different approaches were employed to immunoprecipitated the protein of interest in the lysate of transfected cells as detailed below.

#### **2.2.5.3.1 FLAG-conjugated agarose beads**

ANTI-FLAG®M2 Affinity Gel (Sigma, # A2220) beads were used to pull down FLAG-tagged proteins following the manufacturer's guidelines. Briefly, the beads were mixed thoroughly before use and for a typical Co-IP experiment, 60 µl of the homogenized beads was transferred into 1.5 ml Eppendorf tube. The beads were washed once with 1 ml RIPA lysis buffer by centrifuging the tubes at 500 rcf for 4 minutes at 4°C. The Co-IP samples were prepared by mixing appropriate amounts of protein lysates (usually 0.5 mg) with the FLAG conjugated beads. The volume of the protein/beads mixture was completed to 500 µl with RIPA lysis buffer. The Eppendorf tubes were closed tightly and incubated with gentle rotation for 2-3 hours at 4°C.

After incubation, samples were spun down at 500 rcf for 8 minutes at 4°C then the pellet (beads plus bounded protein complex) was washed 3-4 times with 1 ml RIPA lysis buffer. For each wash, the tubes were rotated 2-3 minutes at 4°C and centrifuged at 500 rcf for 5 minutes. The pellet was resuspended in a suitable amount of 1X SDAS-PAGE loading buffer and boiled at 95°C for 4 minutes followed by incubation on ice for 5 minutes. Beads were pelleted with a short and gentle centrifuge and the supernatants of the Co-IP samples were loaded and run by SDS-PAGE as described in (section 2.2.5.2.1). For each Co-

IP experiment a set of input samples (normal Western blotting samples used to show the IP-efficiency) were also prepared and run on the SDS-PAGE page at the same time.

#### **2.2.5.3.2 Magnetic beads**

Dynabeads<sup>®</sup>Protein G (Invitrogen, # 10003D) was used to pull down proteins with other epitope tags such as MYC-FLYWCH1 (section 3.2.3.2) and/or the endogenous proteins as described previously (Nateri et al., 2005). Here, the beads were manually conjugated to a desired antibody as detailed below. Beads were mixed thoroughly then 60  $\mu$ l of the homogenized beads were transferred to an Eppendorf tube and placed on the magnet to separate the beads from the solution. The supernatant was discarded and the beads were resuspended in 200  $\mu$ l PBS/Tween-20 solution containing distinct concentration of a primary antibody of interest (typically 6  $\mu$ g). Tubes were incubated with rotation for 45 minutes at room temperature. The beads-Ab complex was washed twice in 200  $\mu$ l PBS/Tween-20 solution by gentle pipetting. The magnet was used to separate the supernatant from the beads between each wash. The conjugated beads then used to pull down the protein of interest as outlined above in (section 2.2.5.3.1) with the exception of using the magnet and PBS to pellet and wash the beads during the washing process.

#### **2.2.5.3.3 Agarose beads**

Protein A/G PLUS-Agarose Immunoprecipitation Reagent (Santa Cruz, # sc-2003) was also used to pull down both epitope-tagged and/or endogenous proteins (such as MYC-FLYWCH1 and endogenous TCF4) as summarized below. The protein lysate (0.5 mg) was first mixed with a specific amount of the primary antibody of interest (6-8  $\mu$ g) in 1 ml RIPA lysis buffer. After 1 hour incubation at 4°C, 60  $\mu$ l of the resuspended Protein A/G PLUS-Agarose beads was added to the mixture and incubated with rotation for 2-3 hours at 4°C. The rest of the procedure was carried out as described above in (section 2.2.5.3.1).

## 2.2.6 Functional analysis

### 2.2.6.1 Indirect transcriptional assay

To assess the transcriptional activity of  $\beta$ -catenin in different cell lines, the TOP/FOP-Flash Firefly-luciferase reporter system was employed using the Dual-luciferase kit (Dual-Luciferase® Reporter Assay, Promega, # E1910), as described previously (Nateri et al., 2005). The TOP-Flash construct contains Firefly luciferase coding region under a promoter containing three intact TCF-DNA binding elements (ATCAAAG) upstream to the luciferase gene, whereas FOP-Flash contains three mutated TCF-DNA binding elements (GCCAAAG) and used as a negative control. A constitutively active vector encoding *Renilla* luciferase gene was also used as an internal control.

Experiments were set up by seeding cells of a desired cell line in 24-well plates ( $3 \times 10^5$  cells/well). After overnight incubation, cells were transiently transfected (as outlined above in section 2.2.4.2) with the reporter constructs along with construct (s) of the genes of interest. For all plasmid DNAs used in this experiment except *Renilla*, 0.2  $\mu$ g DNA plus 2  $\mu$ l of the transfection reagent (lipofectamine™ 2000 or FuGENE® HD) were used to transfect cells of a single well of 24-well plates, whereas 0.05  $\mu$ g DNA/well was used for the *Renilla* construct. Transfections were performed in triplicate and the cells were harvested after 36 hours of transfection using 1X passive lysis buffer provided within the Dual-Luciferase kit.

Two types of FLYWCH1 clones, the untagged and MYC-tagged FLYWCH1 (sections 3.2.3.1 & 3.2.3.2) were mainly used in the luciferase assays performed in this work. Both of these clones contain an EGFP reporter gene that is separated from the FLYWCH1 nucleotide sequence by an IRES (internal ribosome entry site) sequence, but both are expressed under the *CMV* promoter (Figure 3-8 & Figure 3-10). The transfection efficiency of all luciferase experiments conducted in this study was visually assessed through monitoring the expression level of the EGFP reporter gene by a fluorescent microscope. Experiments with poor transfection efficiency (less than 50%, judged by the fluorescence level of the EGFP gene) were neglected. Cells were

lysed after 36 hours of transfection based on information discussed in (sections 2.2.4.2).

The activities of the Firefly and *Renilla* luciferase reporters were measured using reagents provided by Promega following the manufacturer's protocol. In brief, small amounts of freshly prepared lysates (10 µl/well) were transferred to a Microplate FluoroNunc 96 well plate (Fisher, # MPA-560-040A) in triplicate. The activity of the firefly luciferase reporter was measured first by adding 50 µl/well Luciferase Assay Reagent II (LAR II) to generate a stabilized luminescent signal which can be detected and read by a Luminoskan Ascent Microplate Luminometer (Thermo Scientific, UK). Immediately after quantifying the firefly luminescence, this reaction was quenched and the *Renilla* luciferase reaction was concomitantly initiated by adding 50 µl/well Stop & Glo® Reagent to the samples in the same plate. This allowed the activities of both firefly and *Renilla* luciferases to be measured sequentially from the same samples.

The measurements were exported to a Microsoft Excel file and analyzed as follows. **First**, the values of the firefly reading (TOP & FOP-FLASH) of all samples (controls and experimental samples) were normalized to the values of *Renilla* according to the following equation,  $\text{Firefly}/\text{Renilla} \times 1000$ . **Second**, the normalized values of the experimental samples were divided on the normalized values of the control samples to produce folds of change in luciferase expression (induction/repression) of the experimental samples (both TOP & FOP-FLASH) in comparison to the control samples. Finally, the normalized values of the control samples were arbitrarily set to number one and then all final values were plotted on a histogram to show the relative changes in luciferase activity. An example of such calculation is given in (*Appendix 14*) by presenting the raw/real data of one of the luciferase experiments performed in this study.

### **2.2.6.2 *In vitro* scratch assay**

The *in vitro* scratch assay was performed as described previously (Babaei-Jadidi et al., 2011, Liang et al., 2007) with slight modifications. Briefly, cells were subcultured and grown in 6-well plates in triplicate. Using a narrow tip marker, the bottom side of the wells was marked with a horizontal line. Cell cultures were transfected at ~80% confluency with a plasmid that encodes the gene of interest such as eGFP-FLYWCH1-WT construct (section 3.2.3.3) or an empty vector such as pEGFP-C2 (*Appendix 6*) to be used as a negative control. The transfection was done as described in (section 2.2.4.2) and the cells were incubated at 37°C for 24 hours (cells should reach 100% confluency during this period to form a monolayer). Then the transfected cells were starved overnight in a serum free RPMI medium to synchronize the cells at G0.

Using p200 pipette tips three parallel wounds were scratched through the cell culture of each well moving perpendicular to the marker line drawn on the bottom of the well. Cell cultures were washed twice with PBS then maintained in complete RPMI medium. The wounds were examined and the first batch of images (zero time) were acquired using the 10X lens of a phase-contrast microscope (Nikon, Model ECLIPSE TE2000-S) supplemented with a digital camera (HAMAMATSU, Model C8484-05G). Images were taken just above and just below each marker line to help orient the captured area in a way to be easily recognized after 24 and/or 48 hours of incubation. A specific name was given to each image indicating the well number and the position of the photo according to the horizontal marker line (above the line or under the line). The imaging process was repeated after 24 hours and/or 48 hours.

The images acquired for each sample were further analyzed quantitatively by using a software called ImageJ which maintained by (Rasband, W.S., ImageJ, U. S. National Institutes of Health, Bethesda, Maryland, USA, <http://imagej.nih.gov/ij/>, 1997-2011). The distances between one side of the scratch and the other (for each image) were measured using the “Freehand Selections” command of the Image J software at certain intervals (e.g. time 0 and time 24 hour). Finally, the percentage of cell movement during the desired time frame was calculated through the equation below:

$$\text{Percentage of cell movement} = 100 - \left( \frac{m_{24}}{m_0} * 100 \right)$$

Where:

$m_0$ = wound measurement at zero time

$m_{24}$ = wound measurement at 24 hours

The rate of cell migration for the transfected cells was determined by comparing the average of the percentage of cell movement of at least six readings for each transfection. A visual evaluation was also performed to provide a secondary assessment of motility.

### ***2.2.6.3 Trans-well cell migration assay***

The trans-well cell migration assay was performed using Boyden trans-well chamber containing polycarbonated filters with 8  $\mu\text{m}$  pore size (Costar, UK) following the manufacturer's guidelines. Briefly, colorectal cancer cells (CRC) such as HCT116 were subcultured and transfected as described in (section 2.2.4.2). The transfected cells were trypsinized and counted after 24 hours of incubation using a Neubauer haemocytometer (*Appendix 3*). Meanwhile, the trans-well chambers were incubated in 600  $\mu\text{l}$  of plain RPMI medium at 37°C for 1 hour in 24-well plates.

The chambers were displaced into new wells of the 24-well plate containing 600  $\mu\text{l}$  of complete RPMI medium supplemented with 20% FBS. Using a narrow tip marker, the bottom side of the wells were marked with 3 horizontal and 3 vertical lines to facilitate cell counting. The trypsinized cells were spun down and resuspended in suitable amounts of complete RPMI medium supplemented with 10% FBS to make a desired final concentration of the cells in the suspension. A distinct amount of cells (typically  $5.0 \times 10^4$  cells/chamber) in a final volume of 100  $\mu\text{l}$  were seeded onto the upper part of the trans-well chambers in triplicate. The number of seeded cells depends on the motility and the adhesiveness property of the cell line of interest. Cells were incubated at

37°C for 24 hours then the total number of migrated cells at the bottom of the plates was manually counted using 10X lens of a bright field microscope. The effect of the gene of interest on the motility of cancer cells was observed by comparing the average number of migrated cells of the experimental samples with the control samples. The experiment was repeated at least on 3 independent occasions and in triplicate format.

#### ***2.2.6.4 Cell cycle analysis***

The propidium iodide (PI) staining method was used to analyze the effect of the gene of interest on the cell cycle of CRC cells as described previously (Babaei-Jadidi et al., 2011, Nateri et al., 2004). Briefly, cells were transfected with desired plasmid DNAs in triplicate and suitable amounts of the transfected cells ( $\sim 3 \times 10^5$  cells) were transferred into flow cytometry tubes and washed twice with PBS. For each wash cells were resuspended in 1 ml PBS and spun down for 5 minutes at 1000 rpm. Cells were fixed by adding 1 ml of 70% cold ethanol dropwise while vortexing the sample then left at 4°C for at least 30 minutes.

The fixed cells were washed twice in 1ml PBS, for each wash samples were spun down for 5 minutes at 1000 rpm. Cells were stained with 300  $\mu$ l of diluted (50  $\mu$ g/ml) propidium iodide (PI) solution (Sigma, # P4864) in PBS containing 0.1  $\mu$ g/ $\mu$ l of RNase A. The number of stained cells in each step of the cell cycle was determined by a Coulter FC 500 flow cytometer (BEKMAN COULTER, UK). Finally, the data was further analyzed by using Windows Multiple Document Interface (WinMDI) and Cylchred-Cell Cycle Analysis software.

#### ***2.2.6.5 Growth curve analysis***

HCT116 cells were transiently transfected with plasmid DNAs of interest. The transfected cells were counted and re-seeded in 24-well plates in triplicate at an initial density of  $5 \times 10^4$  cells/ml. The total number of cells was counted every

24 hours by T10 Automated Cell Counter (BIO-RAD, # 145-0001) following the manufacturer's guidelines for four respective days. The total number of cell counts was plotted on a time versus number graph and the differences between the experimental and control samples were statistically analyzed.

### **2.2.6.6 Immunofluorescent (IF) analysis**

The IF assay, was used to visualize different endogenous or overexpressed proteins and to compare their relative expression levels in different cells. Generally, human cell lines (transfected or untransfected) were grown overnight on coverslips (Size 22x22 mm) in 6-well plates. An optimized IF protocol was applied to stain the cells in three steps as previously described (Ibrahim et al., 2012) and outlined below:

**A) Fixation and permeabilization:** Cells were washed twice in PBS and fixed with 4% PFA (Paraformaldehyde) for 30 minutes at room temperature. The fixed cells were washed twice in PBS for 5 minutes at room temperature and incubated with 800  $\mu$ l of permeabilization solution (0.1% Triton X-100 in PBS) for 30 minutes. After permeabilization, the cells were washed twice in PBS for 5 minutes at room temperature.

**B) Blocking and staining with primary antibody:** The permeabilized cells were blocked with 800  $\mu$ l blocking solution, composed of 3% Bovine Serum Albumin (BSA) in PBS, for 1 hour and washed once in PBS for 5 minutes at room temperature. The blocked cells were incubated overnight at 4°C with 250  $\mu$ l of the primary antibody of interest diluted in 3% BSA. For the dilution factors of the different primary antibodies used in this work see (Table 2-7). Negative controls were incubated with 3% BSA only.

**C) Staining with secondary antibody:** After staining with the primary antibody for overnight, the cells were washed four times in washing solution (1% BSA and 0.1% Tween-20 in PBS) for 10 minutes at room temperature. The secondary antibody was diluted in 3% BSA and gently added on top of the coverslips (350  $\mu$ l per well) including the negative controls. Immediately after

adding the secondary antibody, the plates were wrapped with aluminum foil and incubated in a dark place for 1 hour at room temperature. The stained cells were washed five times in the washing solution for 10 minutes at room temperature. At the end, the coverslips were removed from the wells of the 6-well plates and gently mounted on clean slides in an upside down position with small amount of DAPI. The coverslips were sealed on the slides using nail varnish and stored at 4°C in the dark.

The stained cells were inspected for the fluorescent signal of the proteins of interest using Leica DMI3000 B Inverted microscope (Leica Microsystems, UK). The integrated camera of the Leica microscope was used for the imaging and the software provided by the supplier was used for image analysis following the manufacture's instruction.

#### **2.2.6.7 Phalloidin staining**

Phalloidin is a commonly used dye for the morphological analysis. It can bind F-actin and display the shape of the cells. The initial step of phalloidin staining is similar to the IF protocol in which the cells were grown on coverslips, fixed, and permeabilized with 0.1% Triton X-100 (see section 2.2.6.6). After permeabilization, cells were incubated with diluted (50 µg/ml, in PBS) fluorescent phalloidin conjugate solution (Sigma, # 1951) for 40 minutes in dark. The stained cells were washed 2-3 times in PBS for 5 minutes at room temperature then the coverslips were removed, mounted and analyzed with the Leica microscope as described above in (section 2.2.6.6).

#### **2.2.6.8 In Situ Hybridization (ISH) assay**

##### **2.2.6.8.1 Probe preparation, specificity and verification**

A short fragment of *FLYWCH1* cDNA (651 bp), conserved between mouse and human, was excised from the eGFP-*FLYWCH1*-WT clone (Figure 3-12) by

restriction enzyme digestion using single cutter enzymes *Bam*HI (cutting position 166/170) and *Xho*I (cutting position 811/815). The resultant DNA fragment spans 3 exons of human *FLYWCH1* gene (exons 1-3). The specificity of the probe was confirmed by blasting the nucleotide sequence of the probe to the human and mouse genomic and transcript database using nucleotide BLAST suite facility provided by NCBI (<http://blast.ncbi.nlm.nih.gov/Blast.cgi>). The result of the blast is presented in (Appendices 11 & 12) and the size of the DNA fragment was confirmed by running the digested DNA on 1% agarose gel. Finally, the DNA probe was cloned into the MCS of pcDNA3 vector (Appendix 8) downstream to the T7 promoter using the same enzymes mentioned above. This clone was also verified by restriction enzyme digestion analysis using *Bam*HI/*Xho*I restriction enzymes.

#### **2.2.6.8.2 In vitro transcription and hybridization protocol**

The *FLYWCH1* cDNA probe described above along with tissue microarray (TMA) of human colorectal cancer tissues (provided by prof. Ilyas, Division of Pathology, Nottingham University) and *Apc*<sup>Min/+</sup> mouse intestinal tissues (prepared by Dr Roya Babaei-Jadidi, Dr Nateri's lab) were sent to our collaborator Dr B Spencer-Dene, CRUK-LRI, Histopathology Lab to perform the ISH assay as detailed below. The mouse intestinal tissues were prepared in the form of Swiss rolls by flushing the intestinal segments with cold PBS, threading through with stainless steel rods in a rod holder (Dr Nateri's lab), slicing and opening them longitudinally using a scalpel to expose tissue epithelia to a fixative buffer composed of (10% Neutral Buffered Formalin containing of 100 ml of 37% formaldehyde, 4g of NaH<sub>2</sub>PO<sub>4</sub>, 6.5g of Na<sub>2</sub>HPO<sub>4</sub> in 900 ml of H<sub>2</sub>O), and then rolling them around a metal or wooden stick. These tissues were then processed and embedded in paraffin blocks as described previously (Babaei-Jadidi et al., 2011, Ibrahim et al., 2012, Nateri et al., 2005).

The T7 RNA polymerase was used for *in vitro* transcription of this DNA fragment to generate a human *FLYWCH1* RNA probe using the digoxigenin

(DIG)-RNA labelling mix (Roche; 11277073910). In brief, 4 % paraformaldehyde (PFA)-fixed intestinal Swiss roll preparations were sectioned (8  $\mu\text{m}$ , and placed onto glass slides by floating sections in a water bath at 42°C), dewaxed, rehydrated, digested with 10  $\mu\text{g}/\text{ml}$  proteinase K (37°C for 18 minutes), and then incubated in 0.2 M HCl and refixed. After prehybridization for 1 hour, slides were hybridized overnight at 57°C in buffer containing 50 % deionized formamide, 10 % dextran sulfate, 1X Denhardt's solution, 10 mM Tris-HCl pH 7.6, 600 mM NaCl, 0.25 % Na dodecyl sulfate, 1 mM EDTA, 2 mg/ml transfer 0.2 M, and 2  $\mu\text{g}/\text{ml}$  denatured digoxigenin-labelled cRNA probe. The slides were rinsed in 5X saline-sodium citrate (SSC) buffer at 57°C for 10 min, washed once in 50 % formamide in 2X SSC at 57°C for 30 min, and then once in 2X SSC at 57°C for 30 min and twice in 0.2X SSC for 30 min each at 57°C. After blocking with 1 % blocking reagent (Roche), slides were incubated with sheep antidigoxigenin fab antibody (Roche, 11093274910; 1:1,000) for 2 hours at 37°C. Substrate was developed using NBT/BCIP (nitro-blue tetrazolium chloride and 5-bromo-4-chloro-3-indolyphosphate p-toluidine salt).

### **2.2.7 Statistical analysis**

All statistical evaluations were accomplished by the independent-samples T-test (2-tailed) using SPSS software (IBM SPSS Statistics, version 19) and  $P < 0.05$  was considered to be statistically significant. The error bars shown for all charts represent the standard deviation (STDEV) for the sample's mean, unless otherwise stated. Experiments were performed in triplicates for each case and repeated on at least 2-3 independent occasions.

## **CHAPTER 3**

**Identification and expression of the human**

***FLYWCH1* gene in mammalian cells**

### 3.1 Introduction

Despite the fact that human *FLYWCH1* gene was previously identified (Brandenberger et al., 2004, Stelzl et al., 2005) and its sequence was deposited on the NCBI (National Centre for Biotechnology Information) database (<http://www.ncbi.nlm.nih.gov/gene/84256>), the protein product of this gene was not previously characterized. Therefore, in the current work and for the first time, the FLYWCH1 coding sequence was bioinformatically analyzed and experimentally characterized.

Our bioinformatics analyses show that the *FLYWCH1* gene encodes a protein called FLYWCH1 with five FLYWCH-type Zinc finger motifs. This protein including its FLYWCH motifs is evolutionarily conserved in human, mouse, chimpanzee, dog, cow, and rat. The FLYWCH motifs of FLYWCH1 protein may function as DNA-binding domains (see the discussion). However, there is no evidence for the presence of a transactivation-domain within the coding region of this protein.

Overexpression of proteins is a powerful approach to study their biological and biochemical functions. In this chapter, we, successfully, tagged the full-length *FLYWCH1* cDNA with different epitope tags such as MYC & eGFP, and cloned these sequences into different mammalian expression vectors. The protein expression of these clones and the sub-cellular localization of FLYWCH1 protein were also validated through Western blotting analysis and fluorescent microscopy. The analysis revealed that the expression of eGFP-tagged FLYWCH1 resulted in bright fluorescent spots in the nucleus which was distinct from the expression pattern of eGFP reporter gene in HEK293T and CRC cells, implying that sub-cellular localization may be require for FLYWCH1 function.

## **3.2 Results**

### **3.2.1 Sequence and domain analysis of FLYWCH1**

Human *FLYWCH1* gene is currently recognized under the official name [FLYWCH-type zinc finger 1 (FLYWCH1)] on the NCBI database (Gene ID: 84256, <http://www.ncbi.nlm.nih.gov/gene/84256>). This gene is composed of 2,151 nucleotides encoding 716 aa (aa) residues (Figure 3-1A). To define the presence of conserved domains within the aa sequence of FLYWCH1, related bioinformatic resources such as Domain Mapping of Disease Mutations (DMDM, <http://bioinf.umbc.edu/dmdm/>) (Peterson et al., 2010) and protein family (Pfam, <http://pfam.sanger.ac.uk/>) (Finn et al., 2010) databases were interrogated. The analyses showed that FLYWCH1 contains a tandem array of five FLYWCH-type zinc finger motifs distributed along the protein sequence (Figure 3-1, A & B). The FLYWCH domain was originally described as a Cys<sub>2</sub>His<sub>2</sub> motif (Buchner et al., 2000) and then annotated as FLYWCH domain in the *Drosophila* Mod(mdg4) protein based on the presence of the FLYWCH consensus sequence (F/Y-X<sub>n</sub>-L-X<sub>n</sub>-F/Y-X<sub>n</sub>-WXCX<sub>6-12</sub>CX<sub>17-22</sub>HXH; where X indicates any amino acid) (Dorn and Krauss, 2003).

To validate the presence of such conserved domains in human FLYWCH1 protein, the sequence alignment of FLYWCH motifs was performed. The alignment data revealed that the FLYWCH consensus sequence (F, L, Y, W, C, & H) was highly conserved between zinc finger motifs of this protein (Figure 3-1C). The data also show that each motif is composed of 177 nucleotides encoding 59 aa (Figure 3-1A). Moreover, in addition to the presence of the FLYWCH consensus sequence, most of the other aa residues within the coding sequence of FLYWCH motifs are highly conserved (Figure 3-1C), suggesting that these motifs may have important structural and biological involvement in the function of FLYWCH1.

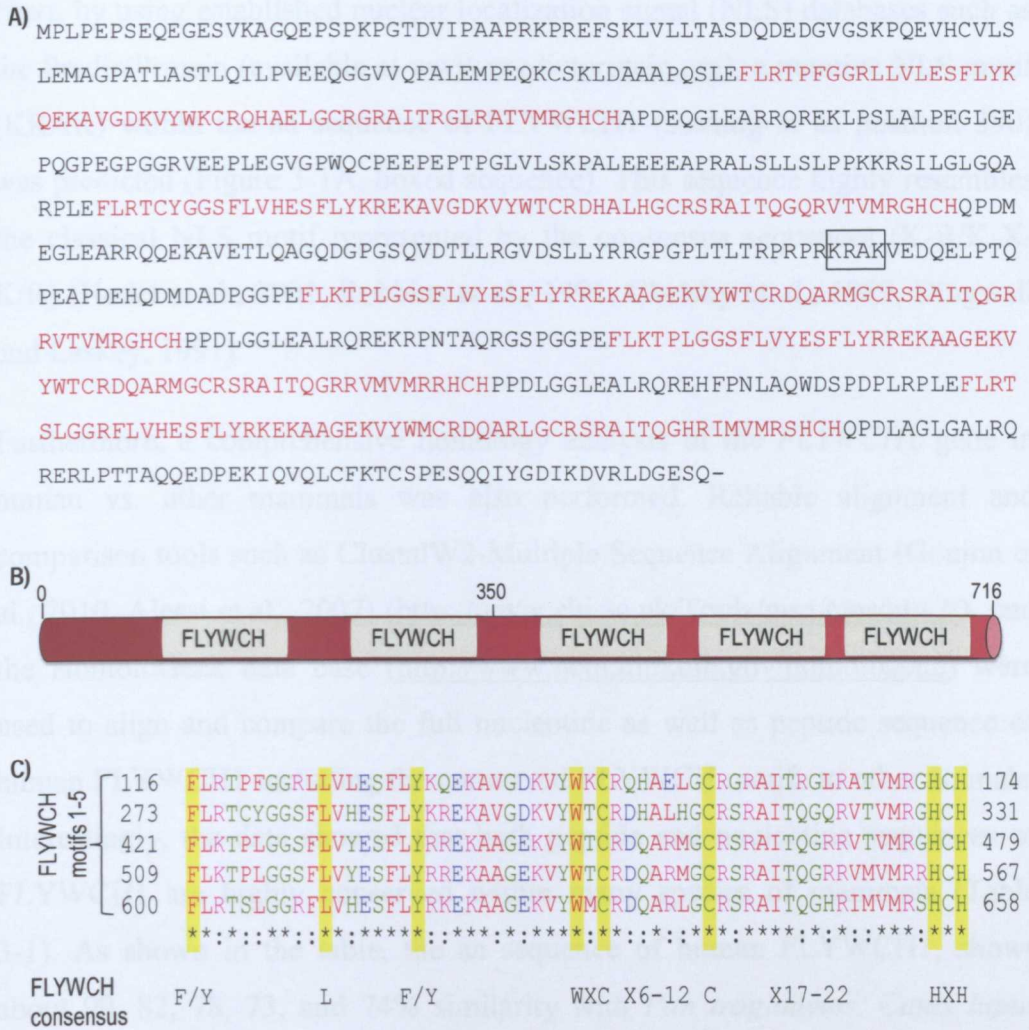


**Figure 3-1: Schematic presentation of FLYWCH motifs within human FLYWCH1 protein. A)** Shows the aa sequence of full-length human FLYWCH1. The deduced aa sequence indicates a complete identity of the FLYWCH1 IMAGE clone nucleotide sequence (see section 3.2.2) translated to protein by ExPASy translate tool (<http://expasy.org/>). The aa composition of FLYWCH motifs are highlighted in red and the predicted NLS motif is boxed. **B)** A diagram shows tandem repeats of five FLYWCH encoding domains across human FLYWCH1 protein. **C)** Alignment of FLYWCH domain sequences shows the core aa residues (F, L, Y, W, C, and H) of FLYWCH consensus sequence highlighted in yellow. The starting and ending residue numbers given for each domain indicate the aa numbering within the FLYWCH1 protein sequence. All identical residues are indicated by asterisks (\*) at the bottom line and the non-identical residues by colons (:).

Next, by using established nuclear localization signal (NLS) databases such as the PredictProtein (available at [www.predictprotein.org](http://www.predictprotein.org)), a putative NLS motif (KRAK) within the aa sequence of FLYWCH1 (starting at aa position 390) was predicted (Figure 3-1A, boxed sequence). This sequence highly resembles the classical NLS motif represented by the consensus sequences (K-R/K-X-K/R) (Hodel et al., 2001, Robbins et al., 1991, Chelsky et al., 1989, Dingwall and Laskey, 1991).

Furthermore, a comprehensive homology analysis of the *FLYWCH1* gene in human vs. other mammals was also performed. Reliable alignment and comparison tools such as ClustalW2-Multiple Sequence Alignment (Goujon et al., 2010, Alessi et al., 2007) (<http://www.ebi.ac.uk/Tools/msa/clustalw2/>) and the HomoloGene data base (<http://www.ncbi.nlm.nih.gov/homologene>) were used to align and compare the full nucleotide as well as peptide sequence of human FLYWCH1 including the conserved FLYWCH motifs to other animals. Interestingly, the data showed that both peptide and nucleotide sequences of FLYWCH1 are highly conserved within many species of mammals (Table 3-1). As shown in the table, the aa sequence of human FLYWCH1, shows about 99, 82, 78, 73, and 74% similarity with *Pan troglodytes*, *Canis lupus familiaris*, *Bos taurus*, *Mus musculus*, and *Rattus norvegicus* respectively.

**Table 3-1: Pairwise alignment scores of FLYWCH1 peptide and nucleotide sequences in human versus other animals.** The HomoloGene automated system was used to perform the protein and nucleotide sequence comparisons, the level of similarity (identity) is shown in percentage (%).

Gene		Identity (%)	
Species	Symbol	Protein	DNA
Homo sapiens	<i>FLYWCH1</i>		
vs. <i>Pan troglodytes</i>	<i>FLYWCH1</i>	98.5	98.8
vs. <i>Canis lupus familiaris</i>	<i>FLYWCH1</i>	81.9	83.9
vs. <i>Bos taurus</i>	<i>FLYWCH1</i>	78.6	83.7
vs. <i>Mus musculus</i>	<i>Flywch1</i>	73.1	76.4
vs. <i>Rattus norvegicus</i>	<i>Flywch1</i>	74.2	78.3

The multiple aa sequence alignment of FLYWCH1 in the above mentioned animals (Table 3-1) also showed conservation of the five FLYWCH domains in all species (Figure 3-2). Moreover, careful examination of FLYWCH1 aa sequence revealed that in addition to the FLYWCH domains, the putative NLS motif (KRAK) which was predicted for human FLYWCH1 (Figure 3-1) was also conserved in all these members (with one exemption) of mammalian FLYWCH1 proteins (Figure 3-2).

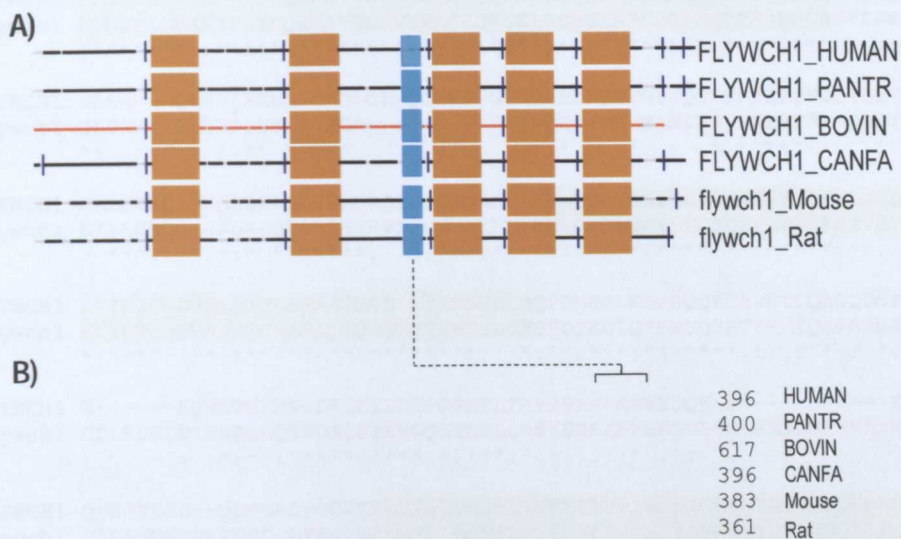


**Figure 3-2: Multiple sequence alignment of FLYWCH1 in different animals. A)** Multiple full-length aa sequence alignment of FLYWCH1 shows the presence of five conserved FLYWCH motifs within several members of FLYWCH1 family of protein as indicated. Dark boxes correspond to FLYWCH domains, while light blue boxes to NLS motifs (KRAK). Lines correspond to non-domain regions; dark lines or boxes show matched parts, while light ones gaps. Vertical dark blue lines indicate splicing boundaries. This alignment was generated using the Tree families database (Tfam accession number TF337169). **B)** Represents alignment of a short aa sequence of FLYWCH1 in the indicated animals shows the predicted conserved NLS motif (KRAK) highlighted in blue.

The full-length aa sequence alignment of FLYWCH1 in the indicated animals in (Figure 3-2) is presented in (Appendix 1). However, the aa sequence alignment of full-length FLYWCH1 in human and mouse (H-FLYWCH1 and



Previous reports have shown that DNA with high GC-content could be more stable than DNA with low GC-content (Hurst and Merchant, 2001, Yakovchuk et al., 2006). To investigate the GC-content ratio of *FLYWCH1* cDNA, a GC ratio calculator tool (available at [http://www.genomicsplace.com/gc\\_calc.html](http://www.genomicsplace.com/gc_calc.html)) was used. The results showed that *FLYWCH1* cDNA contains high GC-content ratio, with 1,456 G's and C's out of 2,151 nucleotides which is equal to 67.7%, indicating that the full-length *FLYWCH1* may normally have a stable structure.

### **3.2.2 Characterization of human FLYWCH1 IMAGE clone**

The IMAGE clone of the human *FLYWCH1* cDNA was purchased from Geneservice (IMAGE ID: 4839062/AK34 P16). The full-length nucleotide sequence of this clone was provided by the supplier and it is also available on the NCBI database (<http://www.ncbi.nlm.nih.gov/nuccore/22382197?report=genbank>) under the name “Homo sapiens FLYWCH-type zinc finger 1, mRNA (cDNA clone MGC: 26050 IMAGE: 4839062), complete CDS” with a GenBank accession number: BC028572.1. This sequence was used as a reference for *FLYWCH1* IMAGE clone cDNA validation and manipulation.

According to the sequence alignment data analysis, the *FLYWCH1* IMAGE clone sequence was matched to the human *FLYWCH1*, a gene that belongs to the mammalian *FLYWCH1* family. This gene comprises eight exons and maps to chromosome 16p13.3. Further genomic information for *FLYWCH1* (Gene ID: 84256) can be found on the NCBI data base at (<http://www.ncbi.nlm.nih.gov/gene/84256>).

The *FLYWCH1* IMAGE clone was received in a slant agar bacterial culture. Upon arrival, a small portion of the culture was re-grown in 5 ml Luria broth (LB) with Ampicillin (Amp) then the plasmid DNA was extracted. According to the information provided by the supplier (Geneservice), the IMAGE clone plasmid DNA is composed of 8,004 base pairs (bp) including the full-length

FLYWCH1 coding region (2,151 bp) fused to 5' and 3' untranslated regions (UTRs) (365 and 2,490 bp, respectively). This DNA fragment has been cloned into the pBluescriptR vector (2,998 bp) (Figure 3-4) by the supplier. It should be mentioned that there is one aa difference between the IMAGE clone provided sequence (Gene ID: BC028572.1) and the gene bank sequence (Gene ID: 84256) of FLYWCH1. However, this difference does not cause any out-of-frame reading of FLYWCH1 nucleotide sequences.

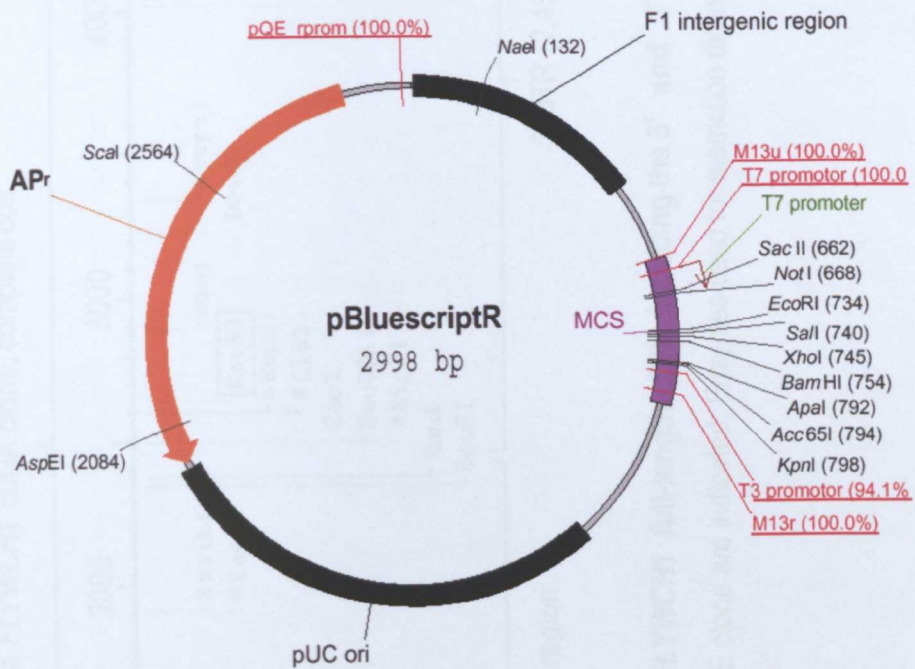


**Figure 3-4: pBluescriptR (KS+) plasmid (Stratagene).** Non-PCR- generated human full-length *FLYWCH1* cDNA was inserted into the pBluescriptR vector by the Geneservice Ltd to produce FLYWCH1 IMAGE clone.

In order to verify the presence of full-length *FLYWCH1* cDNA in the IMAGE clone, a restriction enzyme digestion analysis was carried out. As an initial step, all single cutter restriction enzymes within *FLYWCH1* cDNA including the 5' and 3' UTRs were mapped (Figure 3-5) using version 2.0 of NEBcutter tool (Vincze et al., 2003) available at (<http://tools.neb.com/NEBcutter2/index.php>).

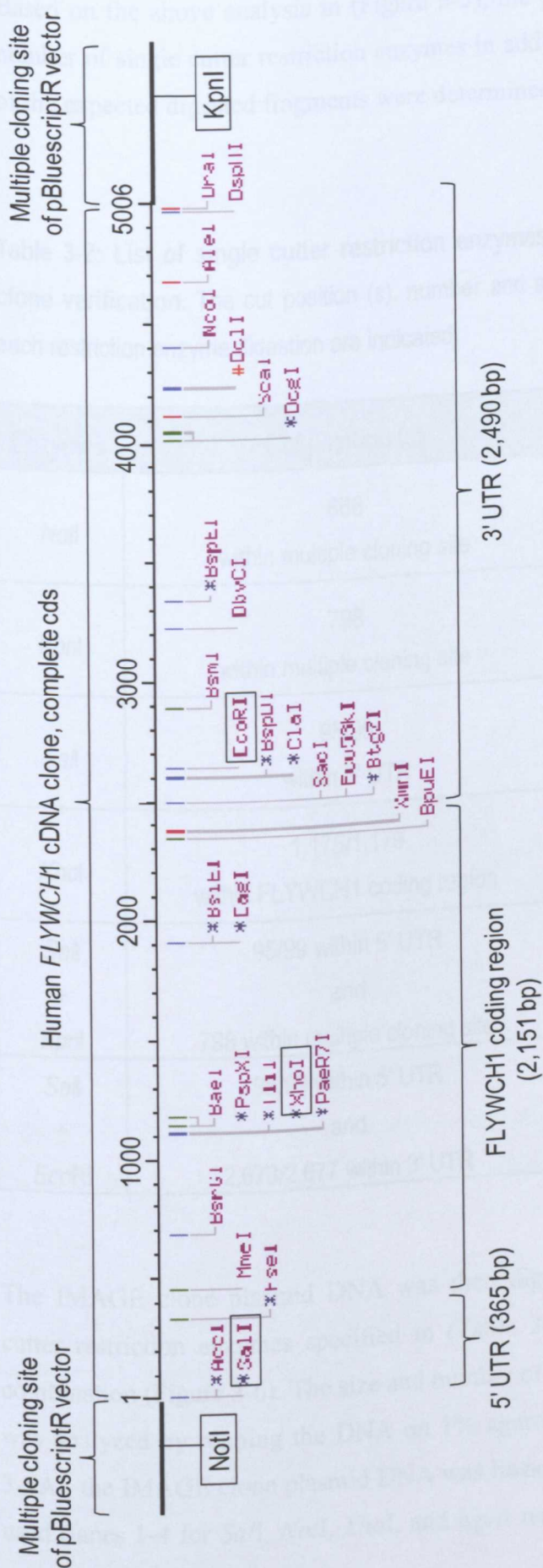


Figure 3-5: Single cutter restriction enzyme's map for *FLYWCH1* full-length cDNA including the 5' and 3' UTRs. All single cutter restriction enzymes within the entire sequence of *FLYWCH1* cDNA in the IMAGE clone are indicated. Enzymes used for restriction digestion analysis of *FLYWCH1* cDNA are boxed.

Based on the above analysis in (Figure 3-5), the precise cut position (s) of a number of single cutter restriction enzymes in addition to the number and size of the expected digested fragments were determined as shown in (Table 3-2).

**Table 3-2: List of single cutter restriction enzymes used for FLYWCH1 IMAGE clone verification.** The cut position (s), number and size of fragments resulted from each restriction enzyme digestion are indicated.

Enzymes	Cut position (s)	Fragments	Size (bp)
<i>NotI</i>	668 within multiple cloning site	1	8,004
<i>KpnI</i>	798 within multiple cloning site	1	8,004
<i>SaII</i>	95/99 within 5' UTR	1	8,004
<i>XhoI</i>	1,175/1,179 within FLYWCH1 coding region	1	8,004
<i>SaII</i> + <i>KpnI</i>	95/99 within 5' UTR and 798 within multiple cloning site	2	4,907 + 3,100
<i>SaII</i> + <i>EcoRI</i>	95/99 within 5' UTR and 2,673/2,677 within 3' UTR	2	5,430 + 2,582

The IMAGE clone plasmid DNA was then digested with the above single cutter restriction enzymes specified in (Table 3-2) either individually or in combination (Figure 3-6). The size and number of the digested DNA fragments was analyzed by running the DNA on 1% agarose gel. As shown in (Figure 3-6A), the IMAGE clone plasmid DNA was linearized by each of the enzymes used (lanes 1-4 for *SaII*, *NotI*, *XhoI*, and *KpnI* respectively). When two single

cutter enzymes were used together such as *SalI/KpnI* and *SalI/EcoRI* (Figure 3-6B), two expected FLYWCH1 DNA fragments; 3,100 and 2,582 bp (lanes 1 and 2 respectively) were released from the pBluscriptR vector. In support of supplier's information, the results of the restriction enzyme digestion confirmed the presence of full-length *FLYWCH1* cDNA in the IMAGE clone.

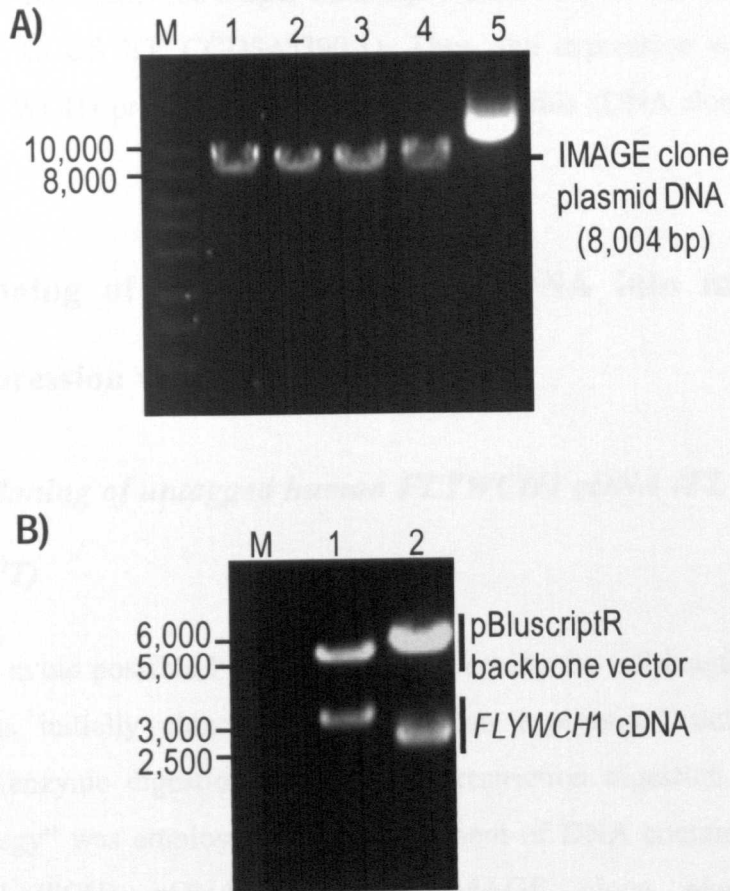


**Figure 3-6: Restriction enzyme digestion analysis of FLYWCH1 IMAGE clone plasmid DNA.** Agarose gel shows **A)** Linearized full-length plasmid DNA (8,004 bp) of FLYWCH1 IMAGE clone digested with single cutter enzymes. Lanes 1-4 correspond to *SalI*, *NotI*, *XhoI*, and *KpnI* respectively, while lane 5 represents the un-cut DNA of the IMAGE clone **B)** Digested DNA with combination of two single cutter enzymes; lane 1 corresponds to *SalI/KpnI* and lane 2 to *SalI/EcoRI*. Fragments of *FLYWCH1* cDNA; 3,100 bp (lane 1) and 2,582 bp (lane 2), were released from the rest of the IMAGE clone sequence (backbone vector + 5' and 3' UTRs) as indicated. Letter M, represents a 1Kb DNA ladder in bp (Sigma).

According to the information available on the NCBI data base, human *FLYWCH1* has two transcript variants; transcript variant (1), this variant represents the longer transcript and encodes the longer isoform (a) ([http://www.ncbi.nlm.nih.gov/protein/NP\\_115672.2](http://www.ncbi.nlm.nih.gov/protein/NP_115672.2)), whereas transcript variant (2) differs in the 3' UTR and coding region compared to variant (1). The resulting isoform (b) is shorter at the C-terminus compared to isoform (a) ([http://www.ncbi.nlm.nih.gov/protein/NP\\_065963.1](http://www.ncbi.nlm.nih.gov/protein/NP_065963.1)). The IMAGE clone used in this study represents the longer transcript which encodes the longer isoform (isoform a; CCDS ID: CCDS45390.1). Thus, the expression of full-length human *FLYWCH1* protein could be obtained using this cDNA clone.

### **3.2.3 Cloning of human *FLYWCH1* cDNA into mammalian expression vectors**

#### **3.2.3.1 Cloning of untagged human *FLYWCH1* cDNA (*FLYWCH1*-WT)**

In order to avoid possible PCR amplification errors, the full-length *FLYWCH1* cDNA was initially cloned into mammalian expression vectors using a restriction enzyme digestion strategy. The restriction digestion or “cut and paste strategy” was employed to cut a fragment of DNA containing the full-length *FLYWCH1* cDNA from the IMAGE clone plasmid vector (pBluescriptR) with *SalI* and *EcoRI* restriction enzymes (Figure 3-7A). A mammalian expression vector (pI-EGFP2) was also digested with the same restriction enzymes to create compatible cohesive ends (Figure 3-7B). pI-EGFP2 is a modified pKW2T vector which was reconstructed to express eGFP (Enhanced Green Fluorescence Protein) (Nateri et al., 2004) (see *Appendix 4*).

As shown in (Figure 3-7A), the size of the DNA fragment (2,582 bp) obtained by this digestion is bigger than the calculated size of the coding region of *FLYWCH1* cDNA (2,151 bp) based on the nucleotide sequence of this gene. This difference is due to the cutting positions of the restriction enzymes used.

*SalI* cuts ~269 bp upstream to the *FLYWCH1* coding region (inside the 5' UTR) and *EcoRI* cuts ~162 bp downstream to the *FLYWCH1* coding region (inside the 3' UTR). Thus, 431 extra nucleotides are fused to the cDNA sequence of *FLYWCH1* obtained by this enzymatic digestion.

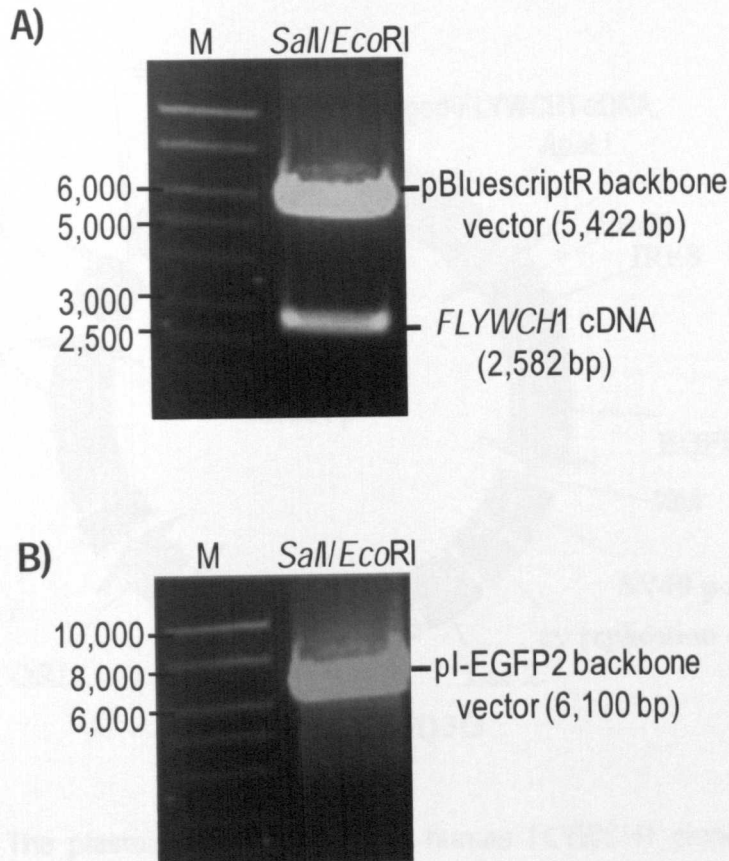


**Figure 3-7: Restriction enzyme digestion analysis of FLYWCH1 IMAGE clone and pI-EGFP2 plasmid vector.** *SalI* and *EcoRI* restriction enzymes were used to **A)** remove a full-length FLYWCH1 containing DNA fragment (2,582 bp) from the rest of the FLYWCH1 IMAGE clone (pBluescriptR vector plus 5' and 3' UTRs), and also to **B)** linearize the pI-EGFP2 vector (6,100 bp) as indicated. Letter M, denotes a 1Kb DNA ladder in bp (Sigma).

The *FLYWCH1* coding region was then inserted into the multiple cloning site of the pI-EGFP2 backbone vector to form a wild-type clone of untagged *FLYWCH1* (*FLYWCH1*-WT, 8682 bp). Therefore, by using this clone the *FLYWCH1* cDNA could be expressed under the *CMV*-promoter in mammalian cells and *SP6*-promoter for in vitro analysis as illustrated in (Figure 3-8).

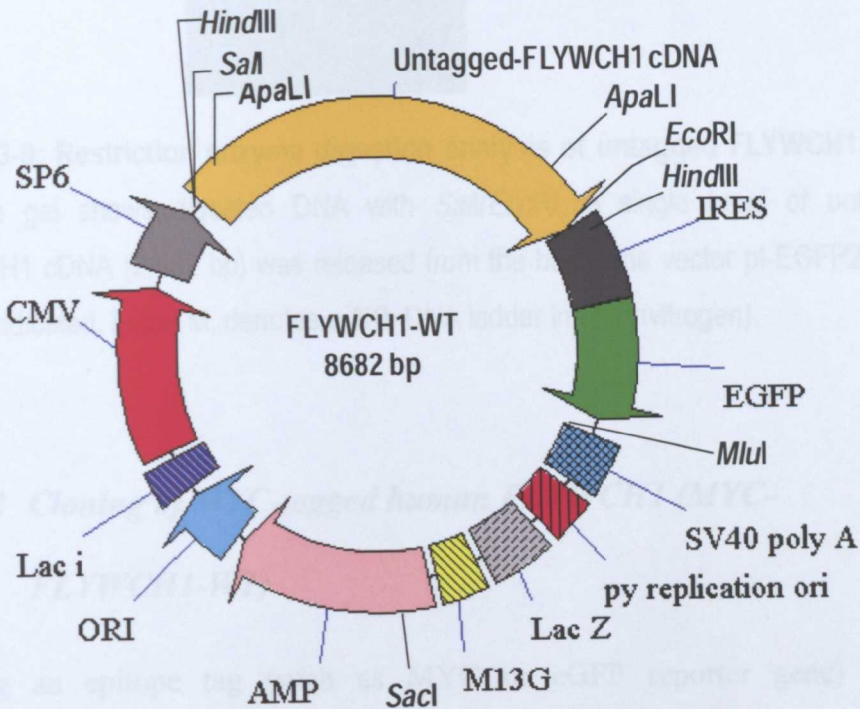


**Figure 3-8: The plasmid map of untagged human *FLYWCH1* clone.** A diagram shows the map of human *FLYWCH1*-WT clone (8,682 bp) with an untagged-*FLYWCH1* cDNA expressed under *CMV*-promoter.

To validate this clone, the plasmid DNA molecules were recovered from several transformed bacterial colonies and examined by the restriction enzyme digestion method using the same enzymes used for cloning (*SalI/EcoRI*). As shown in (Figure 3-9), a single band of DNA (2,582 bp) containing the full-length untagged-*FLYWCH1* cDNA was released from the backbone vector (pI-EGFP2, 6,100 bp). These data confirm the successful cloning of *FLYWCH1* cDNA in pI-EGFP2 mammalian expression vector.

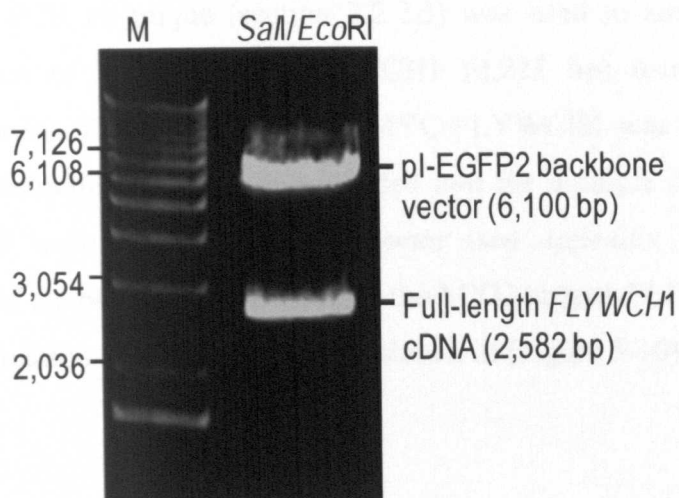


**Figure 3-9: Restriction enzyme digestion analysis of untagged FLYWCH1 clone.** Agarose gel shows digested DNA with *SalI/EcoRI*; a single band of untagged-FLYWCH1 cDNA (2,582 bp) was released from the backbone vector pi-EGFP2 (6,100 bp) as indicated. Letter M, denotes a 1Kb DNA ladder in bp (Invitrogen).

### **3.2.3.2 Cloning of MYC-tagged human FLYWCH1 (MYC-FLYWCH1-WT)**

Adding an epitope tag (such as MYC or eGFP reporter gene) to the exogenously expressed FLYWCH1 not only provides sensitive and specific detection of this protein, but it also simplifies characterization of FLYWCH1 throughout the biochemical and biological analyses. In the current work, the MYC-epitope tag which is a 10 aa segment of the human proto-oncogene c-MYC was fused to the 5'-end of *FLYWCH1* cDNA using PCR (Figure 3-10).

In order to amplify the full-length *FLYWCH1* cDNA fused to the MYC-epitope tag in-frame, specific primers were designed and the FLYWCH1 IMAGE clone plasmid DNA was used as a DNA template for the PCR reaction. The *NheI* restriction enzyme site and two copies of MYC-tag epitope sequence were engineered into the 5'-end of the forward primer, whereas the *EcoRI* restriction enzyme site and two copies of stop codons were added to the 3'-end of the reverse primer (Table 2-2).

The standard PCR technique (section 2.2.2.5) was used to amplify the full DNA sequence of MYC-tagged FLYWCH1 (2,221 bp) using the above described primers. The PCR product of MYC-FLYWCH1 was digested with *NheI/EcoRI* restriction enzymes and inserted into the multiple cloning site of pIRES2-EGFP mammalian expression vector (see Appendix 5). The final composition of the plasmid clone contains the MYC-tagged-FLYWCH1 cDNA under the expression of *CMV*-promoter as shown in (Figure 3-10).

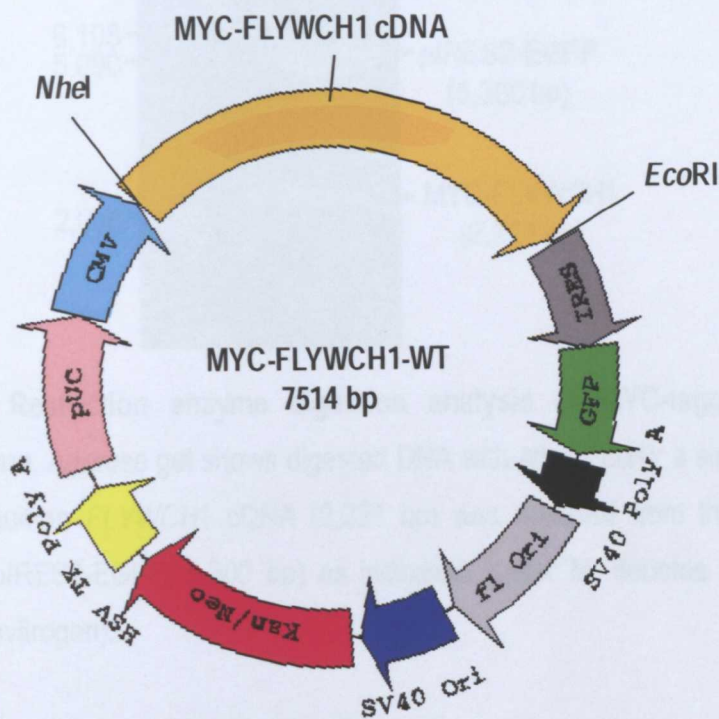


**Figure 3-10:** The plasmid map of MYC-tagged FLYWCH1 clone. A diagram shows the map of MYC-FLYWCH1 plasmid clone (7,514 bp) with MYC-tagged human FLYWCH1 cDNA expressed under *CMV*-promoter.

This clone was validated by restriction enzyme digestion analysis using *NheI* and *EcoRI*. As shown in (Figure 3-11), a single band of MYC-FLYWCH1 (2,221 bp) released from the backbone vector (5,300 bp), confirming that the MYC-epitope-fused *FLYWCH1* cDNA was successfully cloned into the

plasmid vector. The *FLYWCH1* cDNA correct orientation and in-frame construction with the MYC-epitope tag was further verified by automated DNA sequencing (Appendix 9). In addition, the protein expression of this clone was also confirmed by Western blotting analysis (Figure 3-14B). This clone therefore can be broadly applied to overexpress MYC-FLYWCH1 protein in mammalian cells that could be used for different biochemical and functional analysis.

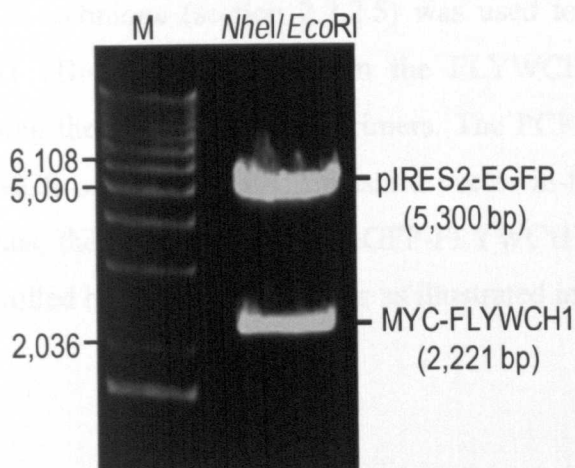


**Figure 3-11: Restriction enzyme digestion analysis of MYC-tagged human FLYWCH1 clone.** Agarose gel shows digested DNA with *NheI/EcoRI*; a single band of MYC-tagged human *FLYWCH1* cDNA (2,221 bp) was released from the backbone vector used (pIRES2-EGFP, 5,300 bp) as indicated. Letter M, denotes a 1Kb DNA ladder in bp (Invitrogen).

### 3.2.3.3 Cloning of eGFP-tagged human FLYWCH1 (eGFP-FLYWCH1-WT)

In order to dissect the cellular localization of FLYWCH1 in mammalian cell culture, cloning of human *FLYWCH1* cDNA fused to eGFP was carried out using the PCR strategy. Specific primers (Table 2-3) were designed and used to amplify the full-length *FLYWCH1* cDNA using the FLYWCH1 IMAGE clone cDNA as a template. Suitable restriction enzyme sites were engineered to the primers to facilitate the cloning process as detailed below. The *Bg/III* restriction site was added to the 5'-end of the forward primer and two extra

nucleotides (A & C) were also added to keep in-frame ORF (Open reading frame) through the nucleotide sequences of the multiple cloning site (MCS) of the plasmid vector (pEGFP-C2) (see Table 2-3). pEGFP-C2, is a mammalian expression vector and contains the enhanced green fluorescent protein (eGFP) reporter gene just upstream to the MCS (see Appendix 6). The *EcoRI* restriction site and two copies of stop codons were also added to the 3'-end of the reverse primer used as shown in (Table 2-3).

The standard PCR technique (section 2.2.2.5) was used to amplify the full-length *FLYWCH1* cDNA (2,151 bp) from the *FLYWCH1* IMAGE clone plasmid DNA using the above described primers. The PCR product was then cloned into the MCS of the pEGFP-C2 plasmid vector in-frame to the eGFP reporter gene. Thus, the expression of the eGFP-*FLYWCH1* fusion protein in this clone is controlled by the *CMV*-promoter as illustrated in (Figure 3-12).

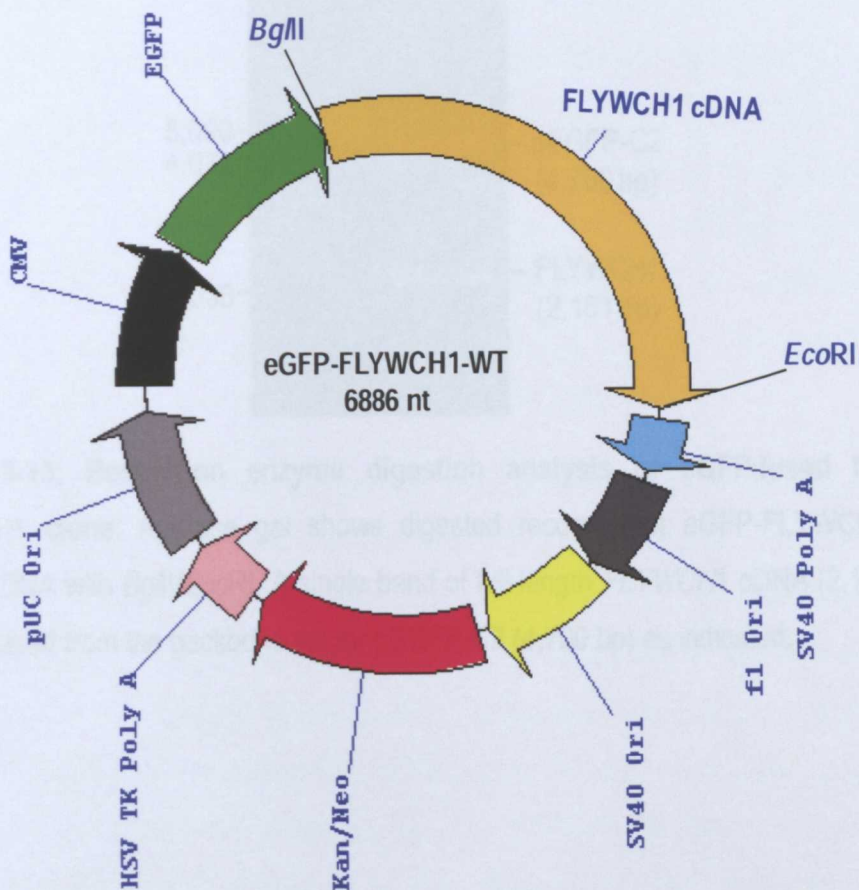


**Figure 3-12:** The plasmid map of the eGFP-fused FLYWCH1 clone. A diagram shows the map of eGFP-FLYWCH1 clone (6,886 bp) with N-terminal eGFP-fused FLYWCH1 cDNA expressed under CMV-promoter.

The successful construction of this clone was confirmed by restriction enzyme digestion analysis using *Bgl*III/*Eco*RI. As shown in (Figure 3-13), a single band of FLYWCH1 cDNA (2,151 bp) was released from the backbone vector (4,700 bp). The in-frame recombination of FLYWCH1 cDNA with the eGFP sequence of the plasmid vector was further verified by Western blotting (Figure 3-14A) and fluorescent microscopic analysis (Figure 3-15). This clone can be used to identify and study the FLYWCH1 gene expression patterns including the sub-cellular localization of this protein.

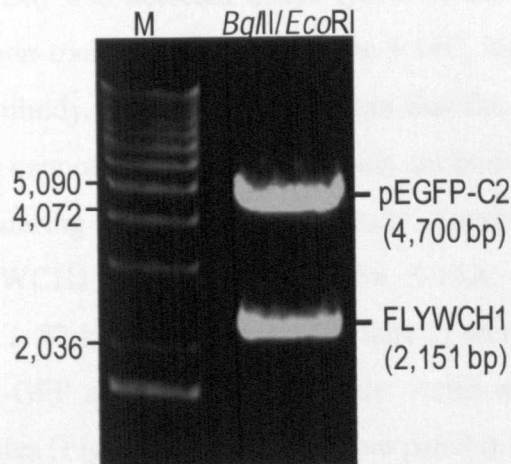


**Figure 3-13:** Restriction enzyme digestion analysis of eGFP-fused human FLYWCH1 clone. Agarose gel shows digested recombinant eGFP-FLYWCH1-WT plasmid DNA with *Bgl*III/*Eco*RI. A single band of full-length FLYWCH1 cDNA (2,151 bp) was released from the backbone vector pEGFP-C2 (4,700 bp) as indicated.

### **3.2.4 Exogenous expression of human *FLYWCH1* cDNA clones in cell culture**

To validate the protein expression of the above FLYWCH1 N-terminal fusion tagged and untagged clones, Western blotting (WB) analysis was carried out. The cDNA of untagged-FLYWCH1 (FLYWCH1-WT), MYC-tagged FLYWCH1 (MYC-FLYWCH1-WT), and eGFP-fused FLYWCH1 (eGFP-FLYWCH1-WT) clones were overexpressed in HEK293T cell line and the protein lysate was examined by Western blotting analysis (see section 2.2.5.2). The lysate of untransfected cells was also used as a negative control. Three types of antibodies; Anti-FLYWCH1, Anti-MYC (E10), and Anti-GFP (Table 2-7) were used to detect untagged, MYC-tagged, and eGFP-tagged FLYWCH1 proteins respectively as detailed below.

As shown in (Figure 3-14), a single band of overexpressed untagged-FLYWCH1 (~80 kDa) was detected in the lysate of the transfected cells but not in the control (non-transfected) cells (Figure 3-14C, lane 1 vs. lane 2) using anti-FLYWCH1 antibody. This finding indicates that the endogenous level of FLYWCH1 protein cannot be detected using this antibody which was the only antibody available during the course of this study. Similarly, a single band of eGFP-tagged FLYWCH1 (~106 kDa) (Figure 3-14A, lane 2) and MYC-tagged-FLYWCH1 (~82 kDa) (Figure 3-14B, lane 2) were also detected using anti-MYC and anti-GFP antibodies respectively. Actin was used as a loading control for all samples (Figure 3-14, A-C, bottom panels).

These data not only confirm the protein expression of all FLYWCH1 different clones in human cell culture, but also verify that the in-frame construction of FLYWCH1 to the MYC-epitope tag and eGFP-fusion proteins was successful. Therefore, these clones can be potentially used to study the biochemical properties of FLYWCH1 which leads to characterization of this protein. In addition, they can also be used for the biological and functional analyses of this gene. One problem we faced during the SDS-PAGE gel electrophoresis throughout this study is related to the visibility of the molecular weight markers at the same exposure time used for the protein bands. In most cases the

protein bands needed less exposure time than the molecular weight markers. Therefore, we could not always show the markers side-by-side with the protein bands on most of the Western blot membranes. However, different technical approaches were practically used to overcome this problem and to precisely evaluate the molecular weight of the protein bands. First, the coloured bands of the molecular markers on the PVDF membrane were highlighted with a normal pen. Then after exposing the membrane with the ECL reagent (section 2.2.5.2.2), different exposure times in addition to visual assessments of the exposed protein bands and the molecular markers were used to carefully determine the molecular weights of the protein of interest.

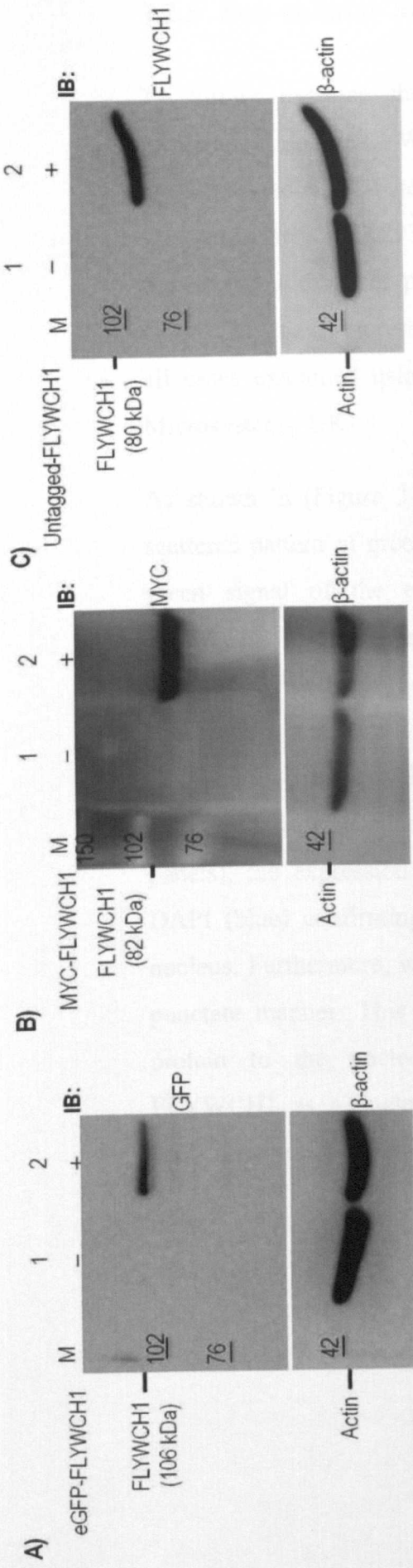


**Figure 3-14: Western blotting analysis of proteins expressed from different human FLYWCH1 clones in cell culture.** HEK293T cells were transiently transfected with **A)** eGFP-FLYWCH1 **B)** MYC-FLYWCH1 and **C)** Untagged-FLYWCH1 clones. The protein lysates were immunoblotted with anti-GFP, anti-MYC (E10), and anti-FLYWCH1 antibodies respectively. Single bands of overexpressed FLYWCH1 protein (lane 2 in all top panels) were detected as indicated. No bands of endogenous FLYWCH1 protein or other unspecific proteins were detected in the lysate of negative controls (i.e. untransfected cells) (lane 1 in all top panels). Actin was used as a loading control. "M", denotes the full range Rain Bow marker from GE Healthcare.

### **3.2.5 Sub-cellular localization of eGFP-FLYWCH1 protein**

To further examine the protein expression pattern and the sub-cellular localization of FLYWCH1, a fluorescent microscopic analysis of overexpressed eGFP-fused FLYWCH1 protein in different human cell cultures was performed. HEK293T, HCT116, and SW480 cell lines were transiently transfected with either pEGFP-C2 vector (control) or eGFP-FLYWCH1-WT clone. The green fluorescent signal of the eGFP reporter gene was observed in all cases examined using a Leica DMI3000 B Inverted microscope (Leica Microsystems, UK).

As shown in (Figure 3-15A, top panels), the control eGFP<sup>+ve</sup>-cells show a scattered pattern of green signal throughout the transfected cells, whereas the green signal of the eGFP reporter gene fused to FLYWCH1 (eGFP-FLYWCH1<sup>+ve</sup>-cells) was restricted to the nucleus in all three cell lines examined (Figure 3-15A, bottom panels). To further confirm the nuclear localization of FLYWCH1, the transfected SW480 cells were stained with a DNA-binding marker, DAPI (4',6-diamidino-2-phenylindole) and visualized under a fluorescent microscope. As shown in (Figure 3-15B, middle & bottom panels), the expression of eGFP-FLYWCH1 (green) was co-localized with DAPI (blue) confirming that FLYWCH1 is expressed and localized to the nucleus. Furthermore, within the nucleus the FLYWCH1 protein appears in a punctate manner. This may suggest a possible localization of FLYWCH1 protein to the nucleolus. Collectively, these data, strongly introduce FLYWCH1 as a nuclear protein judged by the nuclear expression of this protein in three different human cell lines.

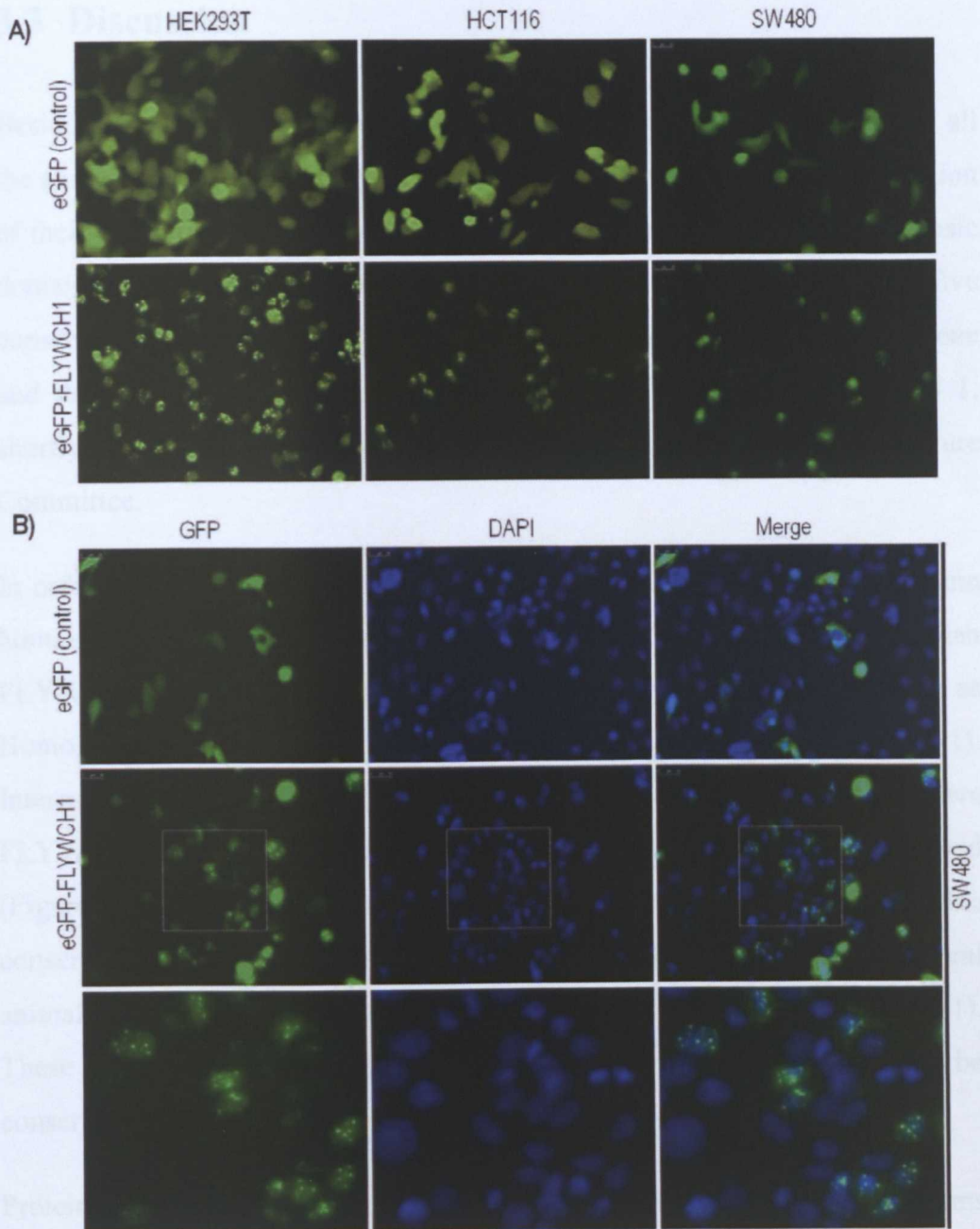


**Figure 3-15: Nuclear localization of human FLYWCH1.** A) Different cell lines (HEK293T, HCT116, and SW480) were transiently transfected with either pEGFP-C2 vector (control) or eGFP-FLYWCH1-WT clone. The transfected cells were subjected to fluorescent microscope analysis. Top panels show the scattered expression of eGFP protein, while bottom panels show the nuclear expression of eGFP-FLYWCH1 protein in the indicated cell lines. B) Transfected SW480 cells (green) were stained with DAPI (blue). Top panels show the expression of eGFP protein, while middle panels show the expression of eGFP-FLYWCH1 protein. Bottom panels are magnified views of the indicated area of eGFP-FLYWCH1 expressing cells (white boxes), emphasizing the punctate nuclear expression of this protein.

### 3.3 Discussion

Beside the substantial progress toward human proteome identification, not all the annotated protein coding genes have been characterized. When the function of their protein products is unknown, genes are often named after the intrinsic domains they contain. The protein product of *FLYWCH1* gene contains five conserved FLYWCH-type zinc finger domains (Figure 3-1). Thus, the gene and its protein product have been named as (FLYWCH-type zinc finger 1, shortly assigned as FLYWCH1) by the HUGO Gene Nomenclature Committee.

In order to further determine the precise positions of FLYWCH motifs within human FLYWCH1 protein and align this sequence with other mammalian FLYWCH1, in the current work, a variety of established databases such as HomoloGene and protein family (Pfam) were employed (Figure 3-1). Interestingly, the analysis revealed that within the sequence of the five FLYWCH motifs of human FLYWCH1, the aa residues are highly conserved (Figure 3-1C). Moreover, the alignment data showed the presence of five conserved FLYWCH domains within the aa sequence of FLYWCH1 in several animals including mouse, rat and chimpanzee (Figure 3-2 and *Appendix 1*). These data suggest that the physiological function of FLYWCH1 may also be conserved in mammals.

Proteins with FLYWCH domains have also been identified in other organisms such as *Drosophila*, in which this domain was initially identified (Buchner et al., 2000, Dorn and Krauss, 2003) and *C. elegans* (Beaster-Jones and Okkema, 2004, Ow et al., 2008). FLYWCH motifs within *Drosophila* proteins may play crucial roles in gene regulation and development through interaction with other transcription factors and/or binding to DNA (Dorn and Krauss, 2003, Dai et al., 2004, Provost and Shearn, 2006). Moreover, FLYWCH-motif containing proteins in *C. elegans* have shown to bind DNA and play crucial roles in the regulatory network of miRNA (Beaster-Jones and Okkema, 2004, Ow et al., 2008, Martinez et al., 2008). Similarly, presence of five FLYWCH domains in human FLYWCH1 and its conservativity in several animals (section 3.2.1)

indicates that these motifs may have crucial contribution to the biological function of mammalian FLYWCH1.

During the course of this study there was no commercially available FLYWCH1 antibody that works endogenously for immunohistochemistry (IHC), immunocytochemistry, Western blotting or ChIP-assay. However, we managed to obtain a mouse polyclonal FLYWCH1 antibody from Abcam (see Table 2-7) which was only detecting the overexpressed level of FLYWCH1 as claimed by the provider (<http://www.abcam.com/FLYWCH1-antibody-ab69284.html>) and also tested in cell culture in this study (Figure 3-14C). In addition, even for the overexpressed protein to be clearly detected, a large amount of protein and a high concentration of antibody were required. Despite these limitations, the FLYWCH1 antibody was used for the initial confirmation of FLYWCH1 expression (Figure 3-14C) and also to confirm its interaction with  $\beta$ -catenin (Figure 4-1). However, this antibody was not used for further analysis in the current study. Alternatively, both MYC and eGFP tagged clones of FLYWCH1 (section 3.2.3) which were effectively detected by MYC and GFP antibodies were used.

As an initial step towards the characterization of human FLYWCH1 protein, both epitope-tagged (MYC and eGFP) and non epitope-tagged *FLYWCH1* cDNA were cloned into different mammalian expression vectors (section 3.2.3) for different objectives. The cloning process was facilitated by obtaining the human *FLYWCH1* cDNA IMAGE clone. This clone provided the intact full-length human *FLYWCH1* cDNA which was used for direct (using restriction enzymes) or indirect (using PCR) cloning of *FLYWCH1*. After validation of the protein expression of FLYWCH1 clones in human cell culture (Figure 3-14), these clones became valuable resources for the forthcoming analyses to investigate the biochemical properties of FLYWCH1 and also to explore the biological impacts of this previously uncharacterized protein in human cell biology.

In agreement with the sub-cellular localization studies performed in this work (Figure 3-1A), the expression of FLYWCH1 was shown to be restricted to the nucleus in different human cell lines (Figure 3-15). These data supports the

presence of the predicted NLS motif in the aa sequence of FLYWCH1. Moreover, as mentioned above, FLYWCH motifs have been reported as DNA-binding domains in *C. elegans* (Beaster-Jones and Okkema, 2004, Ow et al., 2008). Therefore, it is possible that human FLYWCH1 might use its putative NLS and/or FLYWCH motifs to localize into the nucleus and bind DNA which could be required for its function. Moreover, the nuclear localization of FLYWCH1 protein may indicate the possibility that FLYWCH1 functions as a transcription factor. These observations encouraged us to further characterize and investigate the biological function of FLYWCH1 using different biochemical and functional analyses as addressed in the next following chapters.

To sum up, in the current chapter the protein product of the human *FLYWCH1* gene (FLYWCH1) was bioinformatically analyzed and the full cDNA sequence of this gene was successfully tagged and cloned into different mammalian expression vectors. In addition, the expression and nuclear localization of FLYWCH1 protein in different human cell lines was also observed.

## **CHAPTER 4**

# **The Interaction of FLYWCH1 with $\beta$ -catenin in Human Cells**

## 4.1 Introduction

The evolutionarily conserved FLYWCH domain defines several eukaryotic proteins; starting from *Drosophila* (Buchner et al., 2000, Dai et al., 2004, Dorn and Krauss, 2003, Provost and Shearn, 2006, Krauss and Dorn, 2004) to *C. elegans* (Beaster-Jones and Okkema, 2004, Ow et al., 2008, Thatcher et al., 2001), and ending with several uncharacterized proteins in mammals including human FLYWCH1 (see section 3.2.1). The FLYWCH domain in *Drosophila* Mod(mdg4) proteins has a putative role in protein-protein interactions; for example, Mod(mdg4)-67.2 interacts with the DNA-binding protein Su(Hw) via its FLYWCH domain (Gause et al., 2001, Ghosh et al., 2001). However, very little information is available in the literature about the function of proteins with FLYWCH domain in mammals.

Given that FLYWCH1 had been identified in our lab as a potential interacting partner with  $\beta$ -catenin in a yeast-2-hybrid assay (Figure 1-8), we now sought to evaluate whether this interaction occurred in human cells and, if so, where the binding domains are located. We used co-immunoprecipitation with specific antibodies against FLYWCH1 and  $\beta$ -catenin proteins when expressed as fusion proteins with FLAG, MYC or GFP epitopes in human HEK293T cells. Mutants with deletions at the N and C termini of FLYWCH1 and  $\beta$ -catenin showed that amino acids within the C-terminal region of FLYWCH1 (containing 3 FLYWCH motifs) and the N-terminal domain of  $\beta$ -catenin protein (consisting of GSK3- $\beta$ -phosphorylation region) are required for their physical interaction.

## 4.2 Results

### 4.2.1 FLYWCH1 interacts with $\beta$ -catenin in HEK293T cells

To investigate the possible *in vivo* interaction between FLYWCH1 and  $\beta$ -catenin in the cellular context, a co-immunoprecipitation (Co-IP) assay was performed. HEK293T cells were co-transfected with expression plasmids encoding; a constitutively active mutant clone of FLAG-tagged  $\beta$ -catenin (FLAG- $\beta$ -cat<sup>S33A</sup>) in which the phosphorylation site Serine33 (S33) is mutated to Alanine (A) provided by Dr. Nateri (Nateri et al., 2005) and the eGFP fused FLYWCH1 clone (eGFP-FLYWCH1-WT) (see section 3.2.4). The protein lysate was extracted from the cells and subjected to Co-IP using anti-FLAG antibody-conjugated agarose beads as outlined in (section 2.2.5.3.1). Briefly, 500  $\mu$ g of the protein lysate was incubated with 60  $\mu$ l of the FLAG-conjugated beads for 2-3 hours. Non-immunoprecipitated protein lysates were used as controls for the protein expression of plasmid constructs (Input). The standard Western blotting procedure was applied to perform the SDS-PAGE and the immunoblotting as described in (section 2.2.5.2).

The resultant expressed protein of the eGFP-fusion construct of FLYWCH1 (section 3.2.3.3) used in this experiment is composed of full-length FLYWCH1 protein (~80 kDa) fused to EGFP protein (26 kDa) resulting in a fusion protein (EGFP-FLYWCH1) of 106 kDa. This protein is weakly detected by FLYWCH1 antibody on both Input and Co-IP blots (Figure 4-1, Top panel, lanes 2, 3, & 7). However, the detection of eGFP-FYWCH1 protein is enhanced and strongly detected through re-blotting the same membrane with the GFP antibody (Figure 4-1, middle panel, lanes 2, 3, & 7).

As mentioned above the protein lysate of this experiment was immunoprecipitated with FLAG-conjugated beads to pull down FLAG- $\beta$ -cat<sup>S33A</sup> and if FLYWCH1 is interacting with  $\beta$ -catenin, we should see a band of EGFP-FLYWCH1 (106 kDa) in lane 7 of the Co-IP blot where both eGFP-FLYWCH1 and FLAG- $\beta$ -cat<sup>S33A</sup> are co-expressed. Interestingly, the Co-IP blot shows that in addition to  $\beta$ -catenin, a clear band of pulled-down eGFP-

FLYWCH1 protein was also detected by both anti-FLYWCH1 and anti-GFP antibodies (Figure 4-1, lane 7, arrowheads), suggesting that FLYWCH1 may directly interact with the nuclear  $\beta$ -catenin. Notably, this band was only appeared when both FLAG- $\beta$ -cat<sup>S33A</sup> and eGFP-FLYWCH1 were co-expressed together but not individually (Figure 4-1, lanes 5 & 6 vs. lane 7) which confirms the specificity of the binding. Thus, consistent with the RRS yeast-2-hybrid data (Saadeddin A *et al.* unpublished data), these results indicate that FLYWCH1 physically interacts with the unphosphorylated nuclear  $\beta$ -catenin in human cell culture.

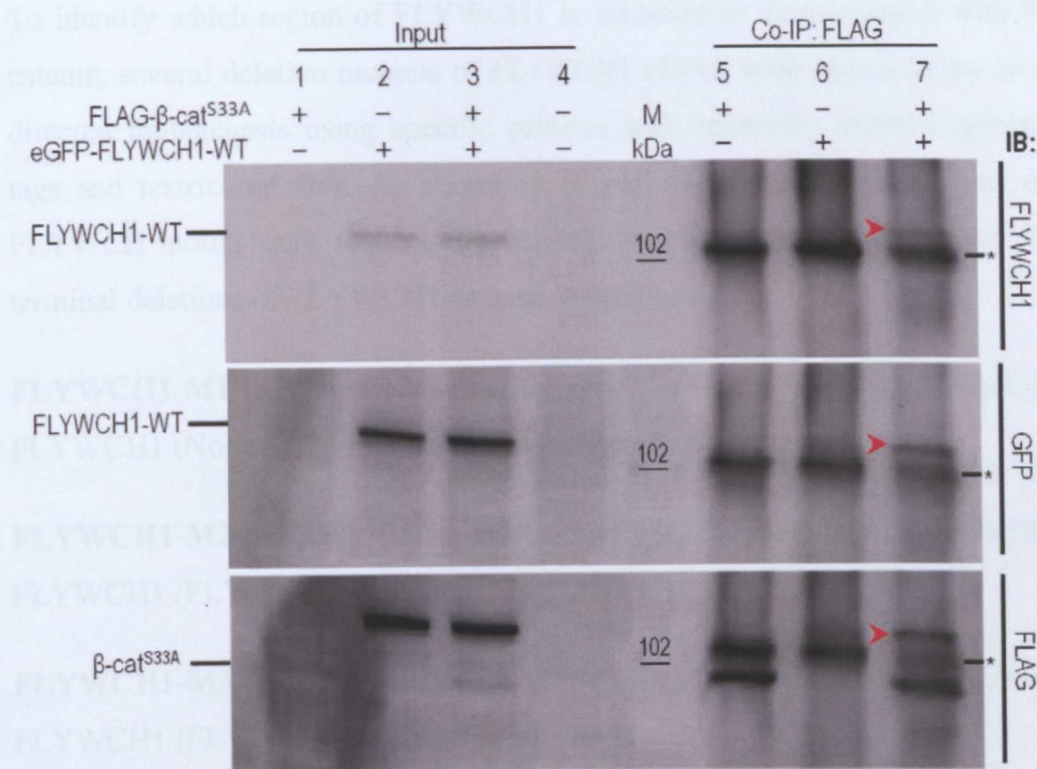


**Figure 4-1: Interaction of FLYWCH1 with  $\beta$ -catenin in human cell culture.** HEK293T cells were co-transfected with FLAG- $\beta$ -cat<sup>S33A</sup> and eGFP-FLYWCH1-WT as indicated. The protein lysates were co-immunoprecipitated using anti-FLAG-conjugated agarose beads. Both the Input and the Co-IP samples were immunoblotted with anti-GFP (top panel), anti-FLYWCH1 (middle panel) and anti-FLAG (bottom panel) antibodies. Arrowheads indicate protein bands of eGFP-FLYWCH1 detected by both anti-FLYWCH1 and anti-GFP antibodies. "M", denotes the full range Rainbow marker from GE Healthcare. Asterisks (\*) indicate unspecific bands. The experiment was repeated on several occasions.

Following our observation that FLYWCH1 directly interacts with the nuclear  $\beta$ -catenin (see above), we next investigated the potential regions involved in FLYWCH1/ $\beta$ -catenin interaction. Thus, the PCR site-directed mutagenesis (Liu and Naismith, 2008, Wang and Malcolm, 2002) was carried out to generate several deletion mutants of both FLYWCH1 and  $\beta$ -catenin proteins as detailed in the following sections.

#### **4.2.2 Site-directed mutagenesis of human FLYWCH1**

To identify which region of FLYWCH1 is involved in its interaction with  $\beta$ -catenin, several deletion mutants of *FLYWCH1* cDNA were generated by site-directed mutagenesis using specific primers with manually inserted epitope tags and restriction sites. As shown in (Figure 4-2), the coding regions of FLYWCH motifs were sequentially deleted over two N-terminal and two C-terminal deletions of FLYWCH1 as summarized below:

**FLYWCH1-M1 ( $\Delta$ N120):** 120aa are deleted from the N-terminus domain of FLYWCH1 (None of the FLYWCH motifs are removed).

**FLYWCH1-M2 ( $\Delta$ N350):** 350aa are deleted from the N-terminus domain of FLYWCH1 (FLYWCH motifs no.1 and 2 are removed).

**FLYWCH1-M3 ( $\Delta$ C120):** 120aa are deleted from the C-terminus domain of FLYWCH1 (FLYWCH motif no.5 is removed).

**FLYWCH1-M4 ( $\Delta$ C350):** 350aa are deleted from the C-terminus domain of FLYWCH1 (FLYWCH motifs no.3, 4, and 5 are removed).

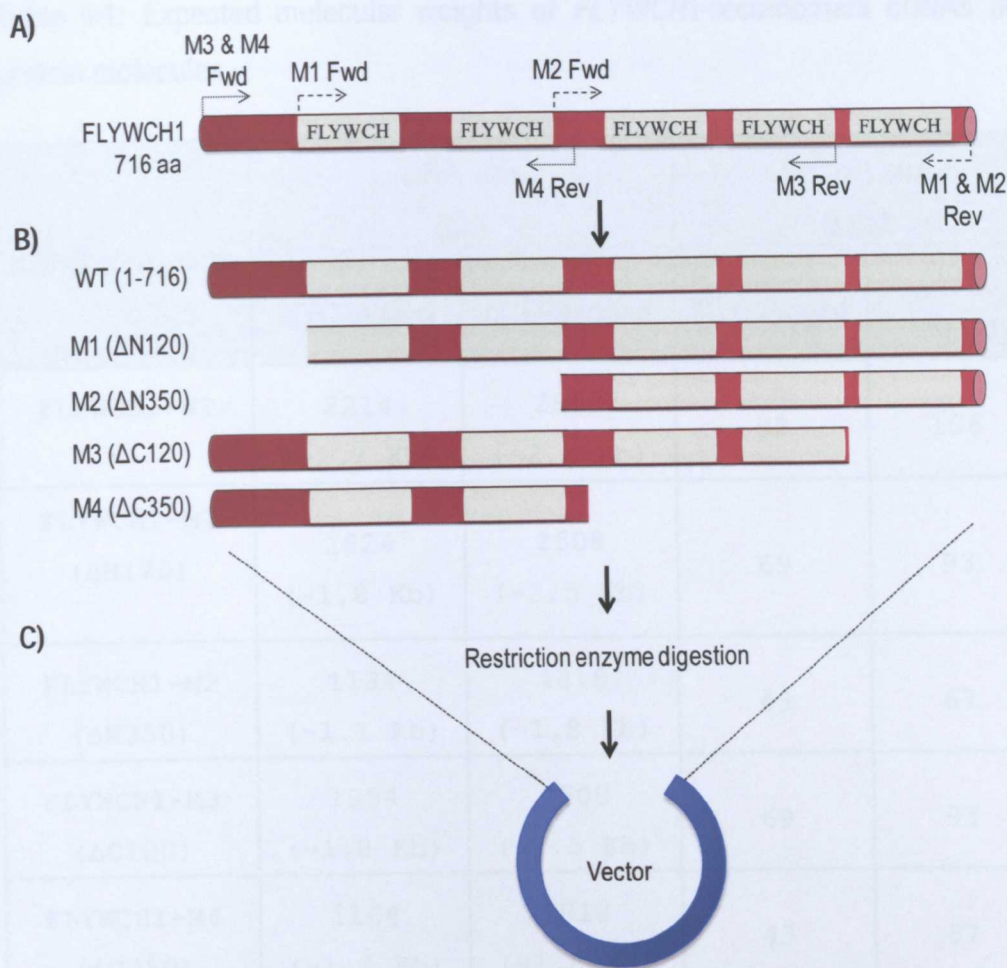


**Figure 4-2: Schematic presentation of *FLYWCH1* PCR-site directed mutagenesis.** A) Represents the full-length coding region of *FLYWCH1*-WT cDNA with sites-specific primer (s) to generate *FLYWCH1* deletion mutants (M1-4) by PCR (B). The PCR product of each deletion mutant was digested with specific restriction enzymes and cloned into the MCS of a mammalian expression vector (C).

The above deletion mutants were tagged with either MYC or eGFP-epitope and cloned into suitable mammalian expression vectors as described below in (sections 4.2.2.1 & 4.2.2.2). The molecular weights of the recombinant cDNAs and proteins encoded by *FLYWCH1* deletions varied according to the size of the deleted cDNA region(s) as shown in (Table 4-1).

Table 4-1: Expected molecular weights of *FLYWCH1*-recombinant cDNAs and protein molecules.

cDNA constructs	DNA size (bp)		Protein size (kDa)	
	MYC-tagged	eGFP-tagged	MYC-tagged	eGFP-tagged
FLYWCH1-WT	2214 (~2.2 Kb)	2868 (~2.8 Kb)	82	106
FLYWCH1-M1 ( $\Delta$ N120)	1824 (~1.8 Kb)	2508 (~2.5 Kb)	69	93
FLYWCH1-M2 ( $\Delta$ N350)	1134 (~1.1 Kb)	1818 (~1.8 Kb)	43	67
FLYWCH1-M3 ( $\Delta$ C120)	1854 (~1.8 Kb)	2508 (~2.5 Kb)	69	93
FLYWCH1-M4 ( $\Delta$ C350)	1164 (~1.2 Kb)	1818 (~1.8 Kb)	43	67

#### 4.2.2.1 MYC-tagged deletion mutants of *FLYWCH1*

To facilitate the immunoblotting detection of *FLYWCH1* proteins encoded by the above clones, the MYC-epitope tag was fused to the 5'-end of the amplified fragment of each deletion. Suitable restriction sites (*NheI* and *EcoRI*) were added to the forward and reverse primers respectively as shown in (Table 2-2). These primers were used to amplify the deletion mutants of *FLYWCH1* that described in (Figure 4-2) by PCR. The PCR products were digested with *NheI/EcoRI* restriction enzymes and subsequently cloned into the pIRES2-EGFP vector (*Appendix 5*). Successful ligation of *FLYWCH1* cDNA fragments was confirmed by restriction enzyme digestion analysis using the same enzymes that were used for cloning (*NheI/EcoRI*).

As shown in (Figure 4-3), the digested DNA fragments of all *FLYWCH1* deletion mutants M1-4 with expected molecular weights (1.8, 1.1, 1.8, and 1.2 Kb respectively) were removed from the backbone vector (5.3 Kb) and visualized on 1% agarose gel. The wild-type clone (MYC-FLYWCH1-WT. 2.2 Kb) was used as a control to compare the size of DNA fragments of mutant clones. These data confirmed the successful cloning of all MYC-tagged *FLYWCH1* cDNA mutants into the pIRES2-EGFP vector. Deletions were also confirmed by additional sequencing analysis.

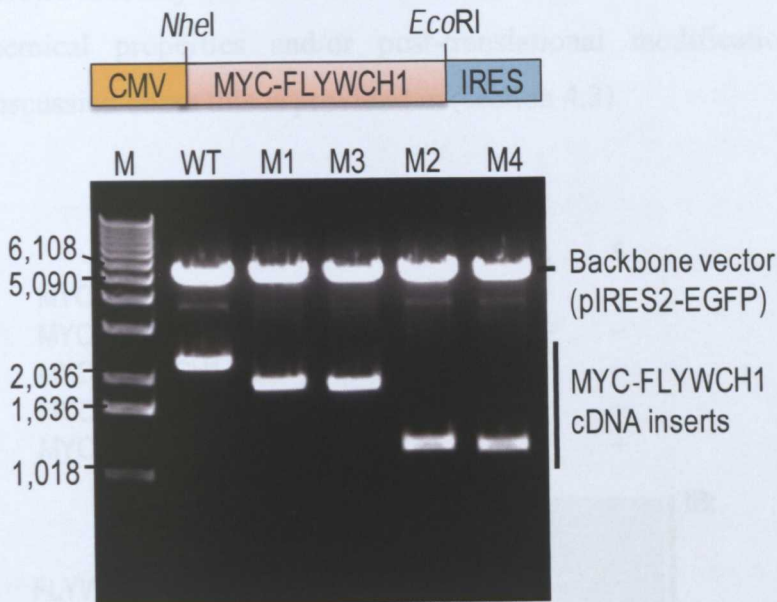


**Figure 4-3: Restriction enzyme digestion analysis of MYC-FLYWCH1 deletion mutant clones.** **Top panel)** A diagram shows the cutting position of *NheI* and *EcoRI* restriction enzymes within the DNA constructs. **Bottom panel)** Agarose gel shows the *NheI/EcoRI* digested DNA fragments (2.2, 1.1, 1.2, 1.8, and 1.8 Kb, left to right) corresponding to the wild-type cDNA clone (WT) and all the deletion mutants of MYC-tagged-FLYWCH1 ( M1, M3, M2, and M4) respectively. Letter M, denotes a 1Kb DNA ladder (Invitrogen).

Next, the protein expression of all MYC-tagged FLYWCH1 clones (WT, M1, M2, M3, and M4) was examined by Western blotting analysis. HEK293T cells were transfected with the above clones and the cell lysate was immunoblotted using anti-MYC antibody. As shown in (Figure 4-4), the results of the Western blot show that all constructs with MYC-tagged *FLYWCH1* cDNAs express relevant proteins, indicating the successful cloning and the in-frame tagging of these clones with MYC epitope. However, it should be noted that the protein products of the C-terminal deletion mutants (M3 & M4) exhibited slower migration on the SDS-PAGE than the N-terminal deletions. Although further examinations are required to experimentally delineate this, but the slow electrophoretic mobility of the C-terminal deletions could be related to their physicochemical properties and/or post-translational modifications. More detailed discussion about this is provided in (section 4.3).

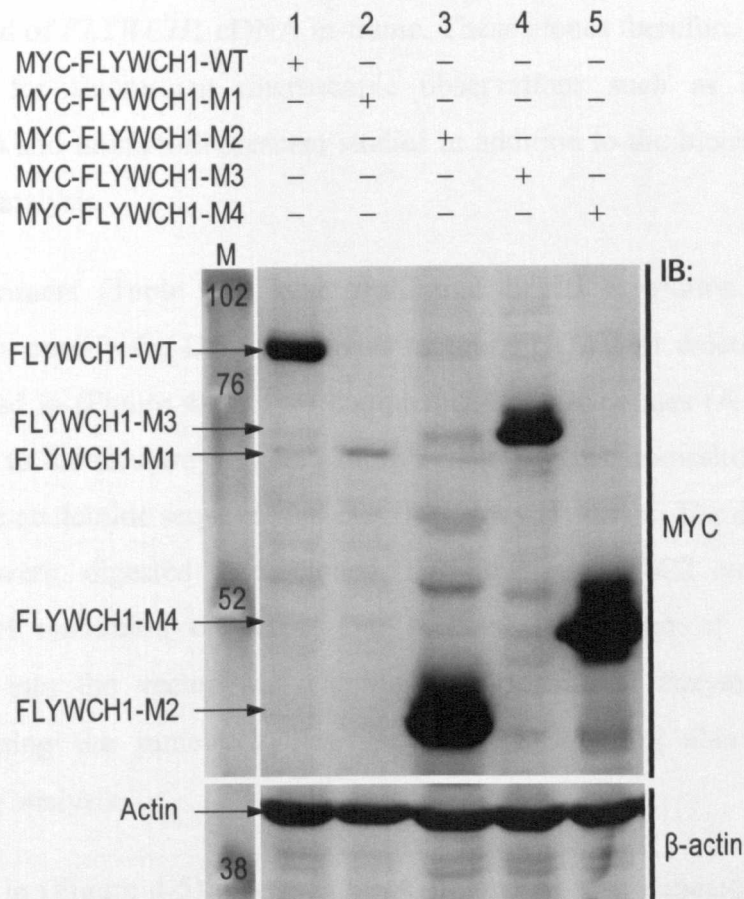


**Figure 4-4: Western blotting analysis of MYC-tagged FLYWCH1 clones.** HEK293T cells were transfected with the wild-type (WT, lane 1) and the deletion mutants of MYC-

tagged FLYWCH1 clones (lanes 2-5 for M1, M2, M3, and M4 respectively). The lysate was immunoblotted with anti-MYC antibody and the protein expression of each clone is shown as indicated.  $\beta$ -actin (bottom panel) was used as a loading control. "M", denotes the full range Rain Bow marker from GE Healthcare. The marker was loaded on the same membrane but separated from the presented blot by other samples. Expression of these clones were detected on several occasions.

#### **4.2.2.2 EGFP-tagged deletion mutants of FLYWCH1**

In order to fuse the above described deletions of *FLYWCH1* cDNA (Figure 4-2) to the eGFP reporter gene, the desired sequences of *FLYWCH1* cDNA were amplified by PCR. The amplified PCR products were then inserted into the multiple cloning site of pEGFP-C2 vector (*Appendix 6*) in such a way that the 3'-end of the eGFP reporter gene (located just upstream to the MCS) fused to the 5'-end of *FLYWCH1* cDNA in-frame. These clones therefore are broadly applicable for fluorescent microscopic observations such as sub-cellular localization and immunofluorescent studies in addition to the biochemical and biological analysis.

Specific primers (Table 2-3) with *Bgl*III and *Eco*RI restriction sites were designed to amplify the DNA fragments of four FLYWCH1 deletion mutants as illustrated in (Figure 4-2). Two complementary nucleotides (A & C) were also added to the forward primers (Table 2-3) to prevent frameshift mutations through the nucleotide sequences of eGFP-FLYWCH1 clone. The desired PCR products were digested and cloned into the pEGFP-C2 vector using *Bgl*III/*Eco*RI restriction enzymes. The successful insertion of FLYWCH1 fragments into the vector was examined by restriction enzyme digestion analysis using the same enzymes used for cloning and also by further sequencing analysis.

As shown in (Figure 4-5), digested DNA fragments with expected molecular weights (1.8, 1.1, 1.8, and 1.1 Kb) corresponding to FLYWCH1 deletion mutants (M1-4 respectively), were removed from the backbone vector (4.7 Kb) and visualized on 1% agarose gel. These data indicate successful insertion of

all FLYWCH1 deletion mutants into the MCS of pEGFP-C2 vector. However, the in-frame recombination of the *FLYWCH1* deletions to the eGFP reporter gene was further investigated through protein expression (Figure 4-6) and sequencing analyses (see below and the discussion section of this chapter).

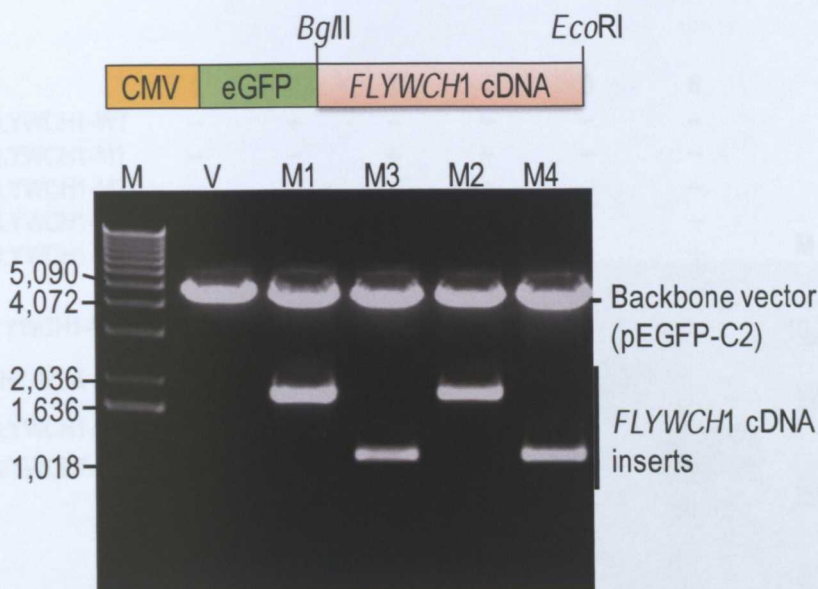


**Figure 4-5: Restriction enzyme digestion analysis of eGFP-FLYWCH1 deletion mutant clones.** **Top panel)** A diagram shows the cutting position of *BglII* and *EcoRI* restriction enzymes within the plasmid constructs. **Bottom panel)** Agarose gel shows digested DNA fragments (1.8, 1.1, 1.8, and 1.1 Kb) of all deletion mutants of FLYWCH1 (M1, M2, M3, and M4 respectively) removed from the pEGFP-C2 backbone vector (V) (4.7 Kb) using *BglII/EcoRI* restriction enzymes as indicated.

Next, the protein expression of all eGFP-tagged mutant clones of FLYWCH1 was examined by Western blotting analysis. HEK293T cells were transfected with these clones and the protein lysate was immunoblotted by anti-GFP antibody. As shown in (Figure 4-6), the expression of all eGFP-tagged FLYWCH1 clones was detected. In addition to the sequencing results, these data further confirmed the in-frame construction of FLYWCH1 coding region to the eGFP reporter gene. Similar to the MYC-tagged deletion mutant clones of FLYWCH1, the C-terminal deletions (especially M4) tend to migrate more

slowly on the SDS-PAGE than the N-terminal deletions. These differences can be explained by changes in the physicochemical properties of these clones and/or post-translational modifications. However, further studies would still be required to examine this possibility. More discussion about this is provided in (section 4.3).

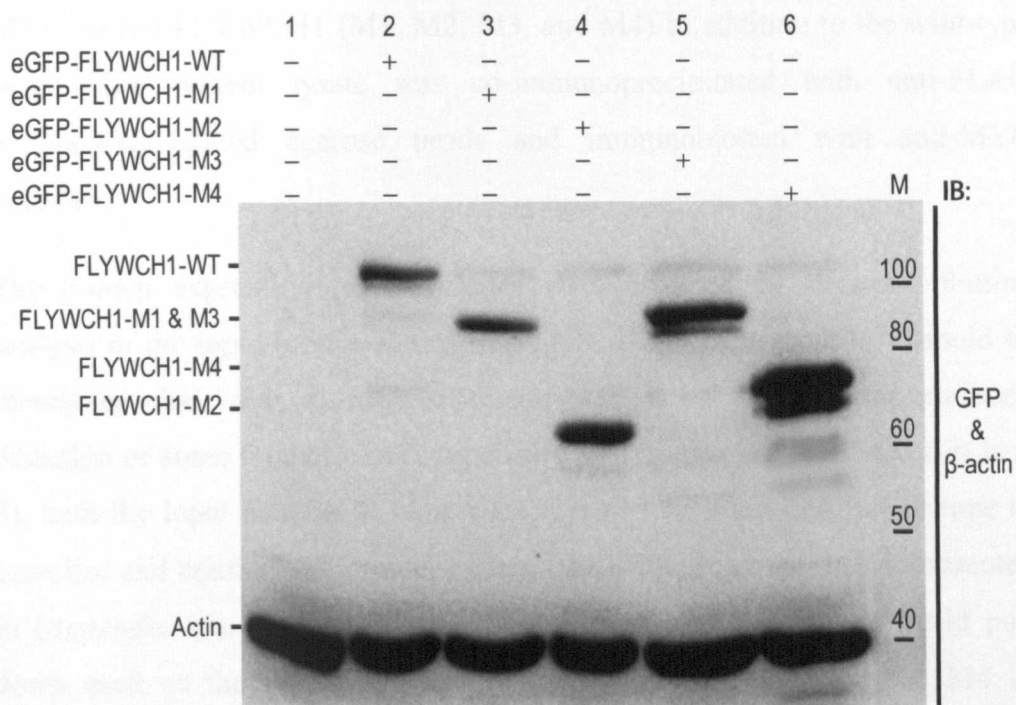


**Figure 4-6: Western blotting analysis of eGFP-FLYWCH1 clones.** HEK293T cells were transfected with the wild-type (WT, lane 2) and the deletion mutants of eGFP-tagged FLYWCH1 clones (lanes 3-6 for M1, M2, M3, and M4 respectively). The lysate was immunoblotted with anti-GFP antibody and the protein expression of each clone was detected as indicated. The lysate of untransfected cells (lane 1) was used as a negative control and  $\beta$ -actin (bottom panel) was used as a loading control. "M", denotes the ColorPlus Protein marker (in kDa) from NEW ENGLAND BioLabs. Expression of these clones were detected on several occasions.

### **4.2.3 Mapping the interaction site of FLYWCH1 with $\beta$ -catenin**

The deletion mutants of MYC-tagged FLYWCH1 were used to map the interaction site of FLYWCH1 with  $\beta$ -catenin using a Co-IP assay. HEK293T cells were co-transfected with expression plasmids encoding a constitutively active form of  $\beta$ -catenin (FLAG-  $\beta$ -catenin<sup>S33A</sup>) and the deletion mutants of MYC-tagged FLYWCH1 (M1, M2, M3, and M4) in addition to the wild-type clone. The protein lysate was co-immunoprecipitated with anti-FLAG antibody-conjugated agarose beads and immunoblotted with anti-MYC antibody.

The protein expressions of all clones were detected by Western blotting analysis of the Input blot as shown in (Figure 4-7, bottom panel). It should be mentioned that, due to low expression efficiency and/or poor antibody detection of some mutant clones especially M1 (Figure 4-7, red boxes in lane 3), both the Input and Co-IP blots were exposed for short and longer time to visualize and confirm the protein expressions. The long exposure is presented in (Appendix 15). The Co-IP data revealed that FLAG- $\beta$ -catenin could pull down each of the wild-type, deletions, M1, M2 and M3, but not M4 of FLYWCH1 (Figure 4-7, top panel) in which FLYWCH motifs number 3-5 are deleted. These results suggest that the C-terminal region of FLYWCH1 containing the last three FLYWCH motifs may be required for its interaction with  $\beta$ -catenin.

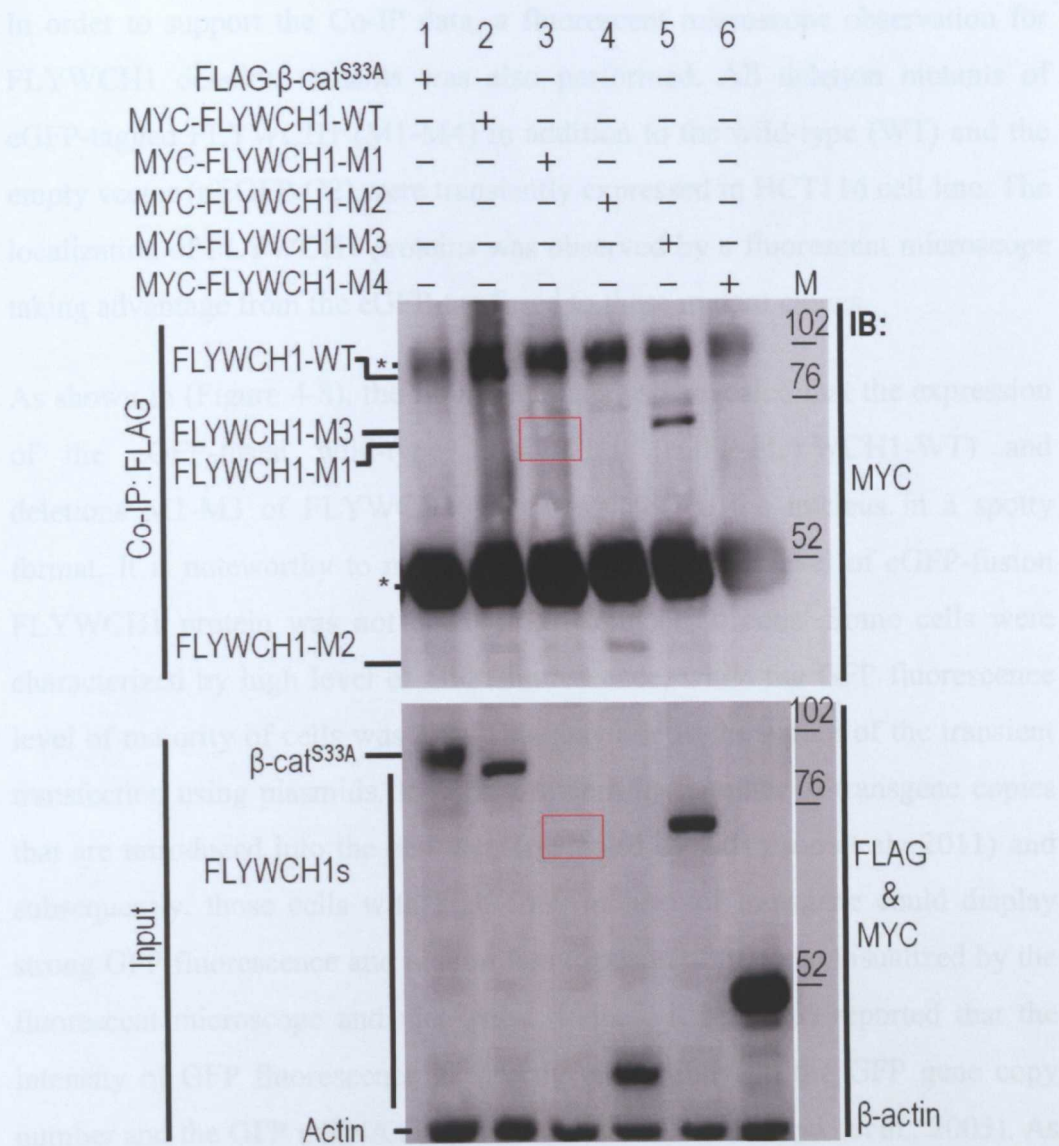


**Figure 4-7: Mapping the interaction site of FLYWCH1 with  $\beta$ -catenin using Co-IP assay.** HEK293T cells were co-transfected with the indicated constructs. The protein lysates were co-immunoprecipitated using anti-FLAG-conjugated agarose beads. **Top panel)** Shows immunoblotting for the Co-IP samples with anti-MYC antibody. **Bottom panel)** Shows immunoblotting for the input samples with anti-FLAG, anti-MYC, and anti- $\beta$ -actin antibodies as indicated. Red boxes indicate weak detection of M1-deletion mutant protein on both Co-IP and Input blots. Explanation about the slow migratory characteristics of deletion mutants M3 & M4 is provided in the text (sections 4.2.2.1 & 4.3). "M", denotes the full range Rain Bow marker from GE Healthcare. Asteriks (\*) indicate unspecific bands. The experiment represents 3 independent Co-IP approaches.

In order to support the Co-IP data, a fluorescent microscope observation for FLYWCH1 deletion mutants was also performed. All deletion mutants of eGFP-tagged FLYWCH1 (M1-M4) in addition to the wild-type (WT) and the empty vector (pEGFP-C2) were transiently expressed in HCT116 cell line. The localization of FLYWCH1 proteins was observed by a fluorescent microscope taking advantage from the eGFP-tag fused to these mutant clones.

As shown in (Figure 4-8), the fluorescent analysis revealed that the expression of the eGFP-fused wild-type FLYWCH1 (eGFP-FLYWCH1-WT) and deletions M1-M3 of FLYWCH1 were restricted to the nucleus in a spotty format. It is noteworthy to mention that the expression level of eGFP-fusion FLYWCH1 protein was not equal in all transfected cells. Some cells were characterized by high level of GFP fluorescence, while the GFP fluorescence level of majority of cells was low. This may due to the nature of the transient transfection using plasmids. In such a system the number of transgene copies that are introduced into the cell vary (reviewed by Adamson et al., 2011) and subsequently, those cells with high copy number of transgene could display strong GFP fluorescence and require less exposure time to be visualized by the fluorescent microscope and vice versa. Indeed, it has been reported that the intensity of GFP fluorescence is directly proportional to the GFP gene copy number and the GFP mRNA abundance in the cells (Soboleski et al., 2005). As a result of this variation, cells with high GFP fluorescence may not show proper punctate nuclear expression at the same exposure time used for the cells with low GFP fluorescence. Instead, false diffusion of the GFP fluorescence outside the nucleus may be seen (Figure 4-8).

Moreover, the green signal of the C-terminal deletion mutant M4 had clearly diffused into the cytoplasm and showed fewer or no spots in the nucleus (Figure 4-8, bottom panel), somehow resembling the expression pattern of the empty vector (Figure 4-8, top panel). These data support the results of the Co-IP experiment and collectively indicate that the C-terminal domain of FLYWCH1 is important for both protein-protein interaction and nuclear localization of this protein.

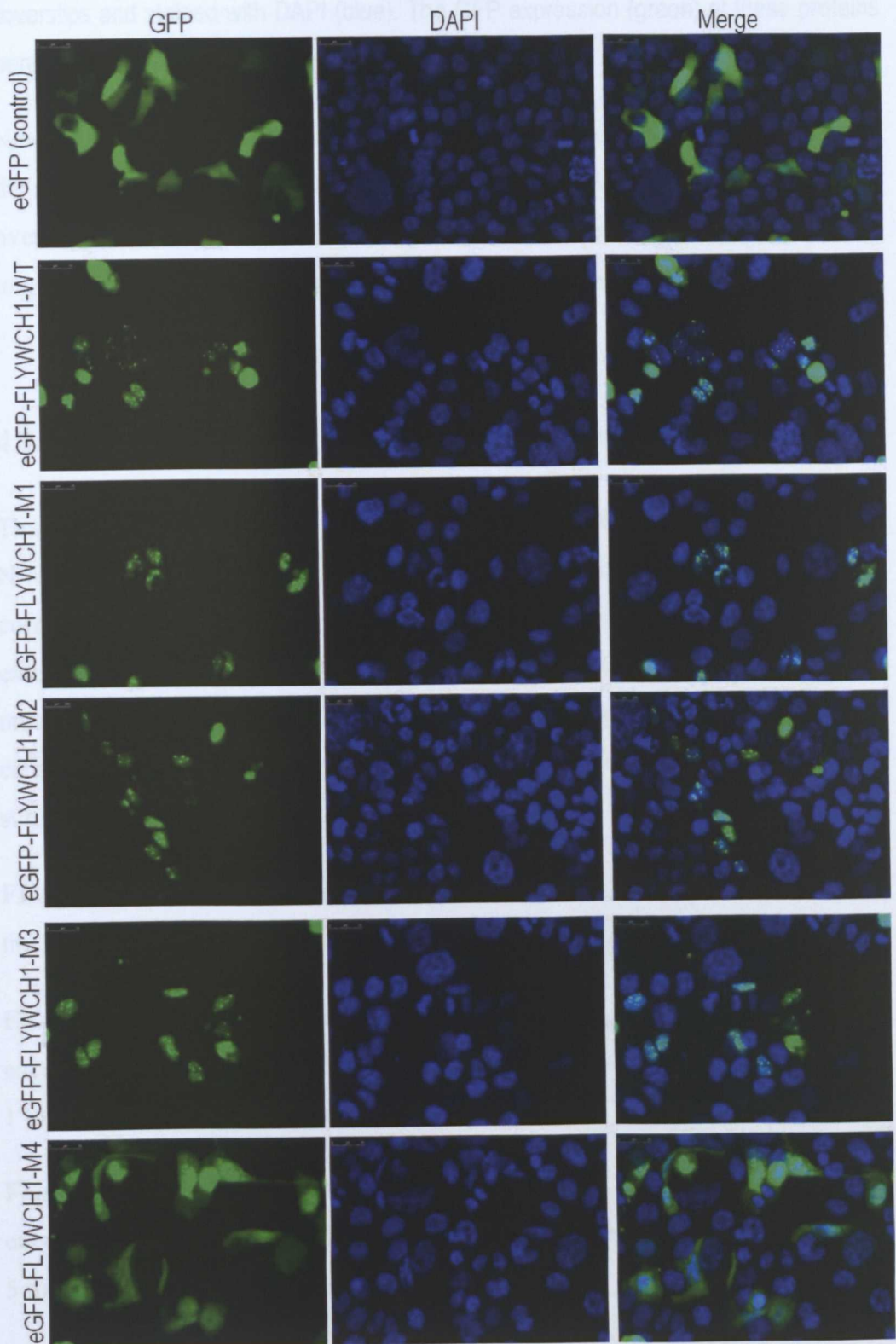


**Figure 4-8:** A C-terminal deletion mutant of FLYWCH1 (FLYWCH1-M4) changed the nuclear localisation of this protein. HCT116 cells were transiently transfected with pEGFP-C2 vector (control), the eGFP-tagged wild-type (WT) and all deletion mutants of eGFP-fused FLYWCH1 (M1-M4). The transfected cells were fixed on

coverslips and stained with DAPI (blue). The GFP expression (green) of these proteins were visualized by a fluorescent microscope as indicated.

Next, in order to identify the interaction domain of  $\beta$ -catenin with FLYWCH1, the site-directed mutagenesis (Liu and Naismith, 2008, Zheng et al., 2004) and overlap extension PCR (Heckman and Pease, 2007) techniques were employed to generate several deletion mutants of  $\beta$ -catenin as described below.

#### **4.2.4 Site-directed mutagenesis of $\beta$ -catenin cDNA**

The amino acid sequence of  $\beta$ -catenin has been divided into three regions; the N-terminus, the C-terminus and the armadillo repeats (Figure 4-9A). In the current work, we employed PCR site-directed mutagenesis and overlap extension PCR, in a similar strategy as outlined above, to generate five deletion mutant clones for  $\beta$ -catenin cDNA as shown in (Figure 4-9). Each deletion caused removal of a complete domain or specific part of a domain as summarized below:

**FLAG- $\beta$ -catenin- $\Delta$ N (N-terminal deletion,  $\Delta$ N126):** Nucleotides encoding the first 126 aa of the N-terminal domain of  $\beta$ -catenin are removed.

**FLAG- $\beta$ -catenin-MD1 (Middle deletion number 1,  $\Delta$ 121-276):** Nucleotides encoding aa number 121 to 276 corresponding to the armadillo repeats number 1 to 4 (R1-4) of  $\beta$ -catenin are removed.

**FLAG- $\beta$ -catenin-MD2 (Middle deletion number 2,  $\Delta$ 270-483):** Nucleotides encoding aa number 270 to 483 corresponding to the armadillo repeats number 5 to 9 (R5-9) of  $\beta$ -catenin are removed.

**FLAG- $\beta$ -catenin-MD3 (Middle deletion number 3,  $\Delta$ 477-713):** Nucleotides encoding aa number 477 to 713 corresponding to the armadillo repeats number 10 to 12 (R10-12) of  $\beta$ -catenin are removed.

**FLAG- $\beta$ -catenin- $\Delta$ C (C-terminal deletion,  $\Delta$ C180):** Nucleotides encoding the last 180 aa of the C-terminal domain of  $\beta$ -catenin are removed.

Specific primers described in (Table 2-4) were used to amplify the above mutations of  $\beta$ -catenin cDNA. The PCR amplicons were gel extracted, digested and cloned into a mammalian expression vector, pcDNA3 (for a complete map of pcDNA3 vector see Appendix 8).

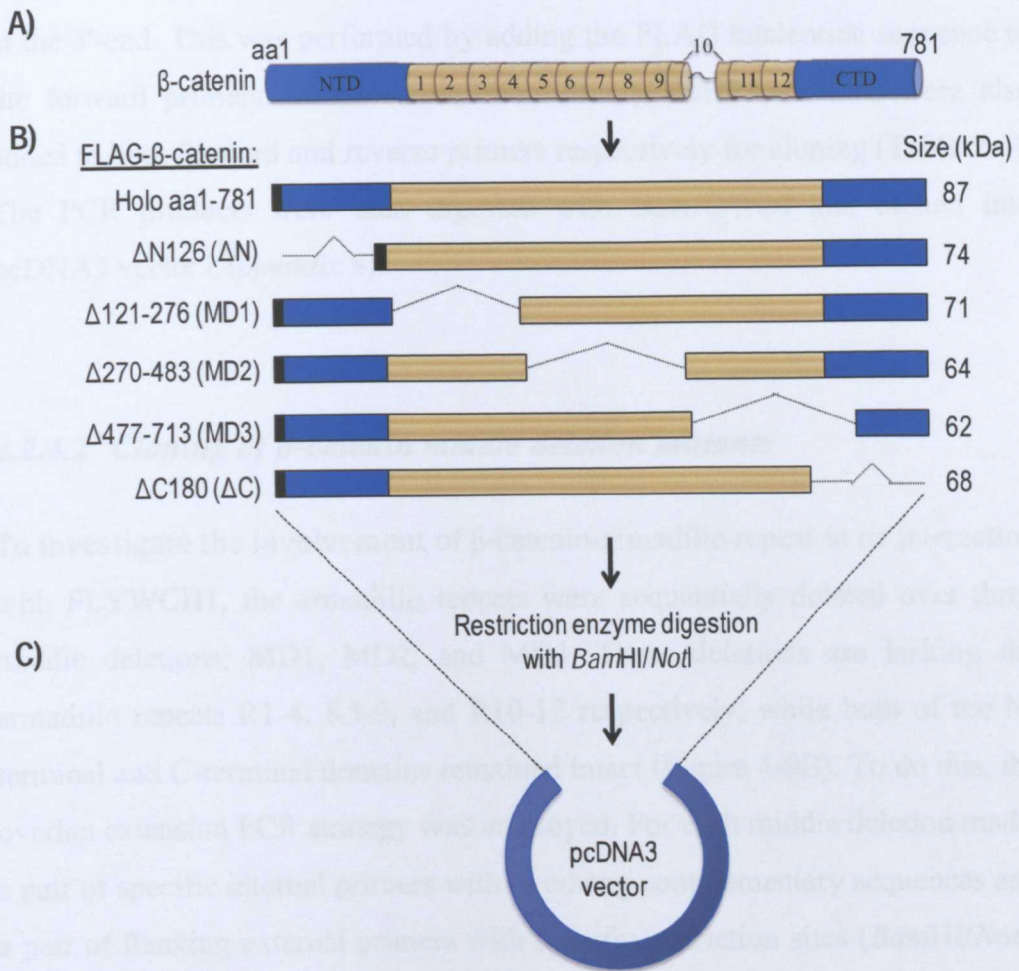


**Figure 4-9: Schematic presentation of  $\beta$ -catenin site-directed mutagenesis.** A diagram shows **A)** the N-terminus (NTD, blue), C-terminus (CTD, blue), and the central armadillo repeats domain (brown) of  $\beta$ -catenin and **B)** the wild-type (holo) and specific deletion mutants of  $\beta$ -catenin amplified by PCR. The PCR product of each deletion was **C)** digested with specific restriction enzymes (*Bam*HI/*Not*I) and cloned into the multiple cloning site of pcDNA3 vector. Black boxes represent FLAG-epitope tag.

#### **4.2.4.1 Cloning of $\beta$ -catenin N-terminal and C-terminal deletions**

In order to examine the involvement of the N- and/or C-terminal domains of  $\beta$ -catenin in the FLYWCH1/ $\beta$ -catenin interaction, the N-terminal ( $\beta$ -catenin- $\Delta$ N126) and C-terminal ( $\beta$ -catenin- $\Delta$ C180) mutant clones of  $\beta$ -catenin were generated by PCR. To facilitate the immunoblotting detection of these deletion mutants, the cDNA of each clone was tagged with the FLAG-epitope sequence at the 5'-end. This was performed by adding the FLAG nucleotide sequence to the forward primers. Suitable restriction sites (*Bam*HI and *Not*I) were also added to both forward and reverse primers respectively for cloning (Table 2-4). The PCR products were then digested with *Bam*HI/*Not*I and cloned into pcDNA3 vector (Appendix 8).

#### **4.2.4.2 Cloning of $\beta$ -catenin middle deletion mutants**

To investigate the involvement of  $\beta$ -catenin-*armadillo* repeat in its interaction with FLYWCH1, the *armadillo* repeats were sequentially deleted over three middle deletions; MD1, MD2, and MD3. These deletions are lacking the *armadillo* repeats R1-4, R5-9, and R10-12 respectively, while both of the N-terminal and C-terminal domains remained intact (Figure 4-9B). To do this, the overlap extension PCR strategy was employed. For each middle deletion made, a pair of specific internal primers with overhang complementary sequences and a pair of flanking external primers with specific restriction sites (*Bam*HI/*Not*I) were designed (Figure 4-10). To facilitate the immunoblotting of these clones, the amplified fragments were tagged with FLAG-epitope. This epitope was fused to the 5'-end of the forward flanking external primers as shown in (Table 2-4).

The overlap extension PCR applied in this study was performed in two steps. *First*, the desired fragments of  $\beta$ -catenin (A and B) were amplified using the FLAG- $\beta$ -catenin-WT cDNA as a template (Figure 4-10A&B). The deletion of interest (fragment C) was introduced by the specific internal primers described in (Table 2-4). As shown in (Figure 4-10A), the forward internal primer

(Internal Fwd) has a short 5'-overhang complementary strand to the reverse internal primer (Internal Rev) indicated by red colour. The complementary strands create overlapping nucleotide sequences within the intermediate amplified DNA fragments (Figure 4-10B).

**Second**, the flanking external primers were used to amplify an integrated strand of  $\beta$ -catenin contains the nucleotide sequence of fragments A and B, but not C (Figure 4-10, C&D) using the purified DNA of fragments A and B as a template. The final PCR product (AB) of each deletion was gel extracted, digested with *Bam*HI/*Not*I restriction enzymes and cloned into pcDNA3 vector (Figure 4-10E).

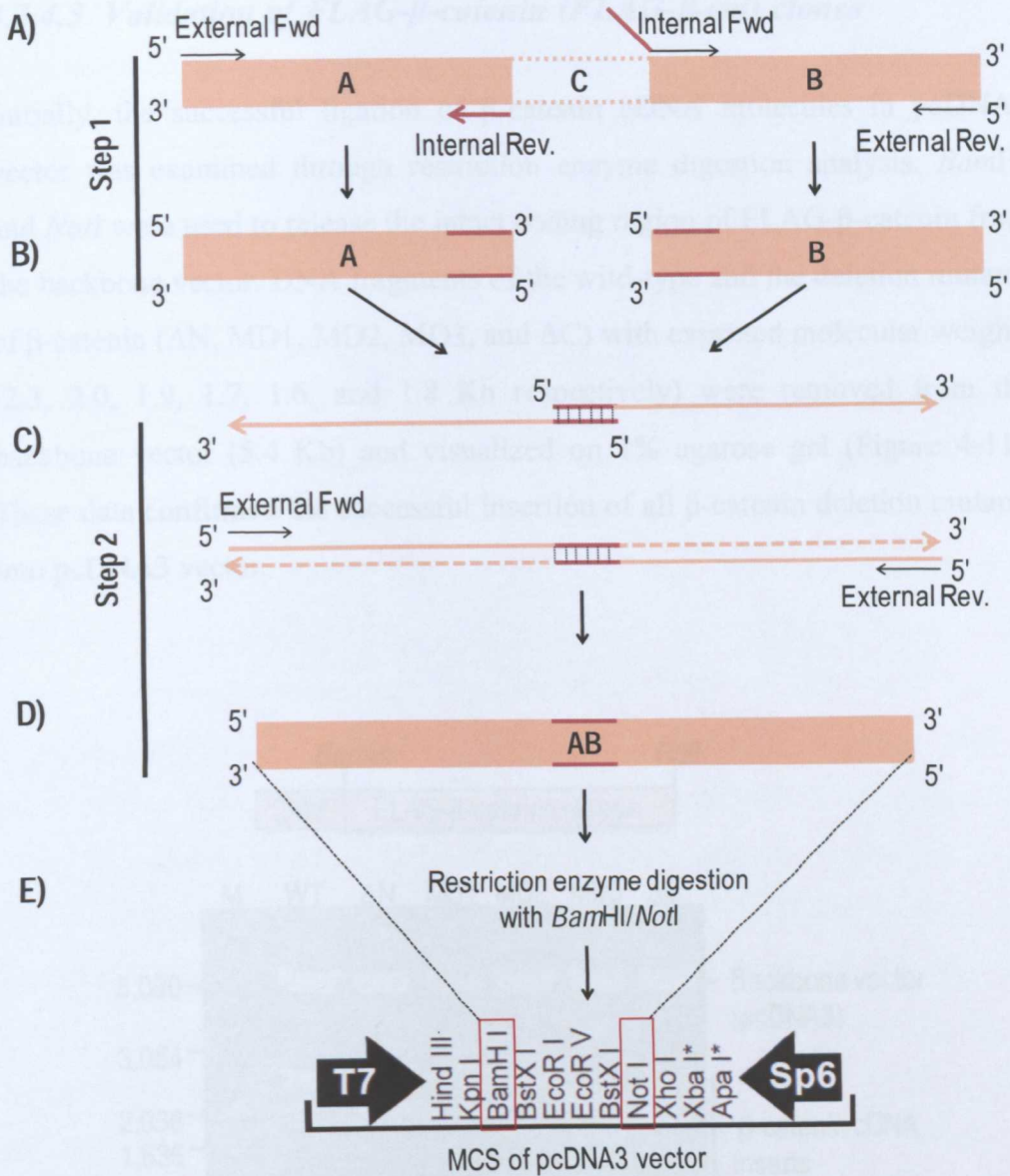
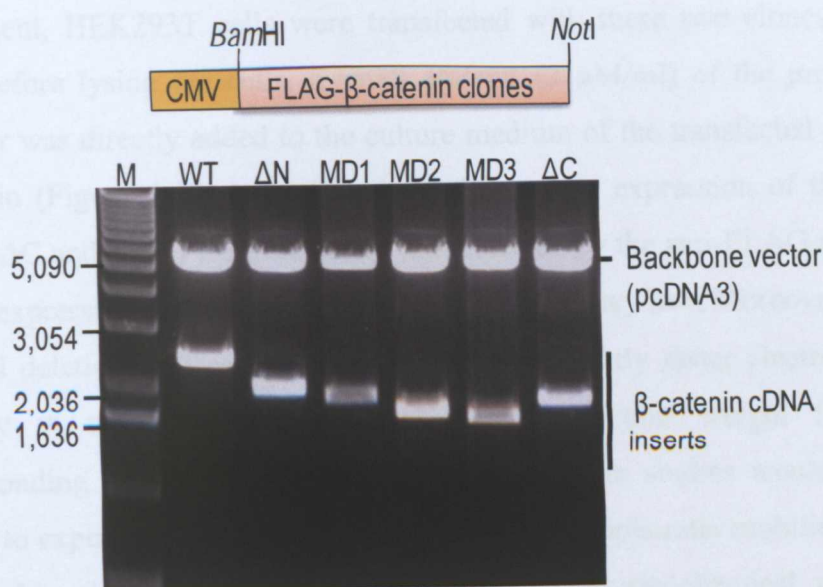


Figure 4-10: Generation of middle deletion mutant clones of  $\beta$ -catenin by overlapping PCR. **A)** Specific fragments of  $\beta$ -catenin cDNA were amplified in the first step of the PCR reaction using both complementary internal and flanking external primers as indicated. **B)** The intermediate PCR products (fragments A and B) with overhanging strands were gel extracted and **C)** used as a template in the second step of the PCR reaction using the flanking external primers only. **D)** The final PCR product (AB) containing the deletion of interest was **E)** digested with *Bam*HI/*Not*I restriction enzymes and inserted into the multiple cloning site of pcDNA3 vector.

#### 4.2.4.3 Validation of FLAG- $\beta$ -catenin (FLAG- $\beta$ -cat) clones

Initially, the successful ligation of  $\beta$ -catenin cDNA molecules in pcDNA3 vector was examined through restriction enzyme digestion analysis. *Bam*HI and *Not*I were used to release the intact coding region of FLAG- $\beta$ -catenin from the backbone vector. DNA fragments of the wild-type and the deletion mutants of  $\beta$ -catenin ( $\Delta$ N, MD1, MD2, MD3, and  $\Delta$ C) with expected molecular weights (2.3, 2.0, 1.9, 1.7, 1.6, and 1.8 Kb respectively) were removed from the backbone vector (5.4 Kb) and visualized on 1% agarose gel (Figure 4-11). These data confirmed the successful insertion of all  $\beta$ -catenin deletion mutants into pcDNA3 vector.



**Figure 4-11: Restriction enzyme digestion analysis of FLAG- $\beta$ -catenin clones.** **Top panel)** An illustration shows the position of *Bam*HI and *Not*I restriction enzymes within  $\beta$ -catenin plasmid constructs. **Bottom panel)** Agarose gel shows *Bam*HI/*Not*I digested DNA fragments (2.3, 2.0, 1.9, 1.7, 1.6, and 1.8 Kb) for the wild-type (WT) and the deletion mutants of FLAG-tagged  $\beta$ -catenin ( $\Delta$ N, MD1, MD2, MD3, and  $\Delta$ C) respectively. M: Marker, bp.

Next, Western blotting analysis was performed to examine the protein expression of these clones in HEK293 cells. The anti-FLAG antibody was used

to detect the protein product of FLAG- $\beta$ -catenin clones in the lysate of transfected cells. Both wild-type (FLAG- $\beta$ -cat-WT) and activated form (FLAG- $\beta$ -cat<sup>S33A</sup>) of FLAG- $\beta$ -catenin clones were used as positive controls for the expression of other clones in this experiment. The protein product of FLAG- $\beta$ -catenin constructs;  $\beta$ -cat<sup>S33A</sup>, WT,  $\Delta$ N, MD1, and MD2 with their relevant molecular weights (87, 87, 74, 71, and 64 kDa respectively) were detected by the FLAG antibody as shown in (Figure 4-12). However, the expression level of the last middle deletion (MD3, 62 kDa) and the C-terminal deletion ( $\Delta$ C, 68 kDa) were not detected on the blot (Figure 4-12, lanes 4 and 7 respectively). This might due to instability and degradation of these proteins by the proteasome degradation system. To check this possibility, a proteasome inhibitor (Sigma, # C2211) was used to prevent the protein degradation and improve the immunodetection of these clones. To do this, in a separate experiment, HEK293T cells were transfected with these two clones and 12 hours before lysing the cells, a small amount (2  $\mu$ M/ml) of the proteasome inhibitor was directly added to the culture medium of the transfected cells. As shown in (Figure 4-12, lanes 8 and 9), the protein expression of these two clones ( $\Delta$ C and MD3) were stabilized and detected by the anti-FLAG antibody, yet the expression and/or detection efficiency is still very low. Moreover, the N-terminal deletion of  $\beta$ -catenin ( $\Delta$ N) exhibited a slightly faster electrophoretic mobility in comparison to its calculated molecular weight from the corresponding nucleotide sequence. Although further studies would still be needed to experimentally describe this, but the electrophoretic mobility shift of a recombinant protein could be related to the physicochemical properties and/or post-translational modifications. More detailed discussion about this is provided in (section 4.3).

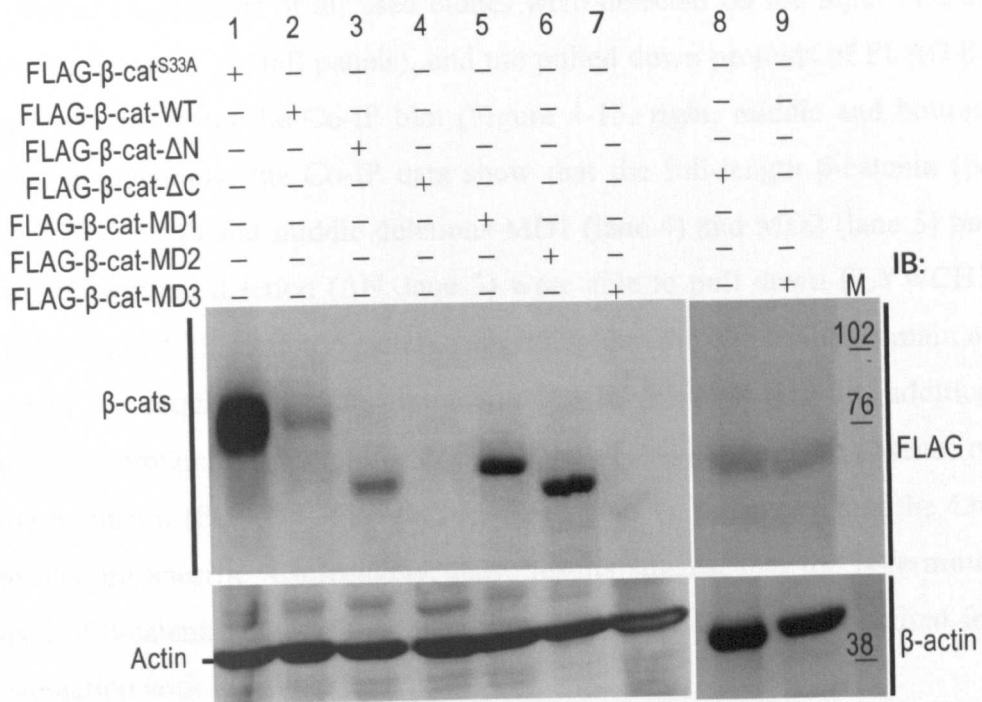


**Figure 4-12: Western blotting analysis of FLAG- $\beta$ -catenin mutant clones.** HEK293T cells were transfected with FLAG- $\beta$ -cat<sup>S33A</sup>, FLAG- $\beta$ -cat-WT, and the deletion mutants of FLAG-tagged  $\beta$ -catenin ( $\Delta$ N,  $\Delta$ C, MD1, MD2, and MD3) respectively. The protein lysate was immunoblotted with anti-FLAG antibody and the protein expressions of FLAG-tagged  $\beta$ -catenin clones were detected on the blot as indicated. Lanes 8 & 9 were treated with proteasome inhibitor. "M", denotes the full range Rain Bow marker from GE Healthcare. This pattern of expression was independently observed on several occasions.

#### 4.2.5 Mapping the interaction site of $\beta$ -catenin with FLYWCH1

To investigate which region of  $\beta$ -catenin is involved in its interaction with FLYWCH1, a Co-IP assay was carried out. HEK293T cells were co-transfected with expression plasmids encoding; eGFP-FLYWCH1-WT and the deletion mutants of FLAG-tagged  $\beta$ -catenin ( $\Delta$ N, MD1, and MD2) in addition to FLAG- $\beta$ -catenin<sup>S33A</sup>. The protein lysate was co-immunoprecipitated with anti-FLAG-conjugated agarose beads and immunoblotted with both anti-GFP and anti-FLAG antibodies.

The protein expressions of all used clones were detected on the Input blot as shown in (Figure 4-13, left panels), and the pulled down proteins of FLAG- $\beta$ -catenin are shown on the Co-IP blot (Figure 4-13, right, middle and bottom panels). Interestingly, the Co-IP data show that the full-length  $\beta$ -catenin ( $\beta$ -catenin<sup>S33A</sup>, lane 2) and middle deletions MD1 (lane 4) and MD2 (lane 5) but not the N-terminal deletion ( $\Delta$ N, lane 3) were able to pull down FLYWCH1 protein (Figure 4-13, right top panel), suggesting that the N-terminal domain of  $\beta$ -catenin is required for its interaction with FLYWCH1. In addition FLYWCH1 protein was not pulled down by the FLAG beads in the absence of FLAG- $\beta$ -catenin (Figure 4-13, right top panel, lane 1), indicating that the Co-IP results are specific. Collectively, these results suggest that the N-terminal domain of  $\beta$ -catenin, but not the armadillo repeats (R1-9) may be required for its interaction with FLYWCH1.

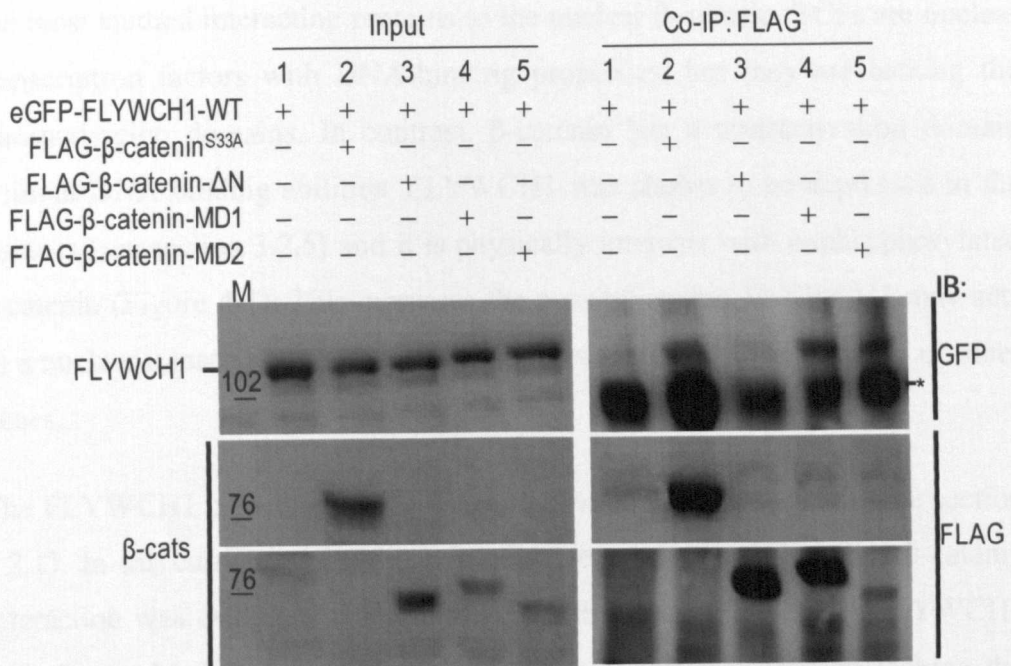


**Figure 4-13: Mapping the interaction site of  $\beta$ -catenin with FLYWCH1 using Co-IP assay.** HEK293T cells were co-transfected with the indicated expression plasmid DNAs. The protein lysates were co-immunoprecipitated using anti-FLAG-conjugated agarose beads and immunoblotted with both anti-GFP and anti-FLAG antibodies. **Left panel)** Shows Western blotting analysis for the input samples. **Right panel)** Shows Western blotting for the Co-IP samples. "M", denotes the full range Rain Bow marker

from GE Healthcare. Asterik (\*) indicates unspecific bands. The experiment represents 2-3 independent Co-IP approaches.

### 4.3 Discussion

In the current work, the *in vivo* interaction between human FLYWCH1 and  $\beta$ -catenin in the cell culture was examined using Co-IP assays. Consistent with the RRS data (Saadeddin A *et al.* unpublished data), the Co-IP results confirmed the association of FLYWCH1 with the unphosphorylated  $\beta$ -catenin ( $\beta$ -cat<sup>S33A</sup>) in the lysate of HEK293T cells (Figure 4-1). Similar to this finding, many other proteins have been reported to interact with the nuclear  $\beta$ -catenin such as T cell factor/lymphoid enhancer factor (TCF/LEF) family of proteins (TCFs) (Graham *et al.*, 2000), CBP (Takemaru and Moon, 2000), ICAT (Tago *et al.*, 2000) and Chibby (Takemaru *et al.*, 2003). Members of TCFs are among the most studied interacting proteins to the nuclear  $\beta$ -catenin. TCFs are nuclear transcription factors with DNA-binding properties, but they are lacking the transactivation domains. In contrast,  $\beta$ -catenin has a transactivation domain without DNA binding abilities. FLYWCH1 was shown to be expressed in the nucleus (see section 3.2.5) and it is physically interacts with unphosphorylated  $\beta$ -catenin (Figure 4-1). This increases the possibility that FLYWCH1 may acts as a nuclear transcription factor and thereby regulates the transcription of other genes.

The FLYWCH1 protein contains five conserved FLYWCH motifs (see section 3.2.1). In the current study, the role of these motifs in FLYWCH1/ $\beta$ -catenin interaction was evaluated through mapping the interaction site of FLYWCH1 with  $\beta$ -catenin. Interestingly, deletion M4, a C-terminal deletion lacking the last three FLYWCH motifs, lost its interaction ability with  $\beta$ -catenin (Figure 4-7). Furthermore, the same deletion lost the nuclear spotty expression pattern of the wild-type clone and showed a scattered green signal throughout the cells resembling the expression of the eGFP reporter gene alone (Figure 4-8). It should be mentioned that deletion M4 also lacks the predicted NLS motif (see section 3.2.1). Collectively, these results suggest that the C-terminal domain of

human FLYWCH1 containing the putative NLS sequence and the last three FLYWCH motifs is not only required for the interaction of FLYWCH1 with  $\beta$ -catenin but it also important for the sub-cellular localization and perhaps for the biological function (s) of this protein.

In the current work we used site-directed mutagenesis to generate several deletion mutant clones of both FLYWCH1 and  $\beta$ -catenin using PCR (Figure 4-9). The 5' end of the coding region of these clones were fused to specific epitope tags and their protein expression was confirmed by Western blotting analysis using SDS-PAGE (sections 4.2.2 & 4.2.4). Although SDS-PAGE is widely used to determine the molecular weight of many proteins based on their electrophoretic mobility, some exceptions always exist (Matagne et al., 1991). Different factors such as protein structure, post-translational modifications, and amino acid composition could affect the nature of the protein including the acidity, hydrophobicity, SDS-loading capacity...etc, and alter its electrophoretic migration (Rath et al., 2009, Garcia-Ortega et al., 2005, Matagne et al., 1991).

Notably, both the C-terminal deletion mutants of MYC-tagged FLYWCH1 (M3 and M4) and the M4-deletion mutant of eGFP-tagged FLYWCH1 run slower on the SDS-PAGE than their N-terminal deletion counterparts (M1 and M2) (Figure 4-4, lanes; 2 & 3 vs. 4 & 5) and (Figure 4-6, lane 4 vs. lane 6) respectively. Furthermore, the protein product of the N-terminal deletion of  $\beta$ -catenin ( $\Delta$ N) showed a smaller band, slightly below its calculated molecular weight (74 kDa) on the SDS-PAGE gel (Figure 4-12, lane 3). Although we are not certain about the exact cause of these variation in molecular weight of the deletion mutants, modifications of the PCR amplified DNA fragments such as frameshift mutations and aminoacid substitutions or post-translational modifications such as phosphorylation and ubiquitination are possible mechanisms that might have affected the nature of these deletion mutant proteins and changed their electrophoretic migration on the SDS-PAGE. In this study, we have used specific primers (Tables 2-2 to 2-4) to amplify specified fragments of both FLYWCH1 and  $\beta$ -catenin clones by PCR. The presence of desired DNA sequences of these clones were confirmed by restriction enzyme

digestion analysis (Figures 4-3, 4-5, & 4.11). Moreover, the in-frame construction of FLYWCH1 and/or  $\beta$ -catenin coding regions to their relevant epitope tags was also confirmed by sequencing. The sequencing data analysis confirmed that the open reading frame was maintained throughout the multiple cloning sites of the plasmid vectors upstream to the coding region of the inserts. An example of the sequencing data analysis is presented in (*Appendix 13*).

Although we have not analyzed the full-length nucleotide sequence of all deletion mutant clones, the sequencing data covered substantial regions upstream and/or downstream to the 5' end of the clones. We have aligned these sequences with the gene bank sequence of the gene of interest and did not find any modifications such as frameshift mutations or amino acid substitutions. Therefore, we assumed that the amino acid composition of these clones may not be modified. Alternatively, it is very much possible that the post-translation modifications and/or changes in the physicochemical properties may be the cause of the low electrophoretic mobility of FLYWCH1 C-terminal deletions. This possibility is further supported by the fact that the protein product of these clones did not migrate to their calculated positions (i.e. migrated slower than expected), giving the notion that these proteins may be subjected to post-translation modifications such as phosphorylation, glycosylation, or ubiquitination. Moreover, the fast electrophoretic mobility of the N-terminal deletion of  $\beta$ -catenin ( $\Delta$ N) can also be explained in the same context as some of the physicochemical properties of proteins such as hydrophobicity can cause faster migration of the modified protein products (Shirai et al., 2008). Thus, further observations in this regard may provide valuable insight toward further characterization of FLYWCH1 and/or  $\beta$ -catenin proteins. Although these areas of study were not further investigated due to time limitations of the present work, various methods such as 2D gel electrophoresis, mass spectrometry, protein crystallography and structure–function predictions (reviewed by Baumann and Meri, 2004) can be used to fully explore the variations of the electrophoretic mobility shifts, exhibited by some deletion mutant clones of FLYWCH1 and  $\beta$ -catenin.

Despite the above considerations, these observations suggest that the amino acid residues within the C-terminal domain of FLYWCH1 and those within the N-terminal domain of  $\beta$ -catenin may have critical involvement in the protein conformation structure and/or folding and thereby may be affecting the function of these proteins. Moreover, despite having the desired recombinant cDNA (lane 2 in Figure 4-3 & Figure 4-5) and equal loading of protein lysates, the M1-deletion mutant of FLYWCH1 (both MYC & eGFP tagged clones) was less expressed in comparison to other deletion mutant clones of FLYWCH1 (Figure 4-4, lane 2 & Figure 4-6, lane 3). These findings indicate that the amino acid residues within the N-terminal region of FLYWCH1 may affect the expression efficiency of this protein.

The primary structure of  $\beta$ -catenin contains 781 amino acids distributed over three regions; the central armadillo (arm) repeats (~550 aa), a distinct amino-terminal (~130 aa) and carboxy-terminal (~100 aa) domains (Huber et al., 1997, Huber and Weis, 2001, Xing et al., 2008). The armadillo repeat region provides the binding surface for the majority of  $\beta$ -catenin partners (more than 20) including members of the TCF/LEF family of proteins (Behrens et al., 1996, Graham et al., 2000, van de Wetering et al., 1997). The N-terminus domain plays an important role in regulation and stability of  $\beta$ -catenin. It provides phosphorylation sites for GSK3 $\beta$  (Barth et al., 1997, Yost et al., 1996) and CK1 $\alpha$  (Liu et al., 2002) which subsequently phosphorylate  $\beta$ -catenin to be recognized and degraded by the proteasomal degradation system. The transactivation function has been assigned to the C-terminus region of  $\beta$ -catenin (van de Wetering et al., 1997) which is crucial for gene activation.

Previous studies have shown that  $\beta$ -catenin can interact with many proteins in the cell. Some of them are membranous, some are located in the cytoplasm and others localized into the nucleus. As part of the classical cadherin junction,  $\beta$ -catenin directly interacts to E-cadherin and  $\alpha$ -catenin to form the cadherin-catenin complex (Aberle et al., 1994). The entire armadillo repeats of  $\beta$ -catenin has shown to be required for its interaction with E-cadherin however the amino acid positions 118 to 149 were determined as the binding site for  $\alpha$ -catenin (Aberle et al., 1996). In the cytoplasm, the free unbound  $\beta$ -catenin is usually

found in a complex which mainly composed of APC, Axin, GSK3 $\beta$  and CK1 $\alpha$ . Deletion mutagenesis studies have shown that the arm repeat region mediates the binding of  $\beta$ -catenin to APC (Rubinfeld et al., 1993, Hulsken et al., 1994), Axin (Behrens et al., 1998, Ikeda et al., 1998), and EGF receptor tyrosine kinase domain (Hoschuetzky et al., 1994).

The  $\beta$ -catenin nuclear interactors are crucial factors that play pivotal roles in gene regulation controlled by the Wnt/ $\beta$ -catenin signalling pathway. The binding sites of the majority of nuclear partners have been mapped to the central arm repeat and the C-terminus domain of  $\beta$ -catenin. It has been reported that members of TCF family interact with the armadillo repeats 3–10 and recruit  $\beta$ -catenin to specific promoters of target genes (Graham et al., 2001, Graham et al., 2000). In addition, the armadillo repeat no.1 (R1) and armadillo repeat no.11 (R11) were also found to be essential for transactivation of Wnt-target genes through interaction with transcriptional co-activators such as BCL9, Pygopus, parafibromin, Brg1, CBP/p300, and MED12 (Barker et al., 2001, Hecht et al., 2000, Kim et al., 2006, Kramps et al., 2002, Mosimann et al., 2006). The  $\beta$ -catenin R11 region has also been shown to interact with many transcriptional inhibitors such as ICAT, HDPR1, and Chibby (Tago et al., 2000, Takemaru et al., 2003 {Yau, 2005 #1186}). Other factors such as Sox proteins were found to bind regions on  $\beta$ -catenin which overlaps with the established TCF binding site (Zorn et al., 1999).

To investigate which part of  $\beta$ -catenin is interacting with FLYWCH1, a series of overlapping deletions across the  $\beta$ -catenin coding region were generated. Each deletion lacks a distinct domain or a specific sequence of the  $\beta$ -catenin coding region, while the rest of the protein remains intact (Figure 4-9). Similar approaches have been previously undertaken to map the interaction site of  $\beta$ -catenin with other nuclear partners (Aberle et al., 1994, Olson et al., 2006). Surprisingly, the mutational analysis data revealed that the armadillo repeats domain of  $\beta$ -catenin is not essential for its interaction with FLYWCH1, but the amino-terminal domain is required (Figure 4-13).

It should be mentioned that in the current work the entire armadillo repeats domain of  $\beta$ -catenin was not used in the Co-IP experiments, but instead

deletions that contain two third of this domain were used (Figure 4-9). Moreover, due to instability and/or low expression efficiency, clear evidence about the interaction of the armadillo repeats 10-12 and the C-terminal domain of  $\beta$ -catenin (covered by deletions MD3 and  $\Delta$ C, respectively) with FLYWCH1 was not obtained in this study (see section 4.2.4.3 & Figure 4-13). Therefore, interaction of FLYWCH1 with the entire armadillo repeats and/or the C-terminal domain of  $\beta$ -catenin cannot be excluded. However, as the N-terminal deletion of  $\beta$ -catenin was sufficient to abolish the interaction between  $\beta$ -catenin and FLYWCH1 even in the presence of intact armadillo and C-terminal domains (Figure 4-13). Therefore, it is unlikely that the C-terminal region of  $\beta$ -catenin play role in its interaction with FLYWCH1. Based on this notion, we assumed that the deletion mutants MD3 and  $\Delta$ C of  $\beta$ -catenin might also interact with FLYWCH1. This view is further supported by our luciferase analyses data discussed in the next chapter.

To sum up, in this study, the human FLYWCH1 was defined as a novel nuclear partner of  $\beta$ -catenin. The N-terminal domain of  $\beta$ -catenin was found to be responsible for its interaction with FLYWCH1, whereas the C-terminal domain of FLYWCH1 was found to be required for this interaction as summarized below in (Figure 4-14).

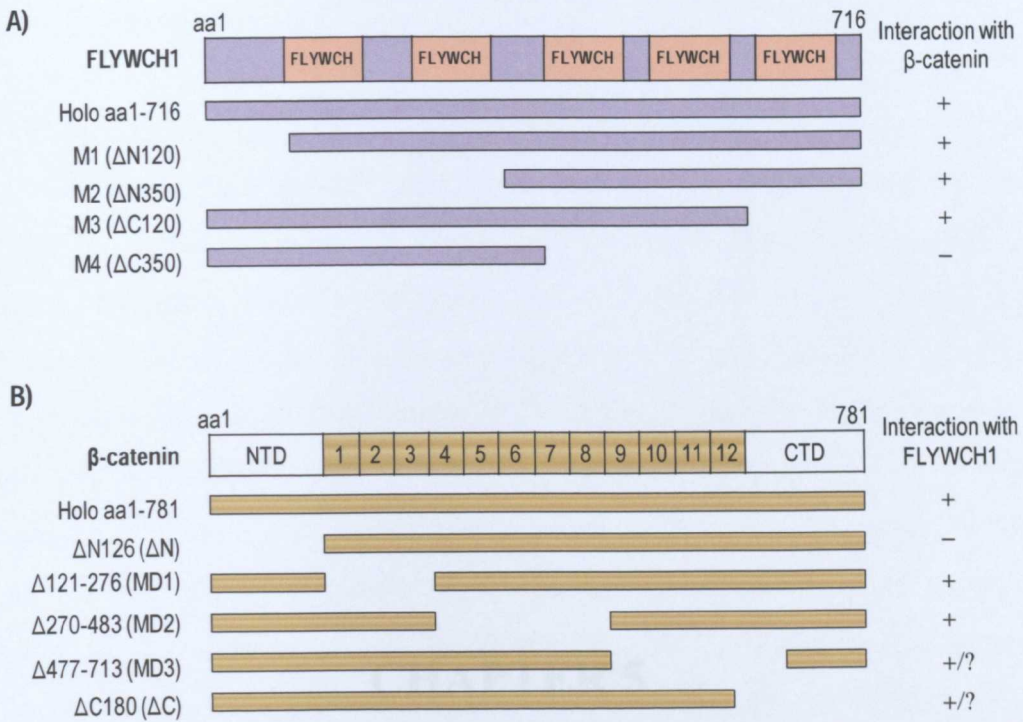


**Figure 4-14: Schematic presentation of the interaction sites between FLYWCH1 and  $\beta$ -catenin.** The interaction ability of FLYWCH1 constructs to bind  $\beta$ -catenin and vice versa is indicated by (+/-) in the right panel of both **A** & **B**. (+) stands for experimentally approved interaction, while (-) for no interaction. (+/?) means interaction is likely occurred but experimentally not approved.

## **CHAPTER 5**

# **Human FLYWCH1 Inhibits Cell Migration and Alters Cell Morphology of Colorectal Cancer (CRC) Cells through Negative Regulation of Wnt/ $\beta$ -catenin Signalling Pathway**

## **5.1 Introduction**

Cell migration involves a precise regulation of a process which becomes altered and/or lost during invasion and metastasis. The process of cell migration demonstrates the phenotypic and genetic modifications required for tumour metastasis including increased cell migration/invasion and pseudopod formation.  $\beta$ -catenin, a key downstream effector of Wnt signalling pathway, plays a crucial role in this process. It can directly modulate gene expression through its interaction with TCF/LEF-transcription factors and also mediate tight intercellular adhesions by linking E-cadherin to the cytoskeleton. The  $\beta$ -catenin/TCF activity is tightly modulated by the nuclear  $\beta$ -catenin partners (either co-activators or co-repressors). Indeed, these cofactors act as potential gatekeepers for the  $\beta$ -catenin/TCF complex, ensuring the proper threshold of  $\beta$ -catenin is achieved before it complexes with TCF family members. Such conventional regulation usually involves a highly specialized set of molecular interactions, which may specifically turn on a particular cell phenotype and may have a crucial effect on the cell signalling network.

In the previous chapter, the physical interaction between FLYWCH1 and  $\beta$ -catenin was reported. Herein, the functional interaction between these two proteins and its consequences are further investigated. The TCF transcriptional (TOP-FALSH/FOP-FLASH) dual luciferase reporter assay was employed to evaluate the effect of FLYWCH1 on the transcriptional activity of  $\beta$ -catenin in human cell culture. The Luciferase data demonstrate a consistent functional interaction between FLYWCH1 and  $\beta$ -catenin resulting in inhibition of Wnt/ $\beta$ -catenin signalling in various cell lines. Subsequently, our further mutational analysis using site directed mutagenesis has identified the FLYWCH1 and  $\beta$ -catenin protein domains that are involved in the repressive activity.

Our results demonstrate a significant inhibition of cell migration by ectopic expression of FLYWCH1. Strikingly, we observed no influence on cell proliferation, whereas the wound closure capacity of FLYWCH1 expressing cells was reduced. In addition, forced expression of FLYWCH1 changed the morphology of CRC cells. Finally, our data shows that the expression of

several downstream Wnt-target genes associated with cell migration was significantly repressed by FLYWCH1. Taken together, our data suggest that FLYWCH1 may regulate cell migration and morphology by repressing Wnt/ $\beta$ -catenin target genes.

## 5.2 Results

### 5.2.1 FLYWCH1 represses $\beta$ -catenin/TCF4 transcriptional activity

To elucidate the consequences of FLYWCH1/ $\beta$ -catenin interaction on the transcriptional activity of  $\beta$ -catenin/TCF4, a TCF transcriptional dual-luciferase reporter assay was performed. The *Renilla*-luciferase reporter was used as an internal control to normalize variations in the transfection efficiency. The TCF-firefly reporters; TOP-FLASH (containing three copies of the TCF binding site, ATCAAAG) and FOP-FLASH (containing three mutated copies of the TCF binding site, GCCAAAG) were used to measure the transactivation activity of  $\beta$ -catenin/TCF complex with the dual-luciferase assay kit (see section 2.2.6.1). In addition to HEK293T cells, two CRC cell lines (HCT116 & SW620) were also used to evaluate the effect of FLYWCH1 on the transcriptional activity of  $\beta$ -catenin. The endogenous level of FLYWCH1 protein is not detectable in HEK293T cells by FLYWCH1 antibody (Figure 3-14C). Moreover, the mRNA expression of FLYWCH1 is very low (almost undetectable) in CRC cells including HCT116 and SW620 (Figure 5-14). Therefore, FLYWCH1 was overexpressed in all these cell lines. HEK293T cells also contain low endogenous active Wnt signals (Porfiri et al., 1997). In contrast, HCT116 and SW620 cells contain high Wnt signals due to different mutations in *APC* gene (Korinek et al., 1997, Morin et al., 1997). In this assay, the effect of the overexpressed FLYWCH1 on the transcriptional activity of both endogenous and overexpressed  $\beta$ -catenin is investigated as detailed below.

HEK293T cells were transiently transfected with plasmids encoding FLAG- $\beta$ -cat<sup>S33A</sup>, and FLYWCH1-WT (encoding the untagged-FLYWCH1 protein; section 3.2.3.1), along with the luciferase reporter constructs; firefly (TOP/FOP-FLASH) and *Renilla*. Cells transfected with the luciferase reporter constructs were used as an experimental control and their luciferase activity were normalized to *Renilla* internal control and then arbitrarily set to 1. The luciferase activities of other experimental plots were also normalized to *Renilla* and compared to the control. The data are presented as folds of induction or reduction as detailed in (section 2.2.6.1). This format of calculation was applied to all TCF-luciferase reporter assays performed in this study.

The luciferase data show that the ectopic expression of FLYWCH1 significantly reduced the TOP-FLASH reporter activity in HEK293T cells without affecting the FOP-FLASH reporter (Figure 5-1A, lane 2 vs. lane 1), indicating that FLYWCH1 could negatively regulate the endogenous transcriptional activity of  $\beta$ -catenin. To further confirm the negative effect of FLYWCH1 on  $\beta$ -catenin, both the stabilized construct of  $\beta$ -catenin (FLAG- $\beta$ -cat<sup>S33A</sup>) and FLYWCH1 were co-expressed in these cells. As shown in the figure, in the absence of FLYWCH1 the FLAG- $\beta$ -cat<sup>S33A</sup> highly induced the TOP-Flash reporter activity by ~100 folds (Figure 5-1B, lane 2 vs. lane 1). However, this induction was dramatically (77%) inhibited by FLYWCH1 (Figure 5-1B, lane 3), suggesting that FLYWCH1 strongly suppresses the  $\beta$ -catenin-mediated transcriptional activation. Notably, no changes for the FOP-FLASH reporter (the negative control) were detected in the entire experiment, indicating that the TOP-FLASH reporter specifically responded to  $\beta$ -catenin/TCF signalling.

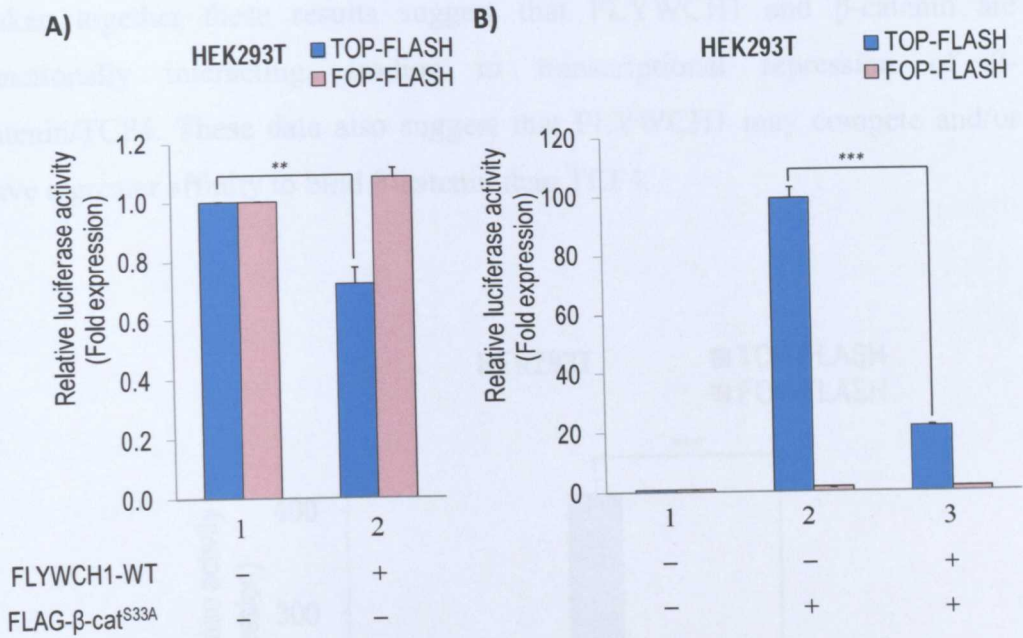


**Figure 5-1: FLYWCH1 represses the transcriptional activity of  $\beta$ -catenin/TCF4.** HEK293T cells were transfected to express FLYWCH1-WT (A) and FLYWCH1-WT plus FLAG- $\beta$ -cat<sup>S33A</sup> (B) in the presence of *Renilla* and TOP-FLASH or FOP-FLASH reporters as indicated. Activity of the firefly luciferase reporters (TOP-FLASH & FOP-FLASH) relative to *Renilla* luciferase transfection control is shown as folds of expression (induction/repression). Data are mean  $\pm$  SD ( $n = 3$ ; \*\*,  $P < 0.01$ ; \*\*\*,  $P < 0.001$ ). Experiment run in triplicate and repeated at least on three independent occasions.

Next, to investigate whether elevated levels of TCF4 could rescue the repressed activity of  $\beta$ -catenin by FLYWCH1, in a separate experiment, both FLAG- $\beta$ -cat<sup>S33A</sup> and TCF4 were coexpressed with or without FLYWCH1-WT construct. The results show that the combination of  $\beta$ -catenin and TCF4 induced the TOP-FLASH reporter activity to a very high level (413 folds) in comparison to the control (Figure 5-2, lane 2 vs. lane 1). However, this induction was dramatically (77%) reduced in the presence of FLYWCH1 (Figure 5-2, lane 3). Notably, the suppression level of FLYWCH1 on  $\beta$ -catenin/TCF4 (77%) (Figure 5-2, lane 3) is comparable to the suppression level of FLYWCH1 on  $\beta$ -catenin alone (77%) (Figure 5-1, lane 3). This finding indicates that TCF4 does

not affect/rescue the transcriptional repression of FLYWCH1 on  $\beta$ -catenin. Taken together these results suggest that FLYWCH1 and  $\beta$ -catenin are functionally interacting, leading to transcriptional repression of  $\beta$ -catenin/TCF4. These data also suggest that FLYWCH1 may compete and/or have a greater affinity to bind  $\beta$ -catenin than TCF4.

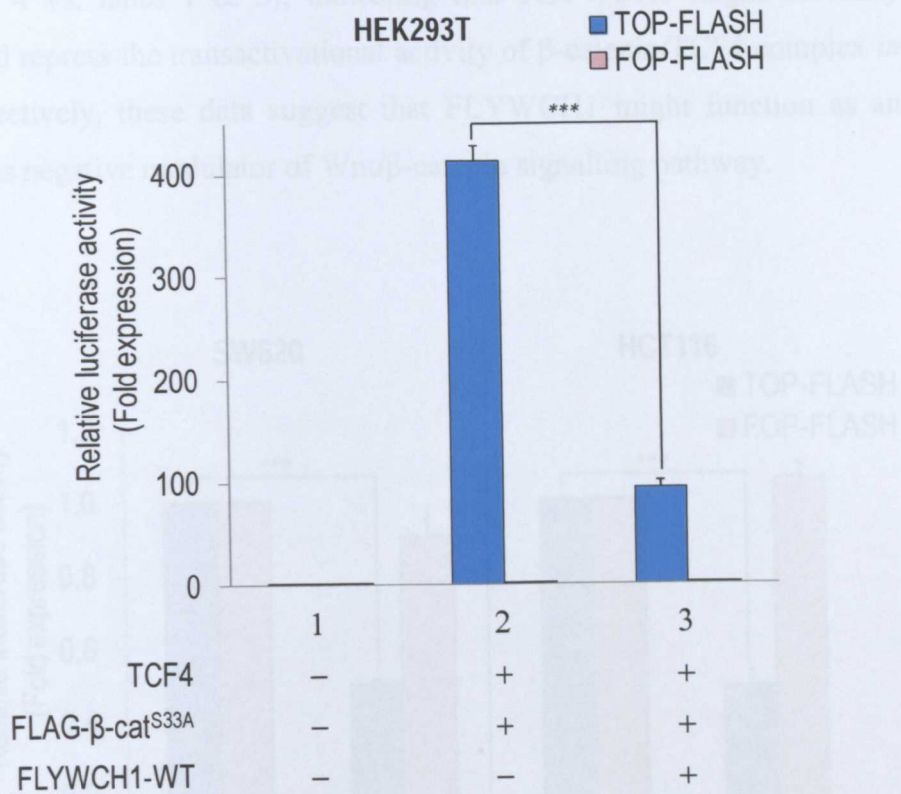


**Figure 5-2: TCF4 does not rescue the transcriptional repression of FLYWCH1 on  $\beta$ -catenin.** HEK293T cells were transfected with the indicated expression plasmids in the presence of *Renilla* and TOP-FLASH or FOP-FLASH reporters. Folds of induction/repression of TOP/FOP-FLASH luciferase activity relative to *Renilla* luciferase are shown as indicated. Data are mean  $\pm$  SD ( $n = 3$ ; \*\*\*,  $P < 0.001$ ). Experiment run in triplicate and repeated on two independent occasions.

To examine the suppression effect of FLYWCH1 on the transcriptional activity of endogenous  $\beta$ -catenin in CRC cells, the *in vivo* transactivational activity of  $\beta$ -catenin/TCF4 in SW620 and HCT116 CRC cell lines was examined. These cell lines contain high level of nuclear  $\beta$ -catenin due to mutations in APC and

$\beta$ -catenin respectively. Therefore, in this experiment we relied on the endogenous level of  $\beta$ -catenin to induce the TOP-FLASH activity. Accordingly, cells were transfected with FLYWCH1 alone in addition to the luciferase reporters.

The results show that the TOP-FLASH reporter activity significantly (50%) reduced by FLYWCH1 in both SW620 and HCT116 cell lines (Figure 5-3, lanes 2 & 4 vs. lanes 1 & 3), indicating that FLYWCH1 might normally interact and repress the transactivational activity of  $\beta$ -catenin/TCF4 complex *in vivo*. Collectively, these data suggest that FLYWCH1 might function as an endogenous negative modulator of Wnt/ $\beta$ -catenin signalling pathway.

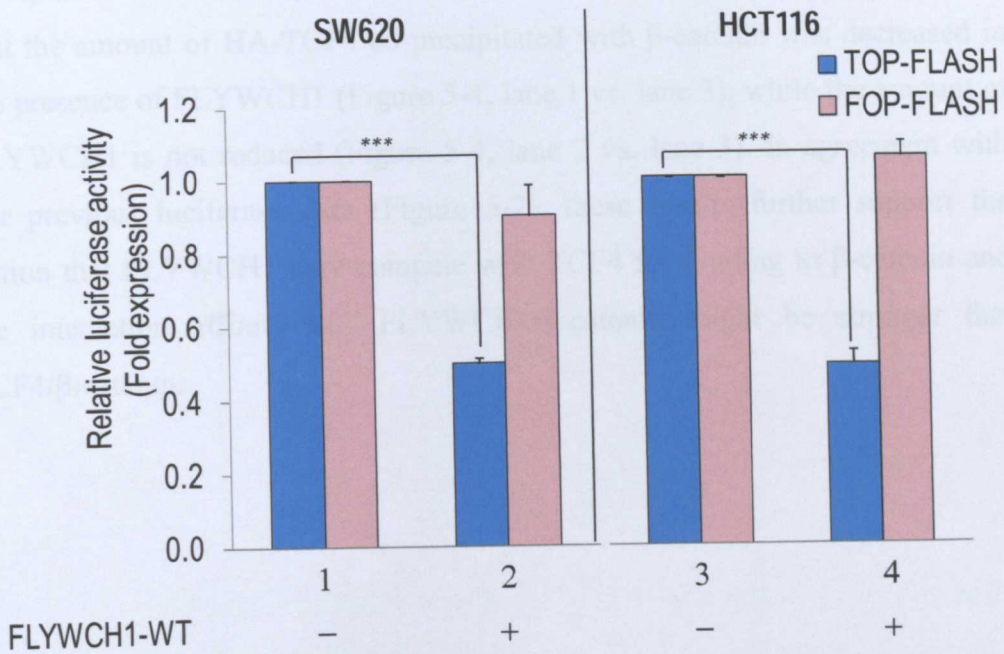


**Figure 5-3: Suppression of endogenous  $\beta$ -catenin/TCF4 by FLYWCH1.** CRC cell lines (SW620 and HCT116) were transiently transfected to express FLYWCH1-WT in the presence of *Renilla* and TOP-FLASH or FOP-FLASH reporters as indicated. The TOP/FOP-FLASH luciferase activity relative to *Renilla* luciferase is presented. Data are mean  $\pm$  SD ( $n = 3$ ; \*\*\*,  $P < 0.001$ ). Experiment run in triplicate and repeated on two independent occasions.

### **5.2.2 FLYWCH1 may compete with TCF4 for binding to $\beta$ -catenin**

To explore the possibility that FLYWCH1 competes with TCF4 for binding to  $\beta$ -catenin, an *in vivo* co-immunoprecipitation (Co-IP) assay in human cell culture was performed. HEK293T cells were co-transfected with expression plasmids encoding; FLAG- $\beta$ -cat<sup>S33A</sup>, eGFP-FLYWCH1-WT, and hemagglutinin tagged TCF4 (HA-TCF4). The protein lysate was co-immunoprecipitated with anti-FLAG-conjugated agarose beads and analysed by Western blotting analysis using anti-HA and anti-GFP antibodies.

The Co-IP blot shows that both HA-TCF4 and eGFP-FLYWCH1 were co-precipitated with FLAG- $\beta$ -cat<sup>S33A</sup> (Figure 5-4). Moreover, the blot also shows that the amount of HA-TCF4 co-precipitated with  $\beta$ -catenin was decreased in the presence of FLYWCH1 (Figure 5-4, lane 1 vs. lane 3), while the amount of FLYWCH1 is not reduced (Figure 5-4, lane 2 vs. lane 3). In agreement with our previous luciferase data (Figure 5-2), these results further support the notion that FLYWCH1 may compete with TCF4 for binding to  $\beta$ -catenin and the interaction affinity of FLYWCH1/ $\beta$ -catenin might be stronger than TCF4/ $\beta$ -catenin.

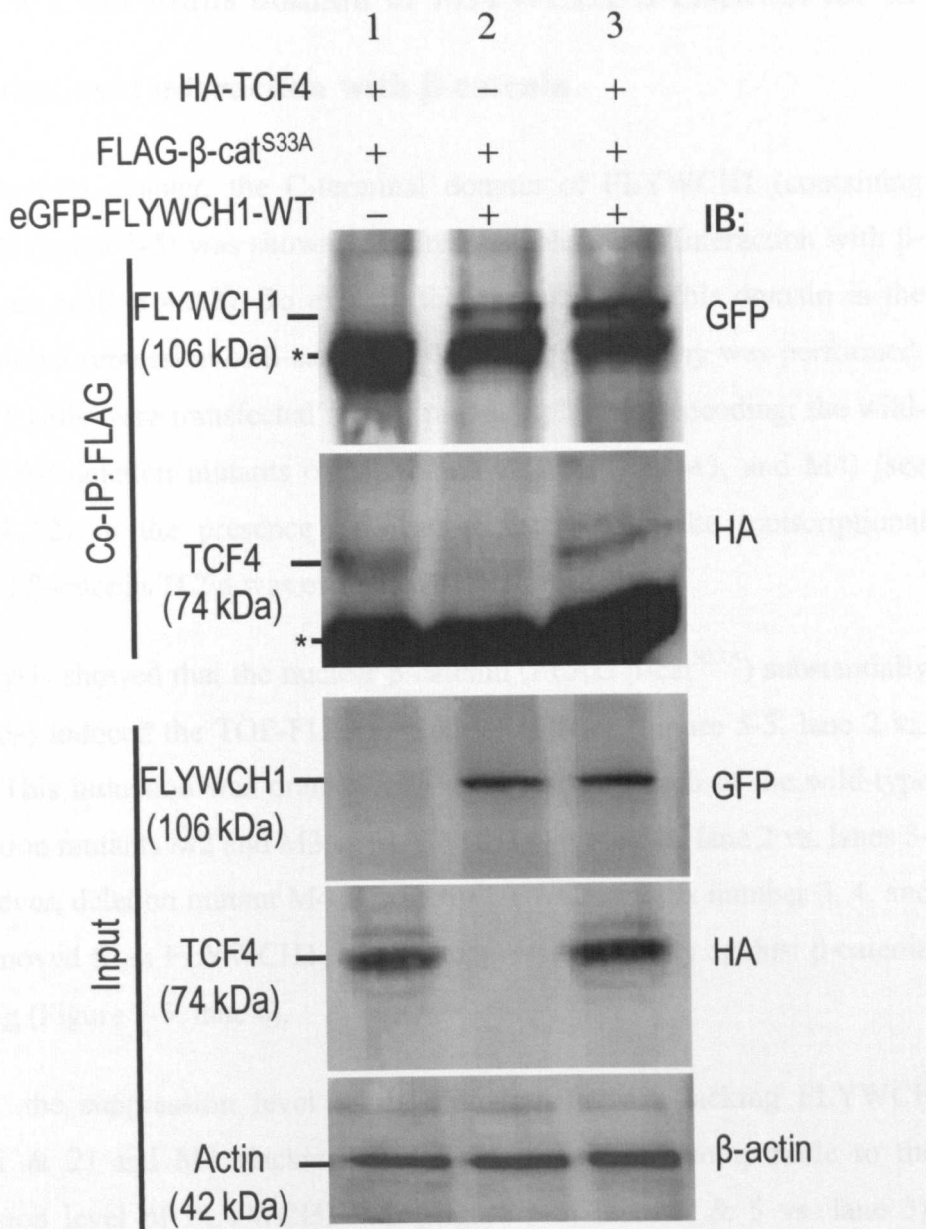


**Figure 5-4: FLYWCH1 competes with TCF4 for interaction with  $\beta$ -catenin.** HEK293T cells were co-transfected to express the FLAG- $\beta$ -cat<sup>S33A</sup>, eGFP-FLYWCH1-WT, and HA-TCF4. The protein lysate was co-immunoprecipitated with anti-FLAG - conjugated agarose beads. Both the Input (**bottom panels**) and Co-IP (**top panels**) samples were immunoblotted with anti-HA and anti-GFP antibodies as indicated. Asteriks (\*) indicate unspecific bands.

### **5.2.3 The C-terminus domain of FLYWCH1 is essential for its functional interaction with $\beta$ -catenin.**

In the previous chapter, the C-terminal domain of FLYWCH1 (containing FLYWCH motifs 3-5) was shown to be responsible for its interaction with  $\beta$ -catenin (see section 4.2.3). To explore the importance of this domain in the transcriptional repression of  $\beta$ -catenin, a TCF luciferase assay was performed. HEK293T cells were transfected with expression plasmids encoding; the wild-type and the deletion mutants of MYC-FLYWCH1 (M2, M3, and M4) (see section 4.2.2) in the presence of FLAG- $\beta$ -cat<sup>S33A</sup> and the transcriptional activity of  $\beta$ -catenin/TCF4 was evaluated as described above.

The analysis showed that the nuclear  $\beta$ -catenin (FLAG- $\beta$ -cat<sup>S33A</sup>) substantially (~95 folds) induced the TOP-FLASH reporter activity (Figure 5-5, lane 2 vs. lane 1). This induction was dramatically suppressed by each of the wild-type and deletion mutants M2 and M3 of FLYWCH1 (Figure 5-5, lane 2 vs. lanes 3-5). However, deletion mutant M4 in which FLYWCH motifs number 3, 4, and 5 are removed from FLYWCH1, lost its suppression activity against  $\beta$ -catenin signalling (Figure 5-5, lane 6).

Notably, the suppression level of deletion mutant M2 (lacking FLYWCH motifs 1 & 2) and M3 (lacking FLYWCH motif 5) is comparable to the suppression level of FLYWCH1-WT (Figure 5-5, lanes 4 & 5 vs. lane 3). These data suggest that motifs 1, 2, and 5 are not mediating the repression activity of FLYWCH1 against  $\beta$ -catenin. Therefore, FLYWCH motifs 3 and 4 within the C-terminal domain of FLYWCH1 might be essential for the functional interaction and suppression activity of FLYWCH1 against  $\beta$ -catenin/TCF4. These observations are in agreement with the previous Co-IP results (see section 4.2.3) and collectively support the concept that FLYWCH1 directly binds to  $\beta$ -catenin through its C-terminal domain and functions as a negative modulator of  $\beta$ -catenin/TCF4-mediated transcriptional activation likely through the FLYWCH motifs number 3 and 4.

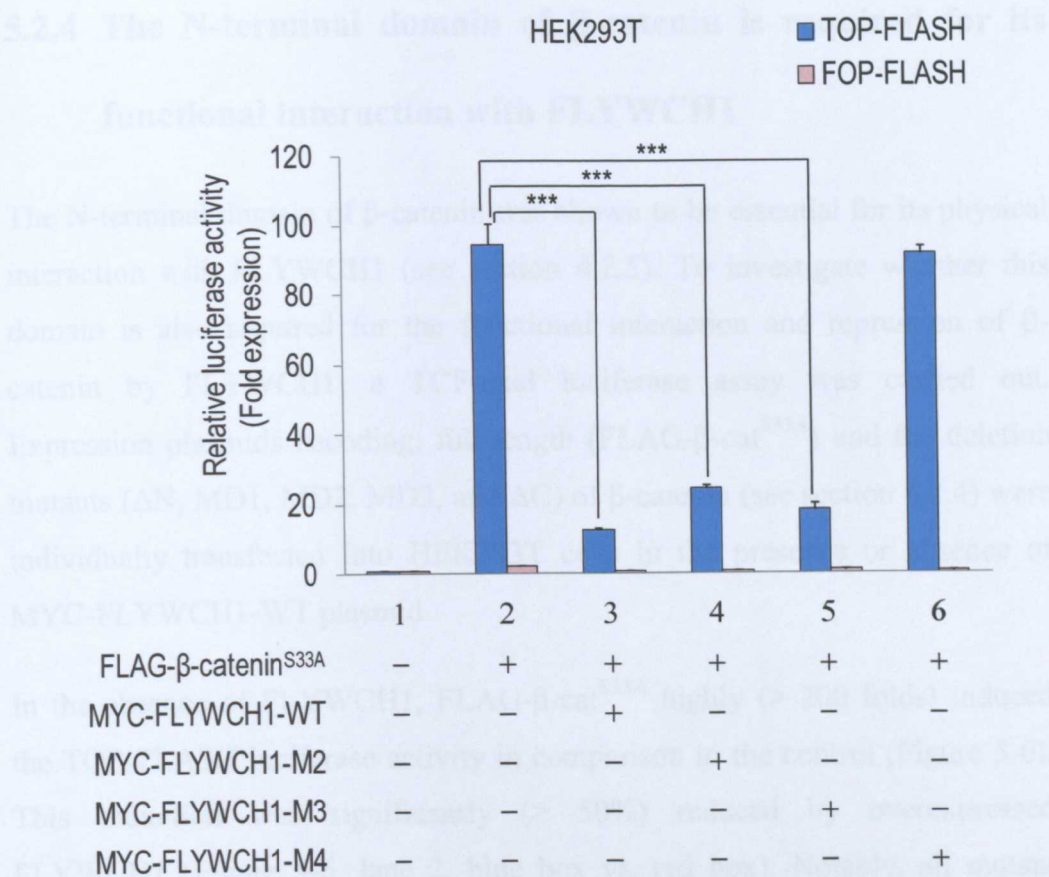


**Figure 5-5: A C-terminal deletion of FLYWCH1 (FLYWCH1-M4) lost its suppression activity against β-catenin/TCF4.** HEK293T cells were transfected to express FLAG-β-cat<sup>S33A</sup> and MYC-tagged constructs of FLYWCH1 (the wild-type and deletion mutants M2, M3, and M4) in the presence of *Renilla* and TOP-FLASH or FOP-FLASH reporters as indicated. The TOP/FOP-FLASH luciferase activity relative to *Renilla* luciferase is presented. Data are mean ± SD ( $n = 3$ ; \*\*\*,  $P < 0.001$ ). Experiment run in triplicate and repeated at least on two independent occasions.

## **5.2.4 The N-terminal domain of $\beta$ -catenin is required for its functional interaction with FLYWCH1**

The N-terminal domain of  $\beta$ -catenin was shown to be essential for its physical interaction with FLYWCH1 (see section 4.2.5). To investigate whether this domain is also required for the functional interaction and repression of  $\beta$ -catenin by FLYWCH1, a TCF-dual luciferase assay was carried out. Expression plasmids encoding; full-length (FLAG- $\beta$ -cat<sup>S33A</sup>) and the deletion mutants ( $\Delta$ N, MD1, MD2, MD3, and  $\Delta$ C) of  $\beta$ -catenin (see section 4.2.4) were individually transfected into HEK293T cells in the presence or absence of MYC-FLYWCH1-WT plasmid.

In the absence of FLYWCH1, FLAG- $\beta$ -cat<sup>S33A</sup> highly (> 200 folds) induced the TOP-FLASH luciferase activity in comparison to the control (Figure 5-6). This induction was significantly (> 50%) reduced by overexpressed FLYWCH1 (Figure 5-6, lane 2, blue box vs. red box). Notably, all mutant clones of  $\beta$ -catenin showed less luciferase activity than the wild-type clone (Figure 5-6, lanes 3-7, blue boxes), especially deletions MD1 (lane 4) and MD2 (lane 5) in which armadillo repeats (R1-4 and R5-9) comprising the TCF4 binding site are deleted. Although the induction activity of  $\beta$ -catenin is influenced by different  $\beta$ -catenin mutations but there is still some activity that could explore the significant role of FLYWCH1 on the transcriptional activity of different domains of  $\beta$ -catenin. As shown in (Figure 5-6), regardless of the level of induction, the luciferase activity of all deletion mutants except  $\Delta$ N was significantly inhibited by FLYWCH1 (Figure 5-6, lanes 4-7, red boxes vs. blue boxes).

Consistent with the previous Co-IP data (section 4.2.5), these results indicate that the N-terminal domain of  $\beta$ -catenin ( $\Delta$ N) may be required for its functional interaction with FLYWCH1. Taken together, these data gives the notion that the N-terminal domain of  $\beta$ -catenin may have essential attribution to both physical and functional interaction of  $\beta$ -catenin with FLYWCH1.

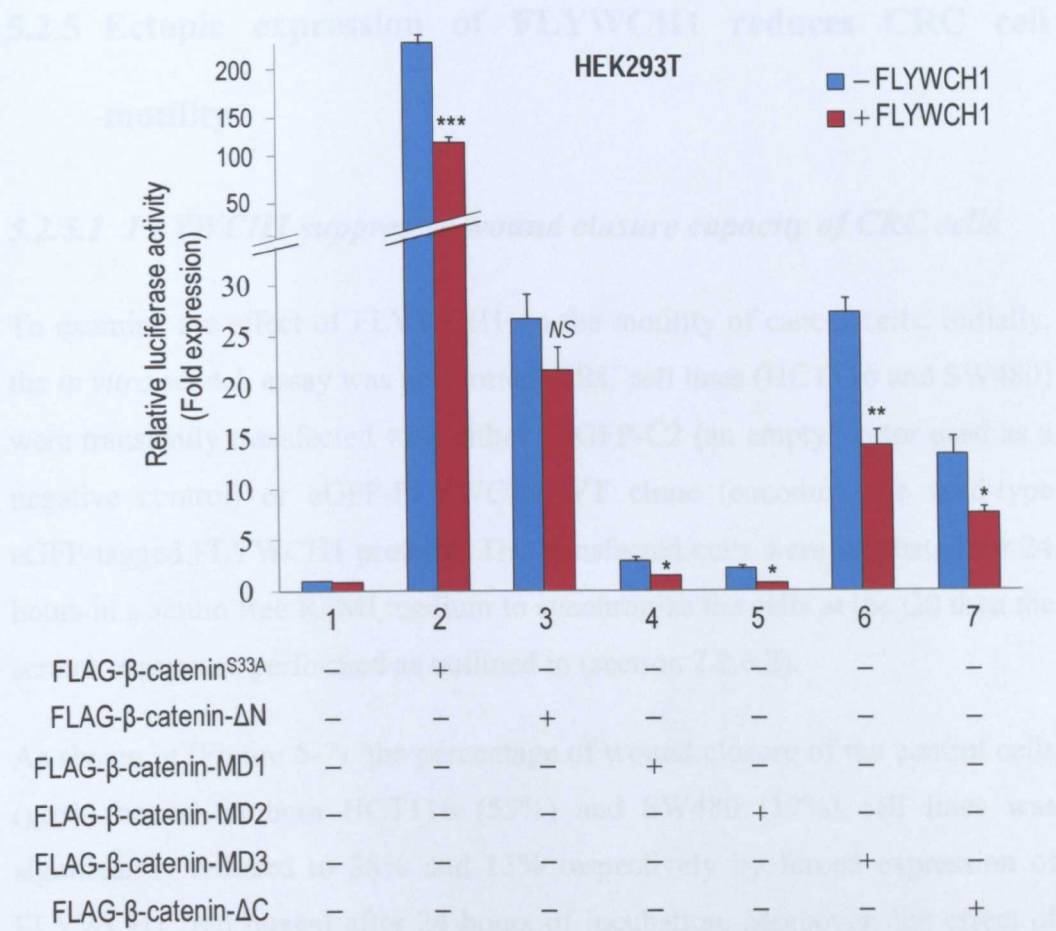


**Figure 5-6: The N-terminal domain of  $\beta$ -catenin is required for its functional interaction with FLYWCH1.** The full-length (FLAG- $\beta$ -cat<sup>S33A</sup>) and the deletion mutants of  $\beta$ -catenin ( $\Delta$ N, MD1, MD2, MD3, and  $\Delta$ C) were separately transfected in HEK293T cells with (red boxes) and without (blue boxes) FLYWCH1. The activity of the firefly luciferase reporter (TOP-FLASH) relative to *Renilla* is shown. Due to differences in the induction levels, the figure is shown in two different scales; low scale (0 to 30) and high scale (50 to 200) as indicated. Data are mean  $\pm$  SD ( $n = 3$ ; \*,  $P < 0.05$ ; \*\*,  $P < 0.01$ ; \*\*\*,  $P < 0.001$ ). Experiment run in triplicate and repeated on two independent occasions.

## **5.2.5 Ectopic expression of FLYWCH1 reduces CRC cell motility**

### ***5.2.5.1 FLYWCH1 suppresses wound closure capacity of CRC cells***

To examine the effect of FLYWCH1 on the motility of cancer cells, initially, the *in vitro* scratch assay was performed. CRC cell lines (HCT116 and SW480) were transiently transfected with either pEGFP-C2 (an empty vector used as a negative control) or eGFP-FLYWCH1-WT clone (encoding the wild-type eGFP-tagged FLYWCH1 protein). The transfected cells were incubated for 24 hours in a serum free RPMI medium to synchronize the cells at the G0 then the scratch assay was performed as outlined in (section 2.2.6.2).

As shown in (Figure 5-7), the percentage of wound closure of the control cells (green boxes) in both HCT116 (55%) and SW480 (17%) cell lines was significantly reduced to 38% and 13% respectively by forced expression of FLYWCH1 (red boxes) after 24 hours of incubation. Moreover, the effect of FLYWCH1 on the wound closure rate of SW480 cells was more pronounced after 48 hours of incubation (Figure 5-7B). This inhibitory effect of FLYWCH1 on wound closure rate of CRC cells could be due to defects in either cell migration or cell proliferation. To further elucidate this, both cell cycle analysis and migration assays were performed as outlined below.

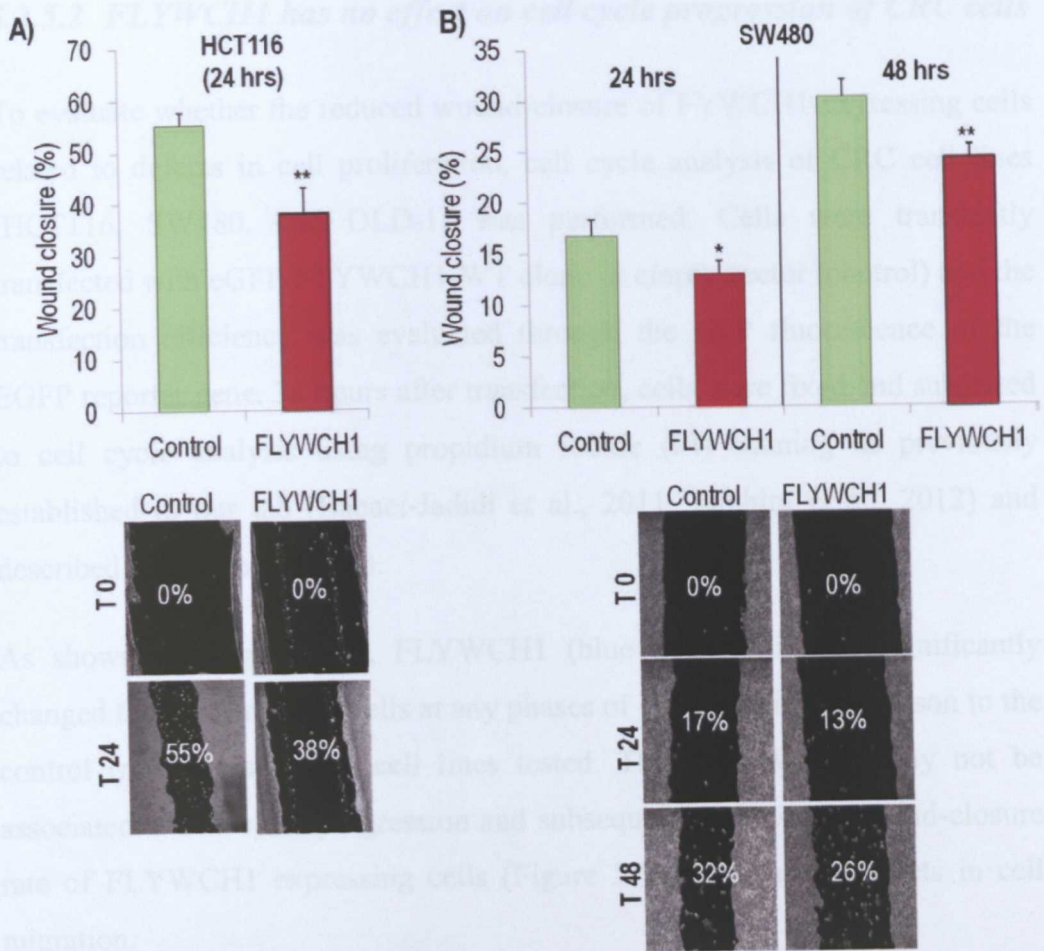


**Figure 5-7: FLYWCH1 reduces wound-closure capacity of CRC cells.** HCT116 and SW480 cells were transiently transfected to express eGFP (control) or eGFP-FLYWCH1-WT protein. The transfected cells were subjected to scratch wound assay. **Top panels)** Charts show the percentage of wound closure for both eGFP (green boxes) and eGFP-FLYWCH1 (red boxes) transfected cells after 24 hours in HCT116 cells **(A)** or 24 & 48 hours in SW480 cells **(B)**. **Bottom panels)** Show representative images of the wounds at time zero (T0) and 24 hours (T24) for HCT116 cells or T0, T24, & T48 for SW480 cells. Data are mean  $\pm$  SD ( $n = 6$ ; \*\*,  $P < 0.01$ ). Experiment run in triplicate and repeated at least on two independent occasions.

### ***5.2.5.2 FLYWCH1 has no effect on cell cycle progression of CRC cells***

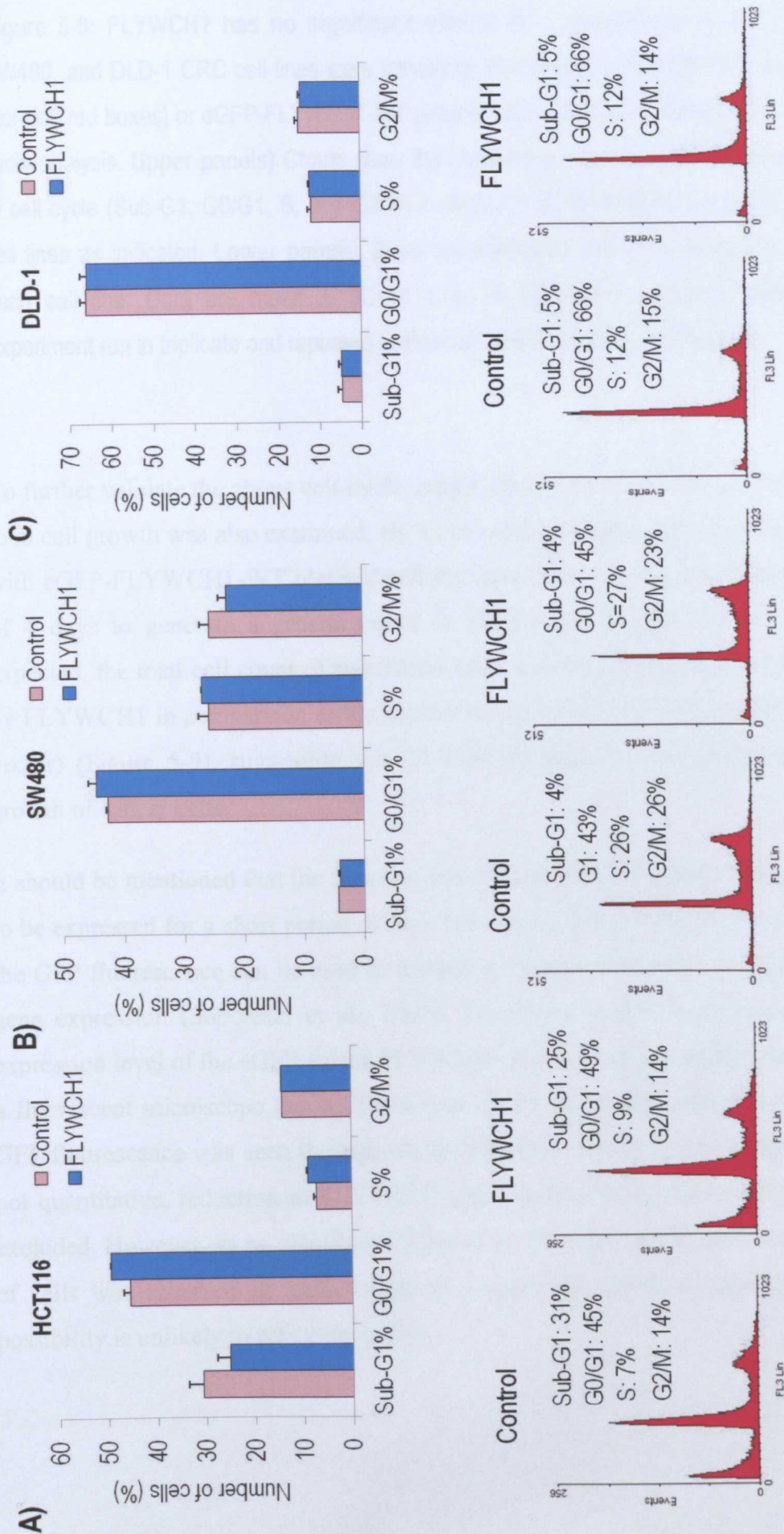
To evaluate whether the reduced wound-closure of FLYWCH1 expressing cells related to defects in cell proliferation, cell cycle analysis of CRC cell lines (HCT116, SW480, and DLD-1) was performed. Cells were transiently transfected with eGFP-FLYWCH1-WT clone or empty vector (control) and the transfection efficiency was evaluated through the GFP fluorescence of the EGFP reporter gene. 36 hours after transfection, cells were fixed and subjected to cell cycle analysis using propidium iodide (PI) staining as previously established in our lab (Babaei-Jadidi et al., 2011, Ibrahim et al., 2012) and described in (section 2.2.6.4).

As shown in (Figure 5-8), FLYWCH1 (blue boxes) did not significantly changed the percentage of cells at any phases of cell cycle in comparison to the control (red boxes) in all cell lines tested. Thus, FLYWCH1 may not be associated to cell cycle progression and subsequently, the slow wound-closure rate of FLYWCH1 expressing cells (Figure 5-7) may due to defects in cell migration.

**Figure 5-8: FLYWCH1 has no significant effects on cell proliferation.** HCT116, SW480, and DLD-1 CRC cell lines were transiently transfected with pEGFP-C2 vector (control, red boxes) or eGFP-FLYWCH1-WT plasmid (blue boxes) and subjected to cell cycle analysis. **Upper panels)** Charts show the percentage of cells in different phases of cell cycle (Sub-G1, G0/G1, S, and G2/M) in **A) HCT116, B) SW480, and C) DLD-1** cell lines as indicated. **Lower panels)** Show representative cell cycle histograms for each cell line. Data are mean  $\pm$  SD ( $n = 3$ ; no significant changes detected). Experiment run in triplicate and repeated at least on three independent occasions.

To further validate the above cell-cycle results, the effect of FLYWCH1 on the total cell growth was also examined. HCT116 cells were transiently transfected with eGFP-FLYWCH1-WT plasmid and the cells were counted over a course of 4 days to generate a growth curve as outlined in (section 2.2.6.5). As expected, the total cell count of transfected cells was not significantly affected by FLYWCH1 in comparison to the control (cells transfected with pEGFP-C2 vector) (Figure 5-9), suggesting that FLYWCH1 might not affect the total growth of cancer cells.

It should be mentioned that the transient transfection allow the gene of interest to be expressed for a short period of time (few days). It has been reported that the GFP fluorescence can be used as a reliable reporter to monitor changes in gene expression (Soboleski et al., 2005). Therefore, in this experiment the expression level of the eGFP-fusion FLYWCH1 protein was examined through a fluorescent microscope during the course of the experiment and detectable GFP fluorescence was seen throughout the indicated times. As this method is not quantitative, reduction in FLYWCH1 gene expression by time cannot be excluded. However, as no significant effect of FLYWCH1 on the total number of cells was observed at early stages of transfection (24 & 48 hours) this possibility is unlikely to affect the results.



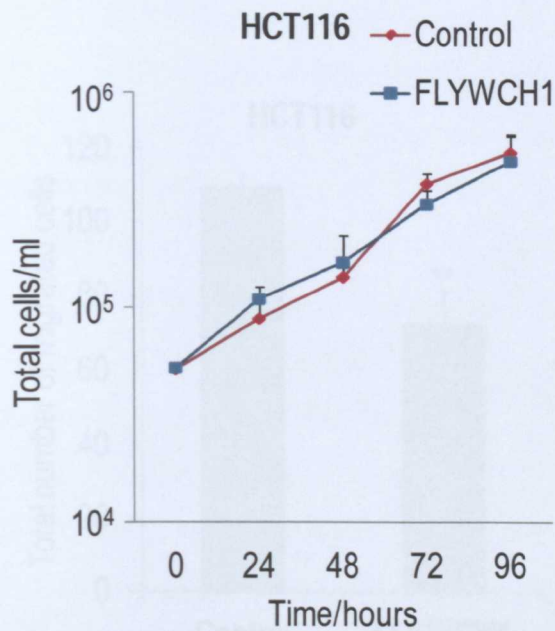


**Figure 5-9: FLYWCH1 does not affect the total cell growth.** Transiently transfected HCT116 cells with either eGFP-FLYWCH1-WT or pEGFP-C2 (control) plasmids were seeded at an initial density of  $5 \times 10^4$  cells/ml. The logarithmic growth curve was generated by counting the total number of cells on daily basis for 4-days (96 hours) as indicated. Y-axis indicates the total number of cells/ml at specific time points given on X-axis. Experiment run in triplicate and data are means  $\pm$  SD ( $n = 3$ ; no significant changes were detected).

### 5.2.5.3 FLYWCH1 reduces migration of CRC cells

To examine the effect of FLYWCH1 on cell motility of CRC cells, a migration assay was performed. HCT116 cells were transiently transfected with eGFP-FLYWCH1-WT clone or pEGFP-C2 vector (control) and the migration ability of the transfected cells was examined using trans-well migration assay as described in (section 2.2.6.3).

The results of the assay showed that overexpressed FLYWCH1 significantly reduced the total number of migrated cells in comparison to the control (Figure 5-10). These data support our previous findings (sections, 5.2.5.1 and 5.2.5.2) and together suggest that FLYWCH1 causes real defects in cell migration which leads to reduced cell motility without affecting cell proliferation.

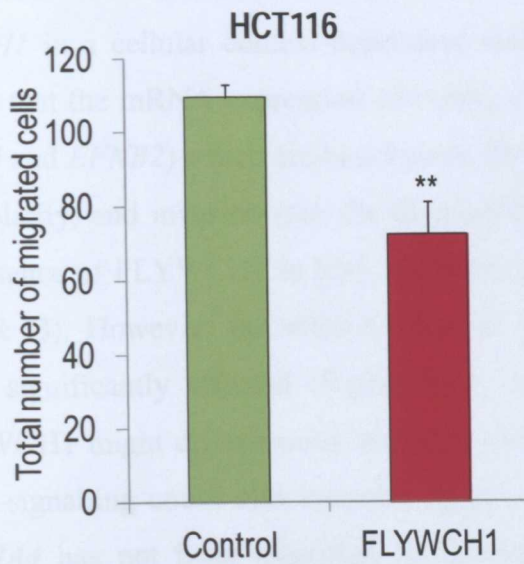


**Figure 5-10: FLYWCH1 reduces the migration of CRC cells.** Chart shows the total number of migrated HCT116 cells transiently transfected with eGFP-FLYWCH1-WT clone (red box) vs. control (green box) using trans-well migration assay. Data are mean  $\pm$  SD ( $n = 3$ ; \*\*,  $P < 0.01$ ). Experiment run in triplicate and repeated at least on three independent occasions.

### **5.2.6 FLYWCH1 modulates the gene expression of migration effectors**

To underline the mechanisms by which FLYWCH1 suppresses cell migration, the gene expression of several migration effectors was analyzed. The mRNA level of several Wnt/ $\beta$ -catenin target genes including *CDH1* (E-cadherin encoding gene), *c-Jun*, *cyclin D1* and Eph/Ephrin molecules was evaluated by qRT-PCR using specific primers (Table 2-5). The cDNA derived from two transiently transfected CRC cell lines (HCT116 and SW480) with either pEGFP-C2 (control) or eGFP-FLYWCH1-WT plasmids was used for the analysis. This method allowed us to compare the mRNA level of the indicated genes (Table 2-5) in FLYWCH1 expressing cells relatively to the control cells (transfected with empty vector). The qRT-PCR analysis revealed that the mRNA level of *CDH1* significantly increased in FLYWCH1 expressing cells

of SW480 but not HCT116 cell line in comparison to the control (Figure 5-11, A & B). This observation indicates that FLYWCH1 may regulate the expression of *CDH1* in a cellular context-dependent manner. Moreover, the analysis also show that the mRNA expression of *c-Jun*, *cyclin D1* and Ephrin molecules (*EPHA4* and *EFNB2*) which are best known for their contribution to cell movement, polarity, and invasion (see the discussion) were significantly reduced in the presence of FLYWCH1 in both HCT116 and SW480 cell lines (Figure 5-11, A & B). However, the mRNA level of *c-Myc*, *EPHB2*, and *EFNB1* were not significantly affected (Figure 5-11, A & B). These data suggest that FLYWCH1 might differentially modulate the expression of Wnt-target genes. Wnt signalling could also modulate gene expression indirectly, for instance, *EPHA4* has not been identified as Wnt-target gene, but its expression was significantly reduced by FLYWCH1. Collectively, these data suggest that FLYWCH1 may affect cell motility through modulation of Wnt-target genes.

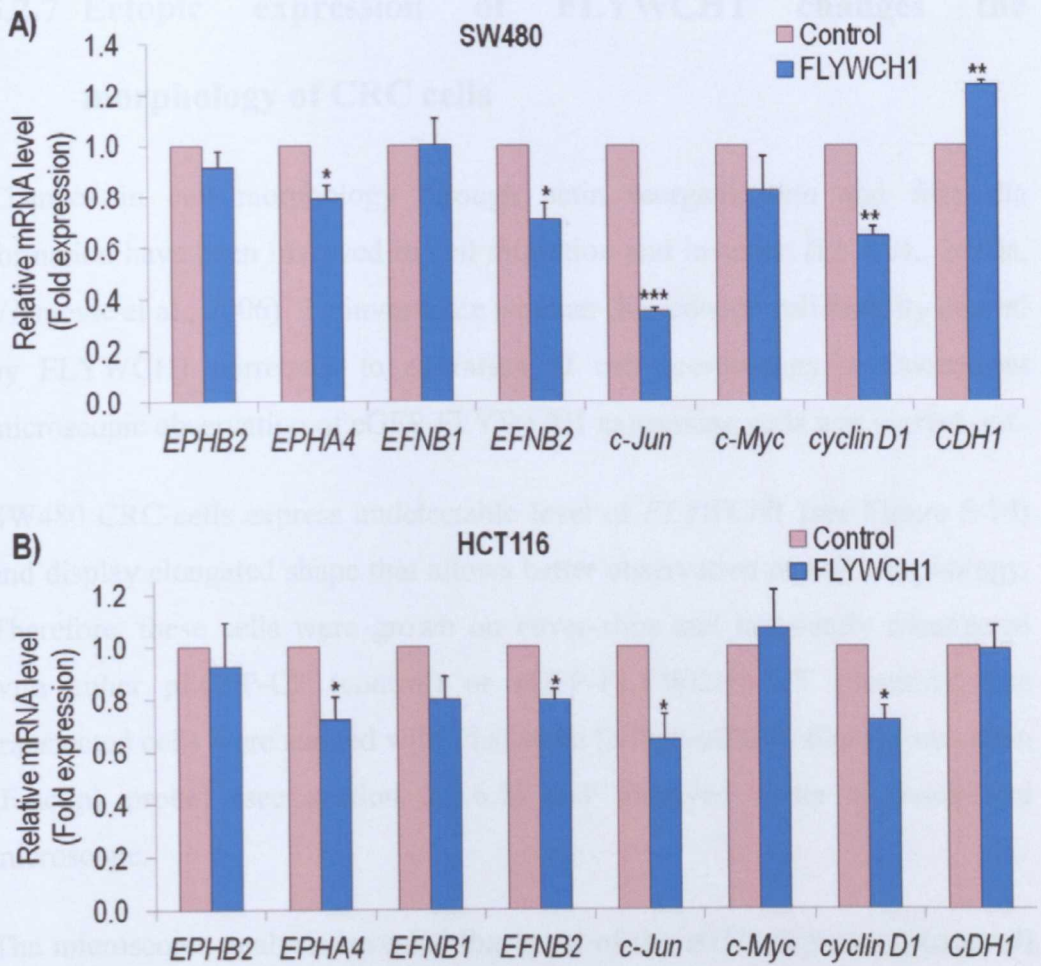


**Figure 5-11: FLYWCH1 modulates the expression of Wnt-target genes.** CRC cell lines **A) SW480** and **B) HCT116** were transiently transfected to express eGFP (control) or eGFP-FLYWCH1-WT (FLYWCH1). The expression of several Wnt-target genes in FLYWCH1 expressing cells (blue boxes) relatively to the control cells (red boxes) is shown as indicated. Data are mean  $\pm$  SD ( $n = 3$ ; \*,  $P < 0.05$ ; \*\*,  $P < 0.01$ ; \*\*\*,  $P < 0.001$ ). Experiment run in triplicate and repeated at least on three independent occasions.

### **5.2.7 Ectopic expression of FLYWCH1 changes the morphology of CRC cells**

Changes in cell morphology through actin reorganization and filopodia formation have been involved in cell migration and invasion (Li et al., 2010a, Vignjevic et al., 2006). To investigate whether the reduced cell motility caused by FLYWCH1 correlates to alteration of cell morphology, a fluorescent microscopic observation of eGFP-FLYWCH1 expressing cells was carried out.

SW480 CRC cells express undetectable level of *FLYWCH1* (see Figure 5-14) and display elongated shape that allows better observation of cell morphology. Therefore, these cells were grown on cover-slips and transiently transfected with either pEGFP-C2 (control) or eGFP-FLYWCH1-WT plasmids. The transfected cells were stained with Phalloidin [a high-affinity filamentous actin (F-actin) probe] (see section 2.2.6.7) and observed under a fluorescent microscope.

The microscopic analysis revealed that most of the eGFP expressing (control) cells display normal, similar to non-transfected cells, morphology in the same field (Figure 5-12, top panel). These cells are characterized by flat, elongated, and branched cells with prominent actin fibres. Conversely, most of the FLYWCH1 expressing cells show different phenotype, characterized by less elongated, circular epithelial-like morphology with actin fibres concentrated at the edge of the cells, whereas non-transfected cells within the same culture/field show normal elongated morphological properties (Figure 5-12, bottom panel). Taken together, these results indicate that FLYWCH1 may regulate cell migration possibly through alterations in cell morphology.

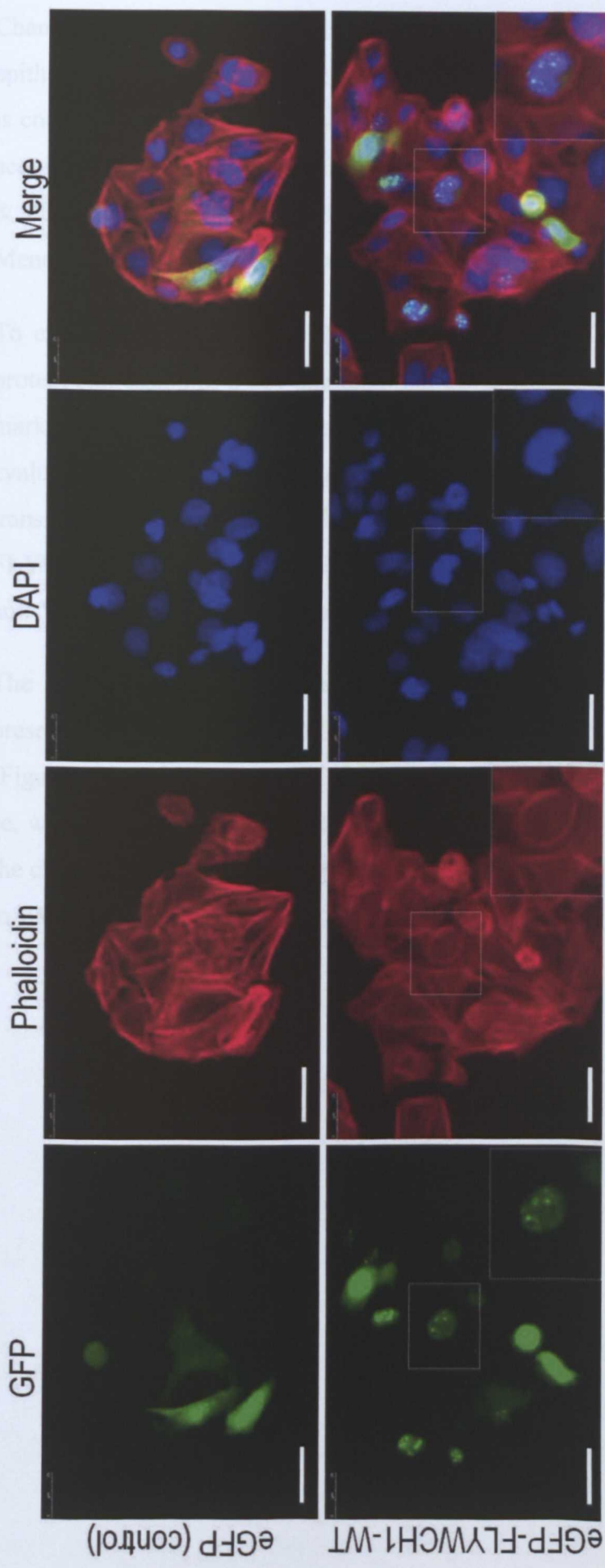


**Figure 5-12: FLYWCH1 changes the morphology of CRC cells.** SW480 cells were transiently transfected to express eGFP (control, top panel) or eGFP-FLYWCH1-WT (bottom panel). Cells were stained with Phalloidin (red) and DAPI (blue) and visualized under a fluorescent microscope. A single FLYWCH1 expressing cell is boxed and magnified (bottom panel) as indicated. Experiment run in triplicate and repeated at least on three independent occasions. Scale bars, 50  $\mu\text{m}$ .

Changes in cell morphology often associated with a cellular process called epithelial to mesenchymal transition (EMT) (Nelson et al., 2008). This process is commonly accompanied by enhanced cell migration and metastasis through acquisition of mesenchymal characteristics (such as up-regulation of Vimentin & ZEB2) and loss of epithelial traits (such as E-cadherin) (Mani et al., 2008, Mendez et al., 2010, Nelson et al., 2008).

To examine whether or not FLYWCH1 associated to the EMT process, the protein expression of a key epithelial marker (E-cadherin) and a mesenchymal marker (Vimentin) in addition to a potential EMT regulator (ZEB2) were evaluated by Western blotting analysis. The protein lysates derived from transiently transfected SW480 cells with either pEGFP-C2 or eGFP-FLYWCH1-WT plasmids were immunoblotted with anti-E-cadherin, anti-GFP, anti-Vimentin and anti-ZEB2 antibodies (see Table 2-7).

The data show that the protein level of E-cadherin was increased in the presence of overexpressed FLYWCH1 in comparison to the control cells (Figure 5-13, lane 1 vs. lane 2). The protein level of ZEB2 was not affected per se, whereas Vimentin was slightly decreased. These data gives the notion that the changes on cell morphology caused by FLYWCH1 might not be associated to EMT through ZEB2 protein.

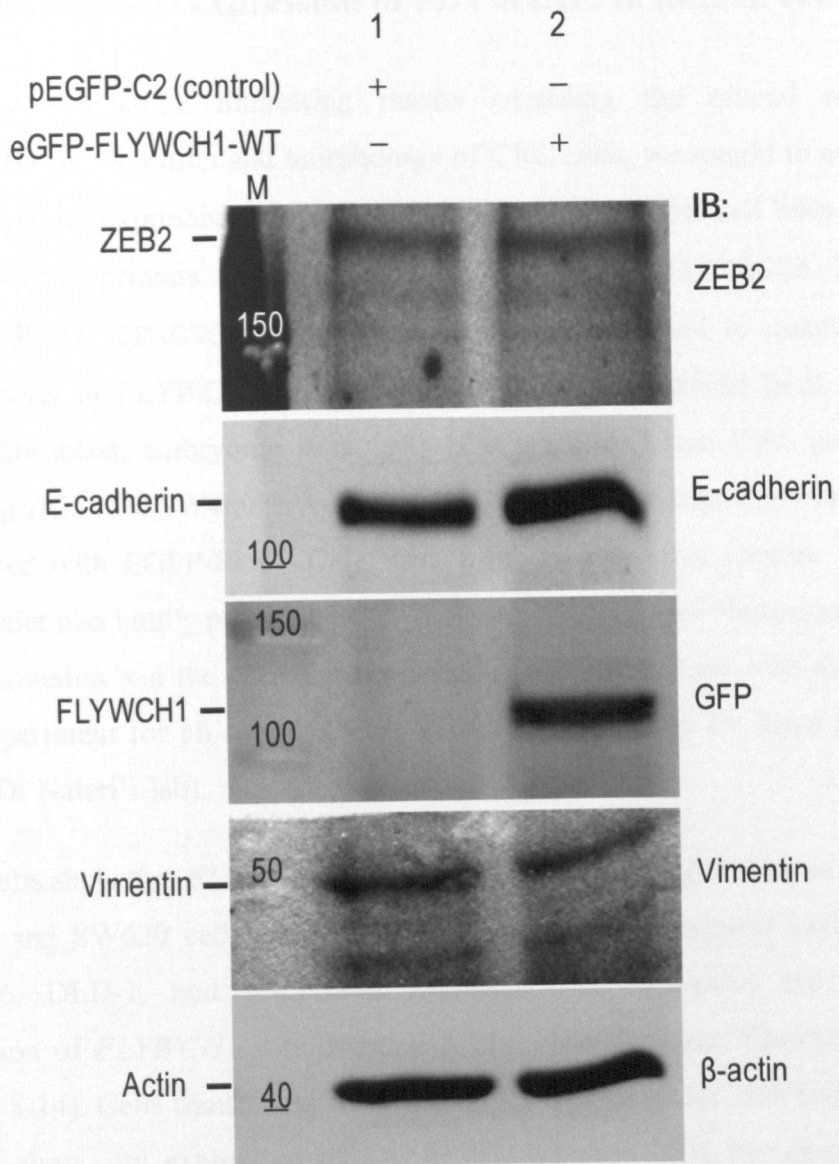


**Figure 5-13: FLYWCH1 enhances the expression of E-Cadherin.** SW480 cells were transiently transfected to express eGFP (lane 1, control) or eGFP-FLYWCH1-WT (lane 2). The protein lysate was immunoblotted with anti-ZEB2, anti-GFP, anti-E-cadherin, anti-Vimentin and anti- $\beta$ -actin antibodies. The expression of each protein is shown as indicated. "M", denotes the ColorPlus Protein marker (in kDa) from NEW ENGLAND BioLabs.

### **5.2.8 Endogenous expression of FLYWCH1 in human cell lines**

Following the above interesting results regarding the crucial role of FLYWCH1 on migration and morphology of CRC cells, we sought to evaluate the endogenous expression of *FLYWCH1* in normal vs. cancer cell lines. To do this, specific primers (forward: 5'-GCAAAGGTCGAAGACCAGGA-3' and reverse: 5'-TTCCTGGTGTACGAGTCCTT-3') were designed to quantify the mRNA level of *FLYWCH1* by qRT-PCR using cDNA derived from normal human fibroblast, embryonic stem cells (ESC) and different CRC cell lines including HCT116, SW480, SW620, and DLD-1. SW480 cells that transiently transfected with EGFP-FLYWCH1 were used as a positive control. Human ESCs pellet was kindly provided by C. Denning, university of Nottingham. The RNA extraction and the cDNA preparation of the ESCs along with the qRT-PCR experiment for all samples were kindly performed by Dr Roya Babaei-Jadidi (Dr Nateri's lab).

The results show that *FLYWCH1* expression level was not detectable in each of SW480 and SW620 cell lines, whereas its expression is slightly detected in HCT116, DLD-1, and ESC cells (Figure 5-14). However, the highest expression of *FLYWCH1* was detected in the normal human fibroblast cells (Figure 5-14). Cells transfected with pEGFP-C2 empty vector (SW480-EGFP) did not show any expression of *FLYWCH1*, whereas cells transfected with EGFP-FLYWCH1 plasmid (SW480-FLYWCH1) show high induction of this gene, indicating the specificity of the PCR reaction. Taken together, these data suggest that *FLYWCH1* is differentially expressed in human cell lines and its expression may be tightly regulated in CRC cells.

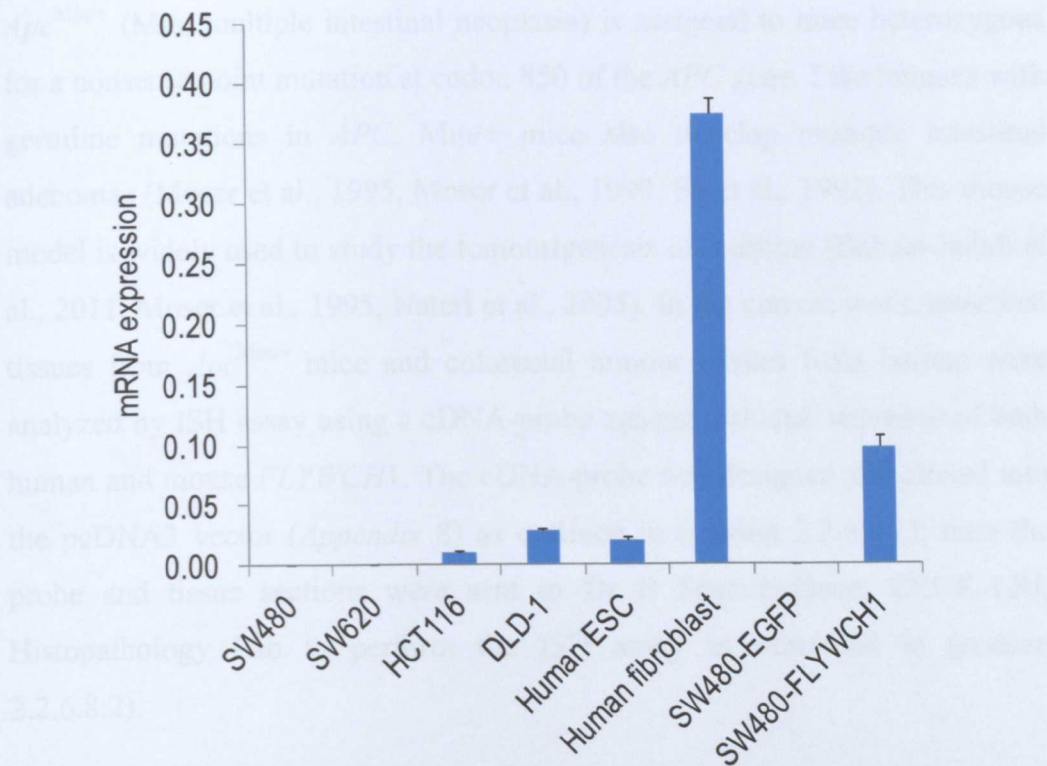


**Figure 5-14: Endogenous expression of *FLYWCH1* in different human cell lines.** The mRNA level of the indicated normal and CRC cell lines was quantified by qRT-PCR. Transiently transfected SW480 cells with *FLYWCH1* (SW480-*FLYWCH1*) were used as a positive control. Experiment run in triplicate and data are mean  $\pm$  SD ( $n = 3$ ). This experiment was kindly performed by Dr Roya Babaei-Jadidi (Dr Nateri's lab) as explained in the text.

### 5.2.9 Endogenous expression of *FLYWCH1* in normal and tumour tissues

Following the above observation of differential *FLYWCH1* expression in CRC cell lines, exploring the endogenous expression of *FLYWCH1* in normal vs. tumour tissues was thought to be important. As there is no commercially available *FLYWCH1*-antibody that works endogenously for immunocytochemistry, Western blot, or ChIP-assays, the In Situ Hybridization (ISH) assay on *Apc*<sup>Min/+</sup> mouse and human colorectal tumour tissues was performed.

*Apc*<sup>Min/+</sup> (Min, multiple intestinal neoplasia) is assigned to mice heterozygous for a nonsense point mutation at codon 850 of the *APC* gene. Like humans with germline mutations in *APC*, *Min/+* mice also develop multiple intestinal adenomas (Moser et al., 1995, Moser et al., 1990, Su et al., 1992). This mouse model is widely used to study the tumorigenesis of intestine (Babaei-Jadidi et al., 2011, Moser et al., 1995, Nateri et al., 2005). In the current work, intestinal tissues from *Apc*<sup>Min/+</sup> mice and colorectal tumour tissues from human were analyzed by ISH assay using a cDNA-probe against a shared sequence of both human and mouse *FLYWCH1*. The cDNA-probe was designed and cloned into the pcDNA3 vector (*Appendix 8*) as outlined in (section 2.2.6.8.1), then the probe and tissue sections were sent to Dr B Spencer-Dene, CRUK-LRI, Histopathology Lab to perform the ISH assay as described in (section 2.2.6.8.2).

In normal gut from *Apc*<sup>Min/+</sup> mice, *Flywch1* expression was not detected in differentiated epithelial cells in the villi, whereas *Flywch1* was highly expressed in a population of crypt based cells (2-6 cells) where the *Lgr5*<sup>+ve</sup> cells are located (Barker et al., 2007) (Figure 5-15A, right panel, magnified box E). In contrast, *Flywch1* expression was down-regulated at the crypt based cells of tumour tissues from *Apc*<sup>Min/+</sup> mice (Figure 5-15A, left panel, magnified box B). This finding indicates that *Flywch1* expression becomes gradually silenced as cells differentiate and also when transformed.

The ISH assay also show that *Flywch1* expression was restricted to the late stages of *Apc*<sup>Min/+</sup> intestinal adenocarcinomas (Figure 5-15A, left panel, magnified box C), and metastatic CRCs in a tissue microarray (TMA) study (Figure 5-15, F & G), indicating that the expression level of *FLYWCH1* may be correlated to pathological staging of CRCs.

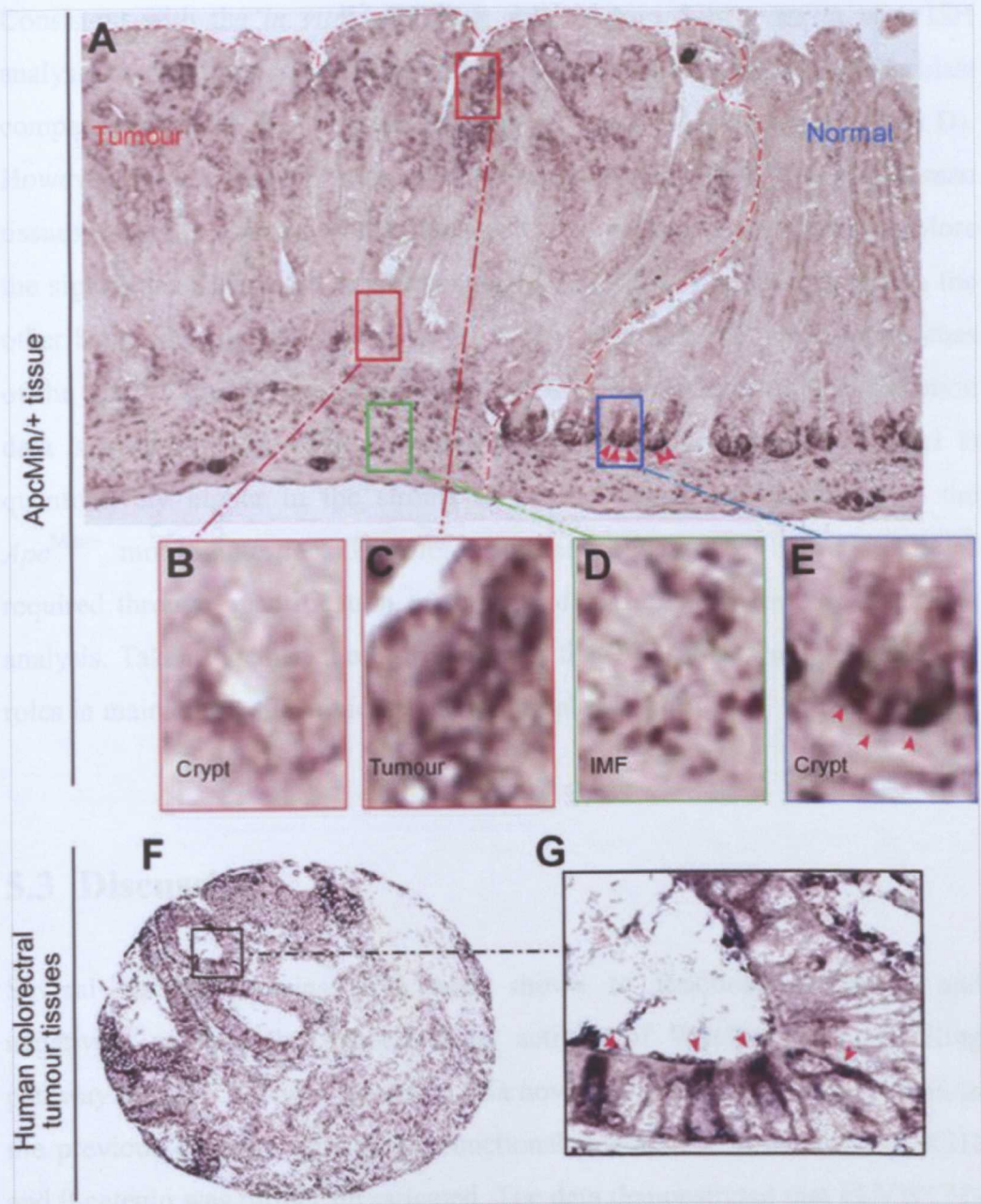


Figure 5-15: Endogenous expression of FLYWCH1 in normal vs. tumour tissues of intestine. ISH for *FLYWCH1* on representative intestinal tissue sections of A) *Apc<sup>Min/+</sup>* mice and E) human colorectal tumours tissues. Red arrowheads indicate *FLYWCH1*<sup>+ve</sup> cells in A) normal crypts of *Apc<sup>Min/+</sup>* murine intestine and F) section of human colorectal tumour tissue. Boxes (B, C, D, E & G) represent magnified views of the indicated area. This experiment was performed in collaboration with Dr B Spencer-Dene, CRUK-LRI, Histopathology Lab.

Consistent with the *in vitro* qRT-PCR data (Figure 5-14), our *in vivo* ISH analysis revealed that *Flywch1* mRNA is highly expressed in the myofibroblast compartment of the *Apc*<sup>Min/+</sup> mouse intestine (Figure 5-15A, magnified box D). However, further quantification of *FLYWCH1* expression in different human tissues including normal, primary and secondary tumours is required to explore the significant differential expression of *FLYWCH1* in human tissues. On the other hand, the expression of *Flywch1* is also evident in the adenocarcinomas of the *Apc*<sup>Min/+</sup> mouse intestine (Figure 5-15A). However, as no quantification data is available, it remains uncertain whether the expression of *Flywch1* is quantitatively higher in the stroma or in the tumour compartment of the *Apc*<sup>Min/+</sup> mouse intestine. Therefore, further validation of these results is required through quantification of the ISH data and/or performing qRT-PCR analysis. Taken together, these data suggest that *FLYWCH1* may play crucial roles in maintaining the homeostasis of normal intestine.

### 5.3 Discussion

Several nuclear proteins have been shown to functionally interact and negatively regulate the transcriptional activity of Wnt/ $\beta$ -catenin signalling pathway. *FLYWCH1* was identified as a novel partner for nuclear  $\beta$ -catenin in the previous chapter. Herein, the functional interaction between *FLYWCH1* and  $\beta$ -catenin was further investigated. The data demonstrated that *FLYWCH1* negatively modulates  $\beta$ -catenin signalling as judged by a dramatic repression of  $\beta$ -catenin transactivational activity by this protein both exogenously in HEK293T cells (Figure 5-1) and endogenously in SW620 and HCT116 cells (Figure 5-3). Furthermore, the luciferase data revealed that the C-terminal truncated form of *FLYWCH1* (deletion mutant M4) lacking motifs number 3, 4 and 5 lost its suppression against  $\beta$ -catenin (Figure 5-5). However, the transcriptional activity of  $\beta$ -catenin was highly repressed by each of the deletion mutants M2 (lacking motifs 1 & 2) and M3 (lacking motif 5) of *FLYWCH1* to a comparable level to the wild-type (WT) clone, indicating the critical involvement of motifs number 3 & 4 in the negative regulation of  $\beta$ -

catenin signalling. These data highlight the importance of FLYWCH1 and its motifs 3 & 4 in the functional interaction of FLYWCH1 with  $\beta$ -catenin.

Negative regulators tightly modulate Wnt pathway through different mechanisms such as enhanced degradation of  $\beta$ -catenin by activated p53 and Nur77 (Sadot et al., 2001, Sun et al., 2011) or competition with members of TCFs for binding to  $\beta$ -catenin in case of Chibby and Sox 9 (Takemaru et al., 2003, Akiyama et al., 2004). Similar to the later reports, our data also suggest that FLYWCH1 might compete with TCF4 for binding to  $\beta$ -catenin and also indicate that the interaction affinity of  $\beta$ -catenin to FLYWCH1 might be stronger than its interaction affinity to TCF4 as shown by the Co-IP (Figure 5-4) and luciferase (Figure 5-2) data. Alternatively, it is also possible that FLYWCH1 may form a complex with both  $\beta$ -catenin and TCF4 and disrupt the transcriptional activity of this complex leading to attenuated  $\beta$ -catenin/TCF4 signalling as it is the case for RUNX3 (Ito et al., 2008). Furthermore, it cannot be excluded that FLYWCH1 may bind to specific elements of DNA through its zinc finger domains and recruit nuclear  $\beta$ -catenin to the promoter of target genes independently to TCFs.

The armadillo repeats (the central domain) and the C-terminal domain of  $\beta$ -catenin are providing interaction sites to many critical partners, especially the N-terminal region of the C-terminal domain which has been described as a key component of the C-terminal transactivation domain (Xing et al., 2008), whereas the N-terminal domain is providing phosphorylation sites (Liu et al., 2002). However, our luciferase results, consistent with our previous Co-IP data (see Figure 4-13), suggested that the N-terminal domain of  $\beta$ -catenin may be required for its functional interaction with FLYWCH1 (Figure 5-6), indicating that, in addition to its role in phosphorylation, The N-terminal domain of  $\beta$ -catenin may also interact with transcription factors and thereby play roles in the transcriptional activity of  $\beta$ -catenin as it has also been suggested by (Tolwinski and Wieschaus, 2004).

Cell migration is one of the critical biological processes regulated by Wnt/ $\beta$ -catenin signalling pathway (Aman and Piotrowski, 2008, Humtsoe et al., 2010, Matsuda et al., 2009).  $\beta$ -catenin, the major player of this pathway, together

with TCFs modulates the expression program of many genes thereby promoting cell migration and/or invasion. Thus, factors that suppress  $\beta$ -catenin transcriptional activity, in principle, should decrease cell motility and migration. Interestingly, the results of *in vitro* scratch assay and trans-well migration assays obtained in this study show that FLYWCH1 decreases cell motility (Figure 5-7 and Figure 5-10) without affecting cell cycle and growth (Figure 5-8 and Figure 5-9). Although plausible data was produced by the approaches applied in this study, some experimental limitations such as using of alternative approaches cannot be excluded. For instance, in the trans-well migration assay, the migrated cells can be counted in different ways, each with distinct advantages or disadvantages. The migration ability of cells can be evaluated through staining and counting the cells that have migrated through and remained attached to the bottom side of the trans-well chambers (Pino et al., 2010). However, this method is very delicate and technically difficult to set up. In addition, this method of cell counting could be very subjective especially when the distribution and/or staining of the cells on the bottom side of the filter are uneven (Staton et al., 2009). On the other hand, this method may be helpful if the protein of interest known to affect the adhesion properties of the cells.

An alternative way to evaluate the results of the trans-well migration assay is to count the cells that migrate down to the lower chamber and attached to the bottom of the well (Entschladen et al., 2005, Elsaba et al., 2010, Al-Ghamdi et al., 2012). This method allows the user to count the viable cells individually excluding any dead cells or debris that might have passed through the chamber. It also helps to study the morphology of the migrated cells through direct visual assessment under microscope without staining. Moreover, one can even re-cultivate these cells and use them for further investigations.

In the current work, we used the later approach to evaluate the effect of FLYWCH1 on the migration properties of HCT116 cells based on the reasons mentioned above. However, using the former method (i.e. staining and counting the cells on the bottom side of the chamber) could give more strength to the results of this assay. Despite of this limitation, the results of the trans-well migration assay (Figure 5-10) was in line with the results of *in vitro*

scratch assay (Figure 5-7) and together suggested that FLYWCH1 may reduce the migration ability of cancer cells.

It has been reported that the results of *in vitro* scratch assay could be associated to effects on cell migration and/or cell proliferation (Coomber and Gotlieb, 1990, Zahm et al., 1997). Therefore, mitosis inhibitors such as mitomycin-C could be used to block cell proliferation and evaluate cell migration alone (Leung et al., 2005). However, this approach is commonly used to evaluate the migration effect of growth factors such as epidermal growth factor (EGF) and transforming growth factor  $\beta$ 1 (TGF $\beta$ 1) that known to affect cell proliferation (Kanazawa et al., 2010, Singer et al., 2009, Rose, 2012). In the present study, we have shown that FLYWCH1 reduces the percentage of wound closure of CRC cells without affecting cell proliferation through cell cycle analysis and growth curve (Figure 5-8 and Figure 5-9) (more information about these assays is given below). Therefore, cell proliferation inhibitors were not used. Additionally, we further confirmed the results of the *in vitro* scratch assay by the trans-well migration assay as mentioned above.

Different cell lines could show different migration capacity (Kubens and Zanker, 1998). In our hand, SW480 cells showed more adhesiveness and slower migration capacity in comparison to HCT116 cells. Therefore, we analyzed the scratch assay for HCT116 cells at time 0 and after 24 hours (Figure 5-7A), as this time was sufficient to detect a significant change between the controls (transfected with empty vector) and experimental samples (transfected with FLYWCH1). Moreover, the edge of the wound was not perceptible at later times. However, for SW480 cells scratches were imaged at time 0, 24, and 48 hours. We noticed that the rate of wound closure was significantly reduced by FLYWCH1 at both 24 and 48 hours time course. However, the reduction was more pronounced at 48 hours as shown in (Figure 5-7B).

Although we have used different established techniques to evaluate the effect of FLYWCH1 on cell migration and proliferation (see above), potential improvement of these technical approaches should be considered. For example, certain factors/drugs that known to either promote or inhibit cell migration

and/or cell proliferation (i.e. positive and negative controls) can be used to further evaluate the effect of FLYWCH1 on these cellular traits. This approach not just helps to show the biological impact of FLYWCH1 more efficiently, but it also ensures that the experimental condition is optimal and the assay worked as expected. Moreover, it is also valuable to compare the migration rate of the control cell lines used in this study with published data. However, researchers often do not show the absolute values of migrated cells of the control samples; instead they arbitrarily normalize control values to number one then show folds of induction or reduction of migrated cells of the experimental samples in comparison to the controls (Pino et al., 2010, Vignjevic et al., 2007). In addition, migration rate of cells in the trans-well assay could be affected by many experimental parameters such as type and the pore size of the chamber, number of seeded cells, incubation period, and serum concentration in the culture medium. These parameters were found to be significantly variable between different laboratories which led to difficulties to perform such a comparison. However, the percentage of wound closure of untreated HCT116 (55%) and SW480 (32%) cells (i.e. controls) obtained in this work is comparable to the wound closure rate of these cells (43% for HCT116 & 29% for SW480) in a recent work published by Fan et al. (2011), though variation in the control wound closure rate in the same paper is also evident (Fan et al., 2011).

Our data also revealed that FLYWCH1 expressing cells are morphologically transformed into less branched, more rounded epithelial-like shape (Figure 5-12). In addition, our western blotting analysis showed up-regulation of E-cadherin without changes in ZEB2 EMT regulator (Figure 5-13). These data suggest that FLYWCH1 may regulate cell migration possibly through alterations in cell morphology that may not be related to ZEB2-mediated EMT. These findings uncovered a novel migratory role of FLYWCH1 in CRC cells and encouraged us to explore the molecular mechanisms underlying this effect in more detail.

Considering the importance of FLYWCH1 as a potential repressor of  $\beta$ -catenin-mediated transcriptional activity (see above), it is plausible that

FLYWCH1 may regulate the expression of Wnt-target genes, especially those which are related to cell migration and morphology. Therefore, in this study the expression of several Wnt-target genes were evaluated by qRT-PCR. Interestingly, our data showed that FLYWCH1 significantly modulates the expression of several key migration effector genes such as *CDH1*, *c-Jun*, and Eph/Ephrin molecules (Figure 5-11, A & B). Each of these genes has critical involvement in cell motility and/or morphology (Haldimann et al., 2009, Hermiston et al., 1996, Katiyar et al., 2007). For example, E-cadherin (encoded by *CDH1*) mediates cytoskeletal rearrangement through actin reorganization which may lead to formation of a distinct phenotype in favour or against cell migration (Alt-Holland et al., 2008, Chen et al., 2012). Accordingly, high level of E-cadherin protein has been widely associated to reduced cell motility (Hermiston et al., 1996, Mao et al., 2008), while its low level often linked to increased cell migration and/or invasion (Alt-Holland et al., 2008, Chen et al., 2012).

In the current work, both the mRNA and the protein levels of E-cadherin were found to be significantly increased by FLYWCH1 in SW480 cells (Figure 5-11A & Figure 5-13). Consistent with the previous reports, the up-regulated E-cadherin led to the acquisition of phenotypic properties that suppressed cell motility in this cell line (Figure 5-7B). Interestingly, our data indicated that the effect of FLYWCH1 on cell morphology and migration may not be related to ZEB2-mediated EMT (see above & section 5.2.7). These findings appreciate the role of FLYWCH1 transcription factor in controlling the key metastasis-suppressing protein, E-cadherin.

Among other Wnt-target genes, *Cyclin D1* was significantly down-regulated by FLYWCH1 (Figure 5-11, A & B). Although *cyclin D1* is widely involved in cell-cycle regulation, cell-cycle independent roles of this gene were also reported (Fernandez et al., 2011, Li et al., 2006a). It has been shown that cyclin D1 affects cell migration and morphology through repression of the metastasis suppressor Thrombospondin 1 (TSP-1) and inhibition of ROCK signalling (Li et al., 2006a). Furthermore, cyclin D1 was also involved in enhanced cell detachment and motility in collaboration with Ral GTPases (Fernandez et al.,

2011). In addition, down-regulation of cyclin D1 through  $\beta$ -catenin siRNA did not affect cell proliferation in U2OS/GR cells (Takayama et al., 2006). Consistence with these findings, our observations suggest that FLYWCH1 might influence the cell-cycle independent roles of cyclin D1 to reduce cell migration without affecting the cell cycle or growth.

*c-Jun* was another strongly down-regulated gene by FLYWCH1 (Figure 5-11, A & B). This gene is frequently overexpressed in diverse tumour types and has been implicated in promoting cellular migration and invasion in addition to proliferation, and angiogenesis (Katiyar et al., 2007, Jiao et al., 2008, Jiao et al., 2010). Moreover, c-Jun is a critical component of the activator protein 1 (AP-1) complex (Eferl and Wagner, 2003) which induces cellular migration and invasion by two regulatory mechanisms. First, by inducing the expression of several critical regulatory genes such as MMP9, CD44, Krp1, stem cell factor (SCF) and CCL5 (Jiao et al., 2010, Katiyar et al., 2007, Ozanne et al., 2007). Second, by suppressing the inhibitors of invasion such as TSC-36, fibronectin, STAT6 and PCDHGC3 (Ozanne et al., 2007). In addition, deletion of c-Jun reduces cellular migration and invasion through inhibition of c-Src and hyperactivation of ROCK II Kinase (Jiao et al., 2008). Ultimately, both up-regulated and down-regulated genes functionally interact to form pseudopods and support the mesenchymal mode of invasion. These findings fit our observations that FLYWCH1 caused migration defects and morphological changes through down-regulation of *c-Jun*.

Our results also showed that the expression of *EPHA4* and *EFNB-B2* was also significantly repressed (Figure 5-11, A & B). Ephrin-B2 has been associated to EMT, stem cell compartment, angiogenesis and metastasis (Haldimann et al., 2009, Kaenel et al., 2012), whereas EphA4 is mainly implicated in Axon Guidance (Wegmeyer et al., 2007). Moreover, targeting EphA4 receptor has been recently considered as a potential task in the therapeutic field for treatment of spinal cord injuries (Goldshmit and Bourne, 2010, Goldshmit et al., 2011). Furthermore, EphA4 is the only receptor that binds both classes (A and B) of ligands (Gale et al., 1996, Pasquale, 2008). Indeed, interaction and coordination between EphA4 and Ephrin-B2 has been reported and contributed

to EMT during somite morphogenesis (Barrios et al., 2003). Thus, down-regulation of both *EPHA4* and *EFNB-B2* by FLYWCH1 might be strongly associated to the reduced cell migration observed in this study.

Despite the fact that FLYWCH1 strongly inhibits  $\beta$ -catenin/TCF4 transcriptional activity, the expression of some but not all Wnt-target genes that examined in this study were affected by forced expressed FLYWCH1. Some genes such as *c-Myc*, *EPHB2* and *EFNB-B1* were not affected, while others were either up-regulated such as *CDH1* or down-regulated such as *c-Jun*, *cyclin D1*, *EPHA4* and *EFNB-B2*. These data indicate that Wnt-target genes differentially responded to FLYWCH1 overexpression. This finding is similar to an earlier report where Wnt-target genes were differentially responded to inhibited  $\beta$ -catenin/TCF signalling (van de Wetering et al., 2002).

Our ISH analysis showed that in normal compartments of *Apc*<sup>Min/+</sup> mouse intestine *Flywch1* was strikingly expressed in the crypt-based cells and down-regulated in differentiated intestinal epithelial cells (Figure 5-15, right panel). Conversely, in tumour tissues *Flywch1* was less expressed in the crypt (Figure 5-15, left panel), while its expression increased in late stages of intestinal adenocarcinomas (Figure 5-15A, left panel, magnified box C). In addition, *FLYWCH1* mRNA expression is restricted to a subpopulation of tumour cells in both humans and *Apc*<sup>Min/+</sup> mouse (Figure 5-15, A & F), suggesting that FLYWCH1 may have crucial roles during tumourigenesis.

On the other hand, some of the FLYWCH1/ $\beta$ -catenin target genes such as *c-Jun* and *EFNB-B2* (see above) were found to be highly expressed in CBS (crypt base columnar) cells of mice intestine, while their expression is decreased at the top of the villi (Batlle et al., 2002, Sancho et al., 2009), indicating important involvement of these genes in intestinal homeostasis (Babaei-Jadidi et al., 2011, Sancho et al., 2009). Moreover, *c-Jun* and Ephrin molecules, including *EFNB-B2*, are widely implicated in intestinal cell migration/positioning, proliferation, and tumourigenesis (Babaei-Jadidi et al., 2011, Batlle et al., 2002, Genander et al., 2009, Holmberg et al., 2006, Nateri et al., 2005, Sancho et al., 2009). It is thus possible that FLYWCH1 exerts its

influence on intestinal homeostasis and/or carcinogenesis through regulating the above genes as key regulators of cancer pathways.

Given the fact that *Flywch1* is highly expressed at the bottom of the crypts of mouse intestine (see above) where the  $Lgr5^{+ve}$  stem cells are located (Barker et al., 2007), and that its expression is restricted to small population of cells in both human and  $APC^{Min/+}$  mouse intestinal tumours (see above), it is therefore, plausible to speculate that FLYWCH1 may regulate intestinal stem cells in normal conditions and control the activity of cancer stem cells during cancer development.

Taken together, the data in this chapter introduced FLYWCH1 as a novel antagonist to the Wnt signalling pathway through functional interaction and inhibition of  $\beta$ -catenin/TCF4 transcriptional activity. The data also highlighted the anti-migratory role of FLYWCH1 transcription factor in colon cancer cell lines and explored the mechanisms by which FLYWCH1 deliver its regulatory function. Based on these data, it is likely that FLYWCH1 inhibits cell motility by regulating the gene expression of critical migration effectors including *cyclin D1*, *c-Jun*, *CDH1*, *EPHA4*, and *EFNB-B2* as illustrated in (Figure 5-16). As changes in cell motility is a key step toward invasion and metastasis, FLYWCH1 may functions as a potential metastasis-suppressing factor which could be of use in the therapeutic field of colon cancer to limit cancer spread. Finally, linking the endogenous expression of *FLYWCH1* in mouse intestine and human tumour tissues to the regulatory effects of FLYWCH1 on key homeostasis factors such as *c-Jun* and Ephrin molecules further highlights the importance of FLYWCH1 in normal vs. cancer development.

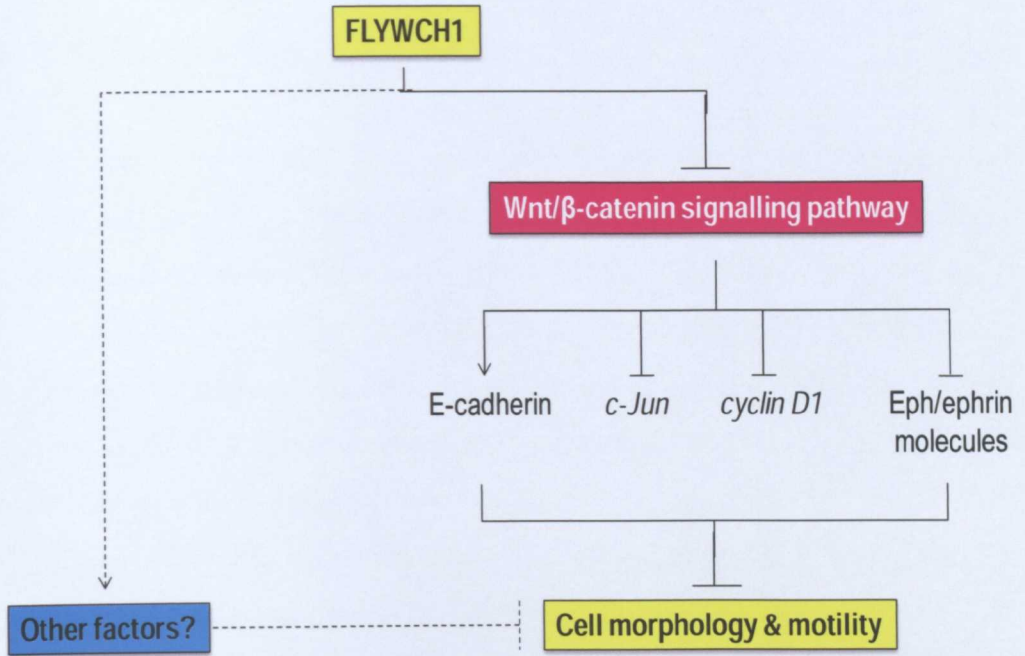


Figure 5-16: A simplified diagram shows the mechanism by which FLYWCH1 reduces cell motility. FLYWCH1 modulates the expression of Wnt/ $\beta$ -catenin target genes through inhibition of the canonical Wnt signalling pathway leading to defects in cell motility through changes in cell morphology. It is also possible that FLYWCH1 may affect cell migration and morphology through other factors.

the Functional Analysis of FLYWCH1

## **CHAPTER 6**

# **Generation of Stably-Transfected Cell lines for the Functional Analysis of FLYWCH1**

## 6.1 Introduction

Stable gene expression is a powerful approach to achieve long-term, reproducible, and large scale protein production. This cost effective method not only helps to overcome the transfection efficiency problems, but it also allows one to perform several biochemical and biological analyses more efficiently. Among different methods, the Lentiviral-based vectors offer an attractive system for efficient gene delivery and integration. The use of this system has been expanded in the past decade and adapted to be used to transduce almost all types of cells such as human monocyte-derived dendritic cells (Rouas et al., 2002), human and mouse ESCs (Gropp and Reubinoff, 2006, Kosaka et al., 2004). In our laboratory, this system has been successfully established to deliver genes of interest into different mammalian cells.

In the current study, a Lentiviral-based gene delivery system was applied to obtain a stable expression of eGFP reporter and eGFP-FLYWCH1 genes in HEK293T and HCT116 cell lines. This system necessitates cloning the nucleotide sequence of these genes into a Lentiviral vector called pLVX-Puro. Herein, the cloning process and the expression pattern of stably expressed FLYWCH1 in these cell lines are evaluated. The preliminary data indicated abnormal protein products expressed by the genome-integrated *FLYWCH1*. Therefore, different approaches such as microscopic observations, Western blotting, genomic PCR analysis, luciferase and migration assays were employed to fully characterize the exogenous FLYWCH1 (both the integrated cDNA sequences and their protein products) in these cell lines. Moreover, the genome-integrated sequence of *FLYWCH1* was PCR amplified and re-cloned into mammalian expression vectors for further characterization and study. Our analyses revealed that the integrated eGFP-FLYWCH1 is spontaneously mutated in both HEK293T and HCT116 stable cell lines resulting in a modified unfunctional FLYWCH1 protein that cannot interact with  $\beta$ -catenin. Subsequently, the mutated protein lost its repression activity on cell migration and morphology. To this end, we were able to obtain a successful integration and expression of full-length *FLYWCH1* cDNA in the HEK293T cell line by

limiting the cell-passage number of stably the transduced cells with Lenti-FLYWCH1. Moreover, within this chapter the morphological changes caused by FLYWCH1 were mechanistically further investigated which indicates up regulation of E-cadherin.

## 6.2 Results

### 6.2.1 Cloning of eGFP and eGFP-FLYWCH1-WT cDNAs into pLVX-Puro

pLVX-Puro is a HIV based Lentivirus expression vector ([www.clontech.com](http://www.clontech.com)). It contains a constitutively active human cytomegalovirus immediately promoter ( $P_{CMV\ IE}$ ) just upstream to the multiple cloning site (MCS) (Figure 6-1A). The *CMV*-promoter also drives the expression of eGFP and eGFP-FLYWCH1 cDNA in both pEGFP-C2 and eGFP-FLYWCH1-WT plasmids (Figure 6-1, B & C). Moreover, the nucleotide sequence of the *CMV*-promoter contains a single unique restriction site for *Sna*BI which is not present elsewhere in these expression plasmids (neither in the backbone nor in the coding region of eGFP or eGFP-FLYWCH1-WT). In addition, the *Eco*RI restriction site is present in the MCS of both pLVX-Puro and pEGFP-C2 vector. Moreover, the *Eco*RI restriction site is also present at the 3'-end of the *FLYWCH1* cDNA cloned in pEGFP-C2 vector (Figure 6-1C). Thus, *Sna*BI/*Eco*RI restriction enzymes were used to excise the full length coding sequence of eGFP and eGFP-FLYWCH1-WT coding regions from pEGFP-C2 plasmid and eGFP-FLYWCH1-WT clone respectively. These DNA fragments were sub-cloned into the pLVX-Puro Lentiviral vector as illustrated in (Figure 6-2). It is noteworthy to mention that *Sna*BI is a blunt end restriction enzyme which allows the two halves of the *CMV*-promoter (the N-terminal half from pLVX-Puro and the C-terminal half from pEGFP-C2 vector or eGFP-FLYWCH1-WT clone) to ligate and restore the complete sequence of *CMV* without introducing extra nucleotides that might interfere and affect the functionality of this promoter.

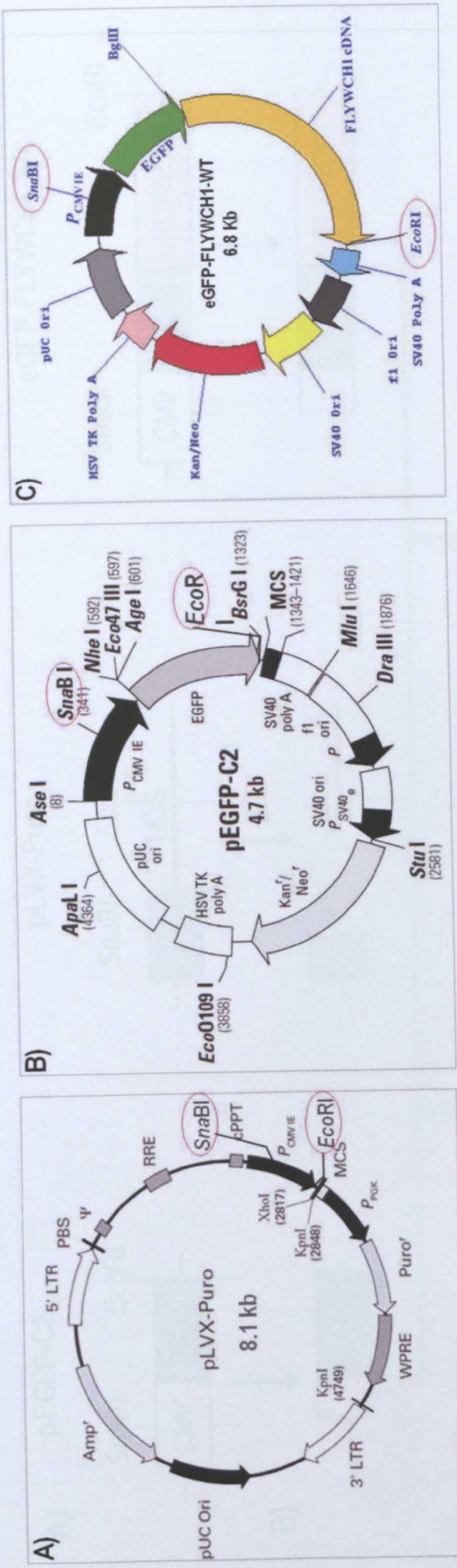
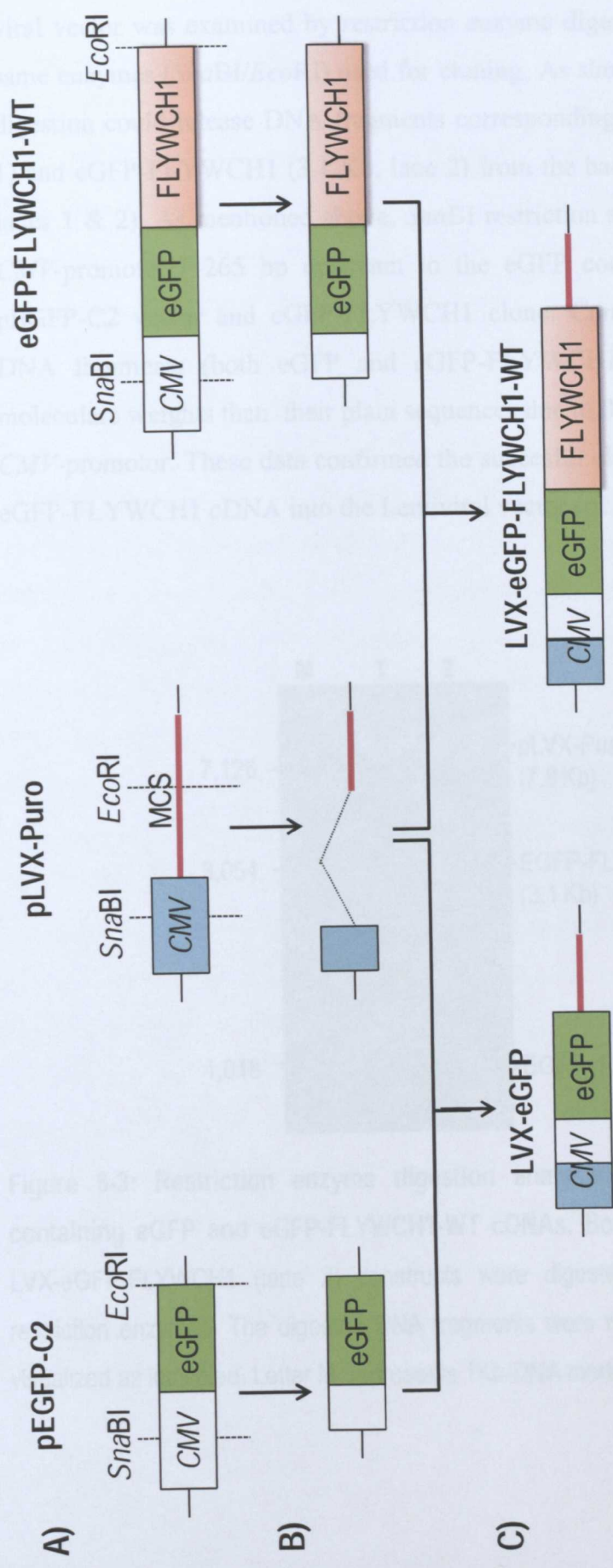
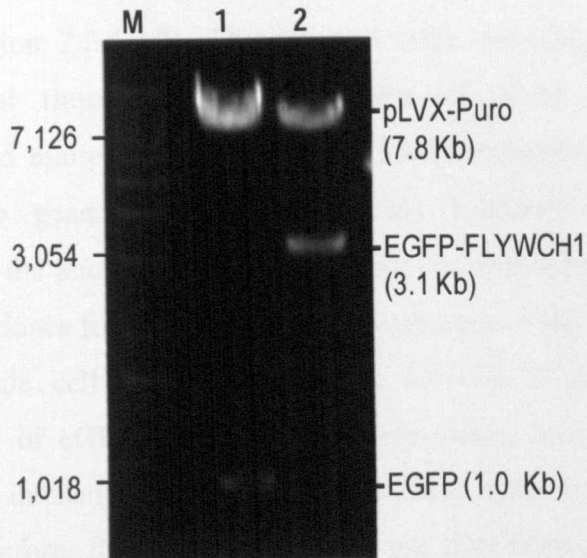


Figure 6-1: The expression plasmids and the strategy in brief, used to clone eGFP and eGFP-FLYWCH1 into the pLVX-Puro. Diagrams show the plasmid maps and the approximate cut positions of *SnaBI* and *EcoRI* restriction enzymes (circled in red) in the A) Lentiviral vector (pLVX-Puro), B) eGFP expression vector (pEGFP-C2), and C) eGFP-FYWCH1-WT clone which contains eGFP-fused full-length FLYWCH1-WT cDNA. The indicated restriction enzymes were used for cloning.



**Figure 6-2: Cloning strategy for LVX-eGFP and LVX-eGFP-FLYWCH1-WT clones.** Schematic presentation shows the cloning strategy of eGFP and eGFP-fused FLYWCH1-WT cDNA into the pLVX-Puro Lentiviral vector using *SnaBI*/*EcoRI* restriction enzymes. The full nucleotide sequence of eGFP (**A, left panel**) and eGFP-tagged FLYWCH1 (**A, right panel**) fused to the 3'-end of the CMV-promoter were **B**) excised by *SnaBI*/*EcoRI* restriction enzymes and **C**) ligated back into a *SnaBI*/*EcoRI* linearized pLVX-Puro vector (**B, middle panel**) to produce recombinant viral vectors expressing eGFP (LVX-eGFP) or eGFP-FLYWCH1 (LVX-eGFP-FLYWCH1-WT) as indicated.

The successful construction of eGFP and eGFP-FLYWCH1 cDNA into the viral vector was examined by restriction enzyme digestion analysis using the same enzymes (*Sna*BI/*Eco*RI) used for cloning. As shown in (Figure 6-3), this digestion could release DNA fragments corresponding to eGFP (1.0 Kb, lane 1) and eGFP-FLYWCH1 (3.1 Kb, lane 2) from the backbone vector (7.8 Kb, lanes 1 & 2). As mentioned above, *Sna*BI restriction site is located inside the *CMV*-promoter (~265 bp upstream to the eGFP coding sequence) in both pEGFP-C2 vector and eGFP-FLYWCH1 clone. Consequently, the digested DNA fragments (both eGFP and eGFP-FLYWCH1) have slightly higher molecular weights than their plain sequences due to this extra-sequence of the *CMV*-promotor. These data confirmed the succesful cloning of both eGFP and eGFP-FLYWCH1 cDNA into the Lentiviral vector (pLVX-Puro).



**Figure 6-3: Restriction enzyme digestion analysis of Lentiviral constructs containing eGFP and eGFP-FLYWCH1-WT cDNAs.** Both LVX-eGFP (lane 1) and LVX-eGFP-FLYWCH1 (lane 2) constructs were digested with *Sna*BI and *Eco*RI restriction enzymes. The digested DNA fragments were run on 1% agarose gel and visualized as indicated. Letter M, represents 1Kb-DNA marker in bp (Invitrogen).

## **6.2.2 Transduction and selection of cells with pLVX-eGFP and pLVX-eGFP-FLYWCH1-WT**

The Lentiviral constructed clones (LVX-eGFP and LVX-eGFP-FLYWCH1-WT) (see section 6.2.1) were used to produce Lentiviral particles using HEK293T cells as a producer cell line for packaging as outlined in (section 2.2.4.3.1). The viral particles were used to deliver eGFP and eGFP-FLYWCH1 cDNA into the genome of HEK293T and HCT116 cell lines in order to obtain stable gene expression of these genes as described in (section 2.2.4.3.2). Briefly, HEK293T cells were co-transfected with expression plasmids encoding components of Lentiviral particles to produce a viral soup. The viral soup was concentrated and used to infect HEK293T and HCT116 cells. The infected cells were maintained and selected with Puromycin to produce stable cell lines expressing either eGFP or eGFP-FLYWCH1 as detailed in (section 2.2.4.3.2). The resistant cells were kept in culture and passaged several times during the process of single clone selection, amplification and maintenance before being used for characterization. In our first attempt to generate stable clones, the transduction efficiency of FLYWCH1 into the above mentioned cell lines was initially low. An average of 2-3 resistant clones for each cell lines were obtained from the 96-well plates method for single cell selection (section 2.2.4.3.2). In addition, the GFP expression level of eGFP-FLYWCH1 in these clones was not equal. Some were losing the intensity of the GFP fluorescence even during the selection procedure. Therefore, the best expressed clone with high GFP fluorescence judged by the fluorescent microscopy was chosen, expanded, and used for further validation and characterization as detailed below (section 6.2.3). However, in the second attempt of stable cell line generation, two clones for each cell line were selected and evaluated by Western blot analysis as detailed in (section 6.2.7).

## **6.2.3 Characterization of cell lines stably expressing eGFP and eGFP-FLYWCH1**

### **6.2.3.1 Evaluation of FLYWCH1 gene expression by Western blotting analysis**

To investigate the stable expression of eGFP and eGFP-FLYWCH1-WT protein in HEK293T and HCT116 cell lines, initially, Western blotting analysis was performed. The protein lysate was extracted from these cell lines, run on SDS-PAGE gel, and immunoblotted with anti-GFP antibody as outlined in (section 2.2.5). The eGFP protein (~26 kDa) was clearly detected in both cell lines (Figure 6-4A, lanes 1 and 3), whereas detection of eGFP-FLYWCH1-WT was ambiguous. The expected molecular weight of this protein (~106 kDa) was only barely detected in HCT116 cells stably expressing eGFP-FLYWCH1-WT (HCT116-FLYWCH1<sup>+ve</sup>) (Figure 6-4A, red-dashed box, lane 4), while a strongly expressed protein band migrating at ~50 kDa was detected in the same lane (boxed in red), suggesting that eGFP-FLYWCH1 protein may be aberrantly expressed (i.e. presumably truncated) in these cells.

In addition, in HEK293T cells stably expressing eGFP-FLYWCH1-WT (HEK293T-FLYWCH1<sup>+ve</sup>), a band of eGFP-FLYWCH1 (just below 100 kDa) was detected. This protein band is slightly smaller than the calculated molecular weight (~106 kDa) of this protein (Figure 6-4A, red box, lane 2). Therefore, it is assumed that FLYWCH1 is either abnormally expressed in this cell line or, alternatively, FLYWCH1 might have been migrated faster on the SDS-PAGE gel. To further elucidate this, the same Lentiviral particles (LVX-eGFP-FLYWCH1-WT) that originally used to transduce and generate the stable cell lines were used to transiently express eGFP-FLYWCH1-WT protein in HEK293T cells. The protein lysates extracted from the transiently infected cells as well as stable cell lines were run on 8% SDS-PAGE gel and immunoblotted with anti-GFP antibody. The low percentage gel was used to separate the band of eGFP-FLYWCH1 from the closely detected possible unspecific bands.

The analysis showed that a band of eGFP-FLYWCH1-WT protein with correct molecular weight (~106 kDa) was detected in the lysate of transiently infected HEK293T cells (Figure 6-4B, red-dashed box, lane 3), whereas a smaller band of eGFP-FLYWCH1 (< 100 kDa) was detected again in the lysate of HEK293T-FLYWCH1<sup>+ve</sup> stable cell line (Figure 6-4B, red box, lane 2) but not in the lysate of the control (HEK293T-eGFP<sup>+ve</sup>) cell line (Figure 6-4B, lane 1). Collectively these findings suggest that the stably expressed eGFP-FLYWCH1 protein might be spontaneously modified in these stable cell lines.

band.

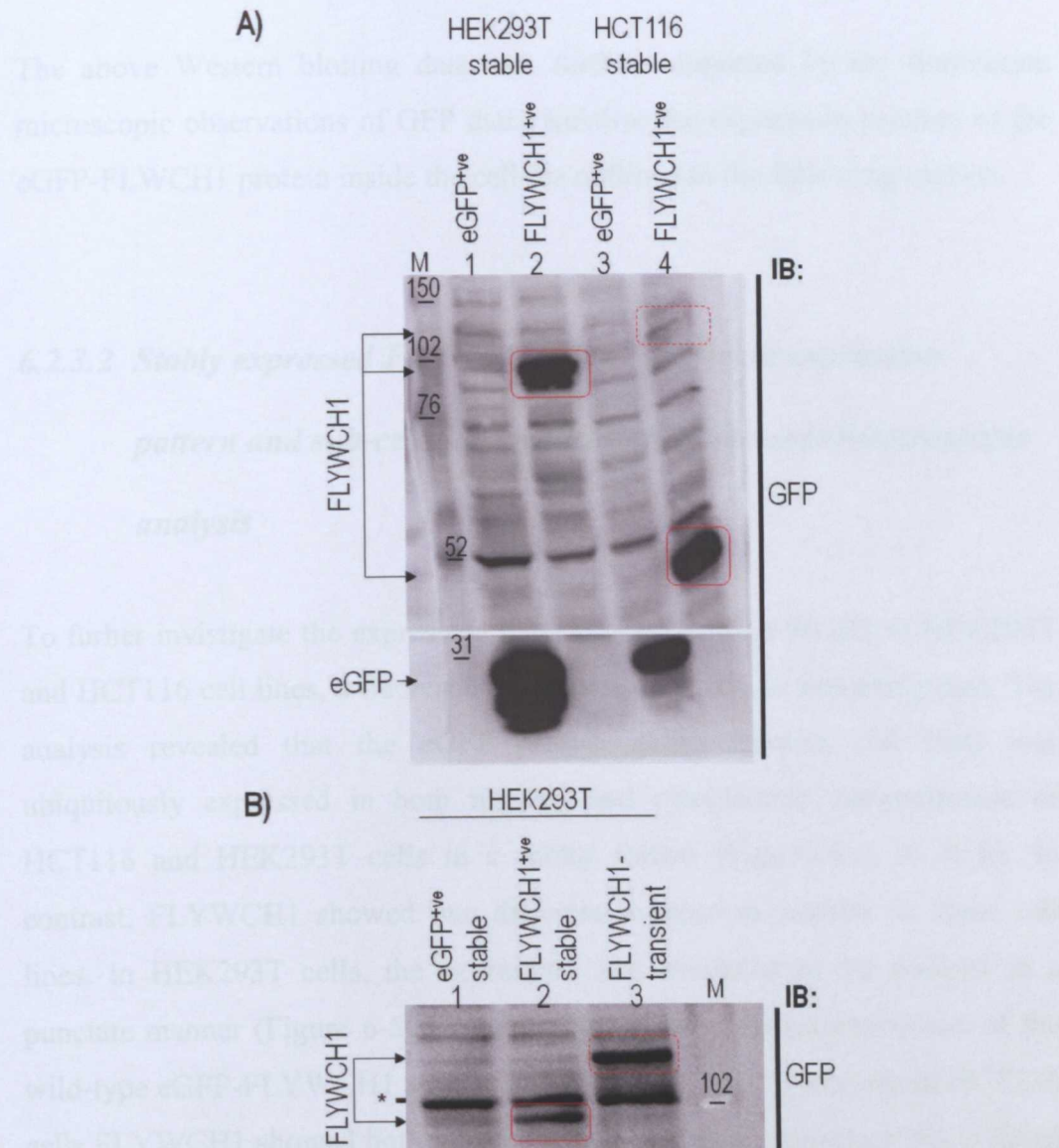


**Figure 6-4: FLYWCH1-WT aberrantly expressed in both HEK293T and HCT116 stable cell lines.** Protein lysates extracted from **A)** HEK293T and HCT116 cell lines

stably expressing eGFP or eGFP-FLYWCH1-WT, and **B**) HEK293T cells stably and transiently expressing these genes were immunoblotted (IB) with anti-GFP antibody. Panel **(A)** shows the expression of eGFP (bottom panel, lanes 1 & 3) and eGFP-FLYWCH1 (top panel, red boxes in lanes 2 and 4) in both cell lines as indicated. Panel **(B)** shows the stable vs. transient expression of the eGFP-FLYWCH1 (red box in lane 2 vs. red-dashed box in lane 3). Two bands of FLYWCH1 with different molecular weights were detected in lane 4 of panel A, for explanation about this see the text. "M", denotes the full range Rain Bow marker from GE Healthcare. Asterisks (\*) indicate unspecific bands.

The above Western blotting data was further supported by the fluorescent microscopic observations of GFP that visualise the expression pattern of the eGFP-FLYWCH1 protein inside the cells as outlined in the following section.

### ***6.2.3.2 Stably expressed FLYWCH1 shows different expression***

#### ***pattern and sub-cellular localization: fluorescent-microscopic analysis***

To further investigate the expression pattern of eGFP-FLYWCH1 in HEK293T and HCT116 cell lines, a fluorescent microscopic analysis was performed. The analysis revealed that the eGFP protein alone (control cell line) was ubiquitously expressed in both nucleus and cytoplasmic compartments of HCT116 and HEK293T cells in a spotty format (Figure 6-5, A & E). In contrast, FLYWCH1 showed two different expression patterns in these cell lines. In HEK293T cells, the expression was restricted to the nucleus in a punctate manner (Figure 6-5G) resembling the transient expression of the wild-type eGFP-FLYWCH1 as addressed in (section 3.2.5), whereas in HCT116 cells FLYWCH1 showed both nucleus and cytoplasmic expression but it failed to form foci (spots) into the nucleus (Figure 6-5C). This pattern of expression is somehow similar to the expression of the mutant clone M4 (Figure 4-8) in

which the C-terminal region of FLYWCH1 was deleted (Figure 4-2). Consistent with the WB data, these observations also suggest that the eGFP-FLYWCH1 is abnormally expressed in HCT116 cells.

Collectively, the WB and fluorescent microscope data indicate that FLYWCH1 aberrantly expressed in both HEK293T and HCT116 stable cell lines. This might be resulted from different modifications, for example *a)* alterations of the genome-integrated *FLYWCH1* cDNA such as point mutations or deletion of large nucleotide sequences, *b)* post-transcriptional or post-translational modifications including ubiquitination and/or degradation of the protein product. Therefore, further analysis of the genomic-integrated sequences of *FLYWCH1* cDNA in these cell lines was initially focused.

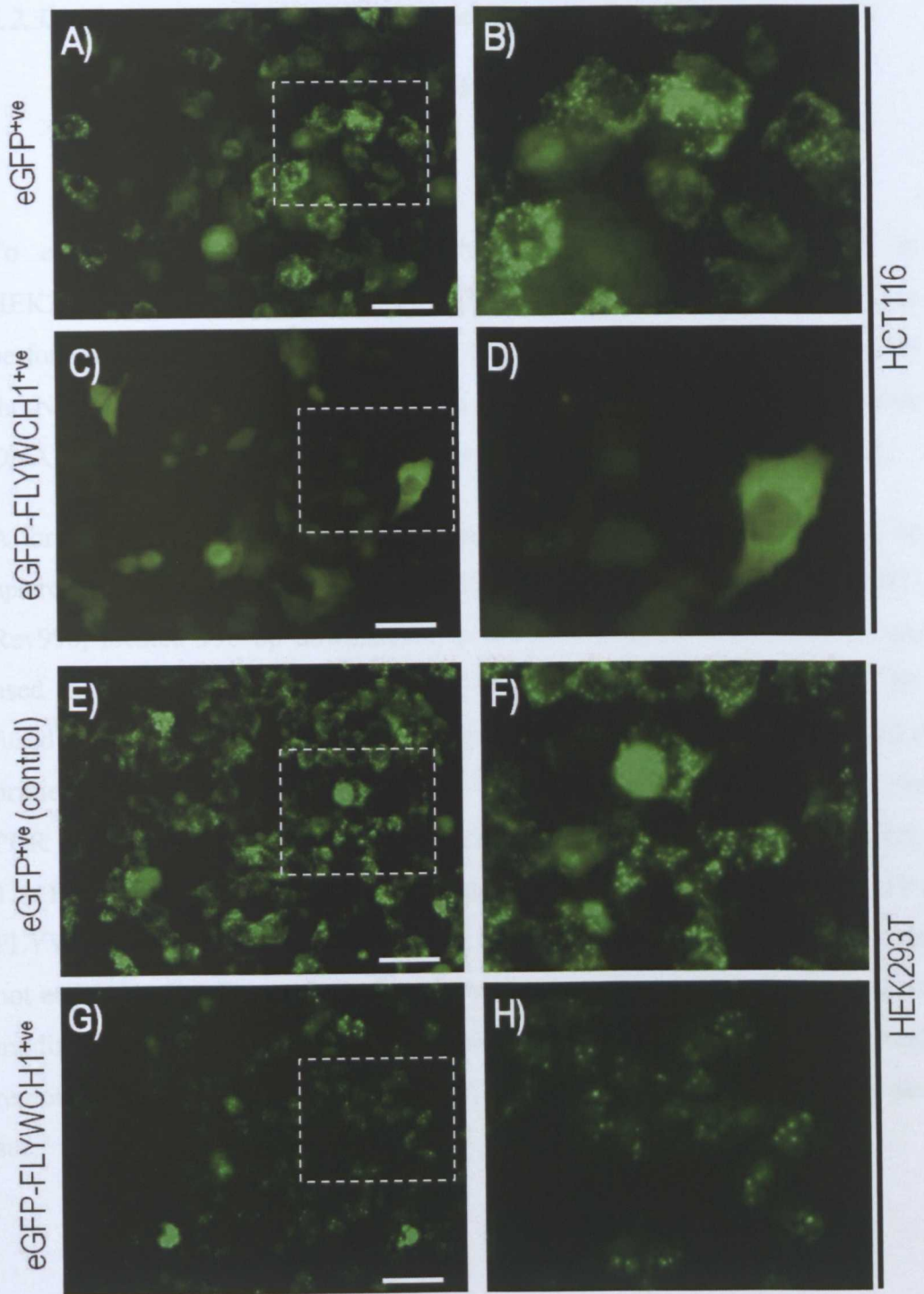


**Figure 6-5: Different localization patterns of stably expressed FLYWCH1.** The protein expression of stably expressed eGFP (A & E) and eGFP-FLYWCH1 (C & G) in both HCT116 and HEK293T stable cell lines are shown as indicated. B, D, F, and H are magnified views of the indicated white boxed area. Data are representative of several attempts to detect eGFP and eGFP-FLYWCH1 in the stable cell lines using fluorescent-microscopic analysis. Scale bars, 50  $\mu$ m.

**6.2.3.3 DNA sequence analysis of genomic PCR products illustrates  
deletional mutation in FLYWCH1 exogenous gene in**

**HEK293T stable cell line**

To explore possible alterations of the genome-integrated *FLYWCH1* in HEK293T stable cell line, a genomic-PCR and DNA sequencing analysis were performed. The standard PCR protocol (section 2.2.2.5) was used to amplify the N-terminal region of the exogenous *FLYWCH1* cDNA from the genomic DNA extract of HEK293T stable cell line using specific primers (Table 2-6).

A forward primer inside the eGFP coding sequence (GFP-Fwd; located 83 bp upstream to the start codon of *FLYWCH1*) and a reverse primer (FLYWCH1-Rev990, located 990 bp downstream to the start codon of *FLYWCH1*) were used to amplify a 1.1 Kb fragment of the N-terminal region of *FLYWCH1* fused to the 3'-end of the eGFP-epitope tag (Figure 6-6A). Using a forward primer inside the eGFP-epitope tag (i.e. GFP-Fwd) provides specificity to the PCR reaction in term of preventing endogenous amplification of *FLYWCH1*. The PCR reaction could specifically amplify the N-terminal region of eGFP-FLYWCH1 (~1.1 Kb) from the genomic DNA derived from FLYWCH1<sup>+ve</sup> but not eGFP<sup>+ve</sup> cells (Figure 6-6B, lane 2 vs. lanes 1). These data suggest that no modifications [such as deletion (s)] happened to the first 1Kb of the N-terminal region of the genome-integrated *FLYWCH1* in HEK293T stable cell lines per see.

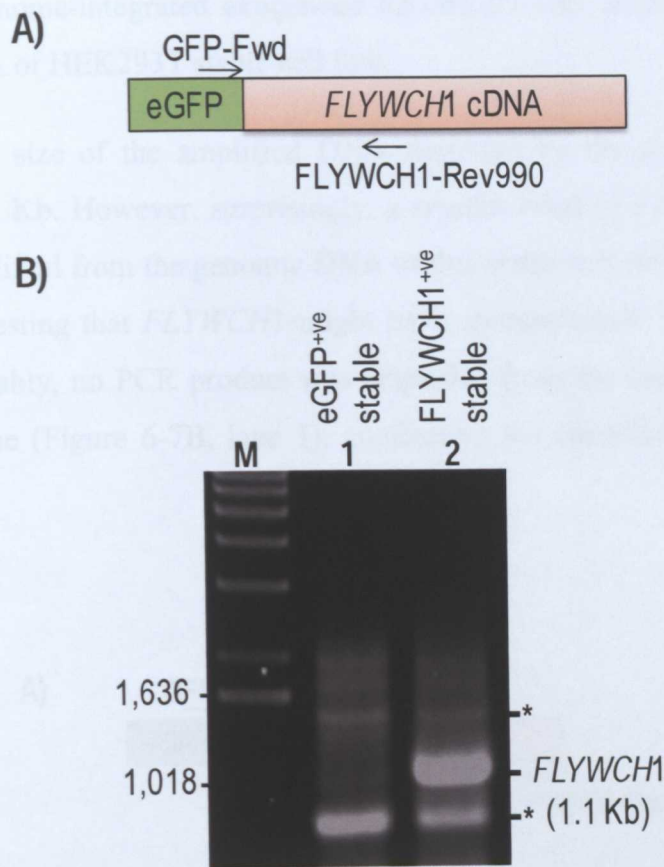


**Figure 6-6: PCR amplification of the N-terminal region of the genomic-integrated exogenous *FLYWCH1*.** A) A diagram shows the approximate positions of the forward (GFP-Fwd) and reverse (FLYWCH1-Rev990) primers used for the PCR reaction. B) Agarose gel shows the amplified N-terminal fragment of *FLYWCH1* (1.1 Kb, lane 2) from the genomic DNA extracted from stably expressing eGFP-*FLYWCH1* (*FLYWCH1*<sup>+</sup>ve) HEK293T stable cell line. The eGFP expressing stable cell line (eGFP<sup>+</sup>ve, lane 1) was used as a negative control. Asterisks (\*) indicate unspecific bands.

The above findings could not explain the aberrant expression pattern of eGFP-*FLYWCH1* protein (see section 6.2.3.1) observed in the lysate of HEK293T stable cell line. Therefore, presence of the full-length coding sequence of exogenous *FLYWCH1* in the genomic DNA of the stable cell line was investigated by standard PCR. Specific primers (Table 2-6), including the same forward primer described above (GFP-Fwd) and a reverse primer (Full-*FLYWCH1*-Rev) marking the 3'-end of *FLYWCH1* cDNA (Figure 6-7A), the

full-length genome-integrated exogenous *FLYWCH1* was amplified from the genomic DNA of HEK293T stable cell line.

The expected size of the amplified DNA fragment by the above described primers is 2.2 Kb. However, surprisingly, a smaller band of *FLYWCH1* (~1.6 Kb) was amplified from the genomic DNA of this stable cell line (Figure 6-7B, lane 2), suggesting that *FLYWCH1* might have spontaneously mutated in this cell line. Notably, no PCR product was amplified from the control (eGFP<sup>+ve</sup>) stable cell line (Figure 6-7B, lane 1), confirming the specificity of the PCR reaction.

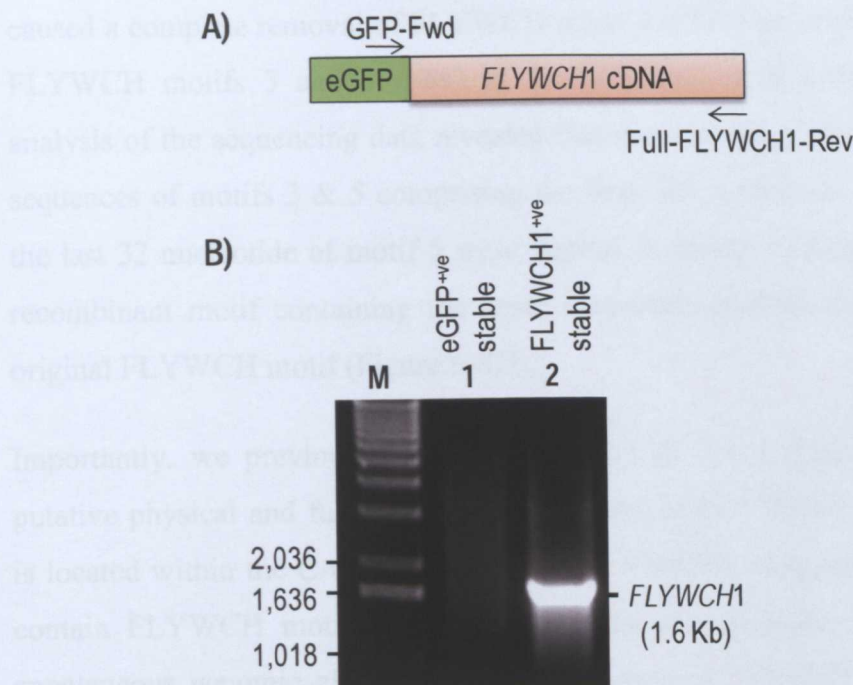


**Figure 6-7: PCR amplification of the full-length genome-integrated *FLYWCH1*.** A) Diagram shows the approximate positions of the forward (GFP-Fwd) and reverse (Full-FLYWCH1-Rev) primers used for the PCR reaction. B) Agarose gel shows amplified DNA fragments of the genome-integrated exogenous eGFP-FLYWCH1 (lane 2) from the genomic DNA extract of HEK293T-FLYWCH1<sup>+ve</sup> but not eGFP<sup>+ve</sup> stable cell line as indicated.

To further evaluate the above observation, the PCR product derived from the genomic DNA of HEK293T-FLYWCH1<sup>+ve</sup> stable cell line was gel extracted and subjected to automated DNA sequencing. The sequencing result was then aligned to the previously approved nucleotide sequence of *FLYWCH1* IMAGE clone [provided by the NCBI gene bank (GeneBank ID: BC028572.1)] using ClustalW2 Alignment database. As shown in (Figure 6-8), the alignment data revealed that the sequence of the PCR amplified DNA contains a relatively large internal deletion (537 bp) mapped to nucleotides 1405-1942 within the C-terminal region of *FLYWCH1* (Figure 6-8C). Surprisingly, the mutated fragment of the exogenous *FLYWCH1* (downstream to the deleted area) was re-ligated with the rest of *FLYWCH1* coding sequence without making any frameshift mutations (Figure 6-8, A & B). Interestingly, the deleted region caused a complete removal of FLYWCH motif 4 (FM4) and partial removal of FLYWCH motifs 3 and 5 (FM3 & FM5) (Figure 6-8C). Moreover, deep analysis of the sequencing data revealed that the remaining (undeleted) partial sequences of motifs 3 & 5 comprising the first 145 nucleotide of motif 3 and the last 32 nucleotide of motif 5 were ligated, in-frame, to restore a complete recombinant motif containing the same nucleotide number (177 bp) as an original FLYWCH motif (Figure 6-8D).

Importantly, we previously (in sections 4.2.3 & 5.2.3) discovered that the putative physical and functional interaction site of FLYWCH1 with  $\beta$ -catenin is located within the C-terminal region of FLYWCH1 especially the area that contain FLYWCH motifs 3 & 4. Thus, one can speculate that the above spontaneous genomic alteration of the exogenous FLYWCH1 in HEK293T-FLYWCH1<sup>+ve</sup> stable cell line may affect the interaction and repression activity of FLYWCH1 against  $\beta$ -catenin signalling.

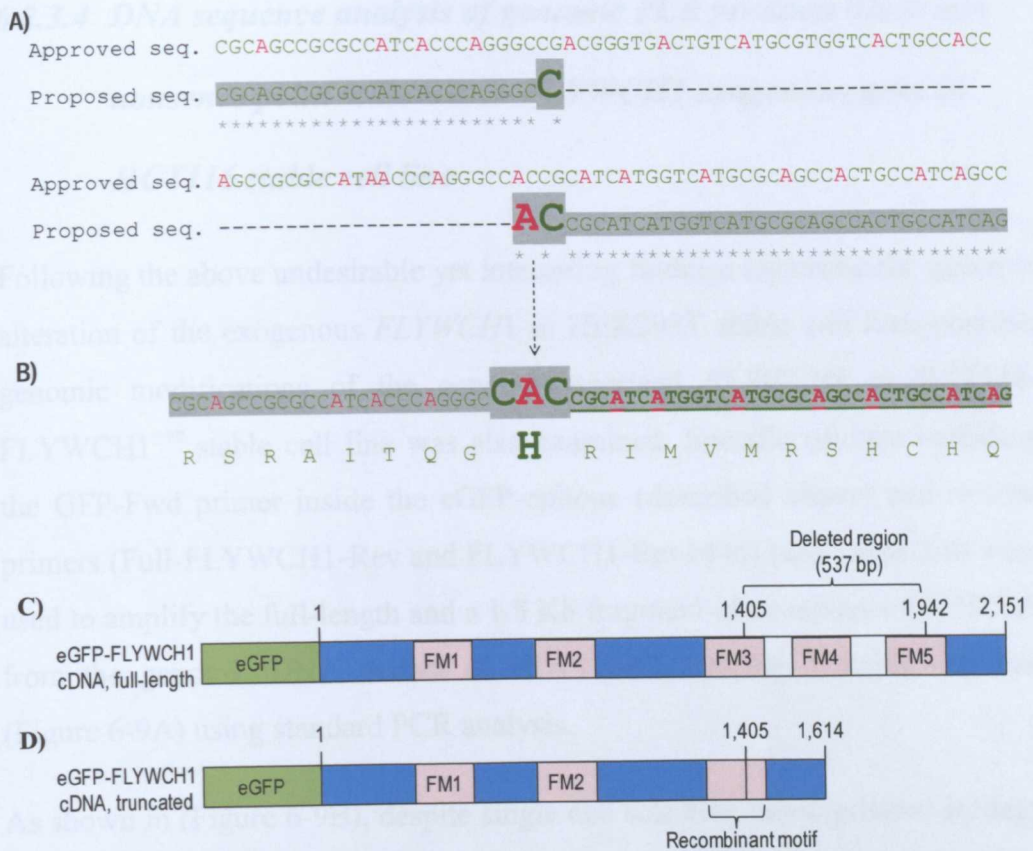


**Figure 6-8: The C-terminus region of the genome-integrated *FLYWCH1* in HEK293T stable cell line contains an internal in-frame deletion mutation.** The proposed full-length genome-integrated *FLYWCH1* (Proposed seq.) was amplified by PCR. **A)** Shows nucleotide sequence alignment of the PCR product to the nucleotide sequence of approved *FLYWCH1* (Approved seq.) using ClustalW2 Alignment tool. Asterisks (\*) indicate identical nucleotides, while dashes (-) indicate missing (deleted) nucleotides. Nucleotides upstream and downstream to the deleted region of the PCR amplified *FLYWCH1* (Proposed seq.) are highlighted in grey and nucleotides marking the 3' and 5'-ends of the deleted region are enlarged in font size. **B)** Shows the in-frame recombined nucleotide and amino acid sequence of *FLYWCH1*. Schematics show **C)** the position of the deleted fragment (537 bp) within the C-terminal region of *FLYWCH1* cDNA highlighting the affected *FLYWCH* motifs and **D)** the truncated *FLYWCH1* cDNA highlighting a new recombinant nucleotide sequence of *FLYWCH* motif. Letters "FM", denote *FLYWCH* motif.

**6.2.3.4 DNA sequence analysis of genomic PCR products illustrates  
nonsense point mutation in FLYWCH1 exogenous gene in  
HCT116 stable cell line**

Following the above undesirable yet interesting findings regarding the genomic alteration of the exogenous *FLYWCH1* in HEK293T stable cell line, possible genomic modifications of the genome-integrated *FLYWCH1* in HCT116-*FLYWCH1*<sup>+ve</sup> stable cell line was also examined. Specific primers including the GFP-Fwd primer inside the eGFP-epitope (described above) and reverse primers (Full-*FLYWCH1*-Rev and *FLYWCH1*-Rev1446) (see Table 2-6) were used to amplify the full-length and a 1.5 Kb fragment of exogenous *FLYWCH1* from the genomic DNA extract of HCT116-*FLYWCH1*<sup>+ve</sup> stable cell line (Figure 6-9A) using standard PCR analysis.

As shown in (Figure 6-9B), despite single cell selection/cloning-based strategy as outlined above, we failed to amplify a clear band of the full-length genome-integrated *FLYWCH1* using GFP-Fwd & Full-*FLYWCH1*-Rev primers. Instead, a smeary PCR product containing multiple bands (from ~2.2 Kb and smaller) of *FLYWCH1* was amplified from the genomic DNA of HCT116-*FLYWCH1*<sup>+ve</sup> stable cell line (Figure 6-9B, lane 2). Notably, none of these bands were amplified from the control (eGFP<sup>+ve</sup>) stable cell lines (Figure 6-9B, lane 1), confirming the specificity of the PCR reaction. Thus, based on this observation, presence of heterogeneous population of cells harbouring the wild-type and different modified/mutated sequences of eGFP-*FLYWCH1* in HCT116 stable cell line was assumed.

In this notion, the PCR was repeated using the GFP-Fwd & *FLYWCH1*-Rev1446 primers to amplify a shorter sequence of the exogenous *FLYWCH1*. The results show that a band of *FLYWCH1* with expected molecular size (~1.5 Kb) was amplified from the genomic DNA of HCT116-*FLYWCH1*<sup>+ve</sup> cell line (Figure 6-9C, lane 2) but not from the control (eGFP<sup>+ve</sup>) cell line (Figure 6-9C, lane 1). This observation suggests that the amplified fragment of the genome-integrated *FLYWCH1* may not contain large deletion mutations (as observed for HEK293T stable cell line) per se. Thus, involvement of other possible

modifications such as point mutations of the exogenous *FLYWCH1* sequence or degradation of the protein product of *FLYWCH1* was concerned.

Figure 6-9: PCR amplification of the genome-integrated *FLYWCH1* from HCT116 stable cell line. A) Diagram shows the approximate positions of the forward (GFP-Fwd) and reverse primers (FLYWCH1-Rev1446 and Full-FLYWCH1-Rev) used for the PCR reaction. B & C) Agarose gels show the amplified DNA fragments of *FLYWCH1* (lane 2 in B & C) from the genomic DNA extract of HCT116-*FLYWCH1*<sup>+ve</sup> but not eGFP<sup>+ve</sup> stable cell line as indicated. For multiple bands of *FLYWCH1* in (B) see the text above.

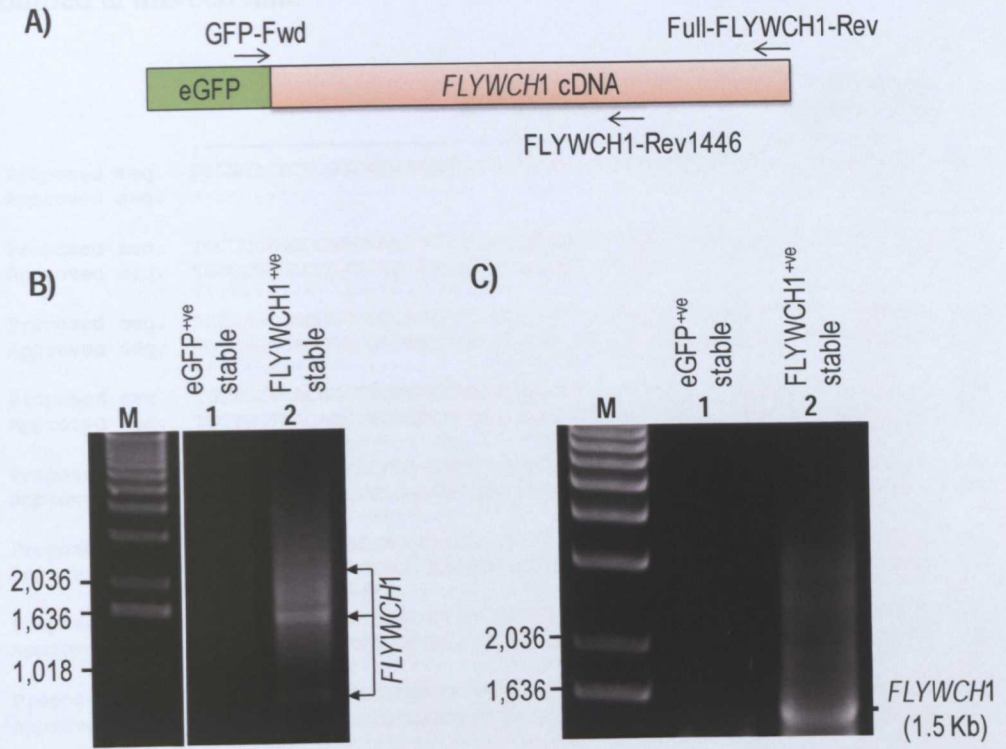


Figure 6-9: PCR amplification of the genome-integrated *FLYWCH1* from HCT116 stable cell line. A) Diagram shows the approximate positions of the forward (GFP-Fwd) and reverse primers (FLYWCH1-Rev1446 and Full-FLYWCH1-Rev) used for the PCR reaction. B & C) Agarose gels show the amplified DNA fragments of *FLYWCH1* (lane 2 in B & C) from the genomic DNA extract of HCT116-*FLYWCH1*<sup>+ve</sup> but not eGFP<sup>+ve</sup> stable cell line as indicated. For multiple bands of *FLYWCH1* in (B) see the text above.

Figure 6-10: The N-terminal region of the genome-integrated *FLYWCH1* sequence.

In order to confirm the nucleotide sequence identity and integrity and also to investigate the presence of possible point mutations within the genome-integrated sequence of *FLYWCH1*, the above amplified DNA fragment (Figure 6-9C) was gel extracted and analyzed by automated DNA sequencing. In the first attempt, the N-terminal region of *FLYWCH1* (~770 bp) was sequenced. The sequencing data revealed that the nucleotide sequence of the proposed

genomic-PCR product of *FLYWCH1* completely (100%) matches the nucleotide sequence of the approved sequence of *FLYWCH1* cDNA (Figure 6-10). These results indicated that the N-terminal region of the exogenous *FLYWCH1* (~770 bp, covered by the sequencing primers used) has not been modified in this cell line.

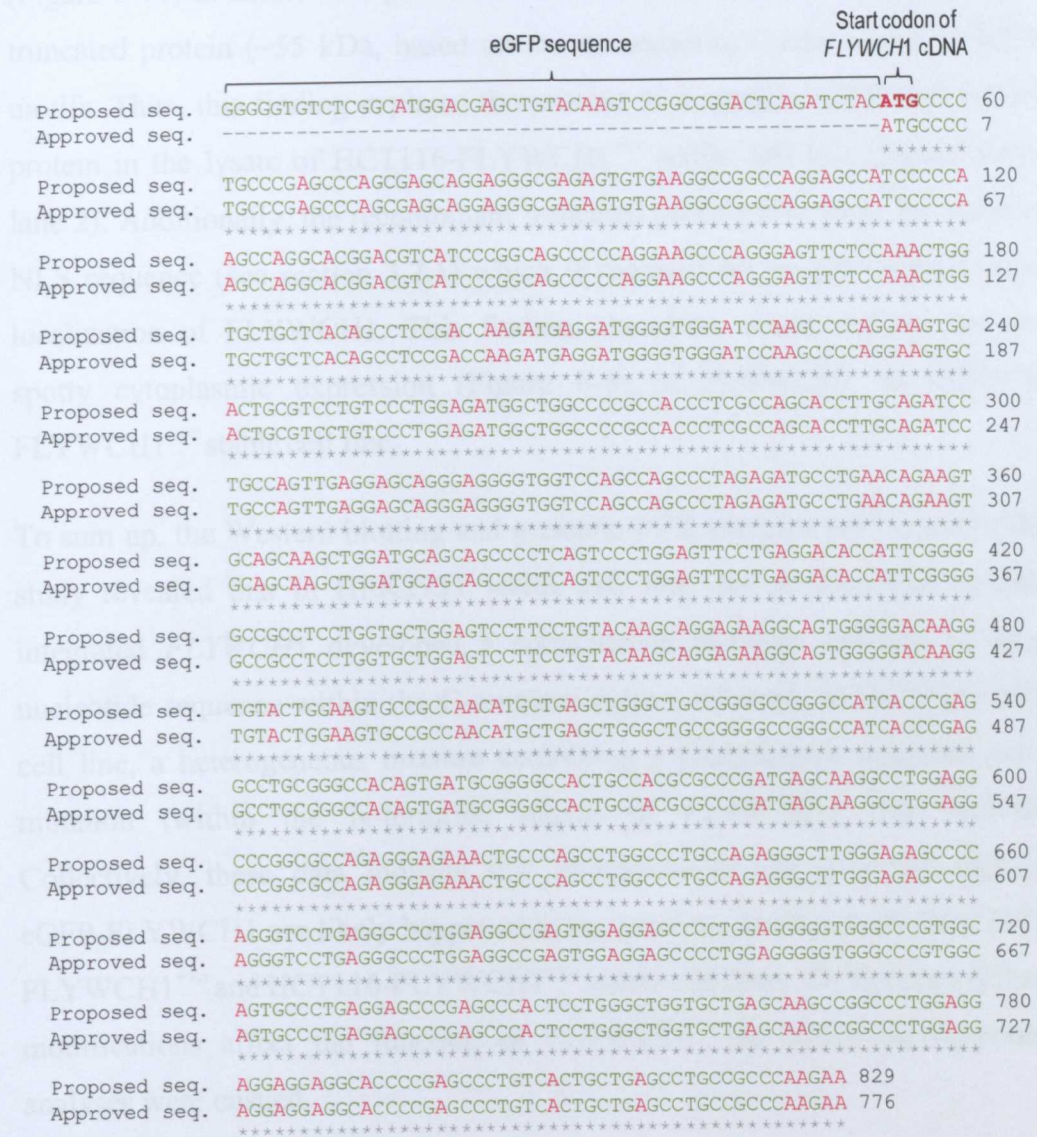
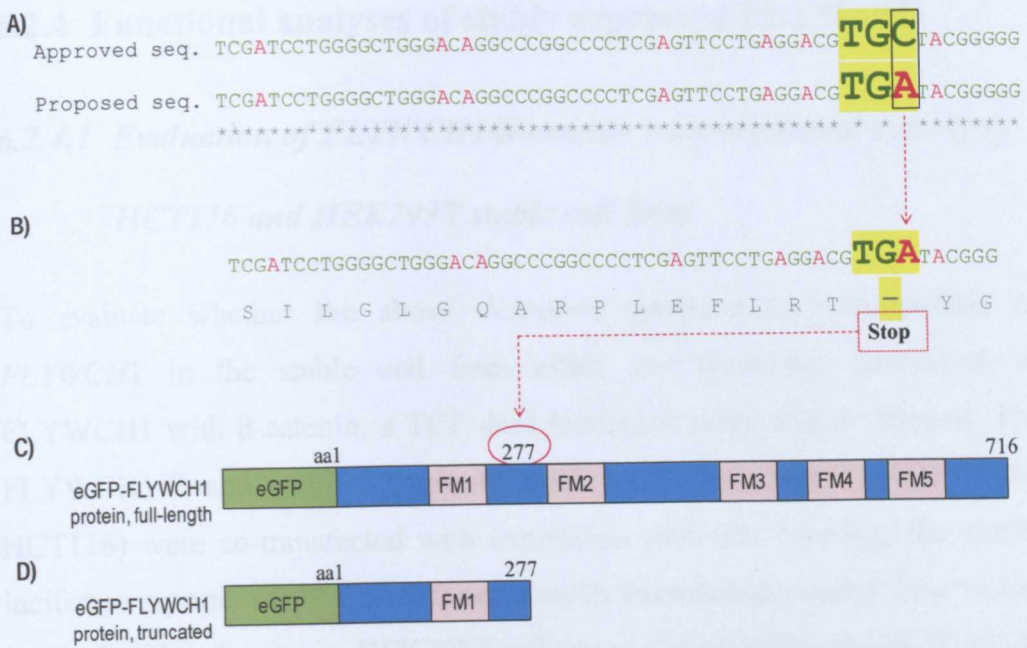


Figure 6-10: The N-terminal region of the genome-integrated exogenous *FLYWCH1* has not been modified in HCT116 cell line. The N-terminal region (~770 bp) of the proposed genome-integrated *FLYWCH1* (Proposed seq.) was amplified by PCR and aligned to the approved gene bank sequence of *FLYWCH1* cDNA (Approved seq.) using ClustalW2 Alignment tool. Asterisks (\*) indicate identical nucleotides. A short sequence of the 3'-end of the eGFP-epitope and the start codon of *FLYWCH1* cDNA are labelled as indicated.

In the second attempt of sequencing, a longer fragment of the PCR amplified exogenous *FLYWCH1* was sequenced and aligned to the gene bank sequence of this gene. Interestingly, the alignment data showed that a single base replacement (C to A) at nucleotide position 831 within the N-terminal region of *FLYWCH1* was occurred. This point mutation caused a stop codon formation (Figure 6-11) at amino acid position 277, which in turn led to production of a truncated protein (~55 kDa, based on the aa sequence) lacks four *FLYWCH* motifs. Thus, this finding explains the present of a smaller eGFP-*FLYWCH1* protein in the lysate of HCT116-*FLYWCH1*<sup>+ve</sup> stable cell line (Figure 6-4A, lane 2). Additionally, the recombinant truncated protein also lacks the putative NLS sequence (see section 3.2.1) which is required for proper spotty/nuclear localization of *FLYWCH1*. This finding, therefore, could explain the non spotty cytoplasmic expression (Figure 6-5) of *FLYWCH1* in HCT116-*FLYWCH1*<sup>+ve</sup> stable cell line.

To sum up, the Western blotting and genomic PCR analyses performed in this study revealed that in HEK293T stable cell line, the predominant genome integrated *FLYWCH1* developed a spontaneous in-frame deletion of large nucleotide sequence within the C-terminal region, whereas, in HCT116 stable cell line, a heterogeneous mixture containing a predominant nonsense point mutation (within the N-terminal region of *FLYWCH1*) was detected. Collectively, these data indicate that alterations of the genome-integrated eGFP-*FLYWCH1* are likely happened at the genomic level in both HEK293T-*FLYWCH1*<sup>+ve</sup> and HCT116-*FLYWCH1*<sup>+ve</sup> stable cell lines. To examine if these modifications affect the function of *FLYWCH1*, the following functional analyses were ensued.



**Figure 6-11: A nonsense point mutation resulted in a stop-codon formation within the N-terminal region of the genome-integrated *FLYWCH1* in HCT116 stable cell line. A) Shows alignment of the PCR amplified sequence of genome-integrated *FLYWCH1* (Proposed seq.) to the gene bank sequence of *FLYWCH1* (Approved seq.). A nonsense point mutation caused by a single nucleotide replacement (C to A) is shown as indicated. B) Shows the resulted stop-codon (TGA) highlighted in yellow. C) Shows the approximate position of the resulted stop-codon within the full-length *FLYWCH1* amino acid sequences. D) Shows the resulted truncated protein that lacks the *FLYWCH* motifs 2, 3, 4, and 5.**

## 6.2.4 Functional analyses of stably expressed FLYWCH1

### 6.2.4.1 Evaluation of FLYWCH1/ $\beta$ -catenin transcriptional activity in

#### *HCT116 and HEK293T stable cell lines*

To evaluate whether the above described spontaneous modifications of *FLYWCH1* in the stable cell lines affect the functional interaction of *FLYWCH1* with  $\beta$ -catenin, a TCF dual luciferase assay was performed. The *FLYWCH1*<sup>+ve</sup> and eGFP<sup>+ve</sup> (control) stable cell lines (both HEK293T and HCT116) were co-transfected with expression plasmids encoding the firefly luciferase reporter (TOP-FLASH) and *Renilla* transfection control. Due to low level of nuclear  $\beta$ -catenin, HEK293T cells were also transfected with FLAG- $\beta$ -catenin<sup>S33A</sup>.

The analysis revealed that the luciferase activity of the firefly reporter in HEK293T-*FLYWCH1*<sup>+ve</sup> stable cell line not reduced by the stable expression of *FLYWCH1* in comparison to the control cell line (Figure 6-12A, lane 2 vs. lane 1), even though it slightly but not significantly induced. In contrast, the firefly luciferase activity in HCT116 cells stably expressing *FLYWCH1* is significantly reduced (Figure 6-12B, lane 2 vs. lane 1). These observations indicate that the spontaneously mutated genome-integrated *FLYWCH1* in HEK293T cell line lost its suppression activity against  $\beta$ -catenin/TCF4, suggesting that the functional interaction of *FLYWCH1* with  $\beta$ -catenin is likely disrupted. This result is in line with our previous finding that deletion mutant M4, in which the C-terminal region of *FLYWCH1* is deleted, significantly lost its suppression activity against  $\beta$ -catenin (see section 5.2.3). Conversely, despite the genomic alterations of *FLYWCH1* in HCT116-*FLYWCH1*<sup>+ve</sup> stable cell line, the endogenous transcriptional activity of  $\beta$ -catenin is still suppressed (Figure 6-12B). This observation further supports our previous view that this cell line may contain a heterogeneous population of cells harbouring the full-length and different modified forms of integrated *FLYWCH1* (see section 6.2.3.4). Subsequently, presence of functional full-length *FLYWCH1*, even in small quantities (small population of cells), could significantly repress the  $\beta$ -catenin transcriptional activity.

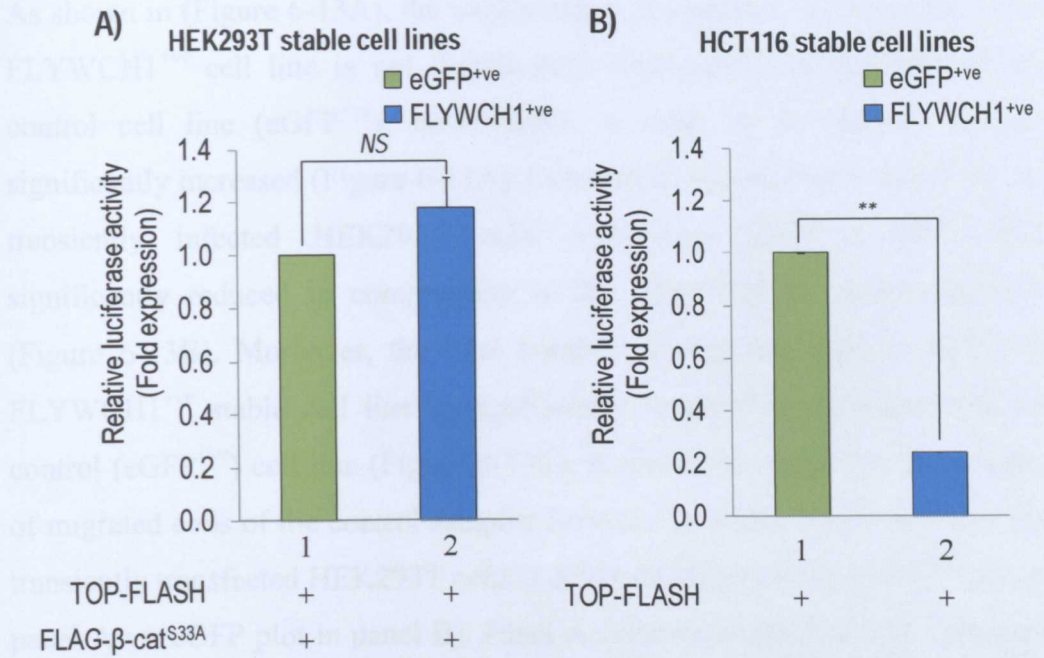


**Figure 6-12: FLYWCH1/β-catenin transcriptional activity in HCT116 and HEK293T stable cell lines.** Cells stably expressing eGFP (eGFP<sup>+ve</sup>, green boxes) and eGFP-FLYWCH1 (FLYWCH1<sup>+ve</sup>, blue boxes) were transiently transfected to express FLAG-β-cat<sup>S33A</sup> and TOP-FLASH reporter in HEK293T (A) and TOP-FLASH alone in HCT116 (B) stable cell lines in addition to the *Renilla* transfection control (added to all samples). Activity of the firefly luciferase reporter (TOP-FLASH) relative to *Renilla* luciferase is shown as indicated. Data are mean ± SD ( $n = 3$ ; \*\*,  $P < 0.01$ ; NS, non-significant). Experiment run in triplicate and repeated on three independent occasions.

#### 6.2.4.2 Evaluation of *FLYWCH1* repression activity on cell migration in HEK293T and HCT116 stable cell lines

Cell migration was significantly reduced by FLYWCH1 transient expression in cancer cells including HCT116 (see Figure 5-10). To examine whether the stable expression of this gene affects cell motility, a migration assay was performed. In addition to HEK293T and HCT116 stable cell lines, a transiently infected HEK293T cells with Lentiviral particles expressing full-length EGFP-FLYWCH1 were also used. The migration ability of the transiently and stably FLYWCH1-expressing cells was evaluated using a trans-well migration assay as outlined in (section 2.2.6.3).

As shown in (Figure 6-13A), the total number of migrated cells in HEK293T-FLYWCH1<sup>+ve</sup> cell line is not significantly decreased in comparison to the control cell line (eGFP<sup>+ve</sup>), nevertheless, it tends to be slightly but not significantly increased (Figure 6-13A). Conversely, the migration ability of the transiently infected HEK293T cells expressing EGFP-FLYWCH1-WT significantly reduced in comparison to the control eGFP expressing cells (Figure 6-13B). Moreover, the total number of migrated cells in HCT116-FLYWCH1<sup>+ve</sup> stable cell line is significantly reduced in comparison to the control (eGFP<sup>+ve</sup>) cell line (Figure 6-13C). It should be noted that the number of migrated cells of the control samples between the stably transfected and the transiently transfected HEK293T cells is different (Figure 6-13, eGFP<sup>+ve</sup> plot in panel A vs. eGFP plot in panel B). Panel A cells were infected with Lentiviral particles containing (LVX-eGFP), while panel B cells were transiently transfected with pEGFP-C2 plasmid vector. Therefore, vehicles for transgene expression (i.e. eGFP) are different between panels A & B. This difference may, subsequently, affect the biological behaviours of HEK293 cells.

Consistent with the results of the luciferase assay (Figure 6-12), these data further support the notion that the stably expressed exogenous *FLYWCH1* in HEK293T-FLYWCH1<sup>+ve</sup> stable cell line, lost its suppression role on cell migration, whereas in HCT116-FLYWCH1<sup>+ve</sup> cell line the suppression effect is still exist.

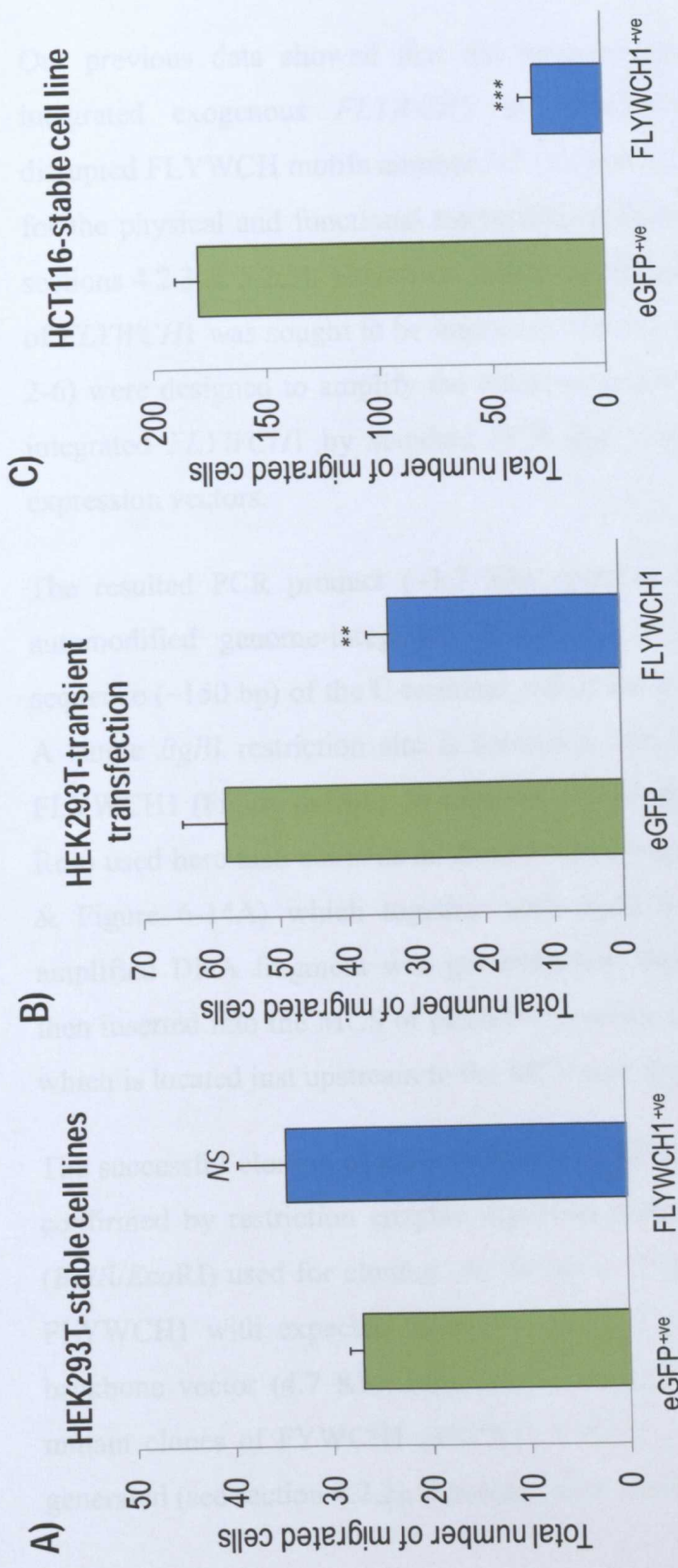


**Figure 6-13: FLYWCH1 repression activity on cell migration in HEK293T and HCT116 stable cell lines. A and B) Show the effect of stable vs. transient expression of FLYWCH1 on migration ability of HEK293T cells. Note that FLYWCH1 is spontaneously mutated in this stable cell line. C) Show the effect of stable expression of FLYWCH1 on migration of HCT116 cells. Cells expressing eGFP (green boxes) were used as control. Data are mean  $\pm$  SD ( $n = 3$ ; \*\*,  $P < 0.01$ ; \*\*\*,  $P < 0.001$ ). Experiment run in triplicate and repeated on two independent occasions.**

## 6.2.5 Cloning the automodified *FLYWCH1* recombinant cDNA into mammalian expression vectors

Our previous data showed that the spontaneous deletion of the genome-integrated exogenous *FLYWCH1* in HEK293T-*FLYWCH1*<sup>+ve</sup> cell line disrupted FLYWCH motifs number 3-5 (section 6.2.3.3) which are responsible for the physical and functional interaction of FLYWCH1 with  $\beta$ -catenin (see sections 4.2.3 & 5.2.3). Therefore, further evaluations for this mutant sequence of *FLYWCH1* was sought to be important. To this end, specific primers (Table 2-6) were designed to amplify the entire sequence of the exogenous genome-integrated *FLYWCH1* by standard PCR and clone it back into mammalian expression vectors.

The resulted PCR product (~1.7 Kb) contains the entire sequence of the automodified genome-integrated *FLYWCH1* (~1.6 Kb) fused to a short sequence (~150 bp) of the C-terminal end of the eGFP-epitope (Figure 6-14B). A single *Bgl*II restriction site is located at the junction between eGFP and FLYWCH1 (Figure 6-14A). In addition, the reverse primer (Full-FLYWCH1-Rev) used here also contains an *Eco*RI restriction site at the 3'-end (Table 2-6 & Figure 6-14A) which together with *Bgl*II were used for cloning. The amplified DNA fragment was gel extracted, digested with *Bgl*II/*Eco*RI and then inserted into the MCS of pEGFP-C2 vector in-frame to the eGFP-epitope which is located just upstream to the MCS (see *Appendix 6*).

The successful cloning of the amplified *FLYWCH1* cDNA into the vector was confirmed by restriction enzyme digestion analysis using the same enzymes (*Bgl*II/*Eco*RI) used for cloning. As shown in (Figure 6-14C), a single band of FLYWCH1 with expected molecular size (~1.6 Kb) was released from the backbone vector (4.7 Kb), indicating a successful cloning. As four deletion mutant clones of FLYWCH1 (eGFP-FLYWCH1- M1 to M4) were previously generated (see section 4.2.2), this clone was named as eGFP-FLYWCH1-M5.

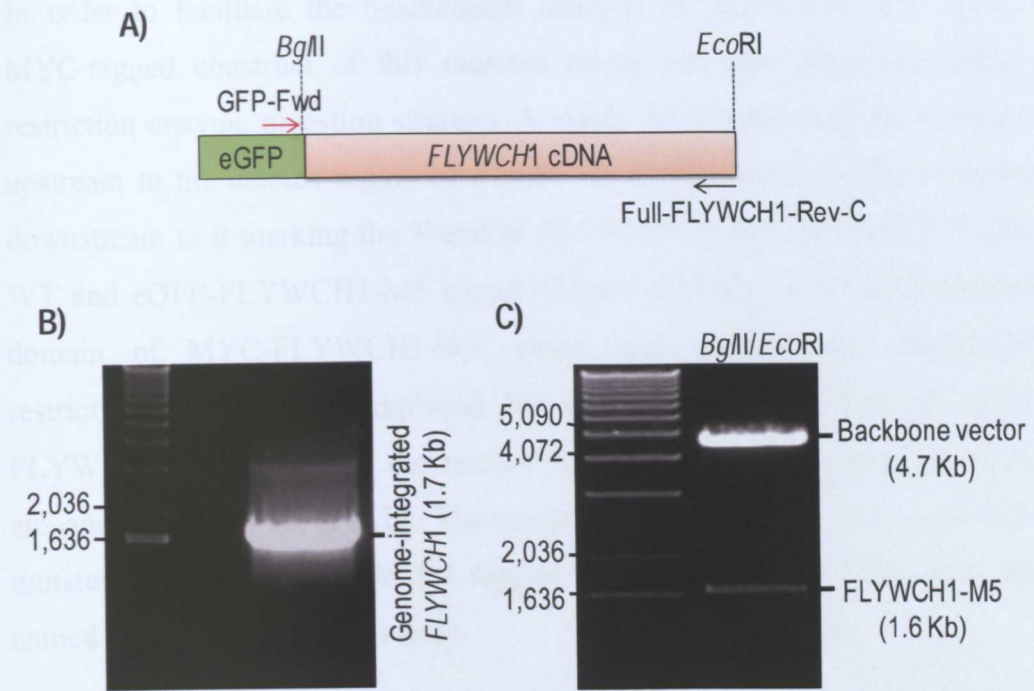


**Figure 6-14: PCR amplification and restriction enzyme digestion analysis of the automodified exogenous *FLYWCH1* cDNA.** A) Diagram shows the approximate positions of the primers used for amplification of the entire sequence of the genome-integrated *FLYWCH1* by PCR. The restriction sites used for cloning are labelled as indicated. B) Agarose gel shows the PCR amplified sequence of *FLYWCH1* from the genomic DNA extract of HEK293T-*FLYWCH1*<sup>+ve</sup> stable cell line. C) Agarose gel shows restriction enzyme digestion analysis of eGFP-*FLYWCH1*-M5 clone with *BglII/EcoRI*. A single band of *FLYWCH1*-M5 cDNA (1.6 Kb) was released from the backbone vector (4.7 Kb) as indicated.

In order to facilitate the biochemical analysis of FLYWCH1-M5 clone, a MYC-tagged construct of this mutated clone was also generated using a restriction enzyme digestion strategy. A single *Xho*I restriction site is located upstream to the deleted region of *FLYWCH1* cDNA, while *Eco*RI is located downstream to it marking the 3'-end of *FLYWCH1* in both MYC-FLYWCH1-WT and eGFP-FLYWCH1-M5 clones (Figure 6-15A). Thus, the C-terminal domain of MYC-FLYWCH1-WT clone was removed by *Xho*I/*Eco*RI restriction enzymes and replaced by the C-terminal domain of eGFP-FLYWCH1-M5 clone (i.e. the mutant fragment) using the same restriction enzymes (Figure 6-15, A & B). The resulted clone (Figure 6-15C) contains the mutated sequence of FLYWCH1 tagged with MYC-epitope. This clone was named as (MYC-FLYWCH1-M5).

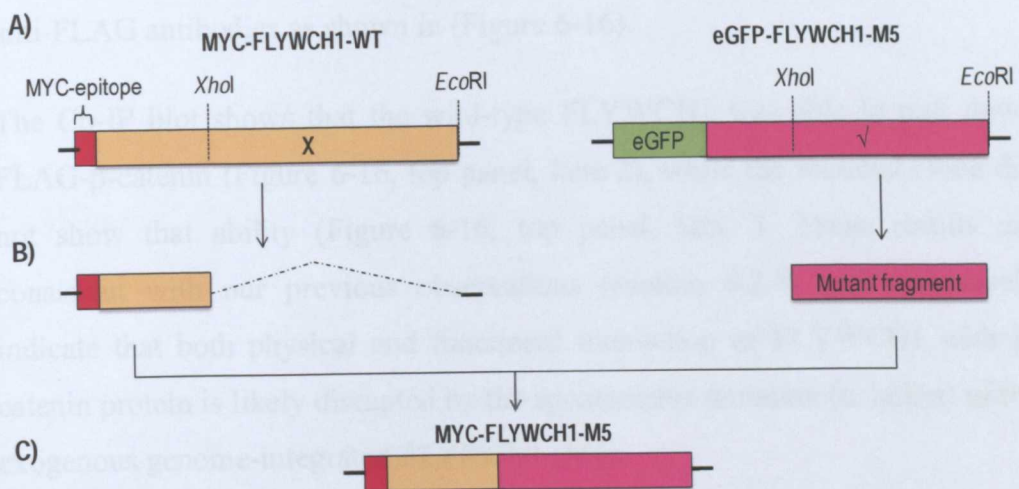


**Figure 6-15: Cloning strategy of MYC-FLYWCH1-M5 plasmid.** Schematic shows **A)** the approximate restriction sites of *Xho*I and *Eco*RI enzymes within the coding sequence of MYC-FLYWCH1-WT (left panel) and eGFP-FLYWCH1-M5 (right panel) clones, **B)** the desired DNA fragments resulted from the enzymatic digestion, and **C)** ligation of the desired DNA fragments to produce a MYC-tagged mutant clone of FLYWCH1 (MYC-FLYWCH1-M5).

## **6.2.6 The automodified clone of FLYWCH1 lost its physical interaction with $\beta$ -catenin**

As mentioned above, the internal mutation of MYC-FLYWCH1-M5 clone disrupted FLYWCH motifs 3-5 within the C-terminal region. It should be mentioned that this region contains the putative interaction site of FLYWCH1 with  $\beta$ -catenin (see sections 4.2.3). To examine whether or not this mutation affect the physical interaction of FLYWCH1 with  $\beta$ -catenin, a Co-IP assay was performed. HEK293T cells were co-transfected with expression plasmids encoding; FLAG- $\beta$ -catenin<sup>S33A</sup>, MYC-FLYWCH1-M5 and MYC-FLYWCH1-WT both separately and in combination. The protein lysate was co-immunoprecipitated with Protein A/G PLUS-Agarose beads which are manually conjugated to anti-MYC antibody (see section 2.2.5.3.3). Both Input and Co-IP samples were analyzed by Western blotting using anti-MYC and anti-FLAG antibodies as shown in (Figure 6-16).

The Co-IP blot shows that the wild-type FLYWCH1 was able to pull down FLAG- $\beta$ -catenin (Figure 6-16, top panel, lane 2), while the mutated clone did not show that ability (Figure 6-16, top panel, lane 3). These results are consistent with our previous observations (section 6.2.4) and collectively indicate that both physical and functional interaction of FLYWCH1 with  $\beta$ -catenin protein is likely disrupted by the spontaneous mutation (deletion) of the exogenous genome-integrated *FLYWCH1* (M5).

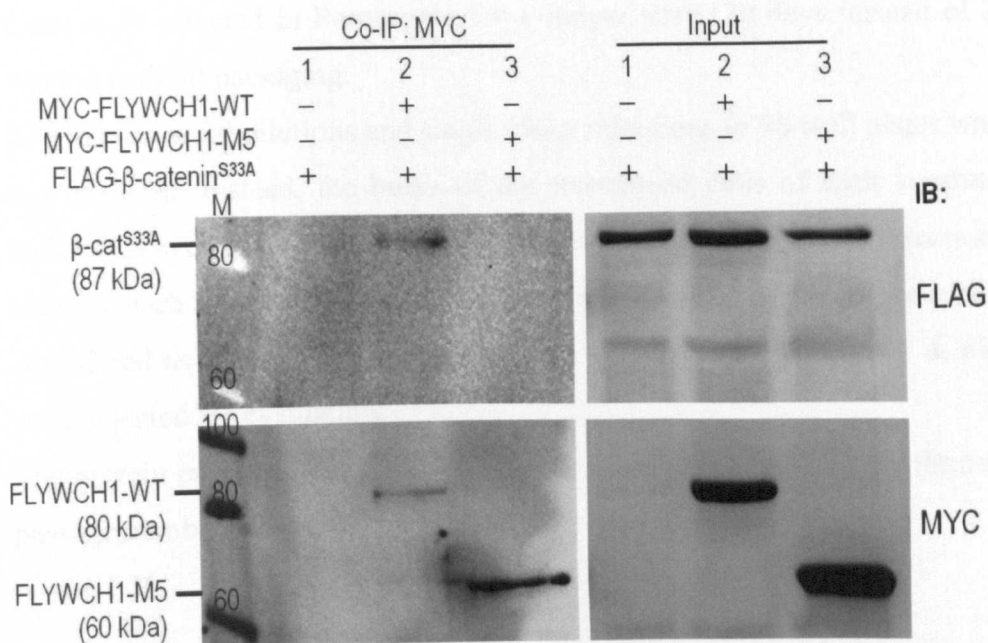


**Figure 6-16: The automutated clone of FLYWCH1 lost its physical interaction with  $\beta$ -catenin.** HEK293T cells were co-transfected to express FLAG- $\beta$ -catenin<sup>S33A</sup>, MYC-FLYWCH1-M5 or MYC-FLYWCH1-WT. The protein lysate was co-immunoprecipitated with anti-MYC-conjugated agarose beads. Both Input and Co-IP samples were immunoblotted with anti-FLAG and anti-MYC antibodies as indicated. "M", denotes the ColorPlus Protein marker (in kDa) from NEW ENGLAND BioLabs.

### 6.2.7 New strategy to generate FLYWCH1<sup>+ve</sup> stable cell lines

As demonstrated above, the exogenous genome-integrated *FLYWCH1* cDNA underwent critical spontaneous alterations in different cell lines. We speculated that several cell passages during selection are likely attributed to the genetic heterogeneity within the parental cells. Therefore, a new strategy to generate stable cell lines expressing eGFP-FLYWCH1 with limited passage number was applied. To do so, the same procedure described earlier in (section 2.2.4.3.2) was used to transduce both HEK293T and HCT116 cells with viral particles containing either eGFP (LVX-eGFP) or eGFP-FLYWCH1 (LVX-eGFP-FLYWCH1). The transduced cells were then selected and maintained in a slightly different way to the standard protocol that described in (section 2.2.4.3.2). The main differences are outlined below:

1. Cells were selected in Puromycin for a longer time (20 days instead of 2 weeks) without passaging.
2. The idea of serial dilutions and single clone selections in 96-well plates was not followed. Instead, the bulks of the transduced cells of each separate well of 24-well plates were considered as a stable clone. After selection, cells of each well were subcultured into one well of a 6-well plate and considered as P0 (passage zero). For each cell line two clones (#1 & #2) were selected for evaluation.
3. The protein expression of FLYWCH1 was evaluated within a very limited passage number, (P0 to P2).

#### ***6.2.7.1 Evaluation Experiments: Western blotting and fluorescent-microscopic analysis of new stable cell lines***

The expression of eGFP-FLYWCH1 in the new stable cell lines was first evaluated by a fluorescent microscope analysis at P0. As shown in (Figure 6-17), FLYWCH1 was expressed in a spotty nuclear format similar to the expression pattern observed for the transiently expressed wild-type FLYWCH1 (see Figure 3-15), suggesting that the wild-type eGFP-FLYWCH1 may be successfully expressed in these cell lines.

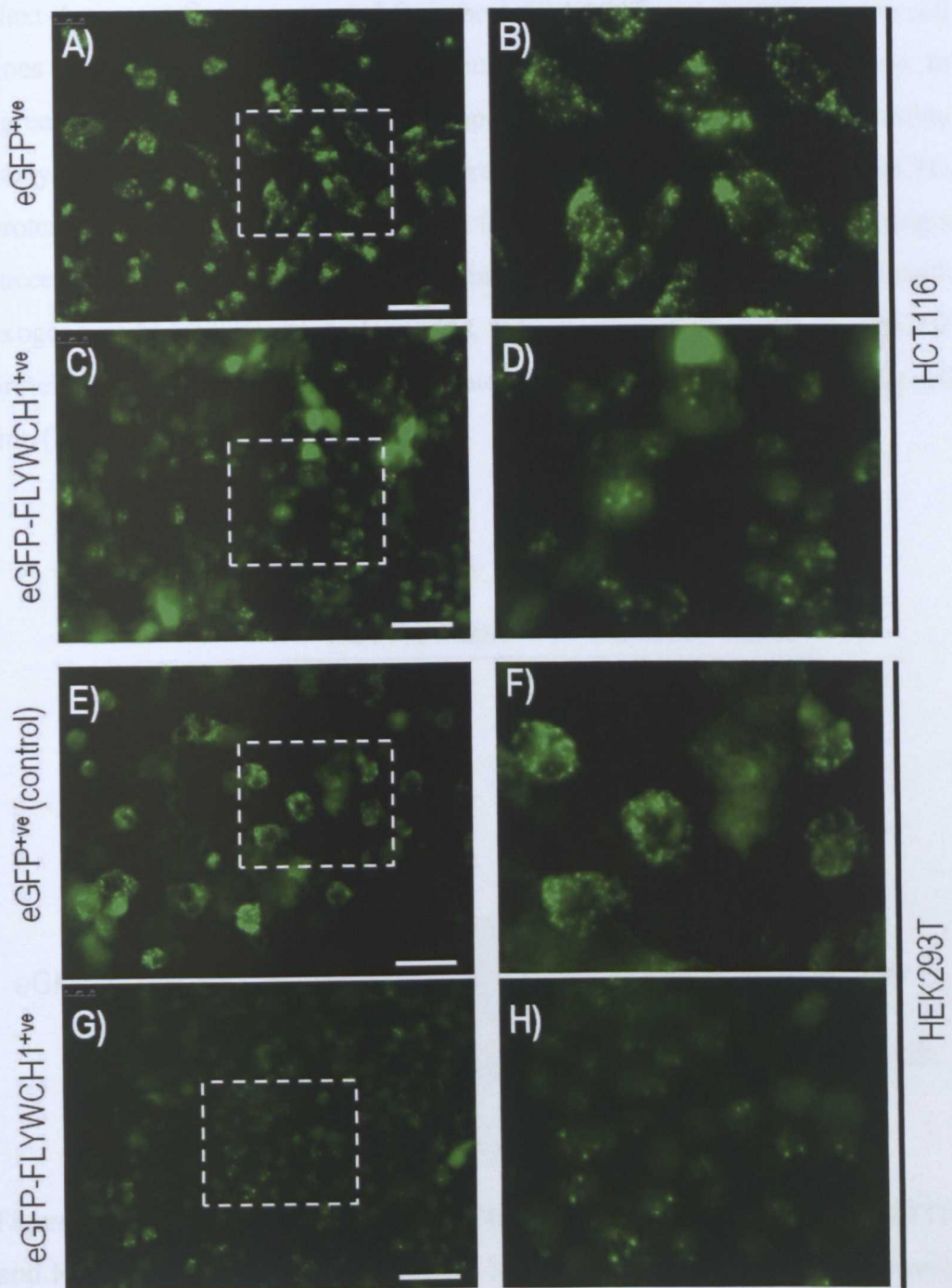
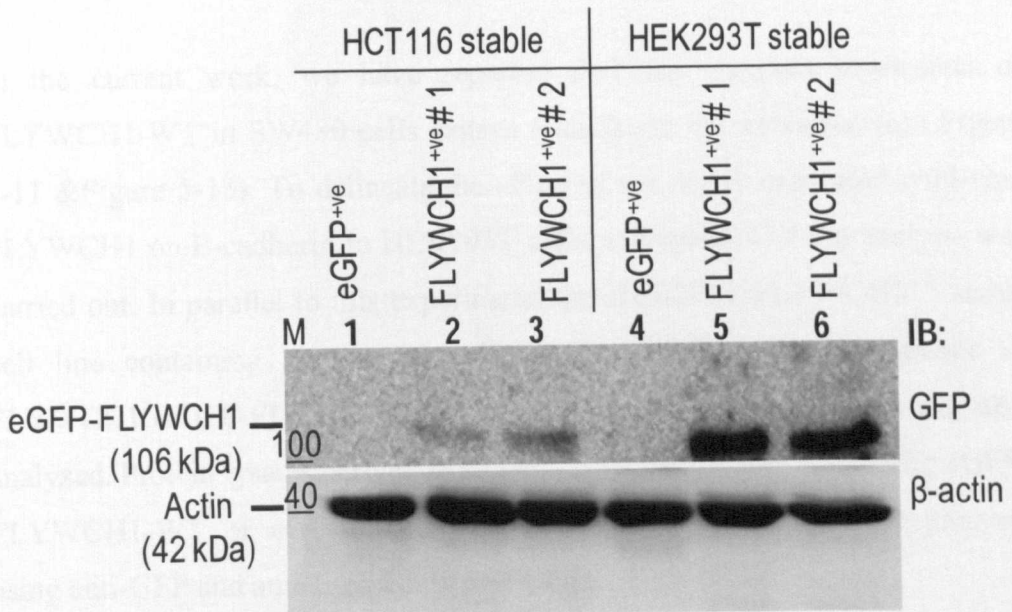


Figure 6-17: Expression pattern of eGFP-FLYWCH1 in both HCT116 and HEK293T stable cell lines. Representative fluorescent images shows the expression pattern of stably expressed eGFP (A & E) and eGFP-FLYWCH1 (C & G) in both HEK293T and HCT116 stable cell lines as indicated. B, D, F, and H) are magnified views of the indicated white boxed area. For both cell lines, Images were taken at P0. Scale bars, 50  $\mu\text{m}$

Next the protein lysate extracted from both HEK293T and HCT116 stable cell lines was run on SDS-PAGE and immunoblotted with anti-GFP antibody. In agreement to the fluorescent-microscope observations, the Western blotting analysis revealed that both cell lines were expressing the wild-type FLYWCH1 protein with expected molecular weight (~106 kDa) (Figure 6-18), indicating a successful genomic integration and protein expression of the full-length exogenous *FLYWCH1* gene. However, the expression of eGFP-FLYWCH1 protein was hardly detectable in the lysate of HCT116-FLYWCH1<sup>+ve</sup> stable cell line (Figure 6-18, lanes 2 & 3).



**Figure 6-18: Evaluation of eGFP-FLYWCH1 protein expression in both HCT116 and HEK293T stable cell lines.** Western blotting analysis shows the expression of eGFP-FLYWCH1-WT in both HCT116 and HEK293T stable cell lines at P0 as indicated using anti-GFP antibody. For each cell line, two clones of eGFP-FLYWCH1 (#1 & #2) were analysed. eGFP<sup>+ve</sup> cells were used as negative controls and  $\beta$ -actin as a loading control. "M", denotes the ColorPlus Protein marker (in kDa) from NEW ENGLAND BioLabs.

Taken together, the above results indicate that wild-type FLYWCH1 (FLYWCH1-WT<sup>+ve</sup>) can be expressed in human cell culture such as HEK293T cells for a limited time (i.e. in a very low passage number). Nevertheless, maintenance of stably expressed FLYWCH1 in CRC cells may not be possible even for a short period of time. Therefore, the HCT116 stable cell line was excluded from further analysis, while the effects of the stably expressed wild-type FLYWCH1 in HEK293T cells was further investigated.

#### ***6.2.7.2 Stably expressed eGFP-FLYWCH1-WT up-regulates E-cadherin in HEK293T stable cell line***

In the current work, we have reported that the transient expression of FLYWCH1-WT in SW480 cells caused E-cadherin up-regulation (see Figure 5-11 & Figure 5-13). To delineate the effect of the stably expressed wild-type FLYWCH1 on E-cadherin in HEK293T cells, a Western blotting analysis was carried out. In parallel to this experiment, the HEK293T-FLYWCH1<sup>+ve</sup> stable cell line containing a spontaneously mutated (unfunctional) sequence of FLYWCH1 (eGFP-FLYWCH1-M5) (see sections 6.2.3.3 & 6.2.3.4) was also analyzed. Protein lysates derived from HEK293T cells stably expressing eGFP-FLYWCH1-WT or eGFP-FLYWCH1-M5 were analyzed by WB analysis using anti-GFP and anti-E-cadherin antibodies.

Visual assessments for the Western blot data show that the expression of E-cadherin clearly up-regulated in FLYWCH1-WT<sup>+ve</sup> cells, while E-cadherin level was not affected in FLYWCH1-M5<sup>+ve</sup> cells in comparison to the control (eGFP<sup>+ve</sup>) cells per se (Figure 6-19, top panel, lane 2 vs. lane 1 in A & C). In addition, the up-regulation of E-cadherin was also evaluated through quantification of the protein bands. The integrated density value (IDV) of E-cadherin and Actin bands were measured by the band analysis tool provided by FluorChem®FC2 Imaging System (Alfa Innotech, UK) following the manufacturer's instruction. The IDV values of E-cadherin bands were then normalized (i.e. divided) to their corresponding loading control (Actin bands). The normalized E-cadherin values of control cells were arbitrarily set to 1 and

the values of other samples were divided to the values of their controls to produce folds of change in the level of E-cadherin (Figure 6-19, B & D).

These findings are in agreement with our previous data regarding up-regulation of E-cadherin by transient expression of FLYWCH1-WT (see Figure 5-13) and together suggest that the expression of E-cadherin may be positively regulated by FLYWCH1 in the context of Wnt/ $\beta$ -catenin signalling pathway.

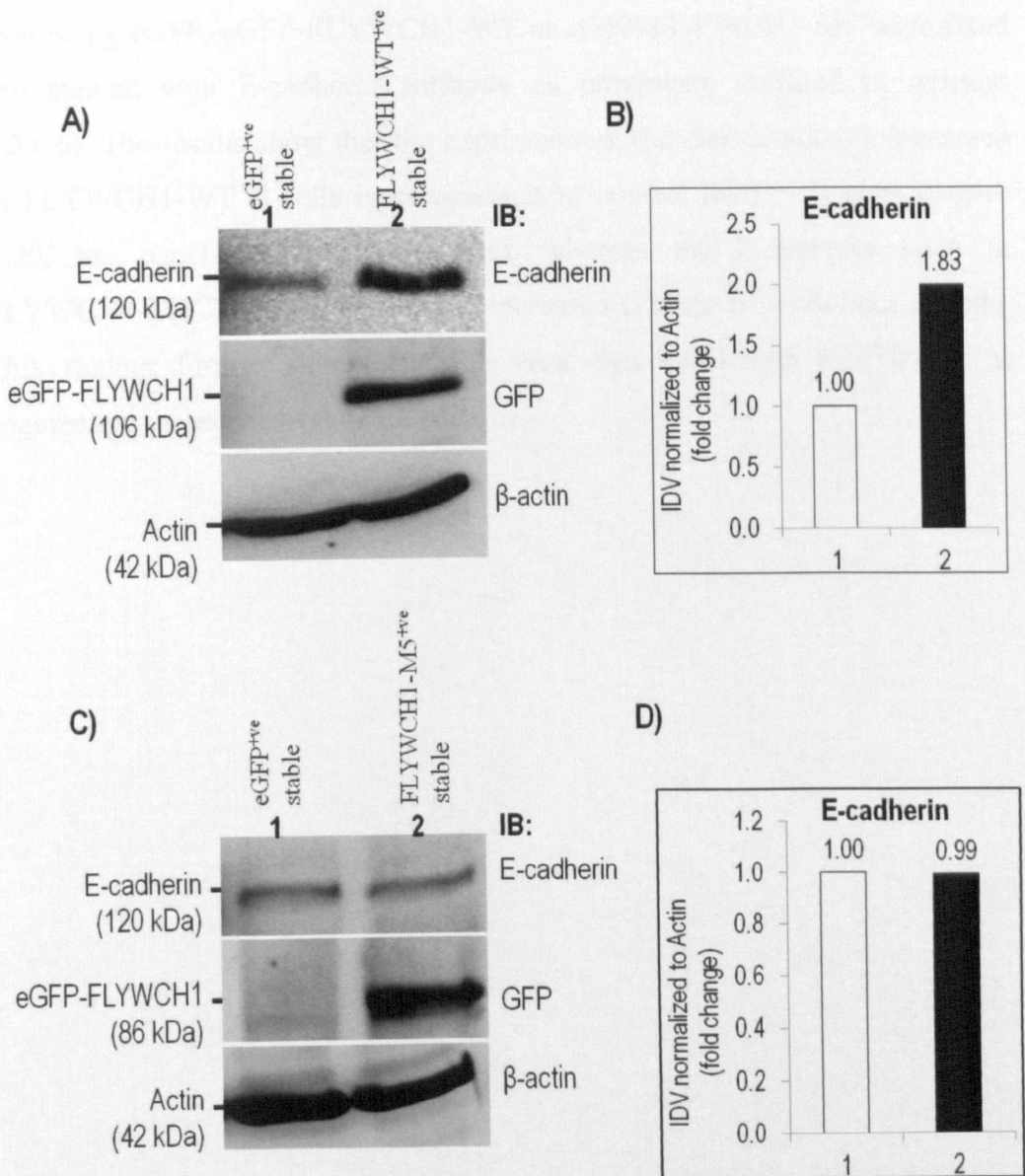


**Figure 6-19: Stably expressed FLYWCH1-WT but not FLYWCH1-M5 up-regulates E-cadherin in HEK293T cells.** Protein lysates extracted from HEK293T cells stably expressing **A)** FLYWCH1-WT and **C)** FLYWCH1-M5 in addition to eGFP<sup>+</sup> stable cell

line in both (A & C) were analyzed by Western blotting using anti-E-cadherin (top panels) and anti-GFP (middle panels) antibodies as indicated.  $\beta$ -actin (bottom panels) was used as a loading control. **B & D)** Show density quantification of E-cadherin protein bands as outlined in the text. Data are representative of three independent experiments.

To further confirm the E-cadherin up-regulation by FLYWCH1, an immunofluorescent (IF) assay was performed. The HEK293T cells that stably expressing eGFP, eGFP-FLYWCH1-WT or eGFP-FLYWCH1-M5 were fixed and stained with E-cadherin antibody as previously outlined in (section 2.2.6.6). The results show that the expression of E-cadherin notably increased in FLYWCH1-WT<sup>+ve</sup> cells in comparison to control (eGFP<sup>+ve</sup>) cells (Figure 6-20, top panels vs. middle panels), whereas the E-cadherin level in FLYWCH1-M5<sup>+ve</sup> cells is less or not increased (Figure 6-20, bottom panels). This finding further strengthens the view that full-length FLYWCH1 is augmenting the expression of E-cadherin.

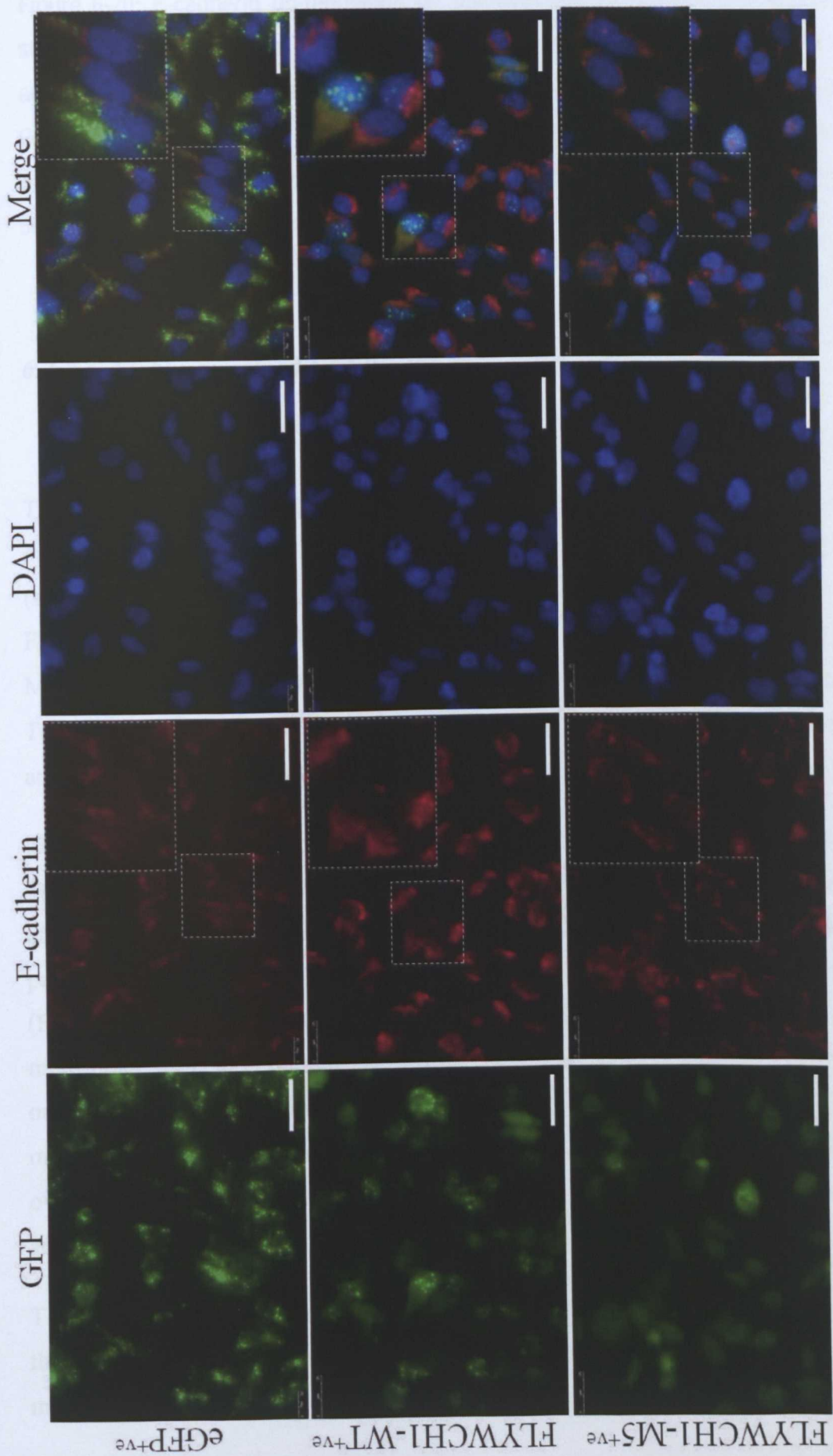


**Figure 6-20: E-cadherin up-regulation by the wild-type FLYWCH1 in HEK293T stable cell lines.** Fixed cells of HEK293T stable cell lines (eGFP<sup>+</sup>, FLYWCH1-WT<sup>+</sup>, and FLYWCH1-M5<sup>+</sup>) were subjected to IF assay using anti-E-cadherin antibody. The GFP (green) and E-cadherin (red) expressions were shown as indicated. Large white-dashed boxes are enlarged views of the indicated small white-boxed area. Scale bars, 50  $\mu$ m.

### ***6.2.7.3 Stably expressed FLYWCH1-WT changed the morphology of HEK293T cells***

The effect of FLYWCH1 mediated E-cadherin up-regulation on the morphology of transiently transfected cells was shown in the previous chapter (see section 5.2.7). Herein, the effect of the stably expressed wild-type eGFP-FLYWCH1 (FLYWCH1-WT<sup>+</sup>) and the deletion mutant M5 (FLYWCH1-M5<sup>+</sup>) on the phenotype of HEK293T stable cell lines was further investigated. To do so, these cell lines were cultured on coverslips, stained with phalloidin and analyzed under a fluorescent microscope.

The analysis show that cells expressing wild-type FLYWCH1 (FLYWCH1-WT<sup>+</sup>) are morphologically transformed, characterized by less branched, less elongated, and more rounded epithelial-like morphology (Figure 6-21, middle panel). In contrast, cells expressing only eGFP (eGFP<sup>+</sup>) or mutant FLYWCH1 (FLYWCH1-M5<sup>+</sup>) displayed distinct characteristics of more elongated and multi-branched cells (Figure 6-21, top & bottom panels). Moreover, the F-actin organization (visualized by phalloidin stain) was also changed. The control and mutant FLYWCH1 expressing cells show prominent actin fibres distributed all over the cells, whereas cells expressing wild-type FLYWCH1 display more actin fibres concentrated at the boundary of the cells.

These observations indicate that FLYWCH1 may control cell morphology through actin cytoskeleton rearrangements and, thereby, modulate cell migration.

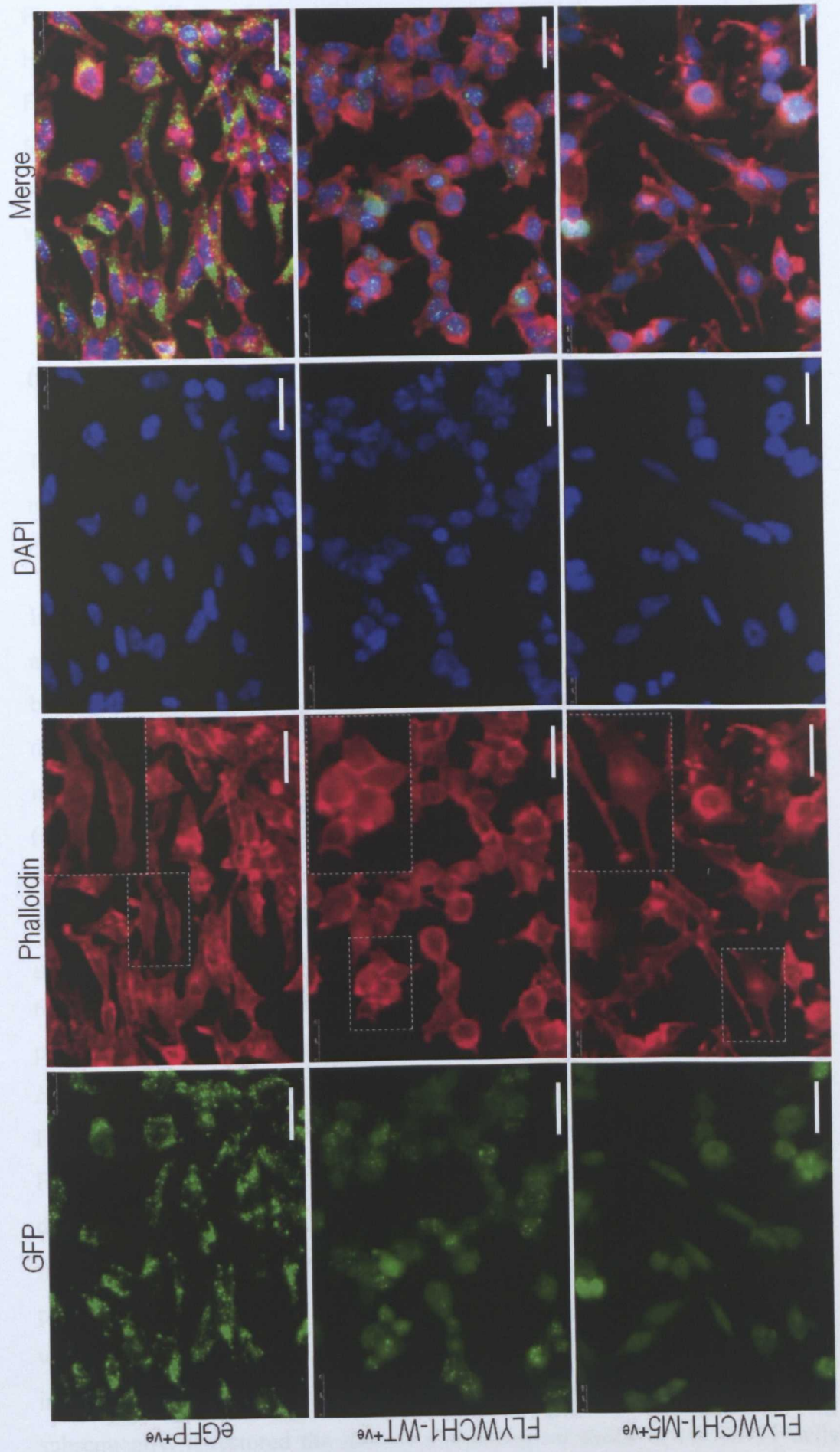


**Figure 6-21: Effects of the stably expressed FLYWCH1 on the morphology of HEK293T cells.** HEK293T cells stably expressing eGFP (eGFP<sup>+</sup>, top panel), wild-type FLYWCH1 (FLYWCH1-WT<sup>+</sup>, middle panel), and deletion mutant M5 (FLYWCH1-M5<sup>+</sup>, bottom panel) (green) were stained with phalloidin (red) and DAPI (blue). The phenotype of these cells is shown as indicated. Large white-dashed boxes are enlarged views of the indicated small white-boxed area. Scale bars, 50  $\mu$ m.

### 6.3 Discussion

The inhibitory effect of FLYWCH1 on cell migration and changes on cell morphology (Chapter 5) encouraged us to establish stable cell lines that constitutively express the FLYWCH1 protein.

In the current work, a Lentiviral-based gene delivery system was successfully applied to achieve an efficient gene delivery and integration (section 6.2.2) in both HEK293T and HCT116 cell lines. However, despite the efficient gene delivery, our attempts to maintain the full-length wild-type sequence of integrated *FLYWCH1* in the genome of these cell lines were not successful (section 6.2.3). Surprisingly, within few passages of these stable cell lines, which were required for the process of single clone selection, maintenance, and amplification, the exogenous genome-integrated *FLYWCH1* underwent various genomic alterations including deletions and point mutations (sections 6.2.3.3 & 6.2.3.4). Occurrence of a nonsense point mutation which resulted in truncated protein and a spontaneous internal deletion of large nucleotide sequence of *FLYWCH1* including its putative interaction site with  $\beta$ -catenin (Figure 6-8 & Figure 6-11), indicate that the forced expressed full-length (wild-type) FLYWCH1 may have outstanding effects on important biological processes that cannot be tolerated by the cell. This view is further supported by the finding that the automutated clone of FLYWCH1 (FLYWCH1-M5) lost its physical (Figure 6-16) and functional (Figure 6-12 & Figure 6-13) interaction with  $\beta$ -catenin. Moreover, this clone was also failed to up-regulate E-cadherin in contrast to the wild-type clone (Figure 6-19 & Figure 6-20) and subsequently, it restored the normal morphological status of HEK293T cells

(Figure 6-21). Thus, it is much more likely that these cell lines developed mechanisms to eliminate the effects of overexpressed FLYWCH1 through modifications that disturb the interaction ability of FLYWCH1 with  $\beta$ -catenin, giving the notion that similar mutations of this gene may normally exist in nature.

Our preliminary data indicated that maintenance of the stably overexpressed wild-type FLYWCH1 in human cell culture may not be possible (sections 6.2.3 & 6.2.7.1). Therefore, generation of inducible gene expression such as doxycycline or tetracycline-inducible expression systems (Grill et al., 2003, Gunther et al., 2002) of FLYWCH1 may greatly help to further investigate the biological roles of this gene in normal versus cancer development.

Following the undesirable yet important consequences of FLYWCH1 stable expression in our first attempt (section 6.2.3), we, therefore, applied a modified strategy to generate stable expression of FLYWCH1 through limiting the passage number of the transduced cells (section 6.2.7). Interestingly, the reduced cell passage method prevented the loss of FLYWCH1 expression and/or alteration in the stable cell lines (section 6.2.7.1). Subsequently, using this strategy enabled us to observe the effect of stably expressed FLYWCH1 on the phenotype of HEK293T cells.

Several morphological alterations including less branched, less elongated, and more rounded epithelial-like morphology was observed for the cells expressing wild-type FLYWCH1 (Figure 6-21, middle panel). Moreover, these cells showed more actin fibres (stained with phalloidin) concentrated at the boundary of the cells. In addition, the protein level of the well known epithelial marker, E-cadherin, was also up-regulated in these cells (Figure 6-19A & Figure 6-20). In contrast, cells expressing mutant FLYWCH1 (FLYWCH1-M5<sup>+</sup><sup>ve</sup>) (Figure 6-21, bottom panel) displayed distinct characteristics of mesenchymal-like cell morphology of more elongated and multi-branched cells with prominent actin fibres distributed all over the cells. These cells did not show up-regulation of E-cadherin (Figure 6-19 & Figure 6-20). Indeed, these cells very much resembled, in their morphology, the control cell line which expressed eGFP protein only (same figures mentioned above).

Consistent to our observations, up-regulation of E-cadherin by different mechanisms has been widely associated to reduced cell motility and invasion in addition to morphological changes from mesenchymal-like to epithelial like shape in various types of cancer (Kajiyama et al., 2003, Wong et al., 2010b, Mao et al., 2008, Meng et al., 2000). Moreover, it has also been reported that E-cadherin mediates cytoskeletal remodelling through actin reorganization leading to formation of a distinct phenotype in favour or against the process of cell migration (Alt-Holland et al., 2008, Chen et al., 2012).

Collectively, our data indicate that FLYWCH1 may function as a potential regulator of cell morphology through up-regulation of E-cadherin and actin cytoskeleton rearrangement which may ultimately affect the process of cell migration and/or invasion.

**CHAPTER 7**  
**General Discussion**

## 7.1 Introduction

Human FLYWCH1 is a conserved member of the mammalian FLYWCH-type zinc finger containing proteins (F-ZFPs). It was believed that FLYWCH1 localize to the nucleus and bind DNA based on the presence of five FLYWCH-type zinc finger DNA-binding motifs. However, no published data about the characterization and/or biological functions of FLYWCH1 was previously available. Thus, in the current study we, for the first time:

1. Bioinformatically and experimentally analyzed the amino acid sequence of human FLYWCH1 and cloned the full-length cDNA sequence of this gene into different mammalian expression vectors.
2. Identified human FLYWCH1 as a novel nuclear  $\beta$ -catenin interacting protein that physically interacts with  $\beta$ -catenin and functionally represses its transcriptional activity in human cell lines.
3. Evaluated the biological activities of FLYWCH1/ $\beta$ -catenin complex in CRC cells.
4. Explored the mechanisms by which FLYWCH1 exerts its influence on cell morphology and migration through evaluating the expression of the downstream target genes that involved in cell motility and cytoskeleton rearrangement.

## 7.2 Novelty of FLYWCH1

As a start point of the present work, a comprehensive online search was performed to find out whether any evidence has been published in the past that could have a direct or even indirect link to FLYWCH1 in human or other animals. The analyses revealed that a part of very limited evidences for the initial identification of *FLYWCH1* gene through large scale screening assays (Brandenberger et al., 2004, Stelzl et al., 2005), no data regarding characterization and/or functional analysis of FLYWCH1 protein was available. Therefore, FLYWCH1 can be considered as a previously uncharacterized protein in mammals and the current work provides the first

report to characterize human FLYWCH1 and appreciate its biological roles in human, particularly, in CRC cells.

### **7.3 Bioinformatics analysis of FLYWCH1**

In this study, sparse information about human *FLYWCH1* was collected from various reliable online recourses and databases such as NCBI (<http://www.ncbi.nlm.nih.gov/gene/84256>), GeneCards (<http://www.genecards.org/cgi-bin/carddisp.pl?gene=FLYWCH1>), and UniProt (<http://www.uniprot.org/uniprot/Q4VC44>). This information was analyzed by the available bioinformatics tools such as basic local alignment search tool (BLAST) (<http://blast.ncbi.nlm.nih.gov/Blast.cgi>), ClustalW2 alignment (<http://www.ebi.ac.uk/Tools/msa/clustalw2/>), HomoloGene (<http://www.ncbi.nlm.nih.gov/homologene/>), and Pfam (<http://pfam.sanger.ac.uk/>). Interestingly, the analysis revealed that the coding sequence of FLYWCH1 protein contains a tandem array of five FLYWCH-type zinc finger motifs (Figure 3-1). Two of these motifs are mapped to the N-terminal region, while the other three are located in the C-terminal region. Notably, a part of FLYWCH motifs, none of the other common protein domains were recognized in FLYWCH1. Moreover, our analyses also revealed that the aa residues of this protein and its FLYWCH motifs are highly conserved in all currently identified members of FLYWCH1 in mammals including human, mouse, chimpanzee, dog, cow, and rat (Table 3-1 & Figure 3-2).

Since the initial identification of F-ZFPs in early 2000s, FLYWCH-domains were found to be involved in protein-protein interactions, DNA-binding, and targeting microRNA genes in both vertebrates and invertebrates (Beaster-Jones and Okkema, 2004, Dorn and Krauss, 2003, Ow et al., 2008). Given that FLYWCH1 protein is highly conserved in several mammals, and considering the importance of the so far identified F-ZFPs in both vertebrate and invertebrates, FLYWCH family of proteins, therefore, may have crucial biological and physiological functions throughout the animal kingdom.

## **7.4 Cloning and characterization of human *FLYWCH1***

The first evidence about the interaction of human FLYWCH1 with  $\beta$ -catenin is originated from a recent screening performed in Dr. Nateri's laboratory (Figure 1-8) (Saadeddin A *et al.* unpublished data). However, the possible *in vivo* interaction of FLYWCH1 with  $\beta$ -catenin in human cell culture was required to be experimentally validated. Lacking previous work on FLYWCH1 protein and subsequently unavailability of examined mammalian expression plasmids encoding *FLYWCH1* protein was the first issue to deal with before starting cell culture experiments.

In the present study, an IMAGE clone of *FLYWCH1*, containing a previously approved (i.e. sequenced) full-length nucleotide sequence of *FLYWCH1* cDNA, was obtained from Geneservice (section 3.2.2). The IMAGE clone facilitated the cloning process of this gene into different mammalian expression vectors (section 3.2.3). This clone (i.e. the IMAGE clone) was used as a template for cloning; either directly through restriction enzyme digestion to clone untagged FLYWCH1 (section 3.2.3.1) or indirectly through PCR amplification which allowed us to tag *FLYWCH1* cDNA with small epitope tags such as MYC-epitope (section 3.2.3.2) or EGFP (section 3.2.3.3) as illustrated in (Figure 7-3). Epitope tagging of *FLYWCH1* cDNA was an essential required step to enhance the immunodetection of this protein, especially as there was no commercially available FLYWCH1 antibody that works endogenously for IHC, immunocytochemistry, WB or ChIP assays during the course of this study.

In the current work, the epitope tagged FLYWCH1 clones were successfully used to express human FLYWCH1 protein in different cell lines and detect the expressed protein by WB analysis using effective commercially available antibodies such as anti-MYC and anti-GFP (Figure 3-14, A & B). Moreover, the EGFP-tagged clone of FLYWCH1 was used to evaluate the expression pattern and the subcellular localization of FLYWCH1 in human cells through dissecting the GFP signal of the EGFP-tag reporter gene fused to the 5'-end of *FLYWCH1* cDNA (Figure 3-15).

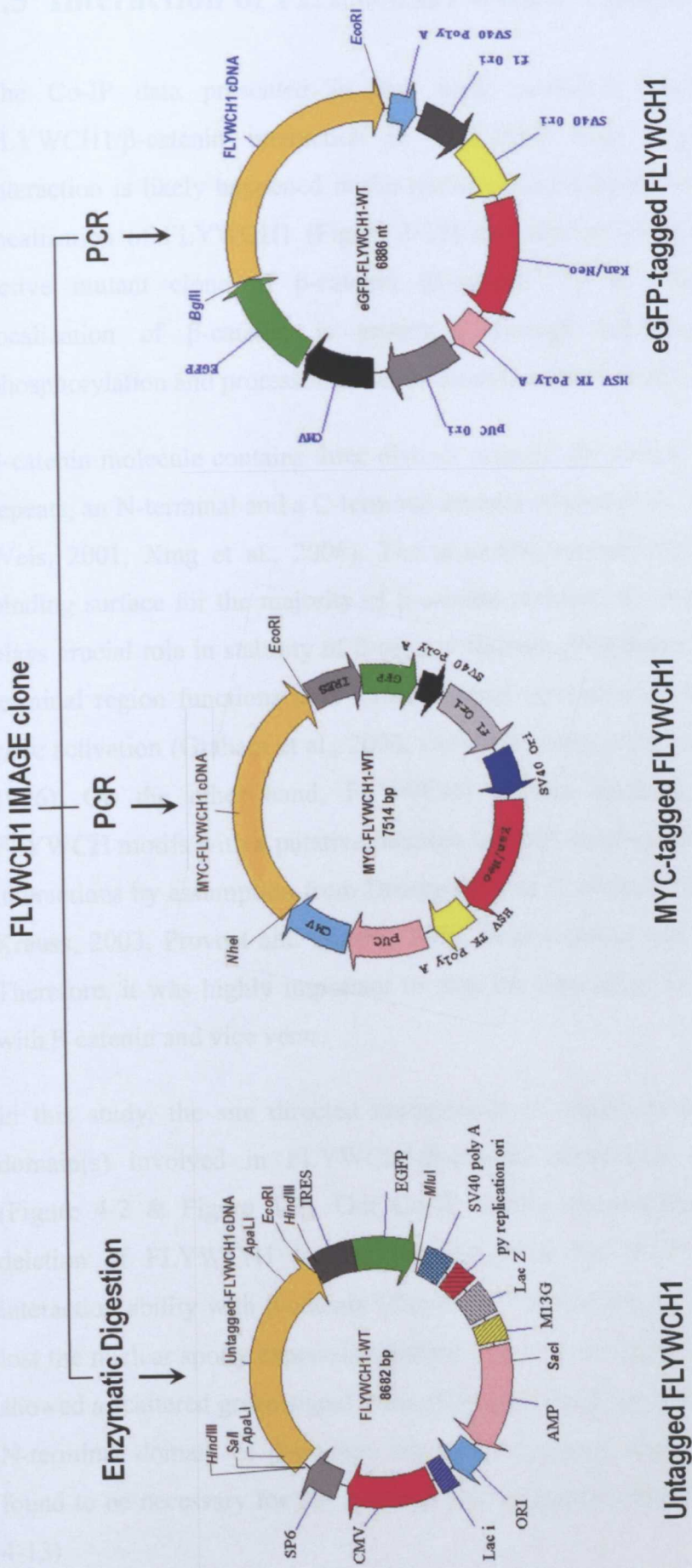


**Figure 7-1: An overview of Human FLYWCH1 cloning.** The full-length human *FLYWCH1* cDNA was obtained from the FLYWCH1 IMAGE clone through (left pane) enzymatic digestion or (middle & right panels) PCR amplification and cloned into different mammalian expression vectors (pI-EGFP2, pIRES2-EGFP, and pEGFP-C2) as indicated. For more details see chapter 3.

## **7.5 Interaction of FLYWCH1 with $\beta$ -catenin**

The Co-IP data presented in this work provided robust evidence of FLYWCH1/ $\beta$ -catenin interaction in HEK293T cells (Figure 4-1). This interaction is likely happened in the nucleus judged by the exclusive nuclear localization of FLYWCH1 (Figure 3-15) and also by using a constitutively active mutant clone of  $\beta$ -catenin ( $\beta$ -catenin<sup>S33A</sup>) in which the nuclear localization of  $\beta$ -catenin is promoted through inhibition of GSK-3 $\beta$  phosphorylation and proteasomal degradation (Liu et al., 2002).

$\beta$ -catenin molecule contains three distinct regions; the central armadillo (arm) repeats, an N-terminal and a C-terminal domain (Huber et al., 1997, Huber and Weis, 2001, Xing et al., 2008). The armadillo repeats region provides the binding surface for the majority of  $\beta$ -catenin partners, the N-terminal domain plays crucial role in stability of  $\beta$ -catenin through phosphorylation, and the C-terminal region functions as a transcriptional activation domain required for gene activation (Graham et al., 2000, van de Wetering et al., 1997, Yost et al., 1996). On the other hand, FLYWCH1 protein contains five conserved FLYWCH motifs with a putative function in DNA-binding and protein-protein interactions by assumption from *Drosophila* and *C. elegans* F-ZFPs (Dorn and Krauss, 2003, Provost and Shearn, 2006, Beaster-Jones and Okkema, 2004). Therefore, it was highly important to map the interaction site of FLYWCH1 with  $\beta$ -catenin and vice versa.

In this study, the site directed mutagenesis is employed to identify which domain(s) involved in FLYWCH1/ $\beta$ -catenin interaction from both sides (Figure 4-2 & Figure 4-9). Our Co-IP results showed that the C-terminal deletion of FLYWCH1 lacking the last three FLYWCH motifs, lost its interaction ability with  $\beta$ -catenin (Figure 4-7). Interestingly, the same deletion lost the nuclear spotty expression pattern observed for the wild-type clone and showed a scattered green signal throughout the cells (Figure 4-8). However, the N-terminal domain of  $\beta$ -catenin, but not the central armadillo repeats, was found to be necessary for the interaction of  $\beta$ -catenin with FLYWCH1 (Figure 4-13).

These results suggest that the last three FLYWCH motifs of human FLYWCH1 are possibly involved in the physical interaction of FLYWCH1 with  $\beta$ -catenin, supporting the assumption of the previous researchers that FLYWCH-type zinc finger motifs may involve in protein-protein interactions, albeit in other organisms such as *Drosophila* (Dorn and Krauss, 2003, Provost and Shearn, 2006). Although the N-terminal domain of  $\beta$ -catenin was mainly associated to kinases such as GSK3 $\beta$  and CK1 $\alpha$  (Barth et al., 1997, Yost et al., 1996, Liu et al., 2002), our data indicated that the N-terminal domain of  $\beta$ -catenin could also physically interact with transcription factors such as FLYWCH1, and thereby, control the transcriptional activity of  $\beta$ -catenin.

The exclusive nuclear localization (Figure 3-15) and the direct interaction of FLYWCH1 with  $\beta$ -catenin (Figure 4-1) in addition to its putative DNA-binding domains (FLYWCH motifs), increased the possibility that FLYWCH1 may acts as a nuclear transcription factor and thereby regulate the transactivation of downstream target genes either through functional interaction with  $\beta$ -catenin or by its own. In this work, we investigated the first possibility and examined the transactivational activity of  $\beta$ -catenin in response to FLYWCH1 through performing a TCF dual-luciferase reporter assay using TOP/FOP-FLASH reporter genes. This method is one of the common indirect transcriptional assays that have been widely used to examine the transactivational activity of  $\beta$ -catenin/TCF complex (Molenaar et al., 1996, van de Wetering et al., 1997, Mahmoudi et al., 2009, Ito et al., 2008).

Intriguingly, our luciferase reporter assays revealed that full-length FLYWCH1 substantially repressed the transactivational activity of  $\beta$ -catenin in variety of human cell lines (Figure 5-1 & Figure 5-3), indicating that FLYWCH1 may act as a repressor for the nuclear  $\beta$ -catenin. Moreover, our deletional analysis showed that the suppression activity of FLYWCH1 against  $\beta$ -catenin was abolished by the C-terminal deletion (Figure 5-5) in which the last three FLYWCH domains of FLYWCH1 protein are deleted (Figure 4-2). Our indirect transcriptional assays, therefore, suggest that in addition to the physical interaction (see above) these motifs may also be required for the functional interaction of FLYWCH1 with  $\beta$ -catenin as summarized in (Figure 7-2).

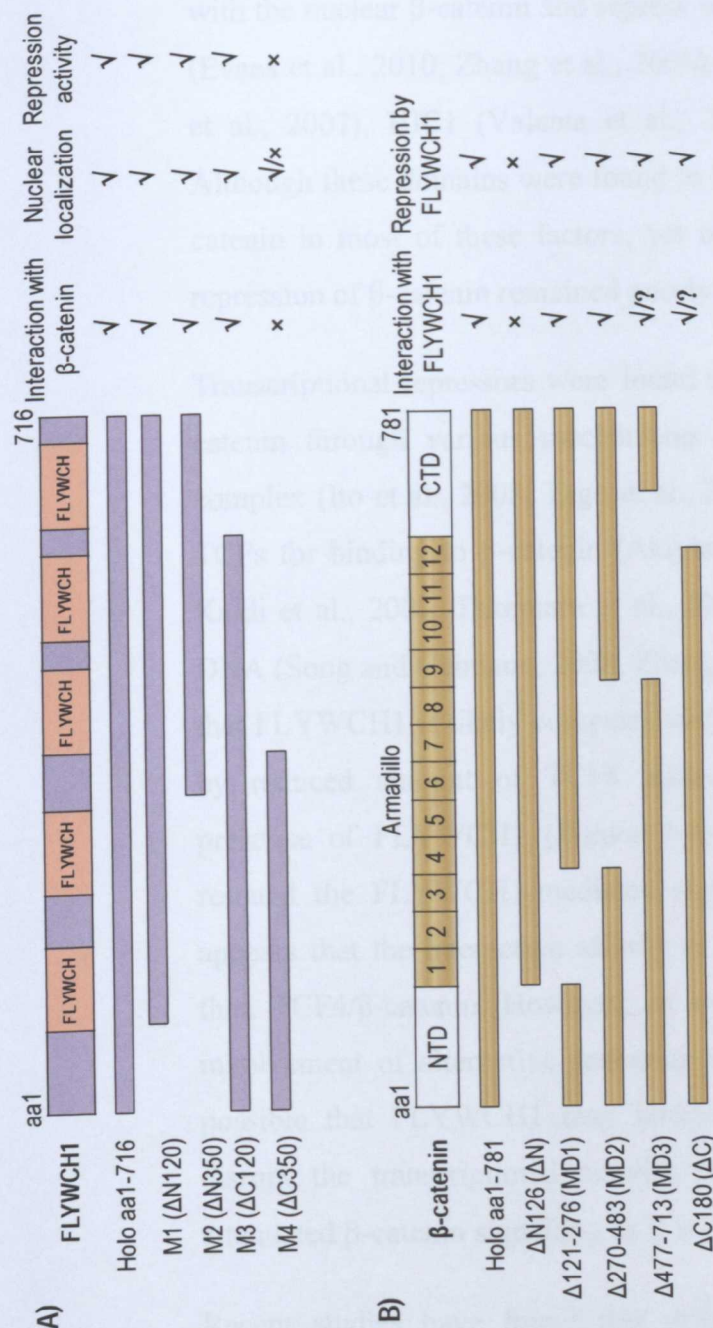


**Figure 7-2: Schematic presentation of protein domains involved in the physical and functional interaction of FLYWCH1 with  $\beta$ -catenin and vice versa.**

A) Shows the nuclear localization, the interaction ability, and the suppression activity of different FLYWCH1 constructs. B) Shows the interaction and repression of different  $\beta$ -catenin mutant clones with/by FLYWCH1. "✓" stands for experimentally approved interaction, repression, and/or nuclear localization, whereas "x" for the opposite status. "✓/x" means the protein is not restricted to the nucleus, while "✓/?" means the interaction is likely occurred but experimentally not approved.

Nuclear  $\beta$ -catenin interacting proteins have been generally divided into two groups; factors that augment the transcriptional activity of  $\beta$ -catenin (co-activators) and those inhibit this activity (co-repressors) (see section 1.2.4). In agreement to our finding, transcription factors harbouring classical C<sub>2</sub>H<sub>2</sub> zinc finger domains such as Krüppel-like C<sub>2</sub>H<sub>2</sub> zinc fingers were found to interact with the nuclear  $\beta$ -catenin and repress its transcriptional activity such as KLF4 (Evans et al., 2010, Zhang et al., 2006), Glis2 (Kim et al., 2007), Glis3 (Ulloa et al., 2007), HIC1 (Valenta et al., 2006), and Osx (Zhang et al., 2008). Although these domains were found to be necessary for the interaction with  $\beta$ -catenin in most of these factors, yet their involvement in the transcriptional repression of  $\beta$ -catenin remained poorly understood.

Transcriptional repressors were found to antagonize the activity of nuclear  $\beta$ -catenin through various mechanisms such as disruption of  $\beta$ -catenin/TCF complex (Ito et al., 2008, Tago et al., 2000, Wu et al., 2010), competing with TCFs for binding to  $\beta$ -catenin (Akiyama et al., 2004, Easwaran et al., 1999, Kaidi et al., 2007, Takemaru et al., 2003), and disruption of TCF binding to DNA (Song and Gelmann, 2008, Zhang et al., 2008). Our Co-IP results showed that FLYWCH1 is likely competes with TCF4 for binding to  $\beta$ -catenin, judged by reduced amount of TCF4 immunoprecipitated with  $\beta$ -catenin in the presence of FLYWCH1 (Figure 5-4). Moreover, as adding TCF4 did not rescued the FLYWCH1-mediated suppression of  $\beta$ -catenin (Figure 5-2), it appears that the interaction affinity of FLYWCH1/ $\beta$ -catenin may be stronger than TCF4/ $\beta$ -catenin. However, as we did not address this issue in detail, involvement of alternative scenarios cannot be excluded. For example, it is possible that FLYWCH1 may interact with both  $\beta$ -catenin and TCF4 and disrupt the transcriptional activity of  $\beta$ -catenin/TCF4 complex leading to attenuated  $\beta$ -catenin signalling as it is the case for RUNX3 (Ito et al., 2008).

Recent studies have found that stabilized  $\beta$ -catenin interacts with certain nuclear cofactors such as Prop1 (Olson et al., 2006) and Oct-4 (Kelly et al., 2011) and regulate crucial aspects of development and pluripotency through TCF-independent mechanisms. In this view, it is possible that FLYWCH1 may bind to specific elements of DNA through its zinc finger domains and recruit

nuclear  $\beta$ -catenin to the promoter of downstream target genes independently to TCFs. This assumption is supported by the finding that FLYWCH1 is efficiently interacts with the nuclear  $\beta$ -catenin and it has five zinc finger domains that may enable this protein to specifically bind DNA. Moreover, the expression of some well known  $\beta$ -catenin/TCF target genes such as *MYC* and *EPHB2* were not affected by FLYWCH1 overexpression in cancer cells, whereas expression of other genes such as *c-Jun*, *cyclin D1*, *EPHA4* and *EFNB-B2* were significantly affected (Figure 5-11). Collectively, these data indicate that FLYWCH1 may specify the downstream target activation of  $\beta$ -catenin/TCF signalling pathway, presumably in TCF-independent manner.

To sum up, the biochemical data presented in this work introduced human FLYWCH1 as a novel nuclear  $\beta$ -catenin interacting protein that antagonizes the activity of the canonical Wnt signalling pathway through physical interaction and transcriptional repression of  $\beta$ -catenin.

## **7.6 Biological significance of FLYWCH1**

Signalling through  $\beta$ -catenin/TCF4 controls many crucial aspects of cell biology such as proliferation, differentiation, migration, and morphology (Logan and Nusse, 2004, Clevers, 2006). Deregulation of this pathway disturbs these cellular processes and leads to development of many diseases including cancer (reviewed by Miller et al., 1999, Polakis, 2000, Clevers, 2006). Given that FLYWCH1 is negatively regulating this pathway (see above), it was of utmost importance to evaluate the biological effects of FLYWCH1/ $\beta$ -catenin interaction on fundamental cellular processes controlled by Wnt/ $\beta$ -catenin signalling pathway. In this notion, different approaches such as cell cycle, *in vitro* scratch assay, and migration assay were applied in this study to elucidate the biological impact of FLYWCH1 on migration, morphology and proliferation of CRC cells.

Alterations in cell motility and morphology are initial steps toward invasion and metastasis, one of the critical hallmarks of cancer (Hanahan and Weinberg,

2011). Wnt/ $\beta$ -catenin signalling pathway, through different mechanisms, often linked to regulation of these biological traits such as modulation of collective cell migration and cell branching (Aman and Piotrowski, 2008, Humtsoe et al., 2010, Matsuda et al., 2009).

The data presented in this work, indicated that FLYWCH1 inhibits cell migration (Figure 5-7 & Figure 5-10) without affecting cell proliferation or growth (Figure 5-8 & Figure 5-9). Moreover, overexpression of FLYWCH1 changed the distribution of actin filaments to be more concentrated at the cell periphery (Figure 5-12). Furthermore, FLYWCH1 altered the morphology of transiently transfected CRC and stably transfected HEK293T cells from multi-branched-elongated phenotype to less-branched-rounded shape (Figure 5-12 & Figure 6-21, respectively).

Defects in cell migration and actin cytoskeleton rearrangement could be related to the mesenchymal epithelial transition (MET) (Nelson et al., 2008), a process which is opposite in meaning to epithelial to mesenchymal transition (EMT) (Baum et al., 2008). In contrast to EMT, MET is characterized by up-regulation of epithelial-specific proteins, including E-cadherin, and down-regulation of mesenchymal-specific molecules, such as Vimentin (Mani et al., 2008, Mendez et al., 2010, Nelson et al., 2008).

Our data showed that the expression of E-cadherin, the well known epithelial marker, was consistently up-regulated by FLYWCH1 in both CRC and HEK293T cells (Figure 5-13 & Figure 6-19, respectively). However, expression of the EMT regulator, ZEB2, was not affected (Figure 5-13). Therefore, it is unlikely that FLYWCH1 may reduce cell migration through ZEB2-dependent EMT. Although involvement of the EMT/MET process through other regulators is not excluded, it is plausible to hypothesize that FLYWCH1 decreases cell migration and mediates the associated cell shape conversions through modulating the genetic program downstream to  $\beta$ -catenin/TCF4 signalling. Especially, as signalling through this pathway controls the expression of various genes that have crucial roles in cell morphology and migration/invasion such as *CDH1*, *c-Jun*, and ephrin

molecules (Alt-Holland et al., 2008, Chen et al., 2012, Jiao et al., 2008, Katiyar et al., 2007, Bochenek et al., 2010, Cortina et al., 2007, Pasquale, 2010).

In favour of this view, our qRT-PCR analysis showed that the expression of *c-Jun*, and *EFNB2* were significantly reduced by FLYWCH1 in CRC cells, while *CDH1* was up-regulated (Figure 5-11). Each of these factors has essential involvement in cell shape determination and motility (see the discussion part of chapter 5), in particular E-cadherin, which has been recently reviewed as a potential molecule associated with the cytoskeletal network during colorectal cancer development and metastasis (Buda and Pignatelli, 2011). Moreover, the qRT-PCR analysis also showed that *Cyclin D1* (another target gene of Wnt pathway) was significantly down-regulated by FLYWCH1, whereas no obvious cell cycle defects was seen. This observation is supported by the discovery of cell cycle independent roles of Cyclin D1, especially those related to cell motility (Fernandez et al., 2011, Li et al., 2006a, Li et al., 2006b). Taken together, these findings uncover a novel anti-migratory role of FLYWCH1 that affect the motility of cancer cells in the context of Wnt/ $\beta$ -catenin signalling pathway.

Our *in vitro* data are further supported by *in vivo* analyses using ISH assay on mouse intestine and human CRC tissues. *Flywch1* was found to be strikingly expressed in the crypt-based cells of the normal compartments of *APC*<sup>Min/+</sup> mouse intestine where the Lgr5<sup>+ve</sup> stem cells are located, while down-regulated in differentiated intestinal epithelial cells (Figure 5-15, right panel). Conversely, in tumour tissues *Flywch1* was less detected in the crypt (Figure 5-15, left panel), while its expression increased in late stages of intestinal adenocarcinomas (Figure 5-15A, left panel, magnified box C). Moreover, *FLYWCH1* mRNA expression was restricted to a subpopulation of tumour cells in both humans and *APC*<sup>Min/+</sup> mouse (Figure 5-15, A & F).

In addition to *FLYWCH1*, the expression of some key regulators of cancer pathways such as *c-Jun* and *EFNB-B2* was found to be up-regulated at the bottom of crypt, while their expression is down-regulated at the top of the villi (Batlle et al., 2002, Sancho et al., 2009). Moreover, *c-Jun* and *EFNB-B2* are widely implicated in intestinal cell migration/positioning, proliferation, and

tumourigenesis (Babaei-Jadidi et al., 2011, Batlle et al., 2002, Genander et al., 2009, Holmberg et al., 2006, Nateri et al., 2005, Sancho et al., 2009). Furthermore, modulation of these genes by FLYWCH1 in CRC cells was also observed in this study (see above). Taken together, these data indicate that FLYWCH1 may play important roles in intestinal homeostasis and/or carcinogenesis through regulating a number of key signalling molecules that are involved in intestinal stem cells maintenance and tumourigenesis such as *c-Jun*, *CDH1*, and Ephrin molecules as outlined in (Figure 7-3).

Although the above data provide valuable insight into the mechanisms by which FLYWCH1 influence cell morphology and migration. Yet, involvement of other regulatory molecules and/or strategies is also feasible. Indeed, there are some preliminary data that FLYWCH1 affects the expression of *Fascin1* and *CDC42*, the key regulators of filopodia formation that have role in collective cell migration and polarity (data not shown, in collaboration with Dr Roya Babaei-Jadidi, Dr Nateri's lab). Moreover, FLYWCH1 was also found to regulate the expression of miRNA-302 family (data not shown, in collaboration with Mr ElSayed Ibrahim, Dr Nateri's lab), the major microRNAs found in human embryonic stem cells with crucial roles in induced pluripotency and stem cells maintenance (Subramanyam et al., 2011, Rosa and Brivanlou, 2011, Barroso-del Jesus et al., 2009, Lin et al., 2010, Lipchina et al., 2012). Therefore, through controlling of these factors FLYWCH1 may play crucial roles in intestinal homeostasis and carcinogenesis. In such a scenario, FLYWCH1 may work independently to TCF4 and/or  $\beta$ -catenin (Figure 7-3).

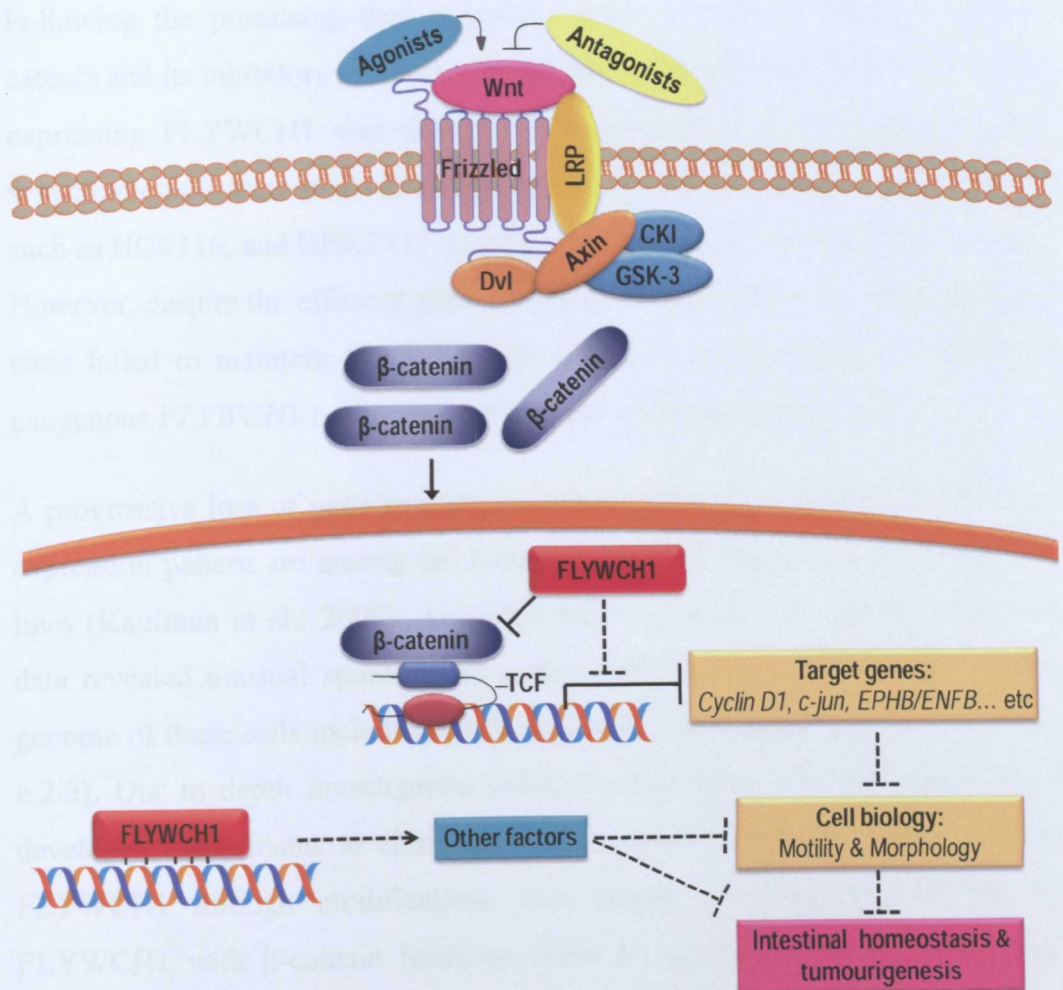


**Figure 7-3: FLYWCH1 may modulate intestinal homeostasis and tumourigenesis through controlling cell migration and morphology.** The nuclear events mediated by the canonical Wnt signalling pathway are mainly controlled by the activity of the downstream target genes of  $\beta$ -catenin/TCF4 in both colorectal cancer development and intestinal homeostasis. Through transcriptional repression of the  $\beta$ -catenin/TCF4 complex, FLYWCH1 controls cell migration and morphology through modulating the expression of several downstream target genes. Therefore, FLYWCH1 may play crucial roles in intestinal homeostasis and carcinogenesis, especially as it's highly expressed in the crypt based cells of intestine and/or a subpopulation of CRC tumour cells. It is also possible that FLYWCH1 may exert its biological influences through targeting other factors that involved in stem cell maintenance, cell morphology, and motility in a TCF4-independent manner (more detail is mentioned in the text above).

Following the promising data regarding interaction of FLYWCH1 with  $\beta$ -catenin and its inhibitory effect on cell migration, generation of cell lines stably expressing FLYWCH1 was thought to be important. In the current work, several attempts were made to stably express FLYWCH1 in different cell lines such as HCT116, and HEK293T using a Lentiviral-based gene delivery system. However, despite the efficient gene delivery, to our surprise, all these attempts were failed to maintain the full-length wild-type sequence of the integrated exogenous *FLYWCH1* in the genome of these cell lines (section 6.2.3).

A progressive loss of gene expression (silencing) and generation of a mosaic expression pattern are among the common reported drawbacks for stable cell lines (Kaufman et al., 2008). Although these problems are not excluded, our data revealed unusual spontaneous gene modifications of FLYWCH1 in the genome of these cells including point mutations and internal deletions (section 6.2.3). Our in depth investigation indicated that these cell lines might have developed mechanisms to eliminate the outstanding effects of overexpressed FLYWCH1 through modifications that disturb the interaction ability of FLYWCH1 with  $\beta$ -catenin (sections 6.2.4 & 6.2.6), giving the notion that mutations of this gene might normally exist in nature.

In this study, we considered the possibility that several cell passages during selection may attributed to the genetic heterogeneity of the parental cells of the stable cell lines. Therefore, a new batch of stable cell lines within a very limited passage number was generated (section 6.2.7). We could not evaluate the effects of stably expressed FLYWCH1 in HCT116 cells due to their rapid loose of FLYWCH1 expression (section 6.2.7.1). However, the effect of FLYWCH1 on cell migration and morphology in HEK293T stable cell lines was further observed (sections 6.2.7.2 & 6.2.7.3). Consistent with the results of the transient transfection (see above), the stably expressed FLYWCH1 changed the morphology of HEK293T cells from elongated to rounded shape (Figure 6-21) and up-regulated E-cadherin (Figure 6-19 & Figure 6-20). These data further highlight the biological roles of FLYWCH1 on cell morphology that could lead to reduced cell migration.

In summary, these data indicate that FLYWCH1 may function as a potential migration suppressor in colon cancer through controlling cell morphology. FLYWCH1 likely exerts this function through modulating the expression of the downstream target genes of  $\beta$ -catenin/TCF4 signalling. Yet, clarifying the full regulatory network and elucidating the precise molecular mechanisms by which FLYWCH1 controls gene expression programs downstream to FLYWCH1/ $\beta$ -catenin signalling, represents an important agenda for future research.

## **7.7 Limitations of this study**

1. One limitation of this study is loss-of-function approach (siRNA) which would be helpful to confirm the negative effect of overexpressed FLYWCH1 on Wnt/ $\beta$ -catenin signalling pathway. It should be mentioned that the absence of specific antibody that could recognize the endogenous expression level of FLYWCH1 was a major barrier to undertake this approach during the course of this study. In addition, most of the CRC cell lines and primary tumour tissues examined in this work expressed almost undetectable level of *FLYWCH1* mRNA (Figure 5-14 & data not shown, in collaboration with Dr Roya Babaei-Jadidi, Dr Nateri's lab). In contrast, the human fibroblast cells show high level of endogenous *FLYWCH1* mRNA measured by qRT-PCR (Figure 5-14). As this observation was obtained at a very late stage of the current study, we did not have chance to perform further experiments using this cell line. Thus, performing siRNA of *FLYWCH1* in this cell line could provide further insight about the biological functions of this gene. However, it would be much better if this approach is performed in cancer cell lines.
2. Another limitation is the absence of xenografts, subcutaneous or metastatic mouse models. Such approaches are necessary to explore and validate the possible anti-tumorigenic potentials of FLYWCH1 expressing cells. This could be accomplished through either loss-of-function or gain-of-function approaches. For which, in both cases stable cell lines were required. We

could not try the gene silencing approach because of the above mentioned reasons. On the other hand, our several attempts to stably express and/or maintain the full-length wild-type sequence of the integrated exogenous *FLYWCH1* in the genome of CRC cell lines were failed (sections 6.2.3 & 6.2.7.1). Hence, further progression toward animal model was affected.

3. Limited technical reproducibility and using of alternative approaches for some assays used in this study cannot be excluded. For example, the trans-well migration assay is a very subjective assay and the migrated cells can be counted in different ways. We have used one method (see section 2.2.6.3) to evaluate the result of this assay. However, using of other methods (discussed in section 5.3) could increase the reproducibility of this assay.
4. PCR amplification error is a common drawback of site directed mutagenesis used in this study to generate deletion mutant clones of *FLYWCH1* and  $\beta$ -catenin. In addition, removing parts of these proteins can cause changes in the physiochemical properties of the mutant clones and may lead to unexpected post-translational modifications. Although we provided plausible data to show the presence of the desired nucleotide sequence and protein expression of these clones, further investigation in this regard (discussed in section 4.3) would help to clarify the exact reasons behind unexpected migration of some of these mutant clones on the SDS-PAGE.
5. Methods used to show competition between *FLYWCH1* and TCF4 to bind  $\beta$ -catenin cannot exclude other possibilities such as forming of ternary complex of *FLYWCH1*/TCF4/ $\beta$ -catenin. Additional Co-IP and luciferase assays using increasing amount of *FLYWCH1* and/or TCF4 would help to further delineate the mechanisms of interaction and suppression of  $\beta$ -catenin by *FLYWCH1*.
6. The *in vitro* use of cell lines for functional analysis does not represent the real *in vivo* environment of cancer due to the lack of tumour microenvironment. Therefore, the *in vitro* biological functions of *FLYWCH1* need to be further validated *in vivo*. The expression profile of

*FLYWCH1* in different stages of cancer may provide valuable information in this regard.

## **7.8 Concluding remarks & future directions**

Considering our investigations regarding *(i)* the novelty of *FLYWCH1* protein, *(ii)* its interaction and transcriptional repression against  $\beta$ -catenin, and *(iii)* its downstream gene regulation (in CRC cells) and expression pattern (in intestine and human CRC tissues), in depth understanding of the enigmatic mechanisms by which *FLYWCH1* antagonize the canonical Wnt signalling pathway and control cell migration and morphology may pave new avenues in the therapeutic field of colon cancer. Yet, implication of *FLYWCH1* in the therapeutic field is currently far from practice. Nevertheless, the findings of this study warrant a larger follow-up investigation of this newly identified protein.

Although plausible data regarding identification, characterization and functional analysis of *FLYWCH1* was presented in this work, a number of complementary investigations and analyses are required to define the involvement of *FLYWCH1* in the biological processes of cell in more detail. Points that need further attention are briefly listed below:

1. Production of a specific and effective antibody that detect the endogenous level of *FLYWCH1*.
2. Gene silencing approach using *FLYWCH1* siRNA technology in cells express high level of *FLYWCH1*, e.g. human fibroblast cells.
3. Observing the endogenous expression of *FLYWCH1* in larger number of cancer cell lines and primary tumours using qRT-PCR. This will provide valuable information about the expression profile of *FLYWCH1* in cancer vs. normal tissues and it also may help to find cancer cell lines that express high level of *FLYWCH1* to be used for the siRNA approach.
4. Inducible system for *FLYWCH1* expression could be helpful to generate cell lines stably expressing this gene. In particular, as the constitutive expression of *FLYWCH1* was not successful in this study.

5. *In vivo* animal studies such as xenograft or knockout mice could be useful to further study the tissue homeostasis and/or tumourigenic properties of FLYWCH1.
6. Investigating the comprehensive gene profile downstream to FLYWCH1/ $\beta$ -catenin signalling could be very helpful to define the precise mechanisms underlying the cellular effects of FLYWCH1.
7. The qRT-PCR analysis performed in this study showed down-regulation of several Wnt target genes by FLYWCH1 at the mRNA level. Western blotting analysis should be performed to examine the negative regulatory effect of FLYWCH1 on the protein expression levels of these genes.
8. The biological effects of FLYWCH1 on cell migration and morphology should be further validated in larger number of cell lines and also by using different alternative approaches.
9. Studies are required to identify the possible regulatory mechanisms that control the expression and/or activity of *FLYWCH1* such as post-transcriptional and/or post-translational modifications.
10. The molecular mechanisms underlying the possible competition between FLYWCH1 and TCF4 for binding to  $\beta$ -catenin need to be further investigated.
11. The ability of FLYWCH1 to bind DNA should be experimentally analyzed. In this case the chromatin immunoprecipitation (ChIP) assay would be useful.
12. The nuclear localization signal (NLS) motif of FLYWCH1 requires further validation. In this case mutational analysis such as point mutation would be the assay of choice.
13. As information about the half life of FLYWCH1 protein is currently unavailable, performing a time course expression of FLYWCH1 in cell culture would help to determine the optimal expression time and give indication about the stability of this protein.
14. The biological effects of FLYWCH1 on cell migration could be further improved by using positive and negative controls (i.e. chemicals/reagents that alter the migration rate). This approach should also be applied to the cell cycle analysis to further validate the results of the PI staining.

## **Appendices**

# Appendix 1: Multiple sequence alignment of FLYWCH1 aa sequence in different animals

<u>NP 115672.2</u>		-----	
<u>XP 510759.2</u>		-----	
<u>XP 547172.2</u>	1	MVIVRATVPAASDPATSGGSHRPHAGRGGQWPAGGARGSAVPATPGDFAA	50
<u>XP 610323.3</u>		-----	
<u>NP 722486.1</u>		-----	
<u>XP 340761.1</u>		-----	
<u>NP 115672.2</u>		-----	
<u>XP 510759.2</u>		-----	
<u>XP 547172.2</u>	51	CSAPLPEEPEKRSSPEERGAALLRMLAAIRSGVPRGGLRSGVARSRPAG	100
<u>XP 610323.3</u>		-----	
<u>NP 722486.1</u>		-----	
<u>XP 340761.1</u>		-----	
<u>NP 115672.2</u>		-----	
<u>XP 510759.2</u>		-----	
<u>XP 547172.2</u>	101	GQWGRGASARLAAAAGA EVHAAAAAEARGPAAARS PEREGSAAAAARVG	150
<u>XP 610323.3</u>		-----	
<u>NP 722486.1</u>		-----	
<u>XP 340761.1</u>		-----	
<u>NP 115672.2</u>		-----	
<u>XP 510759.2</u>		-----	
<u>XP 547172.2</u>	151	ALGPANALRAEEAEPDGVSESPQRPPPPGAPRGQSSWTARFPTREEEEEE	200
<u>XP 610323.3</u>		-----	
<u>NP 722486.1</u>		-----	
<u>XP 340761.1</u>		-----	
<u>NP 115672.2</u>	1	-----MPLPEPSEQEGESVKAGQEP---SPKPGTDV	28
<u>XP 510759.2</u>	1	-----MPLPEPSEQEGESVKAGQEP---SPKPGTDV	28
<u>XP 547172.2</u>	201	EKSLCQGLSVACGTGHRPRMPLPESSEQKGESVKAGQEPSPEPPEPGTDV	250
<u>XP 610323.3</u>	1	-----MPLPEPSEQEGESVKAGQEPSPEPPEPGTDV	31
<u>NP 722486.1</u>	1	-----MPLPEPSEQDCESLRAGQEP-----	20
<u>XP 340761.1</u>	1	-----MPLPEPSEQEGESLRAGQEP-----	20
<u>NP 115672.2</u>	29	IPAAPRKPREFSKLVLLTASDQDEDGVGSKPQEVHCVLSLEMAGPATLA-	77
<u>XP 510759.2</u>	29	IPAAPRKPREFSKLVLLTASNQDEDGVGSKPQEVHCVLSLDMAGPATLA-	77
<u>XP 547172.2</u>	251	VPAAPTKEEFKLVLLTVSTENVGDVDSQPEGGHCVVSLMSGPDTLA-	299
<u>XP 610323.3</u>	32	VLEAPTKEEFSELVLLAASTESGDGMTQPEEVHCVLTLEMADPDTLA-	80
<u>NP 722486.1</u>	21	-SVGARKPQESSNLV-----PARDKERPKPTD---VASQETSSTATLPN	60
<u>XP 340761.1</u>	21	-SRGARKPQESSNLV-----PARDKEKPKPTD---VMSQETSSTTTLPN	60
<u>NP 115672.2</u>	78	STLQILPVVEEQGGVVQPALEMPEQKCSKLD-AAPQSLEFLRTPFGGRLLV	126
<u>XP 510759.2</u>	78	STLQILPVVEEQGGVVQPALEMPEQKCSKLDAAAPQSLEFLRTPFGGRLLV	127
<u>XP 547172.2</u>	300	RMPQILQVEEQVGAVQPTLQAPEQYRSKPD-TAPKPLEFLRTPFGGRLLV	348
<u>XP 610323.3</u>	81	GTPQILPVVEEQCGVVQPRPQTQALKPSKPN-IVTQPLEFLRTPFGGRLLV	129
<u>NP 722486.1</u>	61	NTLQVAPVKKQGRIIH-----RKRSRVDVAVPPQPLEFLKTPFGGRLLV	103
<u>XP 340761.1</u>	61	NTLQALPAKKQGRIIH-----RKRSRVDVAVAPQPLEFLKTPSGSRLLV	103
<u>NP 115672.2</u>	127	LESFLYKQEKAVGDKVYWKCRQHAELGCRGRAITRGLRATVMRGHCHAPD	176
<u>XP 510759.2</u>	128	LESFLYKQEKAVGDKVYWKCRQHAELGCRGRAITRGLRATVMRGHCHTPD	177
<u>XP 547172.2</u>	349	LECFLYKQEKAVGDKVYWKCREHCELGCRGRAITRGPRATVMRGHCHPPD	398
<u>XP 610323.3</u>	130	LESFLYKQEKAVGDKVYWKCREHTELGCRGRAITRGPRATIMRGHCHPPD	179
<u>NP 722486.1</u>	104	HKSFLYKQEKAVGDKVYWKCRQHSELSCRGRAITRGFRVTEMRDHCHPPE	153
<u>XP 340761.1</u>	104	HKSFLYKQEKAVGDKVYWKCRQHSELGCRGRAITRGFRVTEMRDHCHPPE	153

<u>NP 115672.2</u>	177	EQGLE-ARRQREKLPSLALPEGLGEPQ---GPEGP-GGRVEEPLGVGPW	221
<u>XP 510759.2</u>	178	EQGLE-ARRQREKLPSLALPEGLGEPQGPEGPEGP-GGRVEEPLGVGPW	225
<u>XP 547172.2</u>	399	EEGLE-ARRRRQKLPSPSPEGLG-----GPEGPGGRVEEPLGVGPW	441
<u>XP 610323.3</u>	180	EEGLA-ARRRQKRLGALPEGLA-----GSQGP-SSLVEEPLGAGPW	221
<u>NP 722486.1</u>	154	KEGLDRKKRRHRGPPSSALPE-----GAEVQ-----EDEVSLW	186
<u>XP 340761.1</u>	154	KEGLGKKRRQKEKLPSS-----GTEGQ-----GDGVSLW	182
<u>NP 115672.2</u>	222	QCPEEPEPTPGLVLSKPALEEEAAPRALSLLSLPPKKRSILGLGQAR-PL	270
<u>XP 510759.2</u>	226	QCPEEPEPTPGLVLSKPALEEEAAPRALSLLSLPPKKRSILGLGEAR-PL	274
<u>XP 547172.2</u>	442	LCPEEPEPAPTLVLSKPAEEDEGLRALSLSLPPKKRPTLGIGELRPPL	491
<u>XP 610323.3</u>	222	LCPVEPDPTPGPMLSYLVEEDEGLRALALLRPPKKRSTLG-SRGPPPL	270
<u>NP 722486.1</u>	187	LYPVEPEPTPQPSTETP--EEEQGYRSLALQSLPPKKRPTPGVVYR-PL	233
<u>XP 340761.1</u>	183	LYPVEPEPTPQPSIETP--EEEQGYRSLALQSLPPKKRPTPGVVYR-PL	229
<u>NP 115672.2</u>	271	EFLRTCYGGSFVLVHESFLYKREKAVGDKVYWTCDHALHGCRSRAITQGG	320
<u>XP 510759.2</u>	275	EFLRTCYGGSFVLVHESFLYKREKAVGDKVYWTCDQALHGCRSRAITQGG	324
<u>XP 547172.2</u>	492	EFLRTCYGGSFVLVHQSFLYKREKAVGDKVYWTCDHALHSCRSRAITQGG	541
<u>XP 610323.3</u>	271	EFLRTCYGGSFVLVHQSFLYKREKAVGDKVYWTCDHTQHGCRSRAITQGR	320
<u>NP 722486.1</u>	234	EFLKTCYGGTFLVHQSFLYKREKTVGSKVYWTCREHAVHGCRSRAITQGG	283
<u>XP 340761.1</u>	230	EFLKTCYGGTFLVHQSFLYKREKTVGSKVYWTCREHAVHGCRSRAITQGG	279
<u>NP 115672.2</u>	321	RVTVMRGHCHQPDMEGLEARRQEKAVETLQAGQDGPQSG-----VDTL	364
<u>XP 510759.2</u>	325	RVTVMRGHCHQPDVEGLEARRQEKAVETLQAGQDGPQSG-----VDTL	368
<u>XP 547172.2</u>	542	RVTVMRGHCHPPDMEGLEARRQEKAMETLQARPGGPGGQ-----ADQL	585
<u>XP 610323.3</u>	321	RVTVMRGHCHAPDLEGLKARRQERAMAALRAQPGGPGGP-----EDKP	364
<u>NP 722486.1</u>	284	RVTVMRSHCHSPDIEGLQARRQEKTIKKIQARRIGAGDLEDCDDIEDSL	333
<u>XP 340761.1</u>	280	RVTVMRSHCHSPDMEGLQARRQEKTIKKIQARRIGAGDLEDCDDIEDTL	329
<u>NP 115672.2</u>	365	LRGVDSLRYRRGPGPLTL-----TRPRPKKRAKVEDQ	396
<u>XP 510759.2</u>	369	LRGVDSLRYRRGPGPLTL-----SRSRPKKRAKVEDQ	400
<u>XP 547172.2</u>	586	PQGVDSLRCRKGPGTLNL-----SRTRPKRKPVLPA	617
<u>XP 610323.3</u>	365	LQGVDSLRYRRGPGPLTL-----TRPRPKRRLMANDE	396
<u>NP 722486.1</u>	334	LQGVDSLRYRRGQGTTLRSRSKSKSKSKSKSKSKSKSKSKSRSRPKRAKQQE	383
<u>XP 340761.1</u>	330	LQGVDSLRYRRGPGPLTL-----SRSRPKKRAKQQE	361
<u>NP 115672.2</u>	397	ELPTQPEAPDEHQDMDADPGGPEFLKTPLGGSFLVYESFLYRREKAAGEK	446
<u>XP 510759.2</u>	401	ELPAQPEAPDEHQDMDADPGGPEFLKTPLGGSFLVYESFLYRREKAAGEK	450
<u>XP 547172.2</u>	618	QPPALPGSPAEE---DQDKDLGGPEFLRTPLGGSFLVYESFLYRREKAAGEK	665
<u>XP 610323.3</u>	397	ELPAEPQGE---DKDEDPGGPEFLRTPLGGSFLVYESFLYRREKAAGEK	443
<u>NP 722486.1</u>	384	SSQPEP-EE---DQDVPDRGPEFLKTPLGGNFLVYESFLYRREKVAGEK	428
<u>XP 340761.1</u>	362	PLQESPEEE---DQDVPDKGPEFLKTPLGGNFLVYESFLYRREKVAGEK	407
<u>NP 115672.2</u>	447	VYWTCDQARMGCRSRAITQGRVTVMRGHCHPPDLGGLEALRQREKRPN	496
<u>XP 510759.2</u>	451	VYWTCDQARMGCRSRAITQGRVTVMRGHCHPPDLGGLEALRQREKRPN	500
<u>XP 547172.2</u>	666	VYWTCDQARMGCRSRAITQGRVTVMRGHCHPPDLGGLEALRQREKHPG	715
<u>XP 610323.3</u>	444	VYWTCDQARMGCRSRAITQGRVTVMRGHCHPPDLGGLEALRQREKRPG	493
<u>NP 722486.1</u>	429	VYWTCDQARMGCRSRAITQGRVTVMRSHCHPPDLLGLETLRQREKRPG	478
<u>XP 340761.1</u>	408	VYWTCDQARMGCRSRAITQGRVTVMRGHCHPPDLLGLETLRQREKRPG	457
<u>NP 115672.2</u>	497	TAQRGSPGGPEFLKTPLGGSFLVYESFLYRREKAAGEKVYWTCDQARMG	546
<u>XP 510759.2</u>	501	TAQRGSPGGPEFLKTPLGGSFLVYESFLYRREKAAGEKVYWTCDQARMG	550
<u>XP 547172.2</u>	716	AAQRGSPGGPEFLRTPLGGSFLVYESFLYRREKAAGEKVYWTCDQARMG	765
<u>XP 610323.3</u>	494	TAQRGSTGGPEFLRTPLGGSFLVYESFLYRREKAAGEKVYWTCDQARMG	543
<u>NP 722486.1</u>	479	PSQWDGPEGPEFLKTPLGGSFLVYESFLYRREKATGDKVYWTCDQARMG	528
<u>XP 340761.1</u>	458	PAQWDGPEGPEFLKTPLGGSFLVYESFLYRREKATGDKVYWTCDQARMG	507

NLS

<u>NP 115672.2</u>	547	CRSRAITQGRRVMVMRR <b>HCH</b> PPDLGGLEALRQREHFNPNAQWSDPDPLRP	596
<u>XP 510759.2</u>	551	CRSRAITQGRRVMVMRR <b>HCH</b> PPDLGGLEALRQREHFNPNAQWSDPDPLRP	600
<u>XP 547172.2</u>	766	CRSRAITQGQVRVMVMRR <b>HCH</b> PPDLGGLEALRQREQIPSPAQREGSGALQP	815
<u>XP 610323.3</u>	544	CRSRAITQGPRVMVMRR <b>HCH</b> PPDLGGLEALRQREQLPSPAQREGSETPQP	593
<u>NP 722486.1</u>	529	CRSRAITQGQVRVMVMRR <b>HCH</b> PPDMGGLEALRQRENFNPNLTHWEGPEPLQP	578
<u>XP 340761.1</u>	508	CRSRAITQGQVRVMVMRR <b>HCH</b> PPDMGGLEALRQRENFNPNLTHWEGPEPVQP	557
<u>NP 115672.2</u>	597	LEFLRTSLGGRFLVHESFLYRKEKAAGEKVV <b>WM</b> CRDQARL <b>G</b> CRSRAITQ <b>G</b>	646
<u>XP 510759.2</u>	601	LEFLRTSLGGRFLVHESFLYRKEKAAGEKVV <b>WM</b> CRDQARL <b>G</b> CRSRAIT <b>E</b> G	650
<u>XP 547172.2</u>	816	LEFLRTSLGGRFLVYESFLYRKEKAAGEKVV <b>WM</b> CRDQARL <b>G</b> CRSRAITQ <b>G</b>	865
<u>XP 610323.3</u>	594	LEFLRTSLGGRFLVYESFLYRKEKAAGEKVV <b>WM</b> CRDQAR <b>K</b> GCRSRAITQ <b>G</b>	643
<u>NP 722486.1</u>	579	LEFLRTSLGGRFLVYESFLYRKEKAAGEKVV <b>WM</b> CRDQARL <b>G</b> CRSRAITQ <b>G</b>	628
<u>XP 340761.1</u>	558	LEFLQTSLGGRFLVYESFLYRKEKAAGEKVV <b>WM</b> CRDQARL <b>G</b> CRSRAITQ <b>G</b>	607
<u>NP 115672.2</u>	647	HRIMVMRS <b>HCH</b> QPDLAGLEALRQRERLPTTAQQEDPEKI-----QVQ-LCF	691
<u>XP 510759.2</u>	651	HRIMVMRS <b>HCH</b> QPDLAGLEALRQRERLPTTAQQEDPEKI-----QVQ-LCF	695
<u>XP 547172.2</u>	866	QLVTVMRS <b>HCH</b> LPDLAGLEALRQRERLPSVAPQEDPGRQ----ERQELAA	911
<u>XP 610323.3</u>	644	PRVTVMRG <b>HCH</b> PPDLAGLEALRRERQLPSLAQQEDPEKVKLLPEVQ-LCL	692
<u>NP 722486.1</u>	629	RRVMVMRS <b>HCH</b> PPDLAGLEALRQ-----RE-----	653
<u>XP 340761.1</u>	608	RRVMVMRS <b>HCH</b> SPDLAGLEALRQRERERKARERERKARERE-----	646
<u>NP 115672.2</u>	692	KTCSPESQQIYGDIKDVRLDGESQ-----	715
<u>XP 510759.2</u>	696	KTCSPESQQIYGDIKDVRLDGESQ-----	719
<u>XP 547172.2</u>	912	AGVHDAGMGPARDGPKKPLDTETPPPGYAALSRKRPPVSRARDFADFPV	961
<u>XP 610323.3</u>	693	ETCAPECQQSYGKVESTQLDNESQ-----	716
<u>NP 722486.1</u>	654	--KAPSAAKKKKKKKKKK-KGIH-----	673
<u>XP 340761.1</u>	647	--KAPSAAKKKKKKKKKKGSKS-----	667
<u>NP 115672.2</u>		-----	
<u>XP 510759.2</u>		-----	
<u>XP 547172.2</u>	962	CQGPASARAH	971
<u>XP 610323.3</u>		-----	
<u>NP 722486.1</u>		-----	
<u>XP 340761.1</u>		-----	

The amino acid sequence of protein accession numbers; NP\_115672.2 (*Homo sapiens*), XP\_510759.2 (*Pan troglodytes*), XP\_547172.2 (*Canis lupus familiaris*), XP\_610323.3 (*Bos Taurus*), NP\_722486.1 (*Mus musculus*), and XP\_340761.1 (*Rattus norvegicus*) were analysed as indicated. The consensus sequence of FLYWCH motifs (F, L, Y, W, C, & H) is highlighted in yellow, while a conserved possible NLS motif (KRAK) is boxed in red as indicating the putative consensus sequence of the classical NLS motif (K-R/K-X-K/R). For more detail see (section 3.2.1).

## **Appendix 2: Manual plasmid DNA extraction protocol**

### **Steps of manual Miniprep Protocol for Recovery of Plasmid DNA:**

1. Grow cultures overnight in 2 ml Luria broth supplemented with the appropriate antibiotics at 37°C with vigorous shaking (200-250 rpm).
2. Pour 1.0 ml of the culture into eppendorf tubes. Store the unused culture in the fridge.
3. Centrifuge at max speed for 10 minutes (RT or 4°C).
4. Aspirate and discard the supernatant, make the bacteria pellet as dry as possible.
5. Resuspend pellets in 100 µl of ice-cold resuspension buffer (**Solution I**).
6. Add 200 µl of freshly prepared alkaline lysis buffer (**Solution II**). Cap tubes and mix contents by inverting several times (**do not vortex**).
7. Incubate tubes on ice for 5 minutes.
8. Add 150 µl ice-cold neutralization buffer (**Solution III**). Mix by inverting and gentle vortexing.
9. Incubate tubes on ice for 3-5 minutes.
10. Centrifuge tubes at 4°C on high speed for 5 minutes.
11. (**Optional**) Add an equal volume of phenol: chloroform (1:1 v/v). Mix the organic and aqueous phase by vortexing and then centrifuge the emulsion at max speed for 2 minutes at 4°C.
12. Transfer the aqueous upper layer from step 11 or the supernatant from step 10 to fresh eppendorf tubes.
13. Precipitate the DNA by adding 2 volumes of absolute ethanol at room temp. Mix the solution by vortexing and then allow the mixture to stand for 2 minutes at room temperature.
14. Centrifuge tubes at 4°C on high speed for 5 minutes.
15. Remove the supernatant by gentle aspiration. Dry pellets at room temperature for 10 to 15 minutes.
16. Add 1 ml of 70% ethanol to each pellet and invert the closed tubes several times. Centrifuge tubes at 4°C on high speed for 2 minutes.

17. Remove the supernatant by gentle aspiration. Dry pellets at room temperature for 10 to 15 minutes.
18. Gently resuspend pellets in 50  $\mu$ l 1X TE buffer (PH=8) or just use Sigma dH<sub>2</sub>O.

**Solution I (Resuspension buffer):**

4.50 g glucose (50 mm)

1.97 g Tris-Cl (25 mm)

1.86 g EDTA (10 mm)

Dissolve in 500 ml dH<sub>2</sub>O

**Solution II (Alkaline lysis buffer):**

0.2 N NaOH freshly diluted in 1% SDS from a 10 N stock solution of NaOH

**Solution III (Neutralization buffer):**

5 M sodium acetate 60 ml

Glacial acetic acid 11.5 ml

H<sub>2</sub>O 28.5 ml

**TE buffer (Tris EDTA) PH=8**

100 mM tris-HCl (PH=8)

10 mM EDTA (PH=8)

Sterilize solution by autoclaving for 20 minutes at 15 psi.

## **Appendix 3: Cell counting using Neubauer haemocytometer**

This protocol is taken from the Abcam's website:  
[http://www.abcam.com/ps/pdf/protocols/haemocytometer\\_cell\\_counts.pdf](http://www.abcam.com/ps/pdf/protocols/haemocytometer_cell_counts.pdf)

### **A. Preparing haemocytometer**

1. Ensure the haemocytometer is clean using 70% ethanol.
2. Moisten the shoulders of the haemocytometer and affix the coverslip using gentle pressure and small circular motions. The phenomenon of Newton's rings can be observed when the coverslip is correctly affixed, thus the depth of the chamber is ensured.

### **B. Preparing cell suspension**

1. Make sure the cell suspension to be counted is well mixed by either gentle agitation of the flask containing the cells (or other appropriate container). A serological pipette may be used if required.
2. Before the cells have a chance to settle take out about 1 ml of cell suspension using a serological pipette and place in an eppendorf tube.
3. Using a 100  $\mu$ l pipette, mix the cells in this sample again (gently to avoid lysing them). Take out 100  $\mu$ l and place into a new eppendorf, add 100  $\mu$ l trypan blue and mix gently again.

### **C. Counting**

1. Using the Gilson pipette, draw up some cell suspension containing trypan blue. Carefully fill the haemocytometer by gently resting the end of the Gilson tip at the edge of the chambers. Take care not to overfill the chamber. Allow the sample to be drawn out of the pipette by capillary action, the fluid should run to the edges of the grooves only. Re-load the pipette and fill the second chamber if required.
2. Focus on the grid lines of the haemocytometer using the 10X objective of the microscope. Focus on one set of 16 corner square as indicated by the circle in (Figure 1)

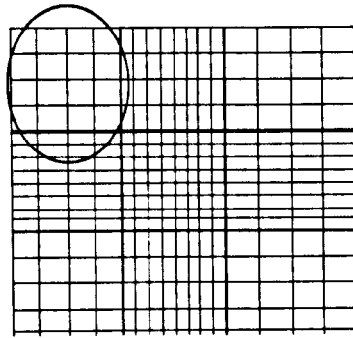


**Figure 1: Gridlines on haemocytometer.**

3. Using a hand tally counter, count the number of cells in this area of 16 squares. When counting, always count only live cells that look healthy (unstained by Trypan Blue). Count cells that are within the square and any positioned on the right hand or bottom boundary line.

Dead cells stained blue with trypan blue can be counted separately for a viability count

4. Move the haemocytometer to another set of 16 corner squares and carry on counting until all 4 sets of 16 corner squares are counted.
5. The haemocytometer is designed so that the number of cells in one set of 16 corner squares is equivalent to the number of cells  $\times 10^4/ml$ .

**Therefore, to obtain the count:**

The total count from 4 sets of 16 corner = (cells / ml  $\times 10^4$ )  $\times$  4 squares from one haemocytometer grid

1. Divide the count by 4
2. Then multiply by 2 to adjust for the 1:2 dilution in trypan blue

These two steps are equivalent to dividing the cell count by 2

As an example:

If the total cell count is 145

The cell density is  $\frac{145}{2} = 72.5 \times 10^4/ml$

#### **D. Viability**

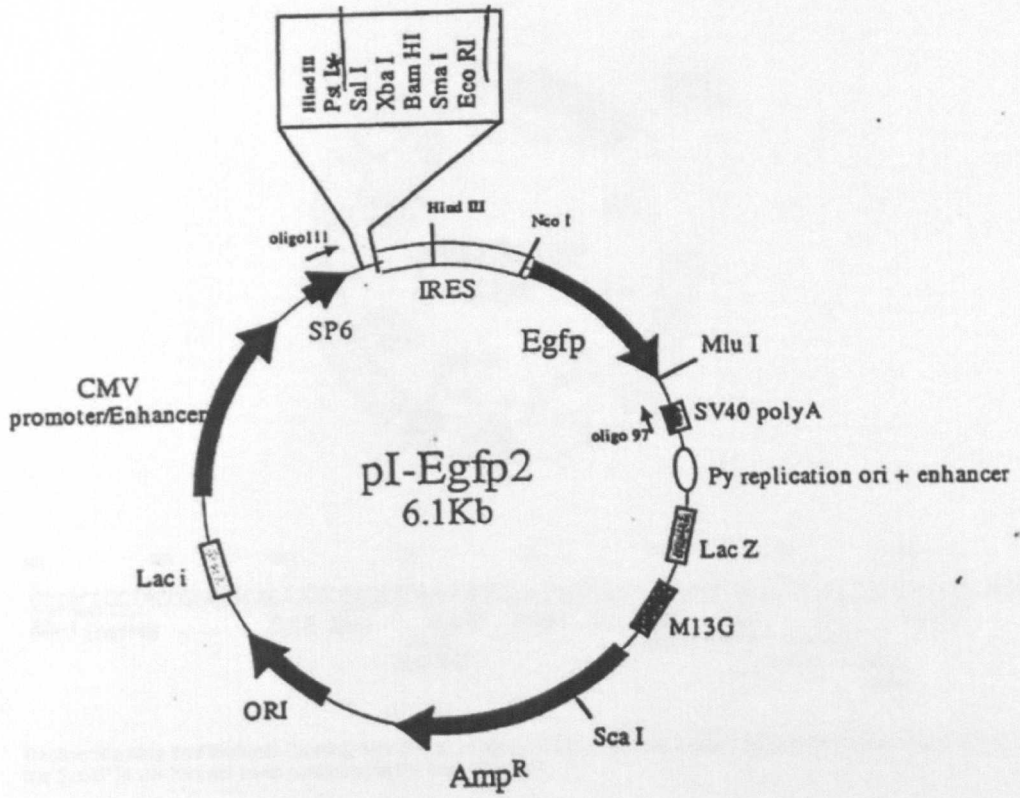
1. The trypan blue is used to stain any dead cells. Cells looking faint or dark blue within the grid being counted are counted as dead cells. To check the viability of the cells requires:

- Live cell count (not including trypan blue cells)
- Total cell count including those stained with trypan blue.

Live cell count/Total cell count = percentage viability.

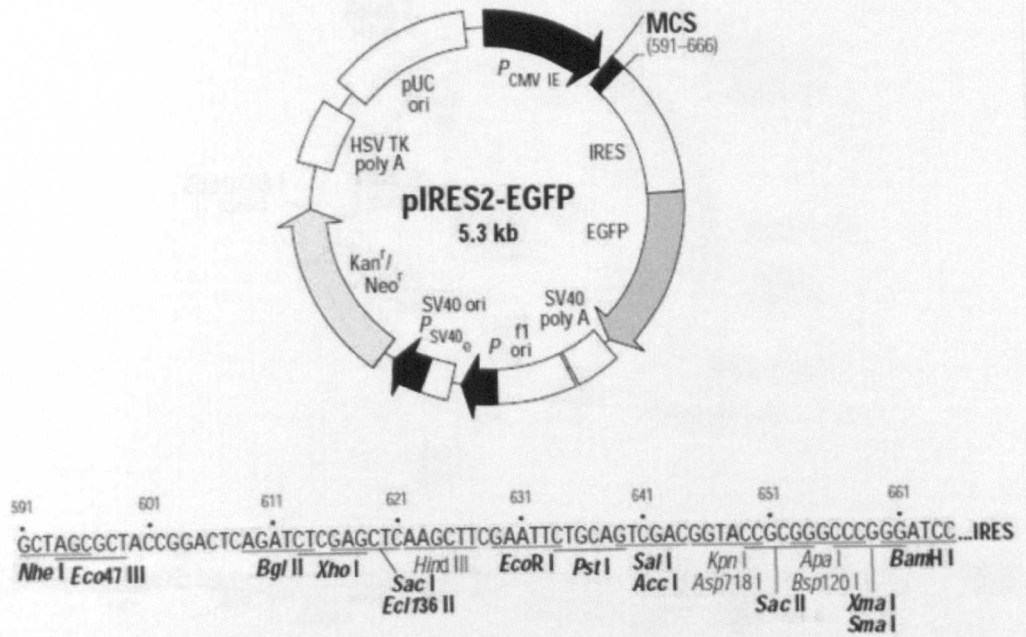
Example;  $\frac{45 \times 10^4/ml}{46 \times 10^4/ml} = 0.978 = 97.8\% \text{ viability}$

### Appendix 4: pI-EGFP2 vector map



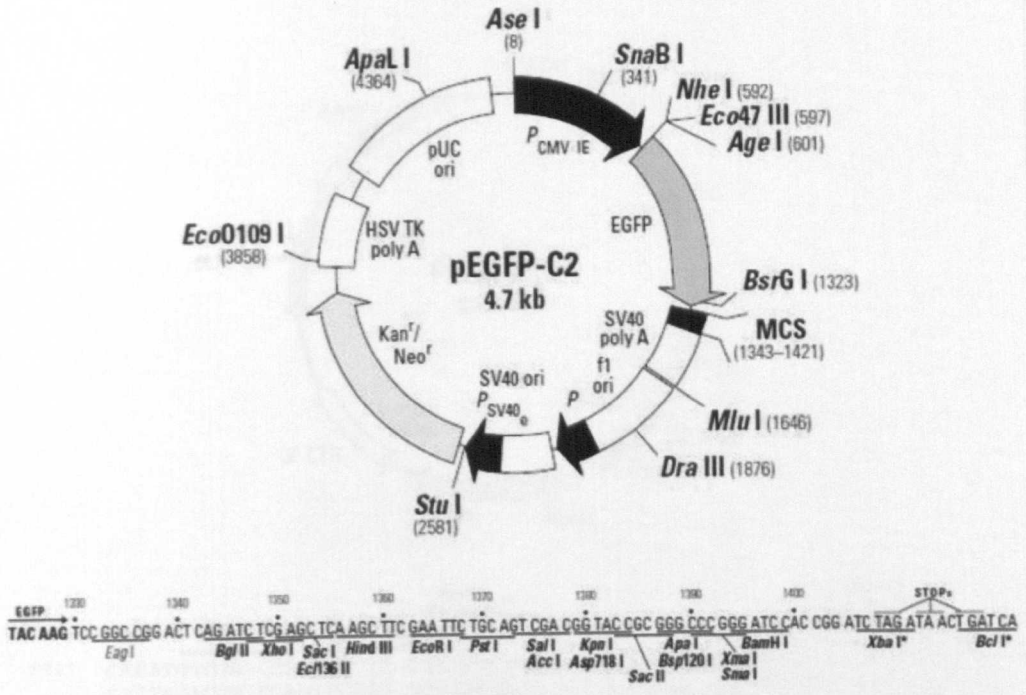
This vector was reconstructed by Dr. Nateri (see section 3.2.3.1).

## Appendix 5: pIRES2-EGFP vector map



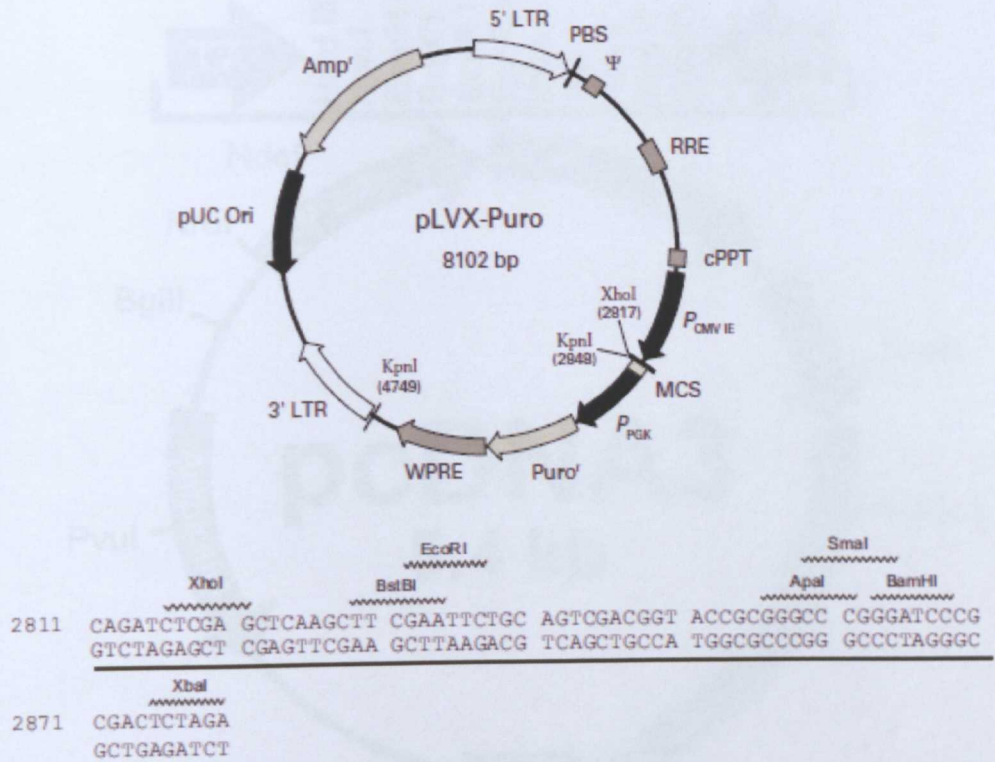
Restriction Map and Multiple Cloning Site (MCS) of pIRES2-EGFP Vector. Unique restriction sites are in bold. Note that the *Eco47 III* site has not been confirmed in the final construct.

## Appendix 6: pEGFP-C2 vector map



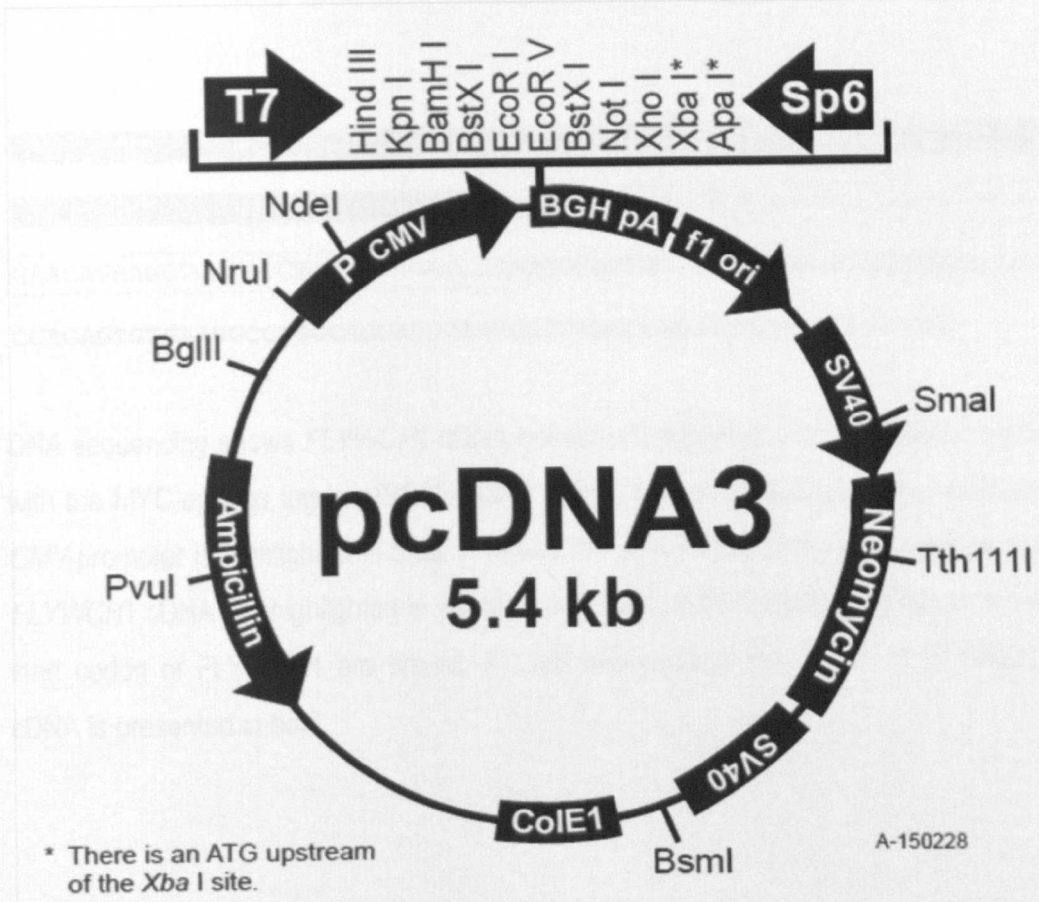
Restriction Map and Multiple Cloning Site (MCS) of pEGFP-C2. (Unique restriction sites are in bold). The *Eag* I site is not unique. The *Xba* I site cannot be used for fusions since it contains an in-frame stop codon. The *Xba* I and *Bcl* I sites (\*) are methylated in the DNA provided by BD Biosciences Clontech. If you wish to digest the vector with these enzymes, you will need to transform the vector into a *dam*<sup>-</sup> host and make fresh DNA.

## Appendix 7: pLVX-Puro vector map



**pLVX-Puro Vector Map and Multiple Cloning Site (MCS).**

Appendix 8: pcDNA3 vector map



## Appendix 9: Sequencing data of MYC-tagged FLYWCH1

```

TCCGCCCATTTGACGCAAATGGGCGGTAGGCGTGTACGGTGGGAGGTCTATATAAGCAGAGC
TGGTTTAGTGAACCGTCAGATCCGCTAGCATGGAGCAGAACTCATCTCTGAAGAAGATCTG
GAACAGAAGCTCATCTCTGAGGAAGATCTGATGCCCTGCCGAGCCAGCGAGCAGGAGGG
CGAGAGTGTGAAGCCGGCCAGGAGCCATCCCCAAGCCAGGCACGGACGTCATCCC

```

DNA sequencing shows *FLYWCH1* cDNA correct orientation and in-frame construction with the MYC-epitope tag in pIRES2-EGFP vector. A short sequence of the upstream *CMV*-promoter is highlighted in blue, whereas the start codon of the MYC-epitope and *FLYWCH1* cDNA are highlighted in yellow. Two copies of MYC-epitope upstream to the start codon of *FLYWCH1* are boxed. A short sequence of the 5' end of *FLYWCH1* cDNA is presented in bold.

## Appendix 10: NCBI primer blast for c-Jun qRT-PCR primers.

	Sequence (5'->3')	Length	Tm	GC%
<b>Forward primer</b>	ACCCAAGATCCTGAAACAG	20	57.11	50.00
<b>Reverse primer</b>	ATCAGGCGCTCCAGCTCG	18	62.22	66.67

**Products on target templates**

>[NM\\_002228.3](#) Homo sapiens jun proto-oncogene (JUN), mRNA

```
product length = 151
Forward primer 1   ACCCCAAGATCCTGAAACAG  20
Template       1132 ..... 1151

Reverse primer 1   ATCAGGCGCTCCAGCTCG  18
Template       1282 ..... 1265
```

>[NM\\_002229.2](#) Homo sapiens jun B proto-oncogene (JUNB), mRNA

```
product length = 181
Forward primer 1   ACCCCAAGATCCTGAAACAG  20
Template       368 ..TA...AC.....C.  387

Reverse primer 1   ATCAGGCGCTCCAGCTCG  18
Template       548 .....T.....C  531
```

>[NM\\_025055.3](#) Homo sapiens coiled-coil domain containing 33 (CCDC33), transcript variant 1, mRNA

```
product length = 2241
Forward primer 1   ACCCCAAGATCCTGAAACAG  20
Template       349 T.....TG.T.....A  368

Reverse primer 1   ATCAGGCGCTCCAGCTCG  18
Template       2589 .G....G.....T  2572
```

## Appendix 11: NCBI nucleotide blast of FLYWCH1 probe against human genomic and transcript database.

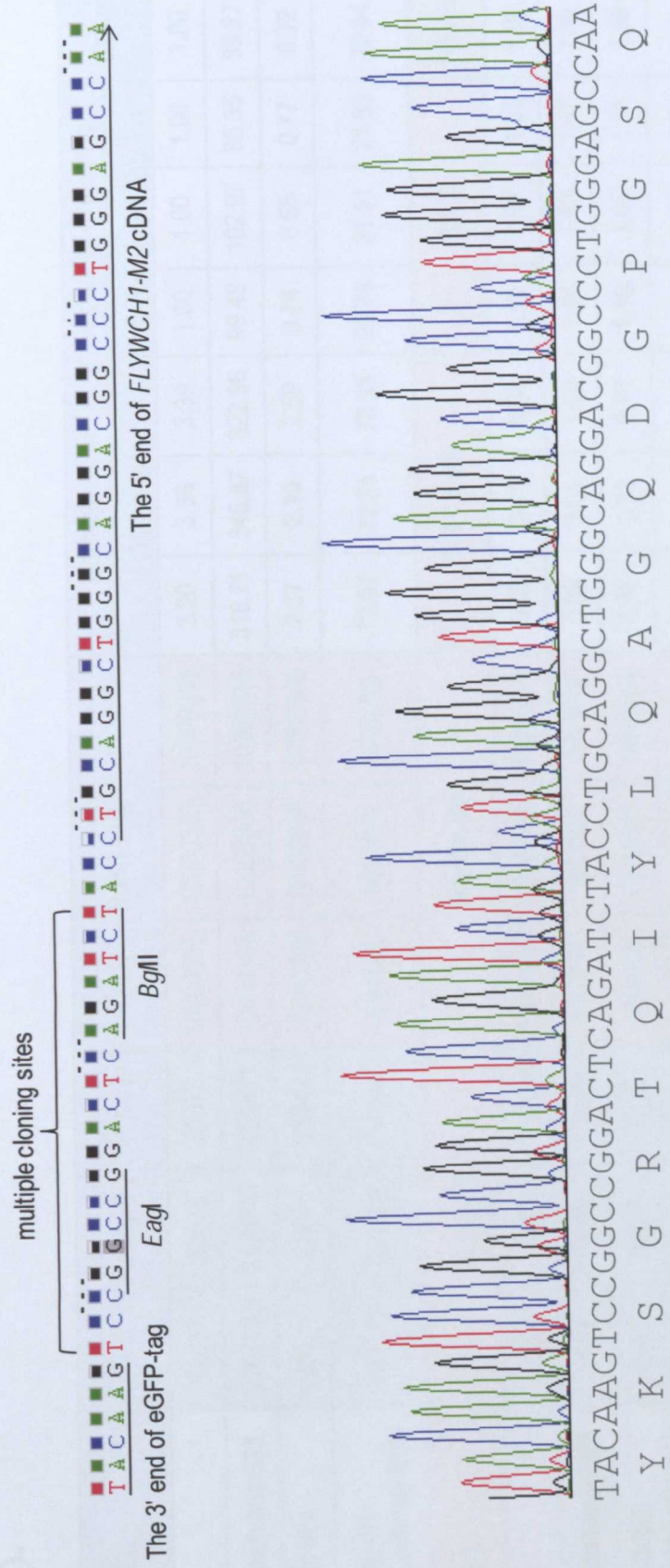
Accession	Description	<u>Max score</u>	<u>Total score</u>	<u>Query coverage</u>	<u>E value</u>	<u>Max ident</u>
<b>Transcripts</b>						
<u>NM_020912.1</u>	Homo sapiens FLYWCH-type zinc finger 1 (FLYWCH1), transcript variant 2, mRNA	<u>1182</u>	1182	100%	0.0	99%
<u>NM_032296.2</u>	Homo sapiens FLYWCH-type zinc finger 1 (FLYWCH1), transcript variant 1, mRNA	<u>1182</u>	1182	100%	0.0	99%
<b>Genomic sequences[show first]</b>						
<u>NT_010393.16</u>	Homo sapiens chromosome 16 genomic contig, GRCh37.p5 Primary Assembly	<u>878</u>	1174	97%	0.0	100%
<u>NW_001838341.1</u>	Homo sapiens chromosome 16 genomic contig, alternate assembly HuRef SCAF_1103279188148, whole genome shotgun sequence	<u>878</u>	1174	97%	0.0	100%
<u>NT_005612.16</u>	Homo sapiens chromosome 3 genomic contig, GRCh37.p5 Primary Assembly	<u>852</u>	852	99%	0.0	91%

## Appendix 12: NCBI nucleotide blast of FLYWCH1 probe against mouse genomic and transcript database.

database.

<u>Accession</u>	<u>Description</u>	<u>Max score</u>	<u>Total score</u>	<u>Query coverage</u>	<u>E value</u>	<u>Max ident</u>
<b>Transcripts</b>						
<u>NM_153791.2</u>	Mus musculus FLYWCH-type zinc finger 1 (Flywch1), mRNA	<u>241</u>	808	42%	9e-61	79%
<u>NM_027236.2</u>	Mus musculus eukaryotic translation initiation factor 1A domain containing (Eif1ad), mRNA	<u>39.2</u>	39.2	3%	5.4	92%
<u>NM_172149.5</u>	Mus musculus BCL2/adenovirus E1B interacting protein 1 (Bnip1), mRNA	<u>39.2</u>	39.2	6%	5.4	80%
<u>NM_134156.2</u>	Mus musculus actinin, alpha 1 (Actn1), mRNA	<u>39.2</u>	39.2	3%	5.4	92%
<b>Genomic sequences[show first]</b>						
<u>NT_039649.8</u>	Mus musculus strain C57BL/6J chromosome 17 genomic contig, GRCm38 C57BL/6J MMCHR17_CTG3_2	<u>237</u>	844	41%	1e-59	80%
<u>NW_001030605.1</u>	Mus musculus strain mixed chromosome 17 genomic scaffold, alternate assembly Mm_Celera 232000009790952, whole genome shotgun sequence	<u>237</u>	844	41%	1e-59	80%

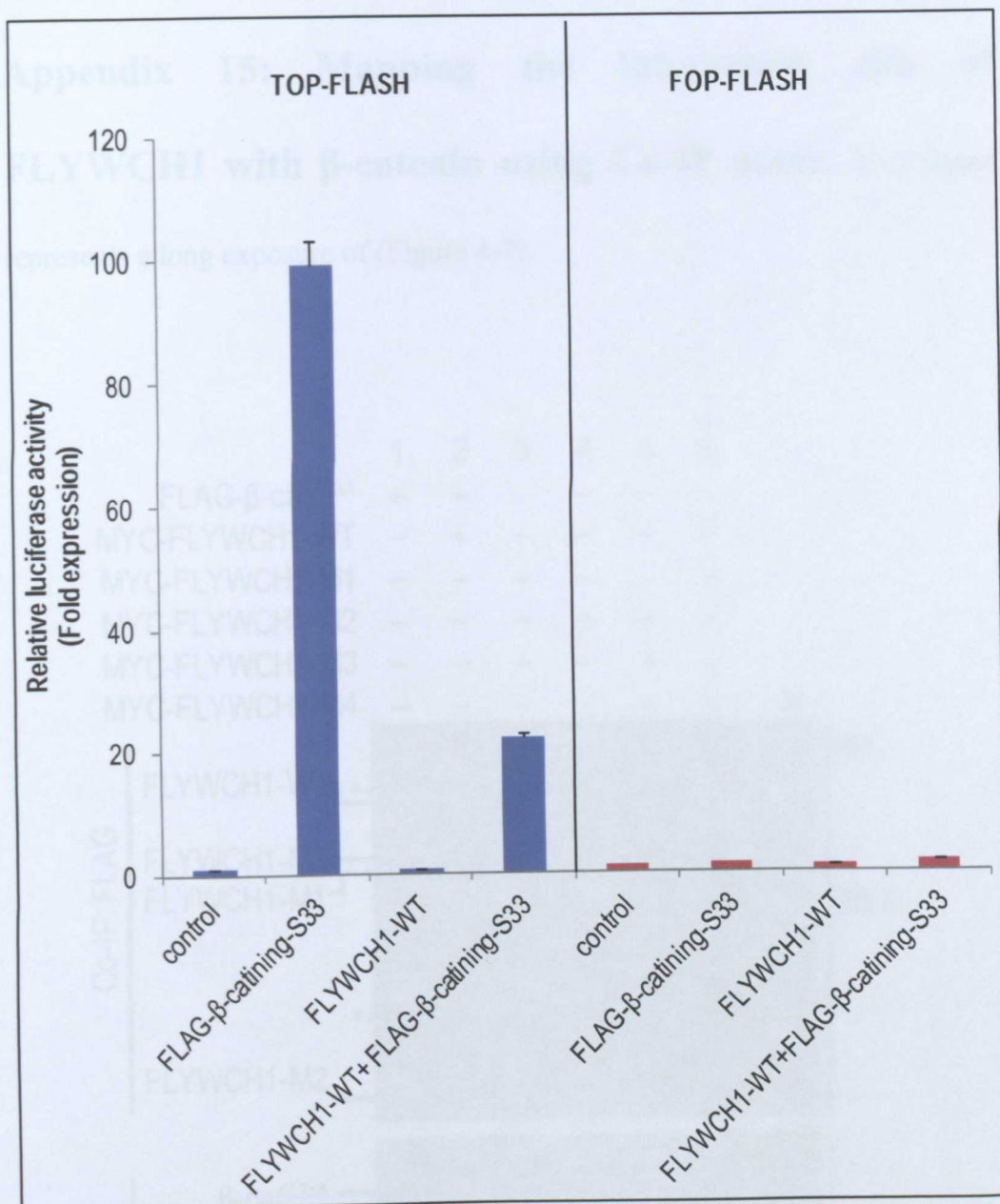
### Appendix 13: Sequencing results for eGFP-FLYWCH1-M2 ( $\Delta$ N350).



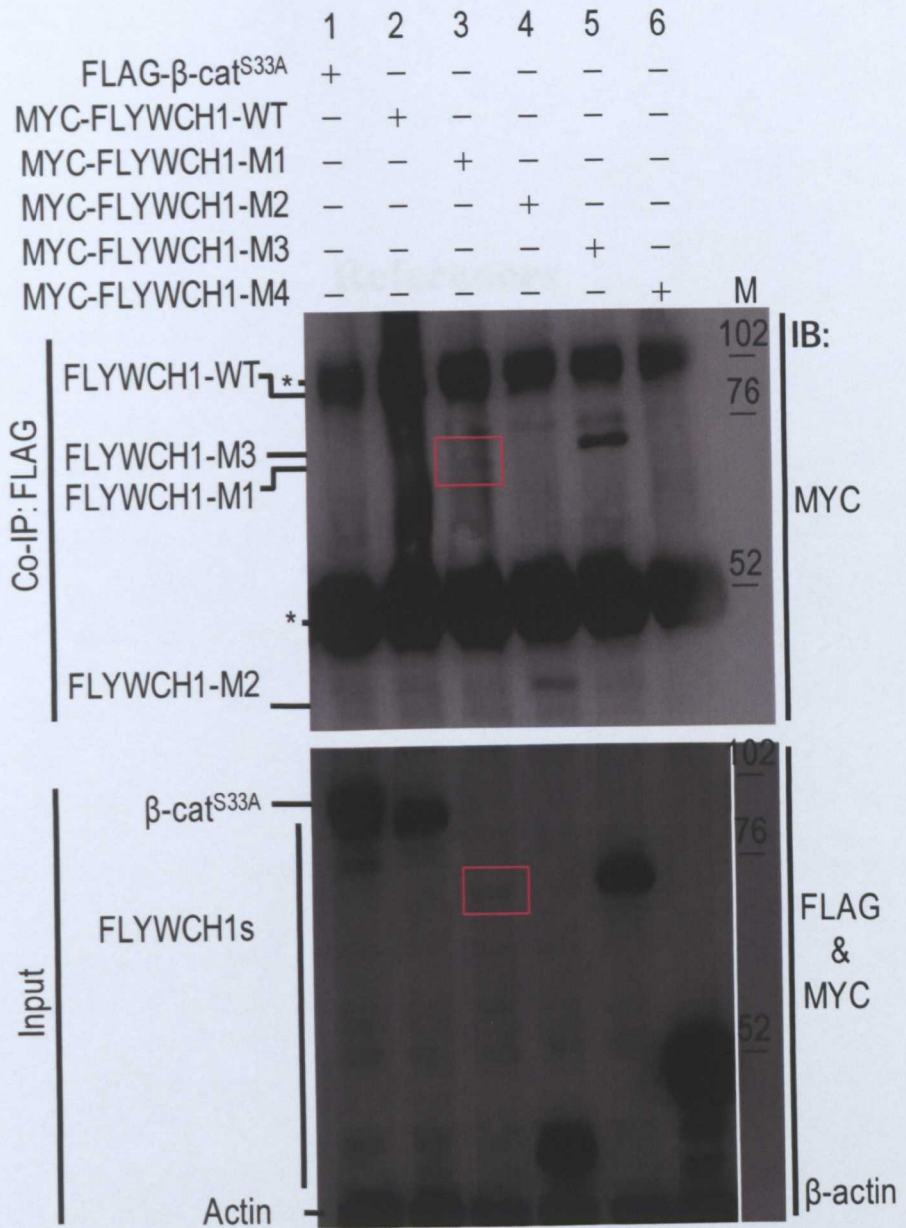
The sequencing data shows the in-frame construction of the 5' end of the deletion mutant FLYWCH1-M2 with the eGFP epitope tag of pEGFP-C2 plasmid vector. The data also shows that the open reading frame is maintained.

**Appendix 14: Raw data shows the calculation method of luciferase assay as outlined in (section 2.2.6.1).**

TOP-Flash	Firefly (F)			Renilla (R)			Normalization			Folds of expression		MEAN	SD
							F/R * 1000			Induction/reduction			
control	32037	33572	33872	10000366	10000365	10000365	3.20	3.36	3.39	1.00	1.00	1.00	0.000
FLAG-β-catining-S33	3187185	3456846	3229671	10000366	10000366	10000365	318.71	345.67	322.96	99.48	102.97	95.35	3.814
FLYWCH1-WT	23664	21888	25942	10000366	10000366	10000366	2.37	2.19	2.59	0.74	0.65	0.77	0.059
FLYWCH1-WT+ FLAG-β-catining-S33	713773	713497	718644	9781649	9880621	9720279	72.97	72.21	73.93	22.78	21.51	21.83	0.660
FOP-Flash	Firefly (F)			Renilla (R)			F/R * 1000			FOLD		MEAN	SD
control	6824	7023	6812	10000362	10000365	10000366	0.68	0.70	0.68	1.00	1.00	1.00	0.000
FLAG-β-catining-S33	9821	9996	9826	9940894	9931985	9793306	0.99	1.01	1.00	1.45	1.43	1.47	0.020
FLYWCH1-WT	6797	6507	7203	9094620	8866517	9590509	0.75	0.73	0.75	1.10	1.05	1.10	0.031
FLYWCH1-WT+FLAG- β-catining-S33	10554	10945	11814	9541398	9826605	9973643	1.11	1.11	1.18	1.62	1.59	1.74	0.080



**Appendix 15: Mapping the interaction site of FLYWCH1 with  $\beta$ -catenin using Co-IP assay.** This figure represents a long exposure of (Figure 4-7).



## **References**

- ABERLE, H., BUTZ, S., STAPPERT, J., WEISSIG, H., KEMLER, R. & HOSCHUETZKY, H. 1994. Assembly of the cadherin-catenin complex in vitro with recombinant proteins. *J Cell Sci*, 107 ( Pt 12), 3655-63.
- ABERLE, H., SCHWARTZ, H., HOSCHUETZKY, H. & KEMLER, R. 1996. Single amino acid substitutions in proteins of the armadillo gene family abolish their binding to alpha-catenin. *J Biol Chem*, 271, 1520-6.
- ADAMSON, A. D., JACKSON, D. & DAVIS, J. R. 2011. Novel approaches to in vitro transgenesis. *J Endocrinol*, 208, 193-206.
- AHMAD, K. F., ENGEL, C. K. & PRIVE, G. G. 1998. Crystal structure of the BTB domain from PLZF. *Proc Natl Acad Sci U S A*, 95, 12123-8.
- AKIYAMA, H., LYONS, J. P., MORI-AKIYAMA, Y., YANG, X., ZHANG, R., ZHANG, Z., DENG, J. M., TAKETO, M. M., NAKAMURA, T., BEHRINGER, R. R., MCCREA, P. D. & DE CROMBRUGGHE, B. 2004. Interactions between Sox9 and beta-catenin control chondrocyte differentiation. *Genes Dev*, 18, 1072-87.
- AL-GHAMDI, S., CACHAT, J., ALBASRI, A., AHMED, M., JACKSON, D., ZAITOUN, A., GUPPY, N., OTTO, W. R., ALISON, M. R., KINDLE, K. B. & ILYAS, M. 2012. C-Terminal Tensin-Like Gene Functions as an Oncogene and Promotes Cell Motility in Pancreatic Cancer. *Pancreas*.
- ALBUQUERQUE, C., BREUKEL, C., VAN DER LUIJT, R., FIDALGO, P., LAGE, P., SLORS, F. J., LEITAO, C. N., FODDE, R. & SMITS, R. 2002. The 'just-right' signaling model: APC somatic mutations are selected based on a specific level of activation of the beta-catenin signaling cascade. *Hum Mol Genet*, 11, 1549-60.
- ALESSI, M., LARKIN, A. L., OGILVIE, K. A., GREEN, L. A., LAI, S., LOPEZ, S. & SNIECKUS, V. 2007. Directed ortho metalation-boronation and Suzuki-Miyaura cross coupling of pyridine derivatives: a one-pot protocol to substituted azabiaryls. *J Org Chem*, 72, 1588-94.
- ALT-HOLLAND, A., SHAMIS, Y., RILEY, K. N., DESROCHERS, T. M., FUSENIG, N. E., HERMAN, I. M. & GARLICK, J. A. 2008. E-cadherin suppression directs cytoskeletal rearrangement and intraepithelial tumor cell migration in 3D human skin equivalents. *J Invest Dermatol*, 128, 2498-507.
- AMAN, A. & PIOTROWSKI, T. 2008. Wnt/beta-catenin and Fgf signaling control collective cell migration by restricting chemokine receptor expression. *Dev Cell*, 15, 749-61.
- AMIT, S., HATZUBAI, A., BIRMAN, Y., ANDERSEN, J. S., BENSHUSHAN, E., MANN, M., BEN-NERIAH, Y. & ALKALAY, I. 2002. Axin-mediated CKI phosphorylation of beta-catenin at Ser 45: a molecular switch for the Wnt pathway. *Genes Dev*, 16, 1066-76.
- ANDONIADOU, C. L., SIGNORE, M., SAJEDI, E., GASTON-MASSUET, C., KELBERMAN, D., BURNS, A. J., ITASAKI, N., DATTANI, M. & MARTINEZ-BARBERA, J. P. 2007. Lack of the murine homeobox

- gene *Hesx1* leads to a posterior transformation of the anterior forebrain. *Development*, 134, 1499-508.
- ANDONIADOU, C. L., SIGNORE, M., YOUNG, R. M., GASTON-MASSUET, C., WILSON, S. W., FUCHS, E. & MARTINEZ-BARBERA, J. P. 2011. HESX1- and TCF3-mediated repression of Wnt/beta-catenin targets is required for normal development of the anterior forebrain. *Development*, 138, 4931-42.
- ANGERS, S. & MOON, R. T. 2009. Proximal events in Wnt signal transduction. *Nat Rev Mol Cell Biol*, 10, 468-77.
- ANGUS-HILL, M. L., ELBERT, K. M., HIDALGO, J. & CAPECCHI, M. R. 2011. T-cell factor 4 functions as a tumor suppressor whose disruption modulates colon cell proliferation and tumorigenesis. *Proc Natl Acad Sci U S A*, 108, 4914-9.
- AOKI, K. & TAKETO, M. M. 2007. Adenomatous polyposis coli (APC): a multi-functional tumor suppressor gene. *J Cell Sci*, 120, 3327-35.
- ARCE, L., YOKOYAMA, N. N. & WATERMAN, M. L. 2006. Diversity of LEF/TCF action in development and disease. *Oncogene*, 25, 7492-504.
- ATCHA, F. A., MUNGUIA, J. E., LI, T. W., HOVANES, K. & WATERMAN, M. L. 2003. A new beta-catenin-dependent activation domain in T cell factor. *J Biol Chem*, 278, 16169-75.
- ATCHA, F. A., SYED, A., WU, B., HOVERTER, N. P., YOKOYAMA, N. N., TING, J. H., MUNGUIA, J. E., MANGALAM, H. J., MARSH, J. L. & WATERMAN, M. L. 2007. A unique DNA binding domain converts T-cell factors into strong Wnt effectors. *Mol Cell Biol*, 27, 8352-63.
- BABAEI-JADIDI, R., LI, N., SAADEDDIN, A., SPENCER-DENE, B., JANDKE, A., MUHAMMAD, B., IBRAHIM, E. E., MURALEEDHARAN, R., ABUZINADAH, M., DAVIS, H., LEWIS, A., WATSON, S., BEHRENS, A., TOMLINSON, I. & NATERI, A. S. 2011. FBXW7 influences murine intestinal homeostasis and cancer, targeting Notch, Jun, and DEK for degradation. *The Journal of Experimental Medicine*, 208, 295-312.
- BAJPAI, R., MAKHIJANI, K., RAO, P. R. & SHASHIDHARA, L. S. 2004. Drosophila Twins regulates Armadillo levels in response to Wg/Wnt signal. *Development*, 131, 1007-16.
- BANZIGER, C., SOLDINI, D., SCHUTT, C., ZIPPERLEN, P., HAUSMANN, G. & BASLER, K. 2006. Wntless, a conserved membrane protein dedicated to the secretion of Wnt proteins from signaling cells. *Cell*, 125, 509-22.
- BARFORD, D. 1995. Protein phosphatases. *Curr Opin Struct Biol*, 5, 728-34.
- BARKER, N. & CLEVERS, H. 2010. Leucine-rich repeat-containing G-protein-coupled receptors as markers of adult stem cells. *Gastroenterology*, 138, 1681-96.
- BARKER, N., HURLSTONE, A., MUSISI, H., MILES, A., BIENZ, M. & CLEVERS, H. 2001. The chromatin remodelling factor Brg-1 interacts

- with beta-catenin to promote target gene activation. *EMBO J*, 20, 4935-43.
- BARKER, N., VAN ES, J. H., KUIPERS, J., KUJALA, P., VAN DEN BORN, M., COZIJNSEN, M., HAEGEBARTH, A., KORVING, J., BEGTHEL, H., PETERS, P. J. & CLEVERS, H. 2007. Identification of stem cells in small intestine and colon by marker gene *Lgr5*. *Nature*, 449, 1003-7.
- BARRIOS, A., POOLE, R. J., DURBIN, L., BRENNAN, C., HOLDER, N. & WILSON, S. W. 2003. Eph/Ephrin signaling regulates the mesenchymal-to-epithelial transition of the paraxial mesoderm during somite morphogenesis. *Curr Biol*, 13, 1571-82.
- BARROSO-DEL JESUS, A., LUCENA-AGUILAR, G. & MENENDEZ, P. 2009. The miR-302-367 cluster as a potential stemness regulator in ESCs. *Cell Cycle*, 8, 394-8.
- BARTH, A. I., POLLACK, A. L., ALTSCHULER, Y., MOSTOV, K. E. & NELSON, W. J. 1997. NH2-terminal deletion of beta-catenin results in stable colocalization of mutant beta-catenin with adenomatous polyposis coli protein and altered MDCK cell adhesion. *J Cell Biol*, 136, 693-706.
- BARTSCHERER, K., PELTE, N., INGELFINGER, D. & BOUTROS, M. 2006. Secretion of Wnt ligands requires Evi, a conserved transmembrane protein. *Cell*, 125, 523-33.
- BATLLE, E., HENDERSON, J. T., BEGTHEL, H., VAN DEN BORN, M. M. W., SANCHO, E., HULS, G., MEELDIJK, J., ROBERTSON, J., VAN DE WETERING, M., PAWSON, T. & CLEVERS, H. 2002. B-Catenin and TCF Mediate Cell Positioning in the Intestinal Epithelium by Controlling the Expression of EphB/EphrinB. *Cell*, 111, 251-263.
- BAUER, A., CHAUVET, S., HUBER, O., USSEGLIO, F., ROTHBACHER, U., ARAGNOL, D., KEMLER, R. & PRADEL, J. 2000. Pontin52 and reptin52 function as antagonistic regulators of beta-catenin signalling activity. *EMBO J*, 19, 6121-30.
- BAUM, B., SETTLEMAN, J. & QUINLAN, M. P. 2008. Transitions between epithelial and mesenchymal states in development and disease. *Semin Cell Dev Biol*, 19, 294-308.
- BAUMANN, M. & MERI, S. 2004. Techniques for studying protein heterogeneity and post-translational modifications. *Expert Rev Proteomics*, 1, 207-17.
- BEASTER-JONES, L. & OKKEMA, P. G. 2004. DNA binding and in vivo function of *C.elegans* PEB-1 require a conserved FLYWCH motif. *J Mol Biol*, 339, 695-706.
- BEHRENS, J., JERCHOW, B. A., WURTELE, M., GRIMM, J., ASBRAND, C., WIRTZ, R., KUHL, M., WEDLICH, D. & BIRCHMEIER, W. 1998. Functional interaction of an axin homolog, conductin, with beta-catenin, APC, and GSK3beta. *Science*, 280, 596-9.

- BEHRENS, J., VON KRIES, J. P., KUHL, M., BRUHN, L., WEDLICH, D., GROSSCHEDL, R. & BIRCHMEIER, W. 1996. Functional interaction of beta-catenin with the transcription factor LEF-1. *Nature*, 382, 638-42.
- BHANOT, P., BRINK, M., SAMOS, C. H., HSIEH, J. C., WANG, Y., MACKE, J. P., ANDREW, D., NATHANS, J. & NUSSE, R. 1996. A new member of the frizzled family from *Drosophila* functions as a Wingless receptor. *Nature*, 382, 225-30.
- BIENZ, M. & CLEVERS, H. 2000. Linking colorectal cancer to Wnt signaling. *Cell*, 103, 311-20.
- BIRD, R. P. 1995. Role of aberrant crypt foci in understanding the pathogenesis of colon cancer. *Cancer Lett*, 93, 55-71.
- BOCHENEK, M. L., DICKINSON, S., ASTIN, J. W., ADAMS, R. H. & NOBES, C. D. 2010. Ephrin-B2 regulates endothelial cell morphology and motility independently of Eph-receptor binding. *J Cell Sci*, 123, 1235-46.
- BOLAND, C. R. & GOEL, A. 2010. Microsatellite instability in colorectal cancer. *Gastroenterology*, 138, 2073-2087 e3.
- BOUWMEESTER, T., KIM, S., SASAI, Y., LU, B. & DE ROBERTIS, E. M. 1996. Cerberus is a head-inducing secreted factor expressed in the anterior endoderm of Spemann's organizer. *Nature*, 382, 595-601.
- BRABLETZ, S., SCHMALHOFER, O. & BRABLETZ, T. 2009. Gastrointestinal stem cells in development and cancer. *J Pathol*, 217, 307-17.
- BRANDENBERGER, R., WEI, H., ZHANG, S., LEI, S., MURAGE, J., FISK, G. J., LI, Y., XU, C., FANG, R., GUEGLER, K., RAO, M. S., MANDALAM, R., LEBKOWSKI, J. & STANTON, L. W. 2004. Transcriptome characterization elucidates signaling networks that control human ES cell growth and differentiation. *Nat Biotechnol*, 22, 707-16.
- BRAYER, K. J. & SEGAL, D. J. 2008. Keep your fingers off my DNA: protein-protein interactions mediated by C2H2 zinc finger domains. *Cell Biochem Biophys*, 50, 111-31.
- BUCHNER, K., ROTH, P., SCHOTTA, G., KRAUSS, V., SAUMWEBER, H., REUTER, G. & DORN, R. 2000. Genetic and molecular complexity of the position effect variegation modifier mod(mdg4) in *Drosophila*. *Genetics*, 155, 141-57.
- BUDA, A. & PIGNATELLI, M. 2011. E-cadherin and the cytoskeletal network in colorectal cancer development and metastasis. *Cell Commun Adhes*, 18, 133-43.
- CADIGAN, K. M. & NUSSE, R. 1997. Wnt signaling: a common theme in animal development. *Genes Dev*, 11, 3286-305.
- CALISTRI, D., RENGUCCI, C., SEYMOUR, I., LEONARDI, E., TRUINI, M., MALACARNE, D., CASTAGNOLA, P. & GIARETTI, W. 2006.

- KRAS, p53 and BRAF gene mutations and aneuploidy in sporadic colorectal cancer progression. *Cell Oncol*, 28, 161-6.
- CAVALLO, R. A., COX, R. T., MOLINE, M. M., ROOSE, J., POLEVOY, G. A., CLEVERS, H., PEIFER, M. & BEJSOVEC, A. 1998. Drosophila Tcf and Groucho interact to repress Wingless signalling activity. *Nature*, 395, 604-8.
- CHELSKY, D., RALPH, R. & JONAK, G. 1989. Sequence requirements for synthetic peptide-mediated translocation to the nucleus. *Mol Cell Biol*, 9, 2487-92.
- CHEN, X., WANG, Y., XIA, H., WANG, Q., JIANG, X., LIN, Z., MA, Y., YANG, Y. & HU, M. 2012. Loss of E-cadherin promotes the growth, invasion and drug resistance of colorectal cancer cells and is associated with liver metastasis. *Mol Biol Rep*, 39, 6707-14.
- CHENG, Y., GENG, H., CHENG, S. H., LIANG, P., BAI, Y., LI, J., SRIVASTAVA, G., NG, M. H., FUKAGAWA, T., WU, X., CHAN, A. T. & TAO, Q. 2010. KRAB zinc finger protein ZNF382 is a proapoptotic tumor suppressor that represses multiple oncogenes and is commonly silenced in multiple carcinomas. *Cancer Res*, 70, 6516-26.
- CHEW, L. J., SHEN, W., MING, X., SENATOROV, V. V., JR., CHEN, H. L., CHENG, Y., HONG, E., KNOBLACH, S. & GALLO, V. 2011. SRY-box containing gene 17 regulates the Wnt/beta-catenin signaling pathway in oligodendrocyte progenitor cells. *J Neurosci*, 31, 13921-35.
- CLARK, C. E., NOURSE, C. C. & COOPER, H. M. 2012. The Tangled Web of Non-Canonical Wnt Signalling in Neural Migration. *Neurosignals*.
- CLEVERS, H. 2006. Wnt/beta-catenin signaling in development and disease. *Cell*, 127, 469-80.
- CLEVERS, H. & BATLLE, E. 2006. EphB/EphrinB receptors and Wnt signaling in colorectal cancer. *Cancer Res*, 66, 2-5.
- CLEVERS, H. & NUSSE, R. 2012. Wnt/beta-Catenin Signaling and Disease. *Cell*, 149, 1192-205.
- CLEVERS, H. & VAN DE WETERING, M. 1997. TCF/LEF factor earn their wings. *Trends Genet*, 13, 485-9.
- COOMBER, B. L. & GOTLIEB, A. I. 1990. In vitro endothelial wound repair. Interaction of cell migration and proliferation. *Arteriosclerosis*, 10, 215-22.
- CORTINA, C., PALOMO-PONCE, S., IGLESIAS, M., FERNANDEZ-MASIP, J. L., VIVANCOS, A., WHISSELL, G., HUMA, M., PEIRO, N., GALLEGO, L., JONKHEER, S., DAVY, A., LLORETA, J., SANCHO, E. & BATLLE, E. 2007. EphB-ephrin-B interactions suppress colorectal cancer progression by compartmentalizing tumor cells. *Nat Genet*, 39, 1376-1383.
- CUNNINGHAM, D., ATKIN, W., LENZ, H. J., LYNCH, H. T., MINSKY, B., NORDLINGER, B. & STARLING, N. 2010. Colorectal cancer. *Lancet*, 375, 1030-47.

- DAHLIN, A. M., PALMQVIST, R., HENRIKSSON, M. L., JACOBSSON, M., EKLOF, V., RUTEGARD, J., OBERG, A. & VAN GUELPEN, B. R. 2010. The role of the CpG island methylator phenotype in colorectal cancer prognosis depends on microsatellite instability screening status. *Clin Cancer Res*, 16, 1845-55.
- DAI, M. S., SUN, X. X., QIN, J., SMOLIK, S. M. & LU, H. 2004. Identification and characterization of a novel *Drosophila melanogaster* glutathione S-transferase-containing FLYWCH zinc finger protein. *Gene*, 342, 49-56.
- DANIELS, D. L. & WEIS, W. I. 2005. Beta-catenin directly displaces Groucho/TLE repressors from Tcf/Lef in Wnt-mediated transcription activation. *Nat Struct Mol Biol*, 12, 364-71.
- DE, A. 2011. Wnt/Ca<sup>2+</sup> signaling pathway: a brief overview. *Acta Biochim Biophys Sin (Shanghai)*, 43, 745-56.
- DE LA ROCHE, M., WORM, J. & BIENZ, M. 2008. The function of BCL9 in Wnt/beta-catenin signaling and colorectal cancer cells. *BMC Cancer*, 8, 199.
- DE LAU, W., BARKER, N., LOW, T. Y., KOO, B. K., LI, V. S., TEUNISSEN, H., KUJALA, P., HAEGEBARTH, A., PETERS, P. J., VAN DE WETERING, M., STANGE, D. E., VAN ES, J. E., GUARDAVACCARO, D., SCHASFOORT, R. B., MOHRI, Y., NISHIMORI, K., MOHAMMED, S., HECK, A. J. & CLEVERS, H. 2011. Lgr5 homologues associate with Wnt receptors and mediate R-spondin signalling. *Nature*, 476, 293-7.
- DELMAS, V., BEERMANN, F., MARTINOZZI, S., CARREIRA, S., ACKERMANN, J., KUMASAKA, M., DENAT, L., GOODALL, J., LUCIANI, F., VIROS, A., DEMIRKAN, N., BASTIAN, B. C., GODING, C. R. & LARUE, L. 2007. Beta-catenin induces immortalization of melanocytes by suppressing p16INK4a expression and cooperates with N-Ras in melanoma development. *Genes Dev*, 21, 2923-35.
- DINGWALL, C. & LASKEY, R. A. 1991. Nuclear targeting sequences--a consensus? *Trends Biochem Sci*, 16, 478-81.
- DORN, R. & KRAUSS, V. 2003. The modifier of mdg4 locus in *Drosophila*: functional complexity is resolved by trans splicing. *Genetica*, 117, 165-77.
- DURANTON, B., HOLL, V., SCHNEIDER, Y., CARNESECCHI, S., GOSSE, F., RAUL, F. & SEILER, N. 2003. Polyamine metabolism in primary human colon adenocarcinoma cells (SW480) and their lymph node metastatic derivatives (SW620). *Amino Acids*, 24, 63-72.
- DUVAL, A., GAYET, J., ZHOU, X. P., IACOPETTA, B., THOMAS, G. & HAMELIN, R. 1999. Frequent frameshift mutations of the TCF-4 gene in colorectal cancers with microsatellite instability. *Cancer Res*, 59, 4213-5.

- EASWARAN, V., PISHVAIAN, M., SALIMUDDIN & BYERS, S. 1999. Cross-regulation of beta-catenin-LEF/TCF and retinoid signaling pathways. *Curr Biol*, 9, 1415-8.
- EFERL, R. & WAGNER, E. F. 2003. AP-1: a double-edged sword in tumorigenesis. *Nat Rev Cancer*, 3, 859-68.
- ELSABA, T. M., MARTINEZ-POMARES, L., ROBINS, A. R., CROOK, S., SETH, R., JACKSON, D., MCCART, A., SILVER, A. R., TOMLINSON, I. P. & ILYAS, M. 2010. The stem cell marker CD133 associates with enhanced colony formation and cell motility in colorectal cancer. *PLoS One*, 5, e10714.
- ENTSCHLADEN, F., DRELL, T. L. T., LANG, K., MASUR, K., PALM, D., BASTIAN, P., NIGGEMANN, B. & ZAENKER, K. S. 2005. Analysis methods of human cell migration. *Exp Cell Res*, 307, 418-26.
- ESSERS, M. A., DE VRIES-SMITS, L. M., BARKER, N., POLDERMAN, P. E., BURGERING, B. M. & KORSWAGEN, H. C. 2005. Functional interaction between beta-catenin and FOXO in oxidative stress signaling. *Science*, 308, 1181-4.
- EVANS, P. M., CHEN, X., ZHANG, W. & LIU, C. 2010. KLF4 interacts with beta-catenin/TCF4 and blocks p300/CBP recruitment by beta-catenin. *Mol Cell Biol*, 30, 372-81.
- FAN, F., SAMUEL, S., GAUR, P., LU, J., DALLAS, N. A., XIA, L., BOSE, D., RAMACHANDRAN, V. & ELLIS, L. M. 2011. Chronic exposure of colorectal cancer cells to bevacizumab promotes compensatory pathways that mediate tumour cell migration. *Br J Cancer*, 104, 1270-7.
- FEARON, E. R. & VOGELSTEIN, B. 1990. A genetic model for colorectal tumorigenesis. *Cell*, 61, 759-67.
- FERNANDEZ, R. M., RUIZ-MIRO, M., DOLCET, X., ALDEA, M. & GARI, E. 2011. Cyclin D1 interacts and collaborates with Ral GTPases enhancing cell detachment and motility. *Oncogene*, 30, 1936-46.
- FEVR, T., ROBINE, S., LOUVARD, D. & HUELSKEN, J. 2007. Wnt/beta-catenin is essential for intestinal homeostasis and maintenance of intestinal stem cells. *Mol Cell Biol*, 27, 7551-9.
- FILALI, M., CHENG, N., ABBOTT, D., LEONTIEV, V. & ENGELHARDT, J. F. 2002. Wnt-3A/beta-catenin signaling induces transcription from the LEF-1 promoter. *J Biol Chem*, 277, 33398-410.
- FINN, R. D., MISTRY, J., TATE, J., COGGILL, P., HEGER, A., POLLINGTON, J. E., GAVIN, O. L., GUNASEKARAN, P., CERIC, G., FORSLUND, K., HOLM, L., SONNHAMMER, E. L. L., EDDY, S. R. & BATEMAN, A. 2010. The Pfam protein families database. *Nucleic Acids Research*, 38, D211-D222.
- FISCHER, A., KLATTIG, J., KNEITZ, B., DIEZ, H., MAIER, M., HOLTSMANN, B., ENGLERT, C. & GESSLER, M. 2005. Hey basic helix-loop-helix transcription factors are repressors of GATA4 and GATA6 and restrict expression of the GATA target gene ANF in fetal hearts. *Mol Cell Biol*, 25, 8960-70.

- FISHEL, R. & WILSON, T. 1997. MutS homologs in mammalian cells. *Curr Opin Genet Dev*, 7, 105-13.
- FODDE, R., SMITS, R. & CLEVERS, H. 2001. APC, signal transduction and genetic instability in colorectal cancer. *Nat Rev Cancer*, 1, 55-67.
- FUERER, C., NUSSE, R. & TEN BERGE, D. 2008. Wnt signalling in development and disease. Max Delbrück Center for Molecular Medicine meeting on Wnt signaling in Development and Disease. *EMBO Rep*, 9, 134-8.
- FUKUSHIMA, H., YAMAMOTO, H., ITOH, F., HORIUCHI, S., MIN, Y., IKU, S. & IMAI, K. 2001. Frequent alterations of the beta-catenin and TCF-4 genes, but not of the APC gene, in colon cancers with high-frequency microsatellite instability. *J Exp Clin Cancer Res*, 20, 553-9.
- GALE, N. W., HOLLAND, S. J., VALENZUELA, D. M., FLENNIKEN, A., PAN, L., RYAN, T. E., HENKEMEYER, M., STREBHARDT, K., HIRAI, H., WILKINSON, D. G., PAWSON, T., DAVIS, S. & YANCOPOULOS, G. D. 1996. Eph receptors and ligands comprise two major specificity subclasses and are reciprocally compartmentalized during embryogenesis. *Neuron*, 17, 9-19.
- GAN, X. Q., WANG, J. Y., XI, Y., WU, Z. L., LI, Y. P. & LI, L. 2008. Nuclear Dvl, c-Jun, beta-catenin, and TCF form a complex leading to stabilization of beta-catenin-TCF interaction. *J Cell Biol*, 180, 1087-100.
- GARCIA-ORTEGA, L., DE LOS RIOS, V., MARTINEZ-RUIZ, A., ONADERRA, M., LACADENA, J., MARTINEZ DEL POZO, A. & GAVILANES, J. G. 2005. Anomalous electrophoretic behavior of a very acidic protein: ribonuclease U2. *Electrophoresis*, 26, 3407-13.
- GAUSE, M., MORCILLO, P. & DORSETT, D. 2001. Insulation of enhancer-promoter communication by a gypsy transposon insert in the *Drosophila cut* gene: cooperation between suppressor of hairy-wing and modifier of *mdg4* proteins. *Mol Cell Biol*, 21, 4807-17.
- GENANDER, M., HALFORD, M. M., XU, N. J., ERIKSSON, M., YU, Z., QIU, Z., MARTLING, A., GREICIUS, G., THAKAR, S., CATCHPOLE, T., CHUMLEY, M. J., ZDUNEK, S., WANG, C., HOLM, T., GOFF, S. P., PETTERSSON, S., PESTELL, R. G., HENKEMEYER, M. & FRISEN, J. 2009. Dissociation of EphB2 signaling pathways mediating progenitor cell proliferation and tumor suppression. *Cell*, 139, 679-92.
- GERASIMOVA, T. I., GDULA, D. A., GERASIMOV, D. V., SIMONOVA, O. & CORCES, V. G. 1995. A *Drosophila* protein that imparts directionality on a chromatin insulator is an enhancer of position-effect variegation. *Cell*, 82, 587-97.
- GERBE, F., VAN ES, J. H., MAKRINI, L., BRULIN, B., MELLITZER, G., ROBINE, S., ROMAGNOLO, B., SHROYER, N. F., BOURGAUX, J. F., PIGNODEL, C., CLEVERS, H. & JAY, P. 2011. Distinct ATOH1 and Neurog3 requirements define tuft cells as a new secretory cell type in the intestinal epithelium. *J Cell Biol*, 192, 767-80.

- GHOSH, D., GERASIMOVA, T. I. & CORCES, V. G. 2001. Interactions between the Su(Hw) and Mod(mdg4) proteins required for gypsy insulator function. *EMBO J*, 20, 2518-27.
- GLINKA, A., DOLDE, C., KIRSCH, N., HUANG, Y. L., KAZANSKAYA, O., INGELFINGER, D., BOUTROS, M., CRUCIAT, C. M. & NIEHRS, C. 2011. LGR4 and LGR5 are R-spondin receptors mediating Wnt/beta-catenin and Wnt/PCP signalling. *EMBO Rep*, 12, 1055-61.
- GLINKA, A., WU, W., DELIUS, H., MONAGHAN, A. P., BLUMENSTOCK, C. & NIEHRS, C. 1998. Dickkopf-1 is a member of a new family of secreted proteins and functions in head induction. *Nature*, 391, 357-62.
- GOLDSHMIT, Y. & BOURNE, J. 2010. Up-regulation of EphA4 on astrocytes potentially mediates astrocytic gliosis after cortical lesion in the marmoset monkey. *J Neurotrauma*, 27, 1321-32.
- GOLDSHMIT, Y., SPANEVELLO, M. D., TAJOURI, S., LI, L., ROGERS, F., PEARSE, M., GALEA, M., BARTLETT, P. F., BOYD, A. W. & TURNLEY, A. M. 2011. EphA4 blockers promote axonal regeneration and functional recovery following spinal cord injury in mice. *PLoS One*, 6, e24636.
- GOLLIN, S. M. 2005. Mechanisms leading to chromosomal instability. *Semin Cancer Biol*, 15, 33-42.
- GOODMAN, R. M., THOMBRE, S., FIRTINA, Z., GRAY, D., BETTS, D., ROEBUCK, J., SPANA, E. P. & SELVA, E. M. 2006. Sprinter: a novel transmembrane protein required for Wg secretion and signaling. *Development*, 133, 4901-11.
- GOSS, K. H. & GRODEN, J. 2000. Biology of the adenomatous polyposis coli tumor suppressor. *J Clin Oncol*, 18, 1967-79.
- GOUJON, M., MCWILLIAM, H., LI, W., VALENTIN, F., SQUIZZATO, S., PAERN, J. & LOPEZ, R. 2010. A new bioinformatics analysis tools framework at EMBL-EBI. *Nucleic Acids Res*, 38, W695-9.
- GRAHAM, F. L., SMILEY, J., RUSSELL, W. C. & NAIRN, R. 1977. Characteristics of a human cell line transformed by DNA from human adenovirus type 5. *J Gen Virol*, 36, 59-74.
- GRAHAM, T. A., FERKEY, D. M., MAO, F., KIMELMAN, D. & XU, W. 2001. Tcf4 can specifically recognize beta-catenin using alternative conformations. *Nat Struct Biol*, 8, 1048-52.
- GRAHAM, T. A., WEAVER, C., MAO, F., KIMELMAN, D. & XU, W. 2000. Crystal structure of a beta-catenin/Tcf complex. *Cell*, 103, 885-96.
- GRILL, M. A., BALES, M. A., FOUGHT, A. N., ROSBURG, K. C., MUNGER, S. J. & ANTIN, P. B. 2003. Tetracycline-inducible system for regulation of skeletal muscle-specific gene expression in transgenic mice. *Transgenic Res*, 12, 33-43.
- GROPP, M. & REUBINOFF, B. 2006. Lentiviral Vector-Mediated Gene Delivery into Human Embryonic Stem Cells. In: IRINA, K. & ROBERT, L. (eds.) *Methods in Enzymology*. Academic Press.

- GUNTHER, E. J., BELKA, G. K., WERTHEIM, G. B., WANG, J., HARTMAN, J. L., BOXER, R. B. & CHODOSH, L. A. 2002. A novel doxycycline-inducible system for the transgenic analysis of mammary gland biology. *FASEB J*, 16, 283-92.
- HALDIMANN, M., CUSTER, D., MUNARINI, N., STIRNIMANN, C., ZURCHER, G., ROHRBACH, V., DJONOV, V., ZIEMIECKI, A. & ANDRES, A. C. 2009. Deregulated ephrin-B2 expression in the mammary gland interferes with the development of both the glandular epithelium and vasculature and promotes metastasis formation. *Int J Oncol*, 35, 525-36.
- HAN, X. H., JIN, Y. R., SETO, M. & YOON, J. K. 2011. A WNT/beta-catenin signaling activator, R-spondin, plays positive regulatory roles during skeletal myogenesis. *J Biol Chem*, 286, 10649-59.
- HANAHAH, D. & WEINBERG, R. A. 2000. The hallmarks of cancer. *Cell*, 100, 57-70.
- HANAHAH, D. & WEINBERG, R. A. 2011. Hallmarks of cancer: the next generation. *Cell*, 144, 646-74.
- HARTERINK, M. & KORSWAGEN, H. C. 2012. Dissecting the Wnt secretion pathway: key questions on the modification and intracellular trafficking of Wnt proteins. *Acta Physiol (Oxf)*, 204, 8-16.
- HARVEY, A. J., BIDWAI, A. P. & MILLER, L. K. 1997. Doom, a product of the *Drosophila* mod(mdg4) gene, induces apoptosis and binds to baculovirus inhibitor-of-apoptosis proteins. *Mol Cell Biol*, 17, 2835-43.
- HAWCROFT, G., GARDNER, S. H. & HULL, M. A. 2003. Activation of peroxisome proliferator-activated receptor gamma does not explain the antiproliferative activity of the nonsteroidal anti-inflammatory drug indomethacin on human colorectal cancer cells. *J Pharmacol Exp Ther*, 305, 632-7.
- HE, T. C., SPARKS, A. B., RAGO, C., HERMEKING, H., ZAWEL, L., DA COSTA, L. T., MORIN, P. J., VOGELSTEIN, B. & KINZLER, K. W. 1998. Identification of c-MYC as a target of the APC pathway. *Science*, 281, 1509-12.
- HEATH, J. K. 2010. Transcriptional networks and signaling pathways that govern vertebrate intestinal development. *Curr Top Dev Biol*, 90, 159-92.
- HEATH, J. P. 1996. Epithelial cell migration in the intestine. *Cell Biol Int*, 20, 139-46.
- HECHT, A., VLEMINCKX, K., STEMMLER, M. P., VAN ROY, F. & KEMLER, R. 2000. The p300/CBP acetyltransferases function as transcriptional co-activators of beta-catenin in vertebrates. *EMBO J*, 19, 1839-50.
- HECKMAN, K. L. & PEASE, L. R. 2007. Gene splicing and mutagenesis by PCR-driven overlap extension. *Nat Protoc*, 2, 924-32.
- HENDRICKX, M. & LEYNS, L. 2008. Non-conventional Frizzled ligands and Wnt receptors. *Dev Growth Differ*, 50, 229-43.

- HERMISTON, M. L., WONG, M. H. & GORDON, J. I. 1996. Forced expression of E-cadherin in the mouse intestinal epithelium slows cell migration and provides evidence for nonautonomous regulation of cell fate in a self-renewing system. *Genes Dev*, 10, 985-96.
- HINO, S., MICHIEUE, T., ASASHIMA, M. & KIKUCHI, A. 2003. Casein kinase I epsilon enhances the binding of Dvl-1 to Frat-1 and is essential for Wnt-3a-induced accumulation of beta-catenin. *J Biol Chem*, 278, 14066-73.
- HOANG, B. H., THOMAS, J. T., ABDUL-KARIM, F. W., CORREIA, K. M., CONLON, R. A., LUYTEN, F. P. & BALLOCK, R. T. 1998. Expression pattern of two Frizzled-related genes, Frzb-1 and Sfrp-1, during mouse embryogenesis suggests a role for modulating action of Wnt family members. *Dev Dyn*, 212, 364-72.
- HODEL, M. R., CORBETT, A. H. & HODEL, A. E. 2001. Dissection of a nuclear localization signal. *J Biol Chem*, 276, 1317-25.
- HOLMBERG, J., GENANDER, M., HALFORD, M. M., ANNEREN, C., SONDELL, M., CHUMLEY, M. J., SILVANY, R. E., HENKEMEYER, M. & FRISEN, J. 2006. EphB receptors coordinate migration and proliferation in the intestinal stem cell niche. *Cell*, 125, 1151-63.
- HOOGEBOOM, D., ESSERS, M. A., POLDERMAN, P. E., VOETS, E., SMITS, L. M. & BURGERING, B. M. 2008. Interaction of FOXO with beta-catenin inhibits beta-catenin/T cell factor activity. *J Biol Chem*, 283, 9224-30.
- HOSCHUETZKY, H., ABERLE, H. & KEMLER, R. 1994. Beta-catenin mediates the interaction of the cadherin-catenin complex with epidermal growth factor receptor. *J Cell Biol*, 127, 1375-80.
- HOVANES, K., LI, T. W., MUNGUIA, J. E., TRUONG, T., MILOVANOVIC, T., LAWRENCE MARSH, J., HOLCOMBE, R. F. & WATERMAN, M. L. 2001. Beta-catenin-sensitive isoforms of lymphoid enhancer factor-1 are selectively expressed in colon cancer. *Nat Genet*, 28, 53-7.
- HSIEH, J. C., KODJABACHIAN, L., REBBERT, M. L., RATTNER, A., SMALLWOOD, P. M., SAMOS, C. H., NUSSE, R., DAWID, I. B. & NATHANS, J. 1999. A new secreted protein that binds to Wnt proteins and inhibits their activities. *Nature*, 398, 431-6.
- HUANG, D. P., NG, M. H., LO, K. W. & LEE, J. C. 1997. Molecular basis of cancer. *Hong Kong Med J*, 3, 186-194.
- HUANG, L., SHITASHIGE, M., SATOW, R., HONDA, K., ONO, M., YUN, J., TOMIDA, A., TSURUO, T., HIROHASHI, S. & YAMADA, T. 2007. Functional interaction of DNA topoisomerase IIalpha with the beta-catenin and T-cell factor-4 complex. *Gastroenterology*, 133, 1569-78.

- HUBER, A. H., NELSON, W. J. & WEIS, W. I. 1997. Three-dimensional structure of the armadillo repeat region of beta-catenin. *Cell*, 90, 871-82.
- HUBER, A. H. & WEIS, W. I. 2001. The structure of the beta-catenin/E-cadherin complex and the molecular basis of diverse ligand recognition by beta-catenin. *Cell*, 105, 391-402.
- HUGHES, M. R. & HUANG, E. H. 2011. Molecular Basis of Hereditary Colorectal Cancer. *Semin Colon Rectal Surg*, 22, 65-70.
- HULSKEN, J., BIRCHMEIER, W. & BEHRENS, J. 1994. E-cadherin and APC compete for the interaction with beta-catenin and the cytoskeleton. *J Cell Biol*, 127, 2061-9.
- HUMTSOE, J. O., LIU, M., MALIK, A. B. & WARY, K. K. 2010. Lipid phosphate phosphatase 3 stabilization of beta-catenin induces endothelial cell migration and formation of branching point structures. *Mol Cell Biol*, 30, 1593-606.
- HURLSTONE, A. & CLEVERS, H. 2002. T-cell factors: turn-ons and turn-offs. *EMBO J*, 21, 2303-11.
- HURST, L. D. & MERCHANT, A. R. 2001. High guanine-cytosine content is not an adaptation to high temperature: a comparative analysis amongst prokaryotes. *Proc Biol Sci*, 268, 493-7.
- IBRAHIM, E. E., BABAEI-JADIDI, R., SAADEDDIN, A., SPENCER-DENE, B., HOSSAINI, S., ABUZINADAH, M., LI, N., FADHIL, W., ILYAS, M., BONNET, D. & NATERI, A. S. 2012. Embryonic NANOG Activity Defines Colorectal Cancer Stem Cells and Modulated through AP1- and TCF-dependent Mechanisms. *Stem Cells*.
- IDOGAWA, M., MASUTANI, M., SHITASHIGE, M., HONDA, K., TOKINO, T., SHINOMURA, Y., IMAI, K., HIROHASHI, S. & YAMADA, T. 2007. Ku70 and poly(ADP-ribose) polymerase-1 competitively regulate beta-catenin and T-cell factor-4-mediated gene transactivation: possible linkage of DNA damage recognition and Wnt signaling. *Cancer Res*, 67, 911-8.
- IDOGAWA, M., YAMADA, T., HONDA, K., SATO, S., IMAI, K. & HIROHASHI, S. 2005. Poly(ADP-ribose) polymerase-1 is a component of the oncogenic T-cell factor-4/beta-catenin complex. *Gastroenterology*, 128, 1919-36.
- IGUCHI, H., URASHIMA, Y., INAGAKI, Y., IKEDA, Y., OKAMURA, M., TANAKA, T., UCHIDA, A., YAMAMOTO, T. T., KODAMA, T. & SAKAI, J. 2007. SOX6 suppresses cyclin D1 promoter activity by interacting with beta-catenin and histone deacetylase 1, and its down-regulation induces pancreatic beta-cell proliferation. *J Biol Chem*, 282, 19052-61.
- IIOKA, H., DOERNER, S. K. & TAMAI, K. 2009. Kaiso is a bimodal modulator for Wnt/beta-catenin signaling. *FEBS Lett*, 583, 627-32.
- IKEDA, S., KISHIDA, S., YAMAMOTO, H., MURAI, H., KOYAMA, S. & KIKUCHI, A. 1998. Axin, a negative regulator of the Wnt signaling

- pathway, forms a complex with GSK-3 $\beta$  and  $\beta$ -catenin and promotes GSK-3 $\beta$ -dependent phosphorylation of  $\beta$ -catenin. *EMBO J*, 17, 1371-84.
- ILYAS, M., TOMLINSON, I. P., ROWAN, A., PIGNATELLI, M. & BODMER, W. F. 1997.  $\beta$ -catenin mutations in cell lines established from human colorectal cancers. *Proc Natl Acad Sci U S A*, 94, 10330-4.
- ISHITANI, T., NINOMIYA-TSUJI, J., NAGAI, S., NISHITA, M., MENEGHINI, M., BARKER, N., WATERMAN, M., BOWERMAN, B., CLEVERS, H., SHIBUYA, H. & MATSUMOTO, K. 1999. The TAK1-NLK-MAPK-related pathway antagonizes signalling between  $\beta$ -catenin and transcription factor TCF. *Nature*, 399, 798-802.
- ISSA, J. P. 2004. CpG island methylator phenotype in cancer. *Nat Rev Cancer*, 4, 988-93.
- ITASAKI, N., JONES, C. M., MERCURIO, S., ROWE, A., DOMINGOS, P. M., SMITH, J. C. & KRUMLAUF, R. 2003. Wise, a context-dependent activator and inhibitor of Wnt signalling. *Development*, 130, 4295-305.
- ITO, K., LIM, A. C., SALTO-TELLEZ, M., MOTODA, L., OSATO, M., CHUANG, L. S., LEE, C. W., VOON, D. C., KOO, J. K., WANG, H., FUKAMACHI, H. & ITO, Y. 2008. RUNX3 attenuates  $\beta$ -catenin/T cell factors in intestinal tumorigenesis. *Cancer Cell*, 14, 226-37.
- IUCHI, S. 2001. Three classes of C2H2 zinc finger proteins. *Cell Mol Life Sci*, 58, 625-35.
- IUCHI, S. & KULDELL, N. 2005. Zinc finger proteins from atomic contact to cellular function. *Molecular biology intelligence unit*. Georgetown, Tex.
- New York, N.Y.: Landes Bioscience/Eurekah.com ;  
Kluwer Academic/Plenum Publishers.
- JAMORA, C., DASGUPTA, R., KOCIENIEWSKI, P. & FUCHS, E. 2003. Links between signal transduction, transcription and adhesion in epithelial bud development. *Nature*, 422, 317-22.
- JENSEN, L. H., DYSAGER, L., LINDEBJERG, J., KOLVRA, S., BYRIEL, L. & CRUGER, D. G. 2010. Molecular biology from bench-to bedside - which colorectal cancer patients should be referred for genetic counselling and risk assessment. *Eur J Cancer*, 46, 1823-8.
- JIA, Z. 1997. Protein phosphatases: structures and implications. *Biochem Cell Biol*, 75, 17-26.
- JIANG, J. & STRUHL, G. 1998. Regulation of the Hedgehog and Wingless signalling pathways by the F-box/WD40-repeat protein Slimb. *Nature*, 391, 493-6.
- JIAO, X., KATIYAR, S., LIU, M., MUELLER, S. C., LISANTI, M. P., LI, A., PESTELL, T. G., WU, K., JU, X., LI, Z., WAGNER, E. F., TAKEYA, T., WANG, C. & PESTELL, R. G. 2008. Disruption of c-Jun reduces cellular migration and invasion through inhibition of c-Src and hyperactivation of ROCK II kinase. *Mol Biol Cell*, 19, 1378-90.

- JIAO, X., KATIYAR, S., WILLMARTH, N. E., LIU, M., MA, X., FLOMENBERG, N., LISANTI, M. P. & PESTELL, R. G. 2010. c-Jun induces mammary epithelial cellular invasion and breast cancer stem cell expansion. *J Biol Chem*, 285, 8218-26.
- JUDSON, H., STEWART, A., LESLIE, A., PRATT, N. R., BATY, D. U., STEELE, R. J. & CAREY, F. A. 2006. Relationship between point gene mutation, chromosomal abnormality, and tumour suppressor gene methylation status in colorectal adenomas. *J Pathol*, 210, 344-50.
- KAENEL, P., ANTONIJEVIC, M., RICHTER, S., KUCHLER, S., SUTTER, N., WOTZKOW, C., STRANGE, R. & ANDRES, A. C. 2012. Deregulated ephrin-B2 signaling in mammary epithelial cells alters the differentiation pathway. *Int J Oncol*, 40, 357-69.
- KAHLER, R. A. & WESTENDORF, J. J. 2003. Lymphoid enhancer factor-1 and beta-catenin inhibit Runx2-dependent transcriptional activation of the osteocalcin promoter. *J Biol Chem*, 278, 11937-44.
- KAIDI, A., WILLIAMS, A. C. & PARASKEVA, C. 2007. Interaction between beta-catenin and HIF-1 promotes cellular adaptation to hypoxia. *Nat Cell Biol*, 9, 210-7.
- KAJIYAMA, H., KIKKAWA, F., KHIN, E., SHIBATA, K., INO, K. & MIZUTANI, S. 2003. Dipeptidyl peptidase IV overexpression induces up-regulation of E-cadherin and tissue inhibitors of matrix metalloproteinases, resulting in decreased invasive potential in ovarian carcinoma cells. *Cancer Res*, 63, 2278-83.
- KANAZAWA, S., FUJIWARA, T., MATSUZAKI, S., SHINGAKI, K., TANIGUCHI, M., MIYATA, S., TOHYAMA, M., SAKAI, Y., YANO, K., HOSOKAWA, K. & KUBO, T. 2010. bFGF regulates PI3-kinase-Rac1-JNK pathway and promotes fibroblast migration in wound healing. *PLoS One*, 5, e12228.
- KATIYAR, S., JIAO, X., WAGNER, E., LISANTI, M. P. & PESTELL, R. G. 2007. Somatic excision demonstrates that c-Jun induces cellular migration and invasion through induction of stem cell factor. *Mol Cell Biol*, 27, 1356-69.
- KAUFMAN, W. L., KOCCMAN, I., AGRAWAL, V., RAHN, H. P., BESSER, D. & GOSSEN, M. 2008. Homogeneity and persistence of transgene expression by omitting antibiotic selection in cell line isolation. *Nucleic Acids Res*, 36, e111.
- KAZANSKAYA, O., GLINKA, A., DEL BARCO BARRANTES, I., STANNEK, P., NIEHRS, C. & WU, W. 2004. R-Spondin2 is a secreted activator of Wnt/beta-catenin signaling and is required for Xenopus myogenesis. *Dev Cell*, 7, 525-34.
- KELLY, K. F., NG, D. Y., JAYAKUMARAN, G., WOOD, G. A., KOIDE, H. & DOBLE, B. W. 2011. beta-catenin enhances Oct-4 activity and reinforces pluripotency through a TCF-independent mechanism. *Cell Stem Cell*, 8, 214-27.

- KIKUCHI, A. 1999. Roles of Axin in the Wnt signalling pathway. *Cell Signal*, 11, 777-88.
- KIKUCHI, A. 2000. Regulation of beta-catenin signaling in the Wnt pathway. *Biochem Biophys Res Commun*, 268, 243-8.
- KIKUCHI, A. & YAMAMOTO, H. 2008. Tumor formation due to abnormalities in the beta-catenin-independent pathway of Wnt signaling. *Cancer Sci*, 99, 202-8.
- KIM, J. H., KIM, B., CAI, L., CHOI, H. J., OHGI, K. A., TRAN, C., CHEN, C., CHUNG, C. H., HUBER, O., ROSE, D. W., SAWYERS, C. L., ROSENFELD, M. G. & BAEK, S. H. 2005. Transcriptional regulation of a metastasis suppressor gene by Tip60 and beta-catenin complexes. *Nature*, 434, 921-6.
- KIM, S., XU, X., HECHT, A. & BOYER, T. G. 2006. Mediator is a transducer of Wnt/beta-catenin signaling. *J Biol Chem*, 281, 14066-75.
- KIM, Y. S., KANG, H. S. & JETTEN, A. M. 2007. The Kruppel-like zinc finger protein Glis2 functions as a negative modulator of the Wnt/beta-catenin signaling pathway. *FEBS Lett*, 581, 858-64.
- KINZLER, K. W. & VOGELSTEIN, B. 1996. Lessons from hereditary colorectal cancer. *Cell*, 87, 159-70.
- KISHIDA, S., YAMAMOTO, H., HINO, S., IKEDA, S., KISHIDA, M. & KIKUCHI, A. 1999. DIX domains of Dvl and axin are necessary for protein interactions and their ability to regulate beta-catenin stability. *Mol Cell Biol*, 19, 4414-22.
- KISHIDA, S., YAMAMOTO, H., IKEDA, S., KISHIDA, M., SAKAMOTO, I., KOYAMA, S. & KIKUCHI, A. 1998. Axin, a negative regulator of the wnt signaling pathway, directly interacts with adenomatous polyposis coli and regulates the stabilization of beta-catenin. *J Biol Chem*, 273, 10823-6.
- KITAGAWA, M., HATAKEYAMA, S., SHIRANE, M., MATSUMOTO, M., ISHIDA, N., HATTORI, K., NAKAMICHI, I., KIKUCHI, A. & NAKAYAMA, K. 1999. An F-box protein, FWD1, mediates ubiquitin-dependent proteolysis of beta-catenin. *EMBO J*, 18, 2401-10.
- KLUG, A. 2010. The discovery of zinc fingers and their development for practical applications in gene regulation and genome manipulation. *Q Rev Biophys*, 43, 1-21.
- KOENEMAN, K. S. 2009. R-spondin2 is a secreted activator of Wnt/beta-catenin signaling and is required for Xenopus myogenesis Kazanskaya O, Glinka A, del BarcoBarrantes I, Stannek P, Niehrs C, Wu W, Division of Molecular Embryology, Deutsches Krebsforschungszentrum, Heidelberg, Germany. *Urol Oncol*, 27, 111.
- KOHN, A. D. & MOON, R. T. 2005. Wnt and calcium signaling: beta-catenin-independent pathways. *Cell Calcium*, 38, 439-46.
- KOMIYA, Y. & HABAS, R. 2008. Wnt signal transduction pathways. *Organogenesis*, 4, 68-75.

- KORINEK, V., BARKER, N., MOERER, P., VAN DONSELAAR, E., HULS, G., PETERS, P. J. & CLEVERS, H. 1998. Depletion of epithelial stem-cell compartments in the small intestine of mice lacking Tcf-4. *Nat Genet*, 19, 379-83.
- KORINEK, V., BARKER, N., MORIN, P. J., VAN WICHEN, D., DE WEGER, R., KINZLER, K. W., VOGELSTEIN, B. & CLEVERS, H. 1997. Constitutive transcriptional activation by a beta-catenin-Tcf complex in APC<sup>-/-</sup> colon carcinoma. *Science*, 275, 1784-7.
- KOSAKA, Y., KOBAYASHI, N., FUKAZAWA, T., TOTSUGAWA, T., MARUYAMA, M., YONG, C., ARATA, T., IKEDA, H., KOBAYASHI, K., UEDA, T., KURABAYASHI, Y. & TANAKA, N. 2004. Lentivirus-based Gene Delivery in Mouse Embryonic Stem Cells. *Artificial Organs*, 28, 271-277.
- KOUZMENKO, A. P., TAKEYAMA, K., ITO, S., FURUTANI, T., SAWATSUBASHI, S., MAKI, A., SUZUKI, E., KAWASAKI, Y., AKIYAMA, T., TABATA, T. & KATO, S. 2004. Wnt/beta-catenin and estrogen signaling converge in vivo. *J Biol Chem*, 279, 40255-8.
- KRAMPS, T., PETER, O., BRUNNER, E., NELLEN, D., FROESCH, B., CHATTERJEE, S., MURONE, M., ZULLIG, S. & BASLER, K. 2002. Wnt/wingless signaling requires BCL9/legless-mediated recruitment of pygopus to the nuclear beta-catenin-TCF complex. *Cell*, 109, 47-60.
- KRAUSS, V. & DORN, R. 2004. Evolution of the trans-splicing Drosophila locus mod(mdg4) in several species of Diptera and Lepidoptera. *Gene*, 331, 165-76.
- KRISHNA, S. S., MAJUMDAR, I. & GRISHIN, N. V. 2003. Structural classification of zinc fingers: survey and summary. *Nucleic Acids Res*, 31, 532-50.
- KUBENS, B. S. & ZANKER, K. S. 1998. Differences in the migration capacity of primary human colon carcinoma cells (SW480) and their lymph node metastatic derivatives (SW620). *Cancer Lett*, 131, 55-64.
- KUBO, K., SAKAMOTO, A., KOBAYASHI, A., RYBKA, Z., KANNO, Y., NAKAGAWA, H. & TAKATSUJI, H. 1998. Cys2/His2 zinc-finger protein family of petunia: evolution and general mechanism of target-sequence recognition. *Nucleic Acids Res*, 26, 608-15.
- KUHNERT, F., DAVIS, C. R., WANG, H. T., CHU, P., LEE, M., YUAN, J., NUSSE, R. & KUO, C. J. 2004. Essential requirement for Wnt signaling in proliferation of adult small intestine and colon revealed by adenoviral expression of Dickkopf-1. *Proc Natl Acad Sci U S A*, 101, 266-71.
- LABBE, E., LETAMENDIA, A. & ATTISANO, L. 2000. Association of Smads with lymphoid enhancer binding factor 1/T cell-specific factor mediates cooperative signaling by the transforming growth factor-beta and wnt pathways. *Proc Natl Acad Sci U S A*, 97, 8358-63.
- LANDER, A. D., KIMBLE, J., CLEVERS, H., FUCHS, E., MONTARRAS, D., BUCKINGHAM, M., CALOF, A. L., TRUMPP, A. &

- OSKARSSON, T. 2012. What does the concept of the stem cell niche really mean today? *BMC Biol*, 10, 19.
- LE, N. H., FRANKEN, P. & FODDE, R. 2008. Tumour-stroma interactions in colorectal cancer: converging on beta-catenin activation and cancer stemness. *Br J Cancer*, 98, 1886-93.
- LEE, M.-G., CHANG, H.-J., LIN, S.-R., CHENG, T.-L., CHANG, H.-R. & TSAO, D.-A. 2010. TCF-4 Microsatellite Instability Mutation and Expression of Splicing Forms in Human Bladder Cancer. 2, 48-52.
- LEON, O. & ROTH, M. 2000. Zinc fingers: DNA binding and protein-protein interactions. *Biol Res*, 33, 21-30.
- LEUNG, T. H., CHING, Y. P., YAM, J. W., WONG, C. M., YAU, T. O., JIN, D. Y. & NG, I. O. 2005. Deleted in liver cancer 2 (DLC2) suppresses cell transformation by means of inhibition of RhoA activity. *Proc Natl Acad Sci U S A*, 102, 15207-12.
- LI, A., DAWSON, J. C., FORERO-VARGAS, M., SPENCE, H. J., YU, X., KONIG, I., ANDERSON, K. & MACHESKY, L. M. 2010a. The actin-bundling protein fascin stabilizes actin in invadopodia and potentiates protrusive invasion. *Curr Biol*, 20, 339-45.
- LI, F. Q., MOFUNANYA, A., FISCHER, V., HALL, J. & TAKEMARU, K. 2010b. Nuclear-cytoplasmic shuttling of Chibby controls beta-catenin signaling. *Mol Biol Cell*, 21, 311-22.
- LI, V. S., NG, S. S., BOERSEMA, P. J., LOW, T. Y., KARTHAUS, W. R., GERLACH, J. P., MOHAMMED, S., HECK, A. J., MAURICE, M. M., MAHMOUDI, T. & CLEVERS, H. 2012. Wnt Signaling through Inhibition of beta-Catenin Degradation in an Intact Axin1 Complex. *Cell*, 149, 1245-56.
- LI, Z., WANG, C., JIAO, X., LU, Y., FU, M., QUONG, A. A., DYE, C., YANG, J., DAI, M., JU, X., ZHANG, X., LI, A., BURBELO, P., STANLEY, E. R. & PESTELL, R. G. 2006a. Cyclin D1 regulates cellular migration through the inhibition of thrombospondin 1 and ROCK signaling. *Mol Cell Biol*, 26, 4240-56.
- LI, Z., WANG, C., PRENDERGAST, G. C. & PESTELL, R. G. 2006b. Cyclin D1 functions in cell migration. *Cell Cycle*, 5, 2440-2.
- LIANG, C.-C., PARK, A. Y. & GUAN, J.-L. 2007. In vitro scratch assay: a convenient and inexpensive method for analysis of cell migration in vitro. *Nat. Protocols*, 2, 329-333.
- LIN, S. L., CHANG, D. C., YING, S. Y., LEU, D. & WU, D. T. 2010. MicroRNA miR-302 inhibits the tumorigenicity of human pluripotent stem cells by coordinate suppression of the CDK2 and CDK4/6 cell cycle pathways. *Cancer Res*, 70, 9473-82.
- LIPCHINA, I., STUDER, L. & BETEL, D. 2012. The expanding role of miR-302-367 in pluripotency and reprogramming. *Cell Cycle*, 11, 1517-23.
- LIU, C., LI, Y., SEMENOV, M., HAN, C., BAEG, G. H., TAN, Y., ZHANG, Z., LIN, X. & HE, X. 2002. Control of beta-catenin

- phosphorylation/degradation by a dual-kinase mechanism. *Cell*, 108, 837-47.
- LIU, H. & NAISMITH, J. H. 2008. An efficient one-step site-directed deletion, insertion, single and multiple-site plasmid mutagenesis protocol. *BMC Biotechnol*, 8, 91.
- LIU, W., DONG, X., MAI, M., SEELAN, R. S., TANIGUCHI, K., KRISHNADATH, K. K., HALLING, K. C., CUNNINGHAM, J. M., BOARDMAN, L. A., QIAN, C., CHRISTENSEN, E., SCHMIDT, S. S., ROCHE, P. C., SMITH, D. I. & THIBODEAU, S. N. 2000. Mutations in AXIN2 cause colorectal cancer with defective mismatch repair by activating beta-catenin/TCF signalling. *Nat Genet*, 26, 146-7.
- LIVAK, K. J. & SCHMITTGEN, T. D. 2001. Analysis of relative gene expression data using real-time quantitative PCR and the 2(-Delta Delta C(T)) Method. *Methods*, 25, 402-8.
- LOEFFLER, M., STEIN, R., WICHMANN, H. E., POTTEN, C. S., KAUR, P. & CHWALINSKI, S. 1986. Intestinal cell proliferation. I. A comprehensive model of steady-state proliferation in the crypt. *Cell Tissue Kinet*, 19, 627-45.
- LOGAN, C. Y. & NUSSE, R. 2004. The Wnt signaling pathway in development and disease. *Annu Rev Cell Dev Biol*, 20, 781-810.
- LORENOWICZ, M. J. & KORSWAGEN, H. C. 2009. Sailing with the Wnt: charting the Wnt processing and secretion route. *Exp Cell Res*, 315, 2683-9.
- LU, W., YAMAMOTO, V., ORTEGA, B. & BALTIMORE, D. 2004. Mammalian Ryk is a Wnt coreceptor required for stimulation of neurite outgrowth. *Cell*, 119, 97-108.
- LUCERO, O. M., DAWSON, D. W., MOON, R. T. & CHIEN, A. J. 2010. A re-evaluation of the "oncogenic" nature of Wnt/beta-catenin signaling in melanoma and other cancers. *Curr Oncol Rep*, 12, 314-8.
- LUO, W., PETERSON, A., GARCIA, B. A., COOMBS, G., KOFAHL, B., HEINRICH, R., SHABANOWITZ, J., HUNT, D. F., YOST, H. J. & VIRSHUP, D. M. 2007. Protein phosphatase 1 regulates assembly and function of the beta-catenin degradation complex. *EMBO J*, 26, 1511-21.
- LUSTIG, B., JERCHOW, B., SACHS, M., WEILER, S., PIETSCH, T., KARSTEN, U., VAN DE WETERING, M., CLEVERS, H., SCHLAG, P. M., BIRCHMEIER, W. & BEHRENS, J. 2002. Negative feedback loop of Wnt signaling through up-regulation of conductin/axin2 in colorectal and liver tumors. *Mol Cell Biol*, 22, 1184-93.
- LYNCH, H. T. & LYNCH, J. 2000. Lynch syndrome: genetics, natural history, genetic counseling, and prevention. *J Clin Oncol*, 18, 19S-31S.
- MACDONALD, B. T., TAMAI, K. & HE, X. 2009. Wnt/beta-catenin signaling: components, mechanisms, and diseases. *Dev Cell*, 17, 9-26.

- MADDEN, S. L., COOK, D. M. & RAUSCHER, F. J., 3RD 1993. A structure-function analysis of transcriptional repression mediated by the WT1, Wilms' tumor suppressor protein. *Oncogene*, 8, 1713-20.
- MAHMOUDI, T., BOJ, S. F., HATZIS, P., LI, V. S., TAOUATAS, N., VRIES, R. G., TEUNISSEN, H., BEGTHEL, H., KORVING, J., MOHAMMED, S., HECK, A. J. & CLEVERS, H. 2010. The leukemia-associated Mlt10/Af10-Dot11 are Tcf4/beta-catenin co-activators essential for intestinal homeostasis. *PLoS Biol*, 8, e1000539.
- MAHMOUDI, T., LI, V. S., NG, S. S., TAOUATAS, N., VRIES, R. G., MOHAMMED, S., HECK, A. J. & CLEVERS, H. 2009. The kinase TNIK is an essential activator of Wnt target genes. *EMBO J*, 28, 3329-40.
- MANI, S. A., GUO, W., LIAO, M. J., EATON, E. N., AYYANAN, A., ZHOU, A. Y., BROOKS, M., REINHARD, F., ZHANG, C. C., SHIPITSIN, M., CAMPBELL, L. L., POLYAK, K., BRISKEN, C., YANG, J. & WEINBERG, R. A. 2008. The epithelial-mesenchymal transition generates cells with properties of stem cells. *Cell*, 133, 704-15.
- MANN, B., GELOS, M., SIEDOW, A., HANSKI, M. L., GRATCHEV, A., ILYAS, M., BODMER, W. F., MOYER, M. P., RIECKEN, E. O., BUHR, H. J. & HANSKI, C. 1999. Target genes of  $\beta$ -catenin-T cell-factor/lymphoid-enhancer-factor signaling in human colorectal carcinomas. *Proceedings of the National Academy of Sciences*, 96, 1603-1608.
- MAO, Q., LI, Y., ZHENG, X., YANG, K., SHEN, H., QIN, J., BAI, Y., KONG, D., JIA, X. & XIE, L. 2008. Up-regulation of E-cadherin by small activating RNA inhibits cell invasion and migration in 5637 human bladder cancer cells. *Biochem Biophys Res Commun*, 375, 566-70.
- MARIKAWA, Y. & ELINSON, R. P. 1998. beta-TrCP is a negative regulator of Wnt/beta-catenin signaling pathway and dorsal axis formation in *Xenopus* embryos. *Mech Dev*, 77, 75-80.
- MARKOWITZ, S. D., DAWSON, D. M., WILLIS, J. & WILLSON, J. K. 2002. Focus on colon cancer. *Cancer Cell*, 1, 233-6.
- MARTINEZ, N. J., OW, M. C., BARRASA, M. I., HAMMELL, M., SEQUERRA, R., DOUCETTE-STAMM, L., ROTH, F. P., AMBROS, V. R. & WALHOUT, A. J. 2008. A *C. elegans* genome-scale microRNA network contains composite feedback motifs with high flux capacity. *Genes Dev*, 22, 2535-49.
- MASON, J. O., KITAJEWSKI, J. & VARMUS, H. E. 1992. Mutational analysis of mouse Wnt-1 identifies two temperature-sensitive alleles and attributes of Wnt-1 protein essential for transformation of a mammary cell line. *Mol Biol Cell*, 3, 521-33.
- MATAGNE, A., JORIS, B. & FRERE, J. M. 1991. Anomalous behaviour of a protein during SDS/PAGE corrected by chemical modification of carboxylic groups. *Biochem J*, 280 ( Pt 2), 553-6.

- MATSUDA, Y., SCHLANGE, T., OAKELEY, E. J., BOULAY, A. & HYNES, N. E. 2009. WNT signaling enhances breast cancer cell motility and blockade of the WNT pathway by sFRP1 suppresses MDA-MB-231 xenograft growth. *Breast Cancer Res*, 11, R32.
- MATTHEWS, J. M. & SUNDE, M. 2002. Zinc fingers--folds for many occasions. *IUBMB Life*, 54, 351-5.
- MENDEZ, M. G., KOJIMA, S. & GOLDMAN, R. D. 2010. Vimentin induces changes in cell shape, motility, and adhesion during the epithelial to mesenchymal transition. *FASEB J*, 24, 1838-51.
- MENG, Q., QI, M., CHEN, D. Z., YUAN, R., GOLDBERG, I. D., ROSEN, E. M., AUBORN, K. & FAN, S. 2000. Suppression of breast cancer invasion and migration by indole-3-carbinol: associated with up-regulation of BRCA1 and E-cadherin/catenin complexes. *J Mol Med (Berl)*, 78, 155-65.
- MI, B., WANG, X., BAI, Y., GONG, W., GENG, Y., WANG, J., ZHANG, H. & JIANG, B. 2009. beta-catenin Expression is Altered in Dysplastic and Nondysplastic Aberrant Crypt Foci of Human Colon. *Appl Immunohistochem Mol Morphol*.
- MICHALEK, J. L., BESOLD, A. N. & MICHEL, S. L. 2011. Cysteine and histidine shuffling: mixing and matching cysteine and histidine residues in zinc finger proteins to afford different folds and function. *Dalton Trans*.
- MIKI, T., YASUDA, S.-Y. & KAHN, M. 2011. Wnt/ $\beta$ -catenin Signaling in Embryonic Stem Cell Self-renewal and Somatic Cell Reprogramming. *Stem Cell Reviews and Reports*, 1-11.
- MILLER, J., MCLACHLAN, A. D. & KLUG, A. 1985. Repetitive zinc-binding domains in the protein transcription factor IIIA from *Xenopus* oocytes. *EMBO J*, 4, 1609-14.
- MILLER, J. R. 2002. The Wnts. *Genome Biol*, 3, REVIEWS3001.
- MILLER, J. R., HOCKING, A. M., BROWN, J. D. & MOON, R. T. 1999. Mechanism and function of signal transduction by the Wnt/ $\beta$ -catenin and Wnt/ $Ca^{2+}$  pathways. *Oncogene*, 18, 7860-72.
- MILLS, J. C. & GORDON, J. I. 2001. The intestinal stem cell niche: there grows the neighborhood. *Proc Natl Acad Sci U S A*, 98, 12334-6.
- MOLENAAR, M., VAN DE WETERING, M., OOSTERWEGEL, M., PETERSON-MADURO, J., GODSAVE, S., KORINEK, V., ROOSE, J., DESTREE, O. & CLEVERS, H. 1996. XTcf-3 transcription factor mediates  $\beta$ -catenin-induced axis formation in *Xenopus* embryos. *Cell*, 86, 391-9.
- MORIN, P. J., SPARKS, A. B., KORINEK, V., BARKER, N., CLEVERS, H., VOGELSTEIN, B. & KINZLER, K. W. 1997. Activation of  $\beta$ -catenin-Tcf signaling in colon cancer by mutations in  $\beta$ -catenin or APC. *Science*, 275, 1787-90.
- MORRIS, E. J., JI, J. Y., YANG, F., DI STEFANO, L., HERR, A., MOON, N. S., KWON, E. J., HAIGIS, K. M., NAAR, A. M. & DYSON, N. J.

2008. E2F1 represses beta-catenin transcription and is antagonized by both pRB and CDK8. *Nature*, 455, 552-6.
- MOSER, A. R., LUONGO, C., GOULD, K. A., MCNELEY, M. K., SHOEMAKER, A. R. & DOVE, W. F. 1995. ApcMin: a mouse model for intestinal and mammary tumorigenesis. *Eur J Cancer*, 31A, 1061-4.
- MOSER, A. R., PITOT, H. C. & DOVE, W. F. 1990. A dominant mutation that predisposes to multiple intestinal neoplasia in the mouse. *Science*, 247, 322-4.
- MOSIMANN, C., HAUSMANN, G. & BASLER, K. 2006. Parafibromin/Hyrax activates Wnt/Wg target gene transcription by direct association with beta-catenin/Armadillo. *Cell*, 125, 327-41.
- MOSIMANN, C., HAUSMANN, G. & BASLER, K. 2009. Beta-catenin hits chromatin: regulation of Wnt target gene activation. *Nat Rev Mol Cell Biol*, 10, 276-86.
- NARAYAN, S. & ROY, D. 2003. Role of APC and DNA mismatch repair genes in the development of colorectal cancers. *Mol Cancer*, 2, 41.
- NATERI, A. S., RIERA-SANS, L., DA COSTA, C. & BEHRENS, A. 2004. The ubiquitin ligase SCFFbw7 antagonizes apoptotic JNK signaling. *Science*, 303, 1374-8.
- NATERI, A. S., SPENCER-DENE, B. & BEHRENS, A. 2005. Interaction of phosphorylated c-Jun with TCF4 regulates intestinal cancer development. *Nature*, 437, 281-5.
- NELSON, C. M., KHAUV, D., BISSELL, M. J. & RADISKY, D. C. 2008. Change in cell shape is required for matrix metalloproteinase-induced epithelial-mesenchymal transition of mammary epithelial cells. *J Cell Biochem*, 105, 25-33.
- NUSSE, R. 2012. Wnt signaling. *Cold Spring Harb Perspect Biol*, 4.
- NUSSE, R., FUERER, C., CHING, W., HARNISH, K., LOGAN, C., ZENG, A., TEN BERGE, D. & KALANI, Y. 2008. Wnt Signaling and Stem Cell Control. *Cold Spring Harb Symp Quant Biol*.
- NUSSE, R. & VARMUS, H. E. 1982. Many tumors induced by the mouse mammary tumor virus contain a provirus integrated in the same region of the host genome. *Cell*, 31, 99-109.
- O'REILLY, D., QUINN, C. M., EL-SHANAWANY, T., GORDON, S. & GREAVES, D. R. 2003. Multiple Ets factors and interferon regulatory factor-4 modulate CD68 expression in a cell type-specific manner. *J Biol Chem*, 278, 21909-19.
- OGINO, S., NOSHO, K., KIRKNER, G. J., KAWASAKI, T., MEYERHARDT, J. A., LODA, M., GIOVANNUCCI, E. L. & FUCHS, C. S. 2009. CpG island methylator phenotype, microsatellite instability, BRAF mutation and clinical outcome in colon cancer. *Gut*, 58, 90-6.
- OISHI, I., SUZUKI, H., ONISHI, N., TAKADA, R., KANI, S., OHKAWARA, B., KOSHIDA, I., SUZUKI, K., YAMADA, G., SCHWABE, G. C.,

- MUNDLOS, S., SHIBUYA, H., TAKADA, S. & MINAMI, Y. 2003. The receptor tyrosine kinase Ror2 is involved in non-canonical Wnt5a/JNK signalling pathway. *Genes Cells*, 8, 645-54.
- OLSON, L. E., TOLLKUH, J., SCAFOGLIO, C., KRONES, A., ZHANG, J., OHGI, K. A., WU, W., TAKETO, M. M., KEMLER, R., GROSSCHEDL, R., ROSE, D., LI, X. & ROSENFELD, M. G. 2006. Homeodomain-mediated beta-catenin-dependent switching events dictate cell-lineage determination. *Cell*, 125, 593-605.
- OW, M. C., MARTINEZ, N. J., OLSEN, P. H., SILVERMAN, H. S., BARRASA, M. I., CONRADT, B., WALHOUT, A. J. & AMBROS, V. 2008. The FLYWCH transcription factors FLH-1, FLH-2, and FLH-3 repress embryonic expression of microRNA genes in *C. elegans*. *Genes Dev*, 22, 2520-34.
- OZANNE, B. W., SPENCE, H. J., MCGARRY, L. C. & HENNIGAN, R. F. 2007. Transcription factors control invasion: AP-1 the first among equals. *Oncogene*, 26, 1-10.
- PARHAM, J. H., IANNONE, M. A., OVERTON, L. K. & HUTCHINS, J. T. 1998. Optimization of transient gene expression in mammalian cells and potential for scale-up using flow electroporation. *Cytotechnology*, 28, 147-55.
- PARK, J. I., KIM, S. W., LYONS, J. P., JI, H., NGUYEN, T. T., CHO, K., BARTON, M. C., DEROO, T., VLEMINCKX, K., MOON, R. T. & MCCREA, P. D. 2005. Kaiso/p120-catenin and TCF/beta-catenin complexes coordinately regulate canonical Wnt gene targets. *Dev Cell*, 8, 843-54.
- PASQUALE, E. B. 2008. Eph-ephrin bidirectional signaling in physiology and disease. *Cell*, 133, 38-52.
- PASQUALE, E. B. 2010. Eph receptors and ephrins in cancer: bidirectional signalling and beyond. *Nat Rev Cancer*, 10, 165-80.
- PAWLOWSKI, J. E., ERTEL, J. R., ALLEN, M. P., XU, M., BUTLER, C., WILSON, E. M. & WIERMAN, M. E. 2002. Liganded androgen receptor interaction with beta-catenin: nuclear co-localization and modulation of transcriptional activity in neuronal cells. *J Biol Chem*, 277, 20702-10.
- PELENGARIS, S. & KHAN, M. 2003. The c-MYC oncoprotein as a treatment target in cancer and other disorders of cell growth. *Expert Opin Ther Targets*, 7, 623-42.
- PELENGARIS, S., KHAN, M. & EVAN, G. 2002. c-MYC: more than just a matter of life and death. *Nat Rev Cancer*, 2, 764-76.
- PETERSON, T. A., ADADEY, A., SANTANA-CRUZ, I., SUN, Y., WINDER, A. & KANN, M. G. 2010. DMDM: domain mapping of disease mutations. *Bioinformatics*, 26, 2458-2459.
- PHAM, P. L., KAMEN, A. & DUROCHER, Y. 2006. Large-scale transfection of mammalian cells for the fast production of recombinant protein. *Mol Biotechnol*, 34, 225-37.

- PINO, M. S. & CHUNG, D. C. 2010. The chromosomal instability pathway in colon cancer. *Gastroenterology*, 138, 2059-72.
- PINO, M. S., KIKUCHI, H., ZENG, M., HERRAIZ, M. T., SPERDUTI, I., BERGER, D., PARK, D. Y., IAFRATE, A. J., ZUKERBERG, L. R. & CHUNG, D. C. 2010. Epithelial to mesenchymal transition is impaired in colon cancer cells with microsatellite instability. *Gastroenterology*, 138, 1406-17.
- PINTO, D. & CLEVERS, H. 2005. Wnt, stem cells and cancer in the intestine. *Biol Cell*, 97, 185-96.
- PINTO, D., GREGORIEFF, A., BEGTHEL, H. & CLEVERS, H. 2003. Canonical Wnt signals are essential for homeostasis of the intestinal epithelium. *Genes Dev*, 17, 1709-13.
- POLAKIS, P. 2000. Wnt signaling and cancer. *Genes Dev*, 14, 1837-51.
- POLIAKOV, A., COTRINA, M. & WILKINSON, D. G. 2004. Diverse Roles of Eph Receptors and Ephrins in the Regulation of Cell Migration and Tissue Assembly. *Developmental cell*, 7, 465-480.
- PORFIRI, E., RUBINFELD, B., ALBERT, I., HOVANES, K., WATERMAN, M. & POLAKIS, P. 1997. Induction of a beta-catenin-LEF-1 complex by wnt-1 and transforming mutants of beta-catenin. *Oncogene*, 15, 2833-9.
- PORT, F. & BASLER, K. 2010. Wnt trafficking: new insights into Wnt maturation, secretion and spreading. *Traffic*, 11, 1265-71.
- POTTEN, C. S. & LOEFFLER, M. 1990. Stem cells: attributes, cycles, spirals, pitfalls and uncertainties. Lessons for and from the crypt. *Development*, 110, 1001-20.
- PROVOST, E. & SHEARN, A. 2006. The Suppressor of Killer of prune, a unique glutathione S-transferase. *J Bioenerg Biomembr*, 38, 189-95.
- RATH, A., GLIBOWICKA, M., NADEAU, V. G., CHEN, G. & DEBER, C. M. 2009. Detergent binding explains anomalous SDS-PAGE migration of membrane proteins. *Proc Natl Acad Sci U S A*, 106, 1760-5.
- REYA, T. & CLEVERS, H. 2005. Wnt signalling in stem cells and cancer. *Nature*, 434, 843-50.
- RICCI-VITIANI, L., LOMBARDI, D. G., PILOZZI, E., BIFFONI, M., TODARO, M., PESCHLE, C. & DE MARIA, R. 2007. Identification and expansion of human colon-cancer-initiating cells. *Nature*, 445, 111-5.
- RIJSEWIJK, F., SCHUERMANN, M., WAGENAAR, E., PARREN, P., WEIGEL, D. & NUSSE, R. 1987. The Drosophila homolog of the mouse mammary oncogene int-1 is identical to the segment polarity gene wingless. *Cell*, 50, 649-57.
- ROBBINS, J., DILWORTH, S. M., LASKEY, R. A. & DINGWALL, C. 1991. Two interdependent basic domains in nucleoplasmin nuclear targeting sequence: identification of a class of bipartite nuclear targeting sequence. *Cell*, 64, 615-23.

- ROOSE, J., HULS, G., VAN BEEST, M., MOERER, P., VAN DER HORN, K., GOLDSCHMEDING, R., LOGTENBERG, T. & CLEVERS, H. 1999. Synergy between tumor suppressor APC and the beta-catenin-Tcf4 target Tcf1. *Science*, 285, 1923-6.
- ROSA, A. & BRIVANLOU, A. H. 2011. A regulatory circuitry comprised of miR-302 and the transcription factors OCT4 and NR2F2 regulates human embryonic stem cell differentiation. *EMBO J*, 30, 237-48.
- ROSE, M. T. 2012. Effect of growth factors on the migration of equine oral and limb fibroblasts using an in vitro scratch assay. *Vet J*, 193, 539-44.
- ROTHENEDER, H., GEYMAYER, S. & HAIDWEGER, E. 1999. Transcription factors of the Spl family: interaction with E2F and regulation of the murine thymidine kinase promoter. *J Mol Biol*, 293, 1005-15.
- ROUAS, R., UCH, R., CLEUTER, Y., JORDIER, F., BAGNIS, C., MANNONI, P., LEWALLE, P., MARTIAT, P. & VAN DEN BROEKE, A. 2002. Lentiviral-mediated gene delivery in human monocyte-derived dendritic cells: optimized design and procedures for highly efficient transduction compatible with clinical constraints. *Cancer Gene Ther*, 9, 715-24.
- RUBINFELD, B., SOUZA, B., ALBERT, I., MULLER, O., CHAMBERLAIN, S. H., MASIARZ, F. R., MUNEMITSU, S. & POLAKIS, P. 1993. Association of the APC gene product with beta-catenin. *Science*, 262, 1731-4.
- RUZOV, A., HACKETT, J. A., PROKHORTCHOUK, A., REDDINGTON, J. P., MADEJ, M. J., DUNICAN, D. S., PROKHORTCHOUK, E., PENNINGS, S. & MEEHAN, R. R. 2009. The interaction of xKaiso with xTcf3: a revised model for integration of epigenetic and Wnt signalling pathways. *Development*, 136, 723-7.
- SAADEDIN, A., BABAEI-JADIDI, R., SPENCER-DENE, B. & NATERI, A. S. 2009. The links between transcription, beta-catenin/JNK signaling, and carcinogenesis. *Mol Cancer Res*, 7, 1189-96.
- SADOT, E., GEIGER, B., OREN, M. & BEN-ZE'EV, A. 2001. Down-regulation of beta-catenin by activated p53. *Mol Cell Biol*, 21, 6768-81.
- SAMPSON, E. M., HAQUE, Z. K., KU, M. C., TEVOSIAN, S. G., ALBANESE, C., PESTELL, R. G., PAULSON, K. E. & YEE, A. S. 2001. Negative regulation of the Wnt-beta-catenin pathway by the transcriptional repressor HBP1. *EMBO J*, 20, 4500-11.
- SANCHO, R., NATERI, A. S., DE VINUESA, A. G., AGUILERA, C., NYE, E., SPENCER-DENE, B. & BEHRENS, A. 2009. JNK signalling modulates intestinal homeostasis and tumourigenesis in mice. *EMBO J*, 28, 1843-54.
- SANGIORGI, E. & CAPECCHI, M. R. 2008. Bmil is expressed in vivo in intestinal stem cells. *Nat Genet*, 40, 915-20.
- SATO, S., IDOGAWA, M., HONDA, K., FUJII, G., KAWASHIMA, H., TAKEKUMA, K., HOSHIKA, A., HIROHASHI, S. & YAMADA, T.

2005. beta-catenin interacts with the FUS proto-oncogene product and regulates pre-mRNA splicing. *Gastroenterology*, 129, 1225-36.
- SAWAMIPHAK, S., SEIDEL, S., ESSMANN, C. L., WILKINSON, G. A., PITULESCU, M. E., ACKER, T. & ACKER-PALMER, A. 2010. Ephrin-B2 regulates VEGFR2 function in developmental and tumour angiogenesis. *Nature*, 465, 487-91.
- SCHEPSKY, A., BRUSER, K., GUNNARSSON, G. J., GOODALL, J., HALLSSON, J. H., GODING, C. R., STEINGRIMSSON, E. & HECHT, A. 2006. The microphthalmia-associated transcription factor Mitf interacts with beta-catenin to determine target gene expression. *Mol Cell Biol*, 26, 8914-27.
- SCOVILLE, D. H., SATO, T., HE, X. C. & LI, L. 2008. Current view: intestinal stem cells and signaling. *Gastroenterology*, 134, 849-64.
- SEGDITSAS, S. & TOMLINSON, I. 2006. Colorectal cancer and genetic alterations in the Wnt pathway. *Oncogene*, 25, 7531-7.
- SEIDENSTICKER, M. J. & BEHRENS, J. 2000. Biochemical interactions in the wnt pathway. *Biochim Biophys Acta*, 1495, 168-82.
- SEMENOV, M. V., HABAS, R., MACDONALD, B. T. & HE, X. 2007. SnapShot: Noncanonical Wnt Signaling Pathways. *Cell*, 131, 1378.
- SERUP, P. 2012. Signaling pathways regulating murine pancreatic development. *Semin Cell Dev Biol*.
- SETO, E., LEWIS, B. & SHENK, T. 1993. Interaction between transcription factors Sp1 and YY1. *Nature*, 365, 462-4.
- SHIMIZU, Y., IKEDA, S., FUJIMORI, M., KODAMA, S., NAKAHARA, M., OKAJIMA, M. & ASAHARA, T. 2002. Frequent alterations in the Wnt signaling pathway in colorectal cancer with microsatellite instability. *Genes Chromosomes Cancer*, 33, 73-81.
- SHIRAI, A., MATSUYAMA, A., YASHIRODA, Y., HASHIMOTO, A., KAWAMURA, Y., ARAI, R., KOMATSU, Y., HORINOUCHE, S. & YOSHIDA, M. 2008. Global analysis of gel mobility of proteins and its use in target identification. *J Biol Chem*, 283, 10745-52.
- SHITASHIGE, M., HIROHASHI, S. & YAMADA, T. 2008. Wnt signaling inside the nucleus. *Cancer Sci*, 99, 631-7.
- SHITASHIGE, M., NAISHIRO, Y., IDOGAWA, M., HONDA, K., ONO, M., HIROHASHI, S. & YAMADA, T. 2007a. Involvement of splicing factor-1 in beta-catenin/T-cell factor-4-mediated gene transactivation and pre-mRNA splicing. *Gastroenterology*, 132, 1039-54.
- SHITASHIGE, M., SATOW, R., HONDA, K., ONO, M., HIROHASHI, S. & YAMADA, T. 2007b. Increased susceptibility of Sfl(+/-) mice to azoxymethane-induced colon tumorigenesis. *Cancer Sci*, 98, 1862-7.
- SHTUTMAN, M., ZHURINSKY, J., SIMCHA, I., ALBANESE, C., D'AMICO, M., PESTELL, R. & BEN-ZE'EV, A. 1999. The cyclin D1 gene is a target of the  $\beta$ -catenin/LEF-1 pathway. *Proceedings of the National Academy of Sciences*, 96, 5522-5527.

- SINGER, S., MALZ, M., HERPEL, E., WARTH, A., BISSINGER, M., KEITH, M., MULEY, T., MEISTER, M., HOFFMANN, H., PENZEL, R., GDYNIA, G., EHEMANN, V., SCHNABEL, P. A., KUNER, R., HUBER, P., SCHIRMACHER, P. & BREUHAHN, K. 2009. Coordinated expression of stathmin family members by far upstream sequence element-binding protein-1 increases motility in non-small cell lung cancer. *Cancer Res*, 69, 2234-43.
- SINNER, D., KORDICH, J. J., SPENCE, J. R., OPOKA, R., RANKIN, S., LIN, S. C., JONATAN, D., ZORN, A. M. & WELLS, J. M. 2007. Sox17 and Sox4 differentially regulate beta-catenin/T-cell factor activity and proliferation of colon carcinoma cells. *Mol Cell Biol*, 27, 7802-15.
- SINNER, D., RANKIN, S., LEE, M. & ZORN, A. M. 2004. Sox17 and beta-catenin cooperate to regulate the transcription of endodermal genes. *Development*, 131, 3069-80.
- SMOLICH, B. D., MCMAHON, J. A., MCMAHON, A. P. & PAPKOFF, J. 1993. Wnt family proteins are secreted and associated with the cell surface. *Mol Biol Cell*, 4, 1267-75.
- SOBOLESKI, M. R., OAKS, J. & HALFORD, W. P. 2005. Green fluorescent protein is a quantitative reporter of gene expression in individual eukaryotic cells. *FASEB J*, 19, 440-2.
- SOLANAS, G. & BATLLE, E. 2011. Control of cell adhesion and compartmentalization in the intestinal epithelium. *Exp Cell Res*, 317, 2695-701.
- SONG, L. N. & GELMANN, E. P. 2008. Silencing mediator for retinoid and thyroid hormone receptor and nuclear receptor co-repressor attenuate transcriptional activation by the beta-catenin-TCF4 complex. *J Biol Chem*, 283, 25988-99.
- SONI, M. & LAI, F. 2011. Cell-based co-transfection microarrays for use with HEK293T cells on a poly D-lysine-coated polystyrene microplate. *Methods Mol Biol*, 706, 13-25.
- SPENCER, G. J., UTTING, J. C., ETHERIDGE, S. L., ARNETT, T. R. & GENEVER, P. G. 2006. Wnt signalling in osteoblasts regulates expression of the receptor activator of NFkappaB ligand and inhibits osteoclastogenesis in vitro. *J Cell Sci*, 119, 1283-96.
- STAPPENBECK, T. S., WONG, M. H., SAAM, J. R., MYSOREKAR, I. U. & GORDON, J. I. 1998. Notes from some crypt watchers: regulation of renewal in the mouse intestinal epithelium. *Curr Opin Cell Biol*, 10, 702-9.
- STATON, C. A., REED, M. W. & BROWN, N. J. 2009. A critical analysis of current in vitro and in vivo angiogenesis assays. *Int J Exp Pathol*, 90, 195-221.
- STELZL, U., WORM, U., LALOWSKI, M., HAENIG, C., BREMBECK, F. H., GOEHLER, H., STROEDICKE, M., ZENKNER, M., SCHOENHERR, A., KOEPPEN, S., TIMM, J., MINTZLAFF, S.,

- ABRAHAM, C., BOCK, N., KIETZMANN, S., GOEDDE, A., TOKSOZ, E., DROEGE, A., KROBITSCH, S., KORN, B., BIRCHMEIER, W., LEHRACH, H. & WANKER, E. E. 2005. A human protein-protein interaction network: a resource for annotating the proteome. *Cell*, 122, 957-68.
- STROVEL, E. T., WU, D. & SUSSMAN, D. J. 2000. Protein phosphatase 2C $\alpha$  dephosphorylates axin and activates LEF-1-dependent transcription. *J Biol Chem*, 275, 2399-403.
- SU, L. K., KINZLER, K. W., VOGELSTEIN, B., PREISINGER, A. C., MOSER, A. R., LUONGO, C., GOULD, K. A. & DOVE, W. F. 1992. Multiple intestinal neoplasia caused by a mutation in the murine homolog of the APC gene. *Science*, 256, 668-70.
- SUBRAMANYAM, D., LAMOUILLE, S., JUDSON, R. L., LIU, J. Y., BUCAY, N., DERYNCK, R. & BLELLOCH, R. 2011. Multiple targets of miR-302 and miR-372 promote reprogramming of human fibroblasts to induced pluripotent stem cells. *Nat Biotechnol*, 29, 443-8.
- SUGIMURA, R. & LI, L. 2010. Noncanonical Wnt signaling in vertebrate development, stem cells, and diseases. *Birth Defects Res C Embryo Today*, 90, 243-56.
- SUN, Z., CAO, X., JIANG, M. M., QIU, Y., ZHOU, H., CHEN, L., QIN, B., WU, H., JIANG, F., CHEN, J., LIU, J., DAI, Y., CHEN, H. F., HU, Q. Y., WU, Z., ZENG, J. Z., YAO, X. S. & ZHANG, X. K. 2011. Inhibition of [beta]-catenin signaling by nongenomic action of orphan nuclear receptor Nur77. *Oncogene*.
- TAGO, K., NAKAMURA, T., NISHITA, M., HYODO, J., NAGAI, S., MURATA, Y., ADACHI, S., OHWADA, S., MORISHITA, Y., SHIBUYA, H. & AKIYAMA, T. 2000. Inhibition of Wnt signaling by ICAT, a novel beta-catenin-interacting protein. *Genes Dev*, 14, 1741-9.
- TAKAYAMA, S., ROGATSKY, I., SCHWARCZ, L. E. & DARIMONT, B. D. 2006. The glucocorticoid receptor represses cyclin D1 by targeting the Tcf-beta-catenin complex. *J Biol Chem*, 281, 17856-63.
- TAKEMARU, K., YAMAGUCHI, S., LEE, Y. S., ZHANG, Y., CARTHEW, R. W. & MOON, R. T. 2003. Chibby, a nuclear beta-catenin-associated antagonist of the Wnt/Wingless pathway. *Nature*, 422, 905-9.
- TAKEMARU, K. I. & MOON, R. T. 2000. The transcriptional co-activator CBP interacts with beta-catenin to activate gene expression. *J Cell Biol*, 149, 249-54.
- TAMAI, K., SEMENOV, M., KATO, Y., SPOKONY, R., LIU, C., KATSUYAMA, Y., HESS, F., SAINT-JEANNET, J. P. & HE, X. 2000. LDL-receptor-related proteins in Wnt signal transduction. *Nature*, 407, 530-5.
- TEN BERGE, D., KOOLE, W., FUERER, C., FISH, M., EROGLU, E. & NUSSE, R. 2008. Wnt signaling mediates self-organization and axis formation in embryoid bodies. *Cell Stem Cell*, 3, 508-18.

- TETSU, O. & MCCORMICK, F. 1999. [beta]-Catenin regulates expression of cyclin D1 in colon carcinoma cells. *Nature*, 398, 422-426.
- THATCHER, J. D., FERNANDEZ, A. P., BEASTER-JONES, L., HAUN, C. & OKKEMA, P. G. 2001. The *Caenorhabditis elegans* *peb-1* gene encodes a novel DNA-binding protein involved in morphogenesis of the pharynx, vulva, and hindgut. *Dev Biol*, 229, 480-93.
- TOLWINSKI, N. S. & WIESCHAUS, E. 2004. A nuclear function for armadillo/beta-catenin. *PLoS Biol*, 2, E95.
- TOUALBI, K., GULLER, M. C., MAURIZ, J. L., LABALETTE, C., BUENDIA, M. A., MAUVIEL, A. & BERNUAU, D. 2007. Physical and functional cooperation between AP-1 and beta-catenin for the regulation of TCF-dependent genes. *Oncogene*, 26, 3492-502.
- TOWNSLEY, F. M., CLIFFE, A. & BIENZ, M. 2004. Pygopus and Legless target Armadillo/beta-catenin to the nucleus to enable its transcriptional co-activator function. *Nat Cell Biol*, 6, 626-33.
- TZENG, S. L., CHENG, Y. W., LI, C. H., LIN, Y. S., HSU, H. C. & KANG, J. J. 2006. Physiological and functional interactions between Tcf4 and Daxx in colon cancer cells. *J Biol Chem*, 281, 15405-11.
- ULLOA, F., ITASAKI, N. & BRISCOE, J. 2007. Inhibitory Gli3 activity negatively regulates Wnt/beta-catenin signaling. *Curr Biol*, 17, 545-50.
- UNO, S., ENDO, K., JEONG, Y., KAWANA, K., MIYACHI, H., HASHIMOTO, Y. & MAKISHIMA, M. 2009. Suppression of beta-catenin signaling by liver X receptor ligands. *Biochem Pharmacol*, 77, 186-95.
- VADLAMUDI, U., ESPINOZA, H. M., GANGA, M., MARTIN, D. M., LIU, X., ENGELHARDT, J. F. & AMENDT, B. A. 2005. PITX2, beta-catenin and LEF-1 interact to synergistically regulate the LEF-1 promoter. *J Cell Sci*, 118, 1129-37.
- VALENTA, T., LUKAS, J., DOUBRAVSKA, L., FAFILEK, B. & KORINEK, V. 2006. HIC1 attenuates Wnt signaling by recruitment of TCF-4 and beta-catenin to the nuclear bodies. *EMBO J*, 25, 2326-37.
- VALENTA, T., LUKAS, J. & KORINEK, V. 2003. HMG box transcription factor TCF-4's interaction with CtBP1 controls the expression of the Wnt target Axin2/Conductin in human embryonic kidney cells. *Nucleic Acids Res*, 31, 2369-80.
- VAN DE WETERING, M., CAVALLO, R., DOOIJES, D., VAN BEEST, M., VAN ES, J., LOUREIRO, J., YPMA, A., HURSH, D., JONES, T., BEJSOVEC, A., PEIFER, M., MORTIN, M. & CLEVERS, H. 1997. Armadillo coactivates transcription driven by the product of the *Drosophila* segment polarity gene dTCF. *Cell*, 88, 789-99.
- VAN DE WETERING, M., SANCHO, E., VERWEIJ, C., DE LAU, W., OVIING, I., HURLSTONE, A., VAN DER HORN, K., BATLLE, E., COUDREUSE, D., HARAMIS, A. P., TJON-PON-FONG, M., MOERER, P., VAN DEN BORN, M., SOETE, G., PALS, S., EILERS, M., MEDEMA, R. & CLEVERS, H. 2002. The beta-catenin/TCF-4

- complex imposes a crypt progenitor phenotype on colorectal cancer cells. *Cell*, 111, 241-50.
- VAN DER FLIER, L. G. & CLEVERS, H. 2008. Stem Cells, Self-Renewal, and Differentiation in the Intestinal Epithelium. *Annu Rev Physiol*.
- VAN DER FLIER, L. G., SABATES-BELLVER, J., OVIING, I., HAEGEBARTH, A., DE PALO, M., ANTI, M., VAN GIJN, M. E., SUIJKERBUIJK, S., VAN DE WETERING, M., MARRA, G. & CLEVERS, H. 2007. The Intestinal Wnt/TCF Signature. *Gastroenterology*, 132, 628-32.
- VAN NOORT, M. & CLEVERS, H. 2002. TCF transcription factors, mediators of Wnt-signaling in development and cancer. *Dev Biol*, 244, 1-8.
- VAN OUYEN, A. & NUSSE, R. 1984. Structure and nucleotide sequence of the putative mammary oncogene int-1; proviral insertions leave the protein-encoding domain intact. *Cell*, 39, 233-40.
- VEEMAN, M. T., AXELROD, J. D. & MOON, R. T. 2003. A second canon. Functions and mechanisms of beta-catenin-independent Wnt signaling. *Dev Cell*, 5, 367-77.
- VIGNJEVIC, D., KOJIMA, S., ARATYN, Y., DANCIU, O., SVITKINA, T. & BORISY, G. G. 2006. Role of fascin in filopodial protrusion. *J Cell Biol*, 174, 863-75.
- VIGNJEVIC, D., SCHOUMACHER, M., GAVERT, N., JANSSEN, K. P., JIH, G., LAE, M., LOUVARD, D., BEN-ZE'EV, A. & ROBINE, S. 2007. Fascin, a novel target of beta-catenin-TCF signaling, is expressed at the invasive front of human colon cancer. *Cancer Res*, 67, 6844-53.
- VINCZE, T., POSFAI, J. & ROBERTS, R. J. 2003. NEBcutter: A program to cleave DNA with restriction enzymes. *Nucleic Acids Res*, 31, 3688-91.
- VITA, M. & HENRIKSSON, M. 2006. The Myc oncoprotein as a therapeutic target for human cancer. *Semin Cancer Biol*, 16, 318-30.
- WANG, S., CHENG, Y., DU, W., LU, L., ZHOU, L., WANG, H., KANG, W., LI, X., TAO, Q., SUNG, J. J. & YU, J. 2012. Zinc-finger protein 545 is a novel tumour suppressor that acts by inhibiting ribosomal RNA transcription in gastric cancer. *Gut*.
- WANG, W. & MALCOLM, B. A. 2002. Two-stage polymerase chain reaction protocol allowing introduction of multiple mutations, deletions, and insertions, using QuikChange site-directed mutagenesis. *Methods Mol Biol*, 182, 37-43.
- WANG, Y., NAKAYAMA, M., PITULESCU, M. E., SCHMIDT, T. S., BOCHENEK, M. L., SAKAKIBARA, A., ADAMS, S., DAVY, A., DEUTSCH, U., LUTHI, U., BARBERIS, A., BENJAMIN, L. E., MAKINEN, T., NOBES, C. D. & ADAMS, R. H. 2010. Ephrin-B2 controls VEGF-induced angiogenesis and lymphangiogenesis. *Nature*, 465, 483-6.
- WEBSTER, M. T., ROZYCKA, M., SARA, E., DAVIS, E., SMALLEY, M., YOUNG, N., DALE, T. C. & WOOSTER, R. 2000. Sequence variants

- of the axin gene in breast, colon, and other cancers: an analysis of mutations that interfere with GSK3 binding. *Genes Chromosomes Cancer*, 28, 443-53.
- WEGMEYER, H., EGEEA, J., RABE, N., GEZELIUS, H., FILOSA, A., ENJIN, A., VAROQUEAUX, F., DEININGER, K., SCHNUTGEN, F., BROSE, N., KLEIN, R., KULLANDER, K. & BETZ, A. 2007. EphA4-dependent axon guidance is mediated by the RacGAP alpha2-chimaerin. *Neuron*, 55, 756-67.
- WILLERT, K., BROWN, J. D., DANENBERG, E., DUNCAN, A. W., WEISSMAN, I. L., REYA, T., YATES, J. R., 3RD & NUSSE, R. 2003. Wnt proteins are lipid-modified and can act as stem cell growth factors. *Nature*, 423, 448-52.
- WONG, S. Y., CHIAM, K. H., LIM, C. T. & MATSUDAIRA, P. 2010a. Computational model of cell positioning: directed and collective migration in the intestinal crypt epithelium. *J R Soc Interface*, 7 Suppl 3, S351-63.
- WONG, T. S., CHAN, W. S., LI, C. H., LIU, R. W., TANG, W. W., TSAO, S. W., TSANG, R. K., HO, W. K., WEI, W. I. & CHAN, J. Y. 2010b. Curcumin alters the migratory phenotype of nasopharyngeal carcinoma cells through up-regulation of E-cadherin. *Anticancer Res*, 30, 2851-6.
- WU, Y., ZHANG, Y., ZHANG, H., YANG, X., WANG, Y., REN, F., LIU, H., ZHAI, Y., JIA, B., YU, J. & CHANG, Z. 2010. p15RS attenuates Wnt/ $\beta$ -catenin signaling by disrupting  $\beta$ -catenin.TCF4 Interaction. *J Biol Chem*, 285, 34621-31.
- XING, Y., TAKEMARU, K., LIU, J., BERNDT, J. D., ZHENG, J. J., MOON, R. T. & XU, W. 2008. Crystal structure of a full-length beta-catenin. *Structure*, 16, 478-87.
- XU, Q., WANG, Y., DABDOUB, A., SMALLWOOD, P. M., WILLIAMS, J., WOODS, C., KELLEY, M. W., JIANG, L., TASMAN, W., ZHANG, K. & NATHANS, J. 2004. Vascular development in the retina and inner ear: control by Norrin and Frizzled-4, a high-affinity ligand-receptor pair. *Cell*, 116, 883-95.
- YAKOVCHUK, P., PROTOZANOVA, E. & FRANK-KAMENETSKII, M. D. 2006. Base-stacking and base-pairing contributions into thermal stability of the DNA double helix. *Nucleic Acids Res*, 34, 564-74.
- YAMADA, Y. & MORI, H. 2007. Multistep carcinogenesis of the colon in Apc(Min/+) mouse. *Cancer Sci*, 98, 6-10.
- YAMAMOTO, H., KISHIDA, S., KISHIDA, M., IKEDA, S., TAKADA, S. & KIKUCHI, A. 1999. Phosphorylation of axin, a Wnt signal negative regulator, by glycogen synthase kinase-3 $\beta$  regulates its stability. *J Biol Chem*, 274, 10681-4.
- YAN, K. S., CHIA, L. A., LI, X., OOTANI, A., SU, J., LEE, J. Y., SU, N., LUO, Y., HEILSHORN, S. C., AMIEVA, M. R., SANGIORGI, E., CAPECCHI, M. R. & KUO, C. J. 2012. The intestinal stem cell

- markers Bmi1 and Lgr5 identify two functionally distinct populations. *Proc Natl Acad Sci U S A*, 109, 466-71.
- YOST, C., TORRES, M., MILLER, J. R., HUANG, E., KIMELMAN, D. & MOON, R. T. 1996. The axis-inducing activity, stability, and subcellular distribution of beta-catenin is regulated in *Xenopus* embryos by glycogen synthase kinase 3. *Genes Dev*, 10, 1443-54.
- ZAHM, J. M., KAPLAN, H., HERARD, A. L., DORIOT, F., PIERROT, D., SOMELETTE, P. & PUCHELLE, E. 1997. Cell migration and proliferation during the in vitro wound repair of the respiratory epithelium. *Cell Motil Cytoskeleton*, 37, 33-43.
- ZHANG, C., CHO, K., HUANG, Y., LYONS, J. P., ZHOU, X., SINHA, K., MCCREA, P. D. & DE CROMBRUGGHE, B. 2008. Inhibition of Wnt signaling by the osteoblast-specific transcription factor Osterix. *Proc Natl Acad Sci U S A*, 105, 6936-41.
- ZHANG, W., CHEN, X., KATO, Y., EVANS, P. M., YUAN, S., YANG, J., RYCHAHOU, P. G., YANG, V. W., HE, X., EVERS, B. M. & LIU, C. 2006. Novel cross talk of Kruppel-like factor 4 and beta-catenin regulates normal intestinal homeostasis and tumor repression. *Mol Cell Biol*, 26, 2055-64.
- ZHANG, W., YANG, J., LIU, Y., CHEN, X., YU, T., JIA, J. & LIU, C. 2009. PR55 alpha, a regulatory subunit of PP2A, specifically regulates PP2A-mediated beta-catenin dephosphorylation. *J Biol Chem*, 284, 22649-56.
- ZHANG, X., GASPARD, J. P. & CHUNG, D. C. 2001. Regulation of vascular endothelial growth factor by the Wnt and K-ras pathways in colonic neoplasia. *Cancer Res*, 61, 6050-4.
- ZHENG, L., BAUMANN, U. & REYMOND, J. L. 2004. An efficient one-step site-directed and site-saturation mutagenesis protocol. *Nucleic Acids Res*, 32, e115.
- ZHOU, Q., GEDRICH, R. W. & ENGEL, D. A. 1995. Transcriptional repression of the c-fos gene by YY1 is mediated by a direct interaction with ATF/CREB. *J Virol*, 69, 4323-30.
- ZHUO, J., TAN, E. H., YAN, B., TOCHHAWNG, L., JAYAPAL, M., KOH, S., TAY, H. K., MACIVER, S. K., HOOI, S. C., SALTO-TELLEZ, M., KUMAR, A. P., GOH, Y. C., LIM, Y. C. & YAP, C. T. 2012. Gelsolin induces colorectal tumor cell invasion via modulation of the urokinase-type plasminogen activator cascade. *PLoS One*, 7, e43594.
- ZORN, A. M., BARISH, G. D., WILLIAMS, B. O., LAVENDER, P., KLYMKOWSKY, M. W. & VARMUS, H. E. 1999. Regulation of Wnt signaling by Sox proteins: XSox17 alpha/beta and XSox3 physically interact with beta-catenin. *Mol Cell*, 4, 487-98.